Self assemblies, ion recognitions by some cyclic imides and related first row transition metal complexes

A Dissertation submitted to the
Indian Institute of Technology Guwahati as
partial fulfillment for the Degree of
Doctor of Philosophy in Chemistry

Submitted by

Jayanta Kumar Nath

Department of Chemistry

Indian Institute of Technology Guwahati

March 2015

Dedicated to My Family

And

Well Wishers….

Statement

I hereby declare that this thesis entitled "**Self assemblies, ion recognitions by some cyclic imides and related first row transition metal complexes**" is the outcome of research work carried out by me under the supervision of Prof. Jubaraj B. Baruah, at the Department of Chemistry, Indian Institute of Technology Guwahati, India.

In keeping with the general practice of reporting scientific observations, due acknowledgement has been made whenever work described here has been based on the findings of other investigators.

IIT Guwahati
March, 2015

Jayanta Kumar Nath

Certificate

This is to certify that Jayanta Kumar Nath has been working under my supervision since August, 2010 as a regular registered Ph. D. student. I am forwarding his thesis entitled "**Self assemblies, ion recognitions by some cyclic imides and related first row transition metal complexes**" being submitted for the Ph. D. (Science) Degree of this Institute.

I certify that he has fulfilled all the requirements according to the rules of this institute regarding the investigations embodied in his thesis and this work has not been submitted elsewhere for a degree.

IIT Guwahati
March, 2015

Prof. Jubaraj B. Baruah

Acknowledgements

This thesis might not have seen through its completion unless I had the support and encouragement of numerous people around me. Today, when I bring it to an end, I would like to express few words of appreciation to the people who actually made this thesis a reality and an unforgettable experience for me.

First and foremost, with a deepest sense of gratitude, I wish to express my sincere thanks to my supervisors, Prof. Jubaraj B. Baruah whose timely help during my crucial phase of my career has made possible to achieve this target. The enlightening experience of doing science under his guidance can hardly be described in words. The numerous discussions and interactions I had with him expanded my horizons to hitherto unknown frontiers of science and knowledge. I am indebt to this wonderful person for all that he has given me and above all for motivating me towards scientific research. My everlasting gratitude goes towards him.

I would like to thank Prof. Annie K. Powel of Karlsruhe Institute of Technology, Germany for magnetic measurements and Dr. Alexander M. Kirillov of Centro de Química Estrutural, Universidade de Lisboa, Portugal for Topological analyses which are included in this thesis.

I would like to acknowledge my sincere gratitude to all my doctoral committee members for their insightful advices and valuable suggestions. I am also grateful to the entire faculty and staff in the Department of Chemistry, Indian Institute of Technology Guwahati for providing a wonderful work atmosphere throughout this period.

I would like to thank my lab mates Dr. W. Marjit Singh, Dr. Rupam Sarma, Dr. Devendra Singh, Dr. Dipjyoti Kalita, Dr. Babulal Das, Dr. Bhaskar Nath, Dr. Bigyan R. Jali, Prithiviraj, Nithi, Krapa, Arup, Abir, Ananta, Rohan whom I had an opportunity to work with and other group members Apurba, Dipankar, Jiban, Subrata, Aswini, Renjith, Laxman, Najbul and other friends for their timely help, support and for the wonderful time we shared during this period. No words can express my thankfulness for giving me their time and companionship, which made the time spent in the laboratory and outside pleasant and memorable. I would like to

give my special thanks to my lab senior Dr. Rupam Sarma and Dr. Bhaskar Nath for their support and valuable suggestions throughout my research career.

This thesis wouldn't have seen the light of this day without the care, encouragement and help of some wonderful persons like Kanaklata Kalita, Dr. Pranjit Barman, Dr. Nityajyoti Kalita, Miss Kalpana Kalita and Mrs. Mira Kalita. I would like to furnish my sincere gratitude to these wonderful people in my life for their constant motivation which made me reach this point.

The financial support from Indian Institute of Technology Guwahati for the research fellowship is duly acknowledged.

I would like to acknowledge all my teachers of Daulasal M. V school, Daulasal High school, Cotton College and Gauhati University for their love and blessings. I also would like to furnish my sincere gratitude to my teacher Monower Hussain of Barkhetri College for his excellent teaching and motivation.

Finally, my Ph. D. endeavor could not have been completed without the endless love, unending support, tolerance and blessings from my family. I wish to express my sincere gratitude to my parents (Late Golak Ch. Nath and Mrs. Bimala Nath), elder brothers (Utpal, Kameswar, Lohit and Pankaj), sister-in-law (Arpana, Dipti, and Archana), nephew (Ishant and Dhritishman) and niece (Jupitara and Himakhshi). They are the main soul and inspiration for each and every step that I achieved in my life.

Jayanta Kr. Nath

Preview

This thesis deals with the studies on syntheses, characterization of various metallacycles, coordination polymers and self-assemblies of naphthalene derivatives such as imides in which naphthalene rings influences their self-assemblies. The content of the thesis is divided into six chapters.

Chapter 1:

Introduction

First chapter of the thesis is on a general introduction on some cyclic aromatic imides to bring forward the necessity of study on supramolecular aspects of dipolar aromatic imides. This chapter includes discussion on structural features and inclusion properties of imides. Supramolecular interactions influencing binding of cations and anions binding to facilitate preferential detections of different ions are discussed. Salient features of imide containing coordination complexes and their roles in biological applications such as binding and photo-cleavage of DNA are discussed. A brief discussion on scope to work with aromatic cyclic imide derivatives is presented at the last part of this chapter.

Chapter 2:

Metal carboxylate complexes formed through hydrolysis of cyclic anhydrides and imide

This chapter deals with the synthesis, characterization and magnetic properties of some transition metal dicarboxylates metallacycles derived from 1,8-naphthalic anhydride. Syntheses of these metallacycles of cobalt (II), nickel (II) and zinc (II) are presented schematically in Scheme **1.1**. In order to effective π-stacking effect in such complexes chelating heterocycles such as 2,2′-bipyridine (*bpy*) and 1,10-phenanthroline (*phn*) were used as co-ligands.

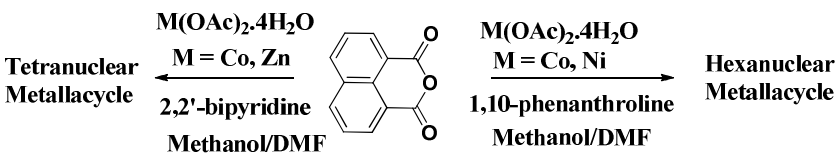

Scheme 1.1

Reaction of 1,8-naphthalic anhydride with cobalt (II) acetate and *bpy*, yielded tetranuclear metallacycle **2.1a;** whereas uses of *phn* instead of *bpy* in a similar reaction yielded hexanuclear metallacycle **2.1b.**

The coordination modes of carboxylate groups and coordination environment around cobalt ions are different in these metallacycles and are shown in Figure **1.1**. The change of bridging mode is guided by π-stacking interactions and is one of the factors due to which nuclearities in two metallacycles differ.

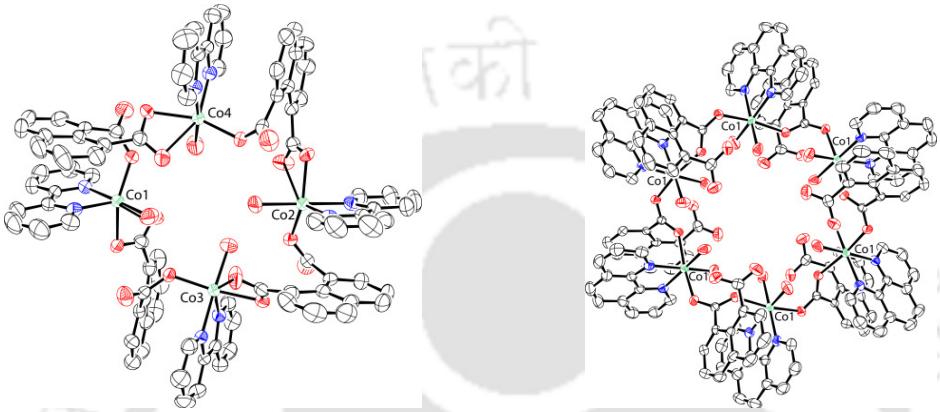

(a) (b)

Figure 1.1*: ORTEP View (30% thermal ellipsoid probabilty) of (a)* ***2.1a*** *and (b)* ***2.1b*** *(hydrogens atoms and lattice waters are omitted).*

Hexa-nuclear nickel (II) metallacycle **2.1c** is isostructural with cobalt (II) metallacyle **2.1b**. On the other hand, reaction of zinc (II) acetate with 1,8-naphthalic anhydride resulted in tetranuclear metallacycle with *bpy* but with *phn* dinuclear zinc (II) metallacycle is formed. Low temperature magnetic studies on **2.1a-2.1c** showed that two cobalt (II) metallacycles (**2.1a-2.1b**) show dominant antiferromagnetic interactions, whereas the nickel (II) metallacycle (**2.1c**) behaves as a spin system S = 3 with intramolecular ferromagnetic interactions.

*Z. Anorg. Allg. Chem.***2013**, *639***,** 2250.

In this section, reactions of phthalic anhydride, naphthalic anhydride, diphenic anhydride in presence of imidazole to prepare mononuclear and polymeric complexes through ring opening reactions are discussed. In case of phthalic anhydride a mononuclear complex of phthalic acid monoester (**2.2a**) transformed to a 2D carboxylate coordination polymer (**2.2b**) through ester hydrolysis were observed and shown in Scheme **1.2**.

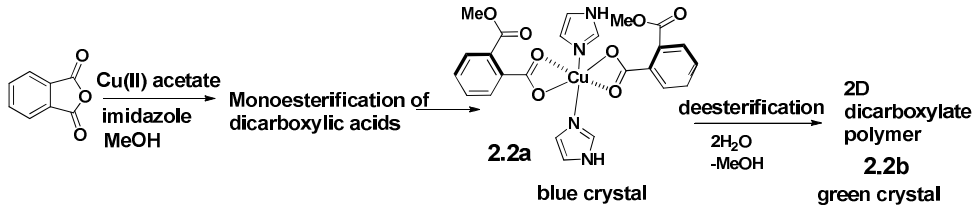

Scheme 1.2

Similar transformation on reaction of naphthalic anhydride also yielded a mononuclear copper complex **2.2c** transformed to a dinuclear copper metallacycle **2.2d** (Scheme **1.3**).

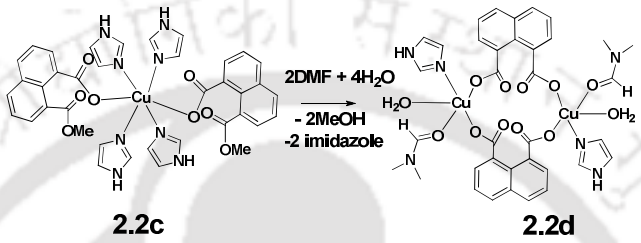

Scheme 1.3

A mononuclear complex was obtained from similar reaction using diphenic anhydride but unlike in above two cases, solvent mediated solid state transformation is not observed in this case. Topological analysis revealed that during transformation of **2.2a** to **2.2b** overall 2D network topology changed from 4-connected **sql** net to a 3-connected **hcb** net. While no topology modification was observed in transformation **of 2.2c** to **2.2d**, in which both structures have topologically equal H-bonded **sql** nets.

RSC Adv. **2014,** *4*, 47876.

Complex formed by the reaction of a cyclic imide possessing flexible imidazole ligand, **L (2.3)** with different copper (II) salts and cadmium (II) acetate are described (Scheme **1.4**).

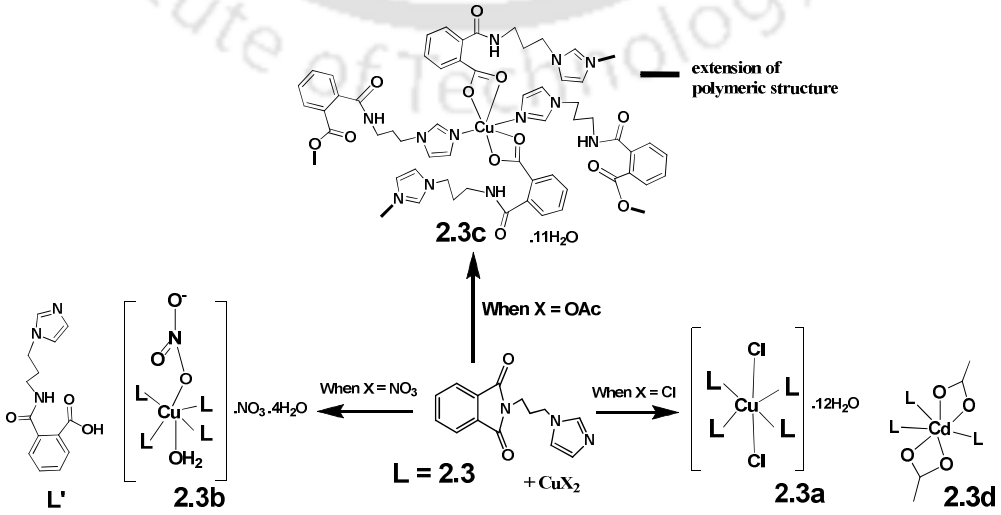

Scheme 1.4

The reaction of copper salts were found to be anion dependent, a mononuclear complexes either in case of cupric chloride or nitrate were formed whereas cupric acetate yielded a coordination polymer (**2.3c**)**.** The coordination polymer was derived from an in-situ generated new ligand **L'**. However no hydrolysis reaction of imide **L** was observed when cadmium (II) acetate was used, it formed a mononuclear complex of **2.3d.** End of this chapter is a summary on the foregoing results describing the propensity of the reactions and role of different factors guiding their synthesis.

Inorg. Chem. Commun. **2013**, *30*, 128.

Chapter 3:

Divalent Manganese, Cobalt, Zinc, Cadmium and Mercury complexes of imidazole tethered to 1,8-naphthalimide

In this chapter synthesis, characterization and photoluminescence properties of divalent transition metal complexes of manganese, cobalt, zinc, cadmium and mercury with N-(3-imidazol-1-yl-propyl)-1,8-naphthalimide ($\mathbf{L^1}$) are discussed.

A series of isomorphous complexes $[M(\mathbf{L^1})_2Cl_2]$ {M = Zn (**3.1a**), Cd (**3.1b**), Hg (**3.1c**)} each having distorted tetrahedral geometry around metal ion were synthesized and characterized. Each of these complexes possesses ligand $\mathbf{L^1}$ in a bend orientation. As a representative structure **3.1a** is shown in Figure **1.2a**. The ratio of ligand to the metal ions varies in the complexes containing thiocyanate as counter anion. The manganese complex with thiocynate ligand, **3.1d** is hexa-coordinated complex, having four $\mathbf{L^1}$ connected through imidazole nitrogen to manganese ion (Figure **1.2b**). An isomorphous cobalt (II) complex is also structurally characterized.

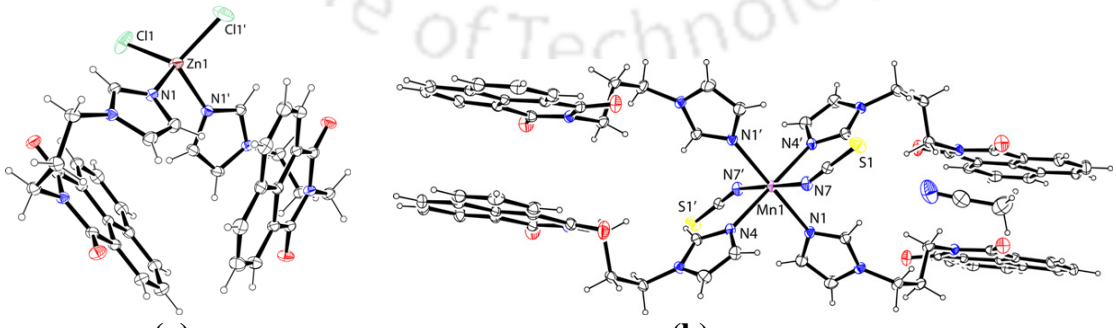

(a) **(b)**

Figure 1.2*: ORTEP view (30% thermal ellipsoid probability) of (a)* ***3.1a*** *and (b)* ***3.1d****.*

On the other hand, 1:2 (metal : ligand) complex was formed in zinc thiocyanate complex and 1:3 (metal : ligand) in cadmium thiocyanate complex. Zinc complex $[Zn(\mathbf{L^1})_2(SCN)_2]$ (**3.1f**) has a distorted tetrahedral geometry whereas in complex $[Cd\mathbf{L^1}_3(SCN)_2DMF]\cdot DMF$ (**3.1g**), cadmium has a distorted octahedral geometry.

Orientation of $\mathbf{L^1}$ and metal ions attached to $\mathbf{L^1}$ decides the solid state fluorescence emission of these complexes. Complexes **3.1a** and **3.1b** show fluorescence emissions at 428 nm and 425 nm respectively which are lower than the fluorescence emission of the ligand $\mathbf{L^1}$ that appears at 461 nm. In mercury complex **3.1c,** emission occurs at 430 nm with higher intensity than ligand $\mathbf{L^1}$**.** On the other hand, complexes **3.1f** and **3.1g** have fluorescence emissions of longer wavelengths. Correlation of these fluorescence behaviors with solid structures are discussed in this chapter. Further, comparison with emission by these compounds in solutions and effect of temperature on the fluorescence changes are discussed.

Inorg. Chem. Front. **2014,** *1*, 342.

Chapter 4:

Transition metal based carboxylate coordination polymers of naphthalimide tethered pyridine and their photoluminescence and magnetic properties

This chapter deals with the synthesis of transition metals (Mn, Co, Ni and Cu) coordination polymers derived from N-(4-pyridylmethyl)-1,8-naphthalimide ligand, $\mathbf{L^2}$ using dicarboxylate as linkers. Ligand $\mathbf{L^2}$ and different carboxylic acids such as fumeric acid (H_2Fum), malonic acid (H_2Mal), adipic acid (H_2Adp) used as a linker in the preparation of transition metal coordination polymers are shown in Scheme **1.5**. All the coordination polymers are characterised by spectroscopic tools and their photoluminescence and magnetic properties are studied.

Manganese (II) coordination polymer **4.1a,** has manganese ions in O_4N_2 environment with distorted octahedral coordination geometry. It shows antiferromagnetic properties and shows slow magnetization relaxation, typical of single chain magnetic (SCM) behavior.

Coordination polymer **4.1b** has an octahedral coordination environment around cobalt (II) centre. Cobalt (II) adipate coordination polymer (**4.1c)** is isostructural with manganese coordination polymer **4.1a**. Coordination polymers **4.1b** and **4.1c** show antiferromagnetic coupling between cobalt (II) ions.

Nickel (II) coordination polymer **4.1d** has have $\pi\cdots\pi$ interactions that help to form 3D supramolecular chains and it shows antiferromagnetic behaviour at low temperature.

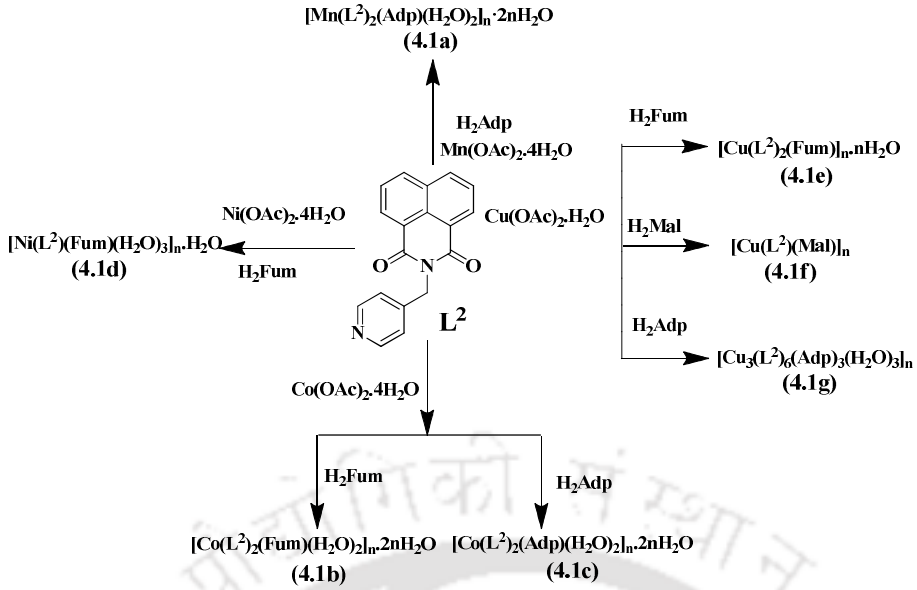

Scheme 1.5

Copper (II) acetate forms coordination polymers of $\mathbf{L^2}$ with malonate, fumarate, and adipate. Among these coordination polymers of copper, copper malonate shows ferromagnetic behavior whereas the other two polymers show antiferromagnetic behavior at low temperature.

Details synthetic procedure, structural description, spectroscopic characterisation and thermal stability of the coordination polymers are included in this chapter.

Cryst. Growth Des. **2014,** *14*, 4735.

Chapter 5:

Anion assisted assemblies of *N,N′*-bis(3-imidazol-1-yl-propyl)naphthalenediimide

In this chapter different anion assisted assemblies of *N,N′*-bis(3-imidazol-1-yl-propyl)naphthalene-diimide, $\mathbf{L^3}$ are discussed. The ligand, forms isostructural and isomorphous protonated 0.5:1 dihydrated salts (**5.1a** and **5.1b**) with hydrochloric and hydrobromic acid respectively. These salts have anion-pi interactions and form hydrogen bonded halide-water chains and is shown in Figure **1.3**. $\mathbf{L^3}$ shows fluorescence quenching on interactions with hydrochloric acid and hydrobromic acid.

The weak interactions in the lattice of perchlorate salt (**5.1c**) contribute to the formation of the 2-D layer structure. Bisulfate salt (**5.1d**) adopts a helical arrangement of cations formed by weak interactions. HPO_4^{2-} anions form water bridged polymeric inter anionic chain-like structure in salt **5.1f**.

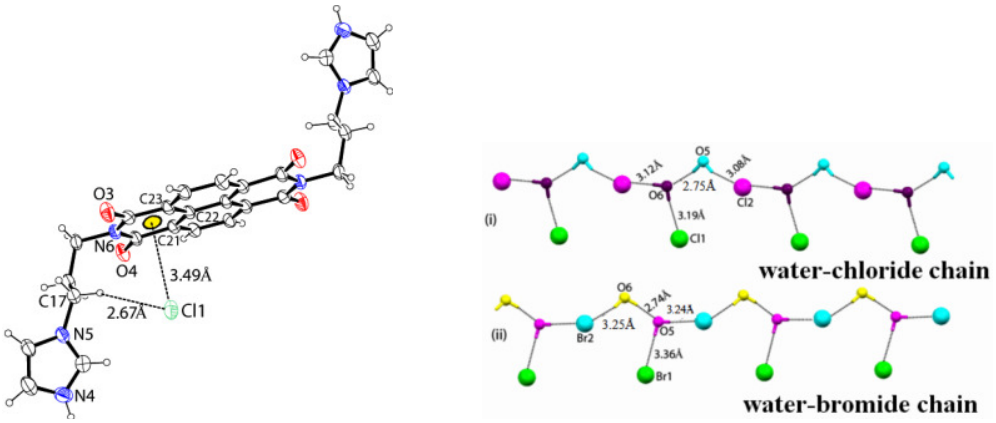

***Figure 1.3**: (a) Anion- π interactions showing position of chloride in **5.1a,** (b) water assisted chain of (i) chloride ions in **5.1a** and (ii) bromide ions in **5.1b**.*

Nitrate salt (**5.1g**) with imide has nitrate anions placed over naphthalenediimide with distance from nitrate plane and the centroid of the naphthalenediimide plane is 3.38Å. In the crystal packing of this salt, planar nitrate anions and imidazole part are sandwiched between the layers of naphthalenediimide rings and the distance of separations lies between 3.4-3.6Å. Whereas in the lattice of salt **5.1h,** SiF_6^{2-} anion form spiral chain like arrangements in between the stacked layer of protonated cations.

Structural analysis of salts and consequence of anion-π interactions reflected in optical spectra are shown in this chapter.

New J. Chem. **2013,** *37*, 1509

Chapter 6:

Self-assemblies of solvates and salts of a chiral zwitterionic host N-(2-imidazol-5-yl-1-carboxyethyl)-1,8-naphthalimide

We found that N-(2-imidazol-5-yl-1-carboxyethyl)-1,8-naphthalimide H**L**^{4} forms varieties of solvates and salts with different solvent molecules (Chart **1**) and with mineral acids respectively. This chapter deals with the self assemblies of solvates and salts of H**L**^{4} and their photoluminescence properties.

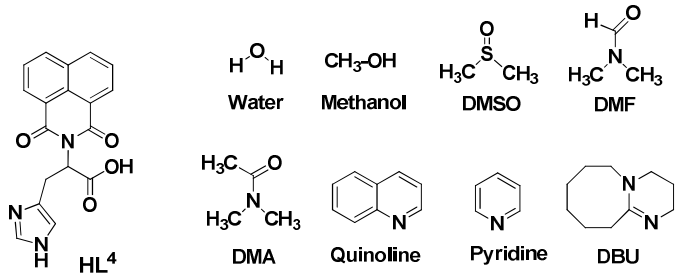

Chart 1

All solvates and salts crystallized in chiral space groups. Their packing patterns were analysed in detail, showing that an interplay of hydrogen bonds, aquation and π-stacking control the formation of distinct 1D, 2D or 3D supramolecular assemblies. The H-bonded 2D underlying networks of all the solvates were topologically classified revealing three distinct topological types, namely an undocumented topology in hydrated H**L**[4] and the **3,4L127** topology in methanol solvate; whereas, **skl** topology was observed in DMSO, DMF, DMA, quinoline, pyridine and dbu solvates. In contrast, bromide, iodide, sulfate and nitrate salts show H-bonded underlying networks that are quite distinct not only in the topology (**2C1** in bromide and iodide salt, **kgd** in sulfate salt and **lon** in nitrate salt) but also in the dimensionality that increases from 1D in halide salts to 2D in sulfate salt and 3D in nitrate salt. The solid state photoluminescence properties of these solvates and salts are also discussed that show higher fluorescence intensity than that of the parent host.

Cryst. Growth Des. **2015**, *15*, 737.

The synthetic procedure and experimental details for each compound or complex are included in the corresponding chapter. The cumulative references are also listed at the end of corresponding chapter. Instrumental details and crystallographic data for all the structures are tabulated in the appendix section of the thesis. A brief summary on the finding of the presented work is compiled at the end of the thesis. The CIF of the crystal structures are presented in a CD as electronic data attached with the thesis

Table of content: **Page no.**

CHAPTER 1

Introduction

1.1 General features of cyclic imides:

Cyclic aromatic imides and their derivatives exhibit various material properties. They find applications in semiconductor,[1] in organic light emitting diode,[2-4] liquid crystal display,[5-6] solar cell[7-8] and energy storage.[9] Moreover due to fluorescence properties and good photostability, some imides have found extensive applications in sensing of cation[10] and anion,[11] fluorescent dyes for polymer materials[12-13] and as biological probes.[14] Imide derivatives have the capability to form host-guest chemistry,[15] can bind with DNA[16] and some imides can also show anticancer activity.[17] Few illustrative examples of cyclic aromatic imides are shown below.

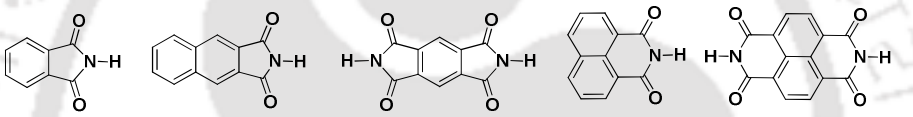

Structural skeleton of above examples are composed of two rings, one is an aromatic ring and other is imide containing ring. Thus, due to the presence of a relatively electron rich aromatic unit connected to an electron deficient imide ring, aromatic imides are dipolar. This allows them to arrange in different ways in the crystal lattices. Relative energies associated with each arrangement differ. Stacking contribution varies in energies in the range of about -12.5 to -16.5 Kcal/mol.[18] In a dipolar molecule such as 1,8-napthalimide, there can be different types of stacking interactions that may arise from the positions and arrangement of the dipoles. It has been established that the order of magnitude of interactions of two π- systems is π-deficient···π-deficient > π-deficient···π-rich > π-rich···π-rich[19] and is shown in Figure **1.1**. Such packing arrangements are guided by interplay of other weak interactions such as C-H···π, O-H···π, O···π and C-H···O which are comparable in energy. Thus various self-assemblies can be generated from imide derivatives. Be a part of a coordination complex or a polymer or a discrete unit each may adopt interesting packing patterns which provides avenues for studying in domain of supramolecular chemistry.

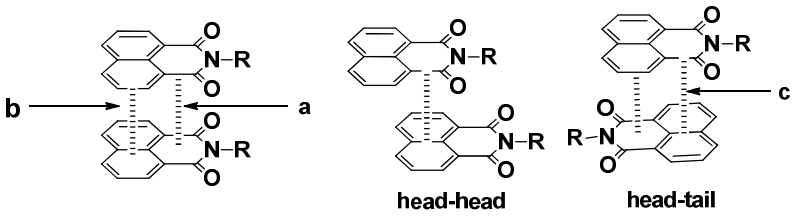

***Figure 1.1**: Different stacking arrangements in 1,8-napthalimide derivatives: (a) π-deficient···π-deficient, (b) π-rich···π-rich and (c) π-deficient···π-rich stacking interactions.*

1.2 Supramolecular assemblies of cyclic imides:

Assembling of structural building blocks into regular arrays with new structural diversity and properties are one of the key features of supramolecular chemistry.[21] Host-guest chemistry[20-21] has tremendous potential to provide strategies to design and build these structures. Non-covalent interactions between π-donor and π-acceptor rings govern the self assemblies in solids or solution state.[22] Weak interactions such as π···π interactions, cation···π, dipole···dipole, ion···dipole also find special significances in assembling processes.[23] Stacking π···π interactions play important roles in packing of crystals containing aromatic moieties[24,25-26] Such interactions help to stabilize three-dimensional helical structures.[27-28] Cyclic imides generally exhibit face-to-face aromatic interactions because it contains electron deficient unit and their rigid, planar structure along with the ability to be easily functionalized with a wide variety of side groups help to tune their packing properties. Cyclic imides are widely studied to construct different host-guest systems using as precursor for intercalations,[29-30] foldamer,[31-32] ion channels,[33] catenanes[34-35] and rotaxanes.[36-37]

Structural and chemical properties make aromatic cyclic imides as ideal candidates for host-guest interactions in particular donor-acceptor charge transfer (CT) type complexes. It has been shown earlier that 2-hydroxyethylphthalimide **1.01** forms 1:1 adducts with 1,3-dihydroxybenzene and 1,3,5-trihydroxybenzene[38] through hydrogen bonding and various weak interaction that leads to supramolecular-layered architectures (Scheme **1.1**).

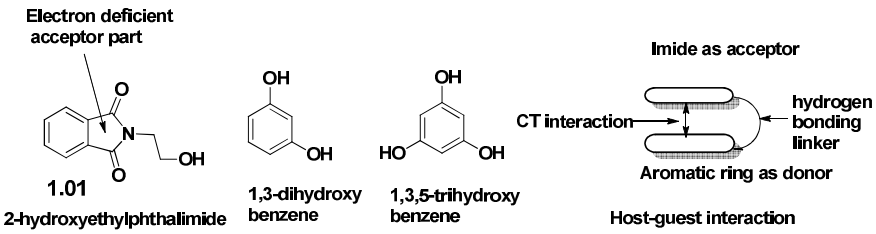

Scheme 1.1

Polyaromatic hydrocarbons are hazardous to mankind because of their carcinogenic and mutagenic properties.[39] For these reasons it is very much essential for their recognition even at low concentration. Compound *N,N´*-bis(glycinyl)pyromellitic diimide (**1.02**) allows intercalation of aromatic hydrocarbons such as anthracene, phenanthrene and perylene as well as tetrathiafulvalene.[40] While forming such species, less directional π-deficient and π-rich stacking interactions has been observed. In these complexes, primary self-assemblies are governed by hydrogen bonds of the carboxylic acid groups to assemble the host molecules into 1D zig-zag chains. The chains linked together to form sheets by π···π stacking interactions between aromatic π-donor guest molecules and electron deficient π-acceptor units of host molecules (Figure **1.2**).

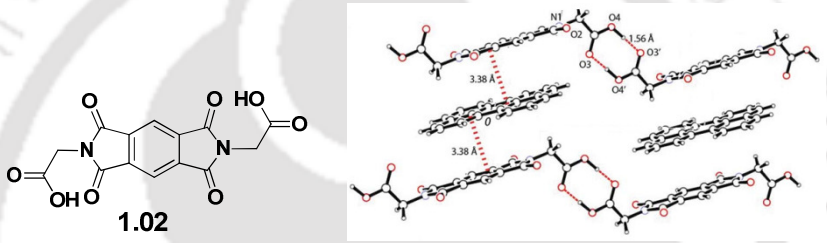

(a) (b)

Figure 1.2*: (a) Structure of* ***1.02****, (b) π···π interactions between* ***1.02*** *and perylene molecules.*

Introducing phenyl group in side chain of **1.02** it was observed that **1.03** forms molecular host-guest assembly with polyaromatic guests such as anthracene and perylene.[41] In this assemblies also π···π interaction plays important role along with conventional hydrogen bonds. C-H···π and π···π interactions of host-guest complex, **1.04** formed between **1.03** and perylene is shown below.

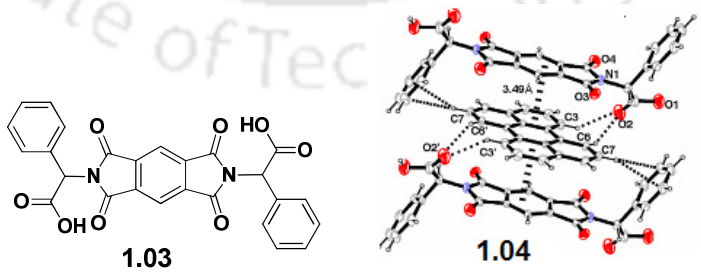

Rotello *et al.* demonstrated molecular recognition processes of naphthalimide through complementary hydrogen bonds in an elegant manner. Based on such a specific binding principle they have showed three components molecular switches. In these examples, host molecules form three point hydrogen bonds with guest naphthalimide.

The electrochemical studies on these adducts have revealed that while guest recognition takes place, the adducts show characteristic redox couples in cyclic voltamograms through their oxidised (N_{ox}) (**1.05**) or radical anions (N_{rad}) (**1.06**).[42]

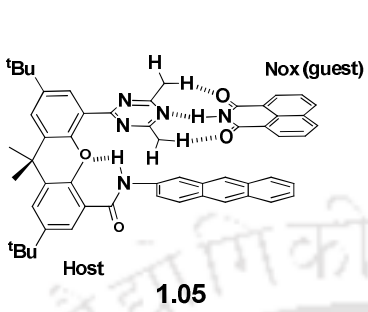

1.05

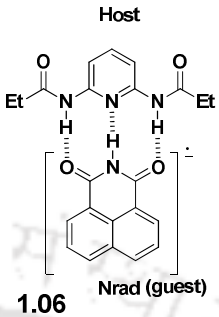

1.06

A series of chiral amino acid functionalized naphthalenediimides (NDIs) derived from L-cysteine (**1.07**), L-lysine and their corresponding methyl esters derivatives were also reported. Sanders *et al*. have shown that these molecules exhibit molecular recognition through formation of host-guest assemblies. These molecules form supramolecular helical nanotubes (**1.08**) in aprotic solvents. The dimension of the nano-tubes is 115 nm which are suitable to encapsulate polyaromatic compounds such as pyrene and their derivatives. Such assemblies are primarily formed by hydrogen bonds and are stabilized by other weak interactions. Pyrene and it's derivatives gets encapsulated and the encapsulated nano-tubes shows color in solution. Circular dichroism spectroscopy indicates that the nano-tube remains intact after encapsulation of guest molecules.[43] However, no significant color changes were observed if the larger analogues of pyrene were added to the nano-tubes as they are not fit into the cavities. Thus system is suitable to serve as important receptor for molecular recognition.

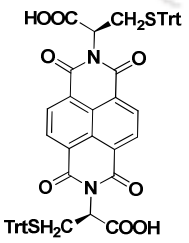

1.07 (Trt = Trityl group)

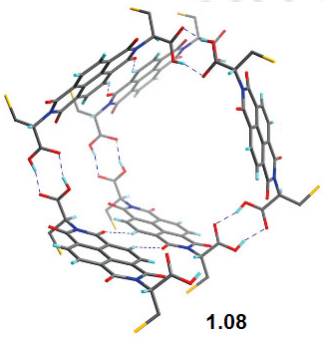

1.08

Bispyridyl based pyromellitic diimide **1.09**, shows selectivity to sense various aromatic diols.[44] Receptor **1.09** is highly selective that forms charge transfer complexes showing different colors and intensity of colors depends on the phenols and naphthols. The charge

transfer band is useful to simultaneously report multiple characteristics about a guest such as size, recognition ability, and electronic structure.[45] Thus, the differences in colorimetric responses observed in this case is due to a combination of the abilities of guests to form hydrogen-bonded complexes and the electronic structure of the guest. Host guest complex **1.10** formed between **1.09** and 1,3-dihydroxybenzene is shown in Chart **1.1**.

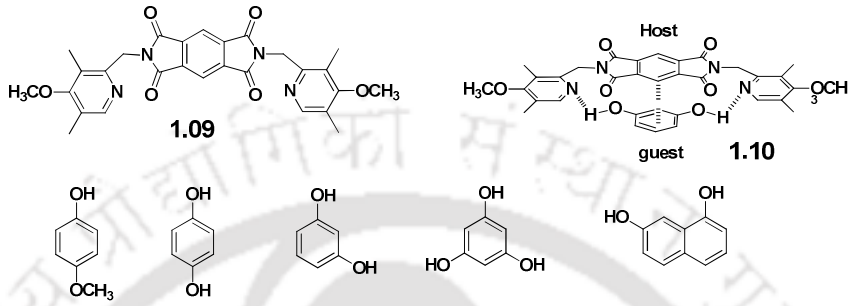

Chart 1.1

Macrocyclic receptors bearing pyromellitic diimide or naphthalenediimide, **1.11** and **1.12** bind with a wide range of electron-donor substrates.[46] Their bindings are assisted by π-stacking donor-acceptor interactions. These receptors are colorless but addition of π-electron donor molecules such as pyrene, perylene, 2,6-dimethoxynaphthalene, tetrathiafulvalene and pyren-1-ol to the solutions produced intense colors. Such color changes are assigned to intermolecular charge-transfer absorptions. ^{1}H-NMR showed large ring-current-induced complexation shifts in each case during interactions at different proportions. 1:1 complex (**1.13**) is formed between macrocycle **1.12** and perylene.

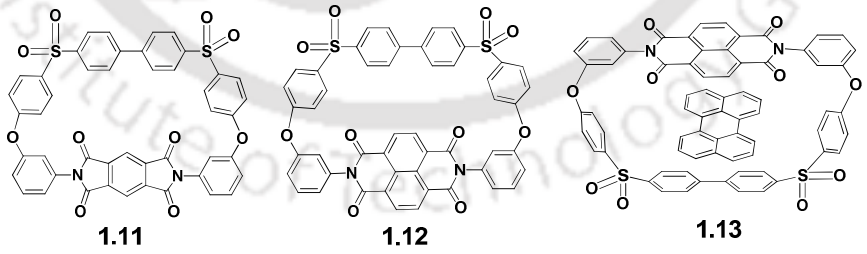

Pyromellitic diimide based cyclophane-type macrocycles with large ring size macrocyclic receptors were also reported by Shinmyozu *et al*. These receptors form tubular structures that selectively encapsulate electron rich guest molecules like p-xylene and toluene.[47] High selectivity was observed in 1:1 host-guest complex, **1.15** formed between the electron-deficient host **1.14** and electron-rich guests (*p*-xylene)$_3$. The host-guest structure was confirmed by X-ray crystallography and NMR techniques. In this case driving force is due

to charge transfer interactions where guest molecule is arranged in a parallel fashion with the benzene ring of the pyromellitic diimide moiety. This serves as an example to show the importance of a charge transfer type π···π interactions to form inclusion complex.

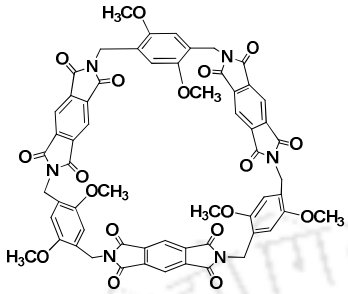

1.14

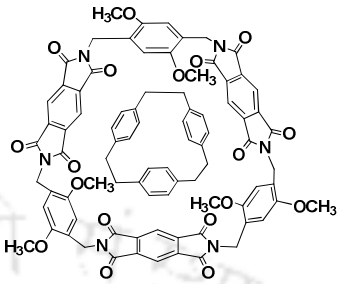

1.15

Calix[4]arene based naphthalimide derivatives (**1.16)** were reported and these type of receptors recognize aromatic molecules such as benzene, naphthalene, anthracene, pyrene and their derivatives. Guest binding properties were studied using fluorescence and UV-visible absorption spectroscopy.[48] Changes in fluorescence intensity was observed to be more in the case of compounds containing more number of aromatic rings. This was attributed to more π···π interactions present in such systems. An illustrative example **1.17** shows the binding of naphthaldehyde with **1.16**.

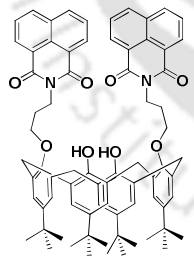

1.16

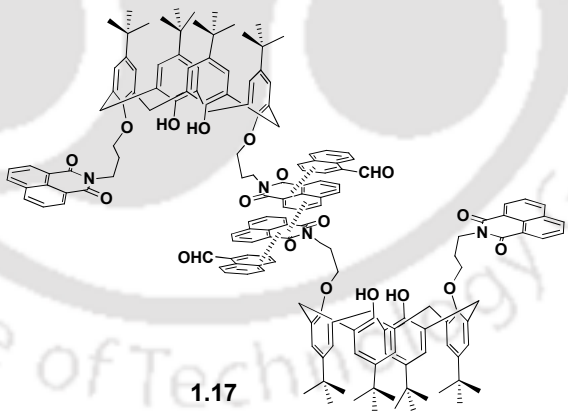

1.17

Several phthalimide and naphthalimide tethered carboxylic acids (**1.18a-1.18f**) were reported to form inclusion complexes with pyridine and quinoline. Crystal structures revealed that these complexes were formed by different hydrogen bonded motif. Depending on the assembly formed and method of preparation, the host molecules accommodate guest molecules in different ratios. [49] In these examples pseudo polymorphs of such inclusion complexes were shown. For example **1.18a** can accommodate one pyridine molecule whereas**1.18c** can accommodate three molecules of pyridine molecules.

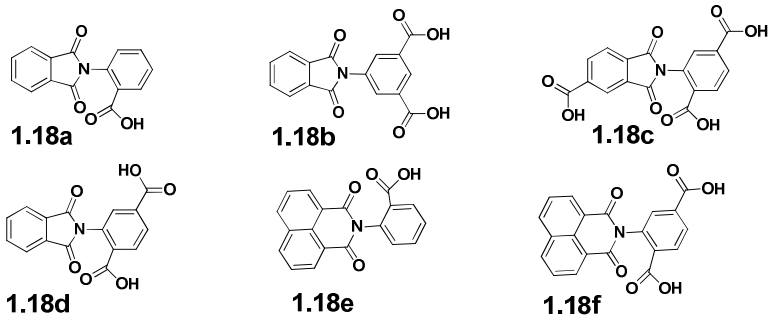

4-Amino-1,8-naphthalimide chromophore (**1.19**) were attached to cucurbit[6]uril and cucurbit[7]uril to generate different receptors with hydrophobic pockets of definite sizes. It was found that cucurbit[6]uril encapsulated a portion of the dye and such inclusion complexes have high binding constants. Strength of binding in such inclusion complexes was found to be invariant of pH of the media. Binding of dye is accompanied by fluorescence quenching and a bathochromic shift of charge-transfer absorption band of the dye. From quenching of fluorescence spectra, 1:1 host-guest complexation was established. Comparatively, cucurbit[7]uril derivative encapsulated the dye much less efficiently and it showed a significant fluorescence enhancement in contrast to fluorescence quenching shown while interacting with cucurbit[6]uril derivative. From such a study, dye-cucurbit[6]uril (**1.20**) derivative has been identified as potential host for the detection of biogenic amines under physiological pH conditions and at low analyte concentrations.[50]

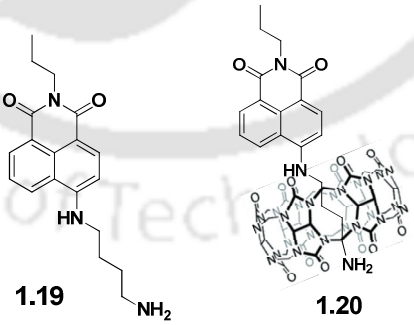

From the above discussions and examples it is clear that π···π interactions in host-guest assemblies are prominent features and such interactions along with interplays of with other weak interactions such as C-H···O or C-H···π interactions help the assembly formation. Examples provided in this section have clearly depicted that directional nature of weak interactions and inherent dipolar nature of aromatic imides has made them to be potential

host molecules for binding to various neutral molecules providing avenues to study molecular recognition properties.

1.3 Cyclic imides as sensors for anions:

Nature provides us many examples of anion binding motifs. Such motifs are primarily based on hydrogen-bonding interactions and they may be in charged or neutral states.[51] On the other hand, luminescent and colorimetric ion sensing is a rapidly developing field.[52-54] 1,8-Naphthalimide based structures connected to a receptor derived from molecules such as urea[55], thiourea[56] and amide[57-58] have been extensively used for anion recognition. Sensing as well as recognition is routinely carried out in organic, aqueous solutions, or within various polymeric networks. In such cases use of confined media such as hydrogels is of worth noting.[59] In the last decade, owing to many demonstrated examples of naphthalimide-based anion sensors,[60-61] versatility of this class of molecules within this fast growing field of research has made a big impact. Synthetic modifications on an imide can be done on aromatic naphthalene moiety or at N-imide site. Fuctionalization at both the sites are relatively easy; thus allows scope for incorporating varieties of functional groups at these sites. UV-visible absorption and fluorescence emission spectra of naphthalimide can be easily tuned through judicious structural design. The optical properties of many naphthalimide derivatives depend on environments more importantly on solvents. Thus they can either solvochromic or solvatoemissive which makes them advantageous for study as receptors in biological system or in ordinary condition for molecular recognitions. Their optical responses to different analytes are different but with selective manner. Moreover, hydrogen-bonded receptors, as well as charged assisted anion receptors have been extensively used for anion recognition and sensing. Generally photo-induced electron transfer (PET) and internal charge transfer (ICT) are the most extensively studied processes to sense anions. Both these paths independently or in combined manner are effective to cause specific changes in optical spectra. In PET probes, a fluorophore is usually connected via a spacer to a receptor containing electronegative atoms such as nitrogen atom. Relatively high energy nonbonding electron pair presents in a receptor can transfer an electron to excited fluorophore, leading to the quenching of fluorescence. Upon binding to anion fluorescence emission get quenched due to enhanced PET from the receptor to the excited state of the fluorophore. However, upon coordination to a metal cation, reduction potential of a receptor increases so that corresponding energy

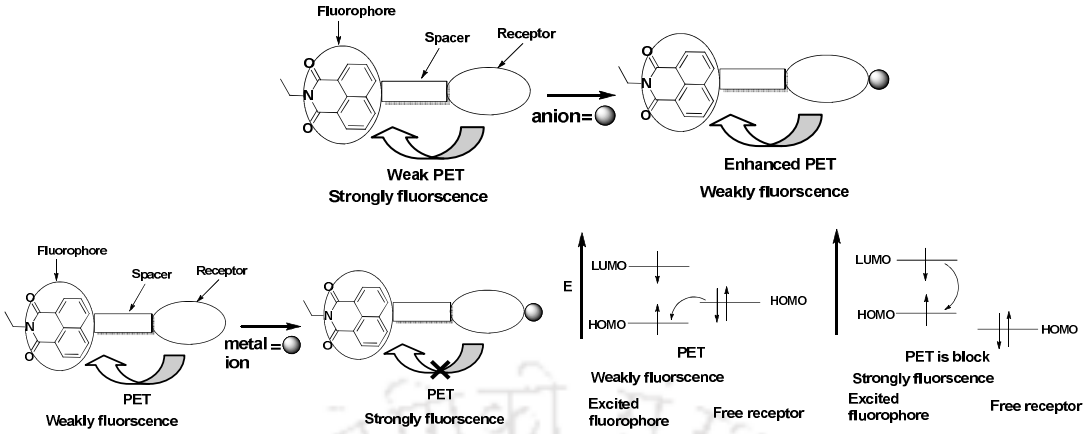

Scheme 1.2

of highest occupied molecular orbital is lower than that of fluorophore. As a consequence, PET process from receptor to fluorophore is prohibited. In this process fluorescence intensity enhances. Polarity of a solvent can affect the oxidation potential of the receptor, thus use of highly polar solvent, PET-mediated quenching effect of the fluorescence occurs more quickly in polar solvent.

There are many examples of sensors for detecting ions which are designed with sequence of arrangements of components as fluorophore-spacer-receptor, they operates through PET mechanism (Scheme **1.2**).[62-63] Thiourea functional unit connected to naphthalimide have been extensively reported as colorimetric anion sensors.[64-66] Thiourea based naphthalimide receptor for anions have generated large interest due to ease to synthesize and handle at ambient conditions. In such sensors, thiourea parts act as anion receptors and naphthalimide moiety acts as a fluorophore. ^{1}H-NMR spectroscopy has been used as tool for detection of anions. Thiourea unit directly connected to naphthalimide unit has also been reported to recognize different anions.[67]

Receptors **1.21-1.29** behave as dual responsive chemosensor for selective detection of different anions such as F^-, Cl^-, $H_2PO_4^-$, AcO^-, OH^- ion.[68-75] These receptors display dual sensing actions for specific anion. Upon addition of an anion, they give rise to large changes in the UV-visible spectra (red shift) and show quenching of fluorescence intensity. Changes take place due to formation of 1:1 complex either through hydrogen bond without proton transfer or through proton transfer of amino moiety. Formation of 1:1 stoichiometric complex is established by ^{1}H-NMR titration experiments; where substantial chemical shift for the naphthalimide N-H and thiourea N-H protons were observed. A few common naphthalimide based anion sensors are shown in Table **1.1**.

***Table 1.1**: Examples of some common naphthalimide based anion sensors.*

Sensor	Anion	Sensor	Anion	Sensor	Anion
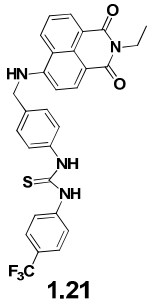 **1.21**	F^- Ref. 68	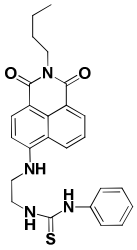 **1.22**	$H_2PO_4^-$ Ref. 69	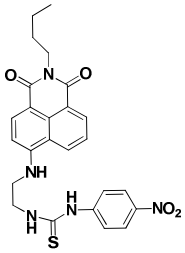 **1.23**	F^- and AcO^- Ref. 70
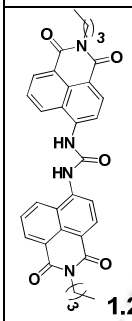 **1.24**	F^- and OH^- Ref. 71	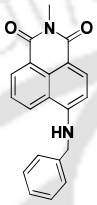 **1.25**	F^- Ref. 72	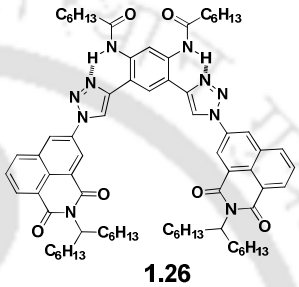 **1.26**	Cl^- Ref. 73
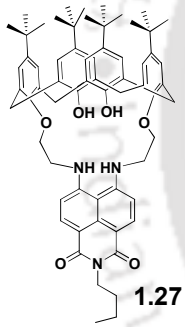 **1.27**	F^- Ref. 74	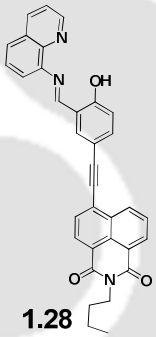 **1.28**	F^- Ref. 75	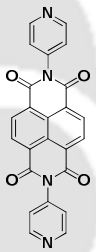 **1.29**	F^- Ref. 78

Anion-π interaction is a quadrupolar interaction that occurs between an appropriately placed anion over a π-cloud. Naphthalimide based compounds are well known for anion-π interactions which are reflected in their absorption and emission spectra.[76]

One illustrative interaction of chloride interacting cyano substituted naphthalenediimide derivative is shown in Figure **1.3a**. Figure **1.3b** shows the bromide and chloride interactions with N-phenyl substituted naphthalenediimide and showing the positions of anions over the ring and also the experimentally observed distances between anion and π-clouds. On the basis of such observations, naphthalenediimide based molecules were employed for selective anion recognition through anion-π interactions.[77] Anion-π interactions and charge transfer or electron transfer involving F^- ions to naphthalenediimides are reflected in their emission and absorption spectra. Utilities of such effects were shown in π-electron deficient colorless naphthalenediimide receptors

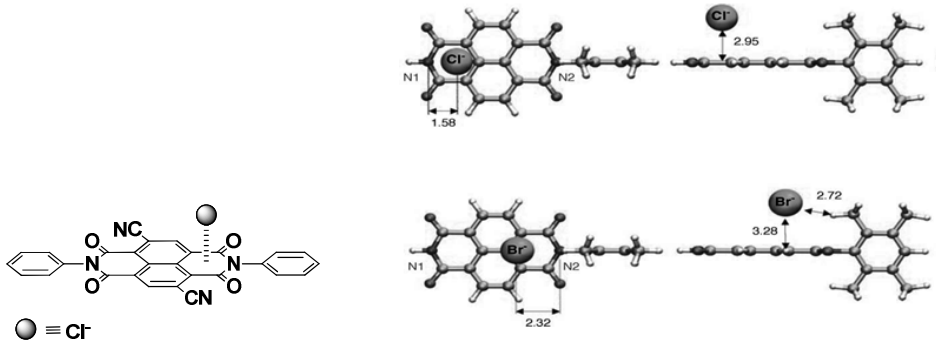

(a) (b)

***Figure 1.3**: (a) An example of a Cl⁻-π interaction, (b) Structures showing π-interactions of Cl⁻ and Br⁻ ions with substituted naphthalendiimide (from two different directions).*

bearing bis-pyridyl groups (**1.29**) shown in Table **1.1**. Strong electronic interactions between lone-pair electrons on F^- ions and π^*-orbitals of naphthalenediimide unit led to development of an orange color due to formation radical anion of naphthalenediimide. Further reduction of such radicals by another F^- ion, generate colored dianion of naphthalenediimide. Such color changes are useful to selectively detect F^- ions and they operate in a very specific manner over various other anions.[78]

Another methodology to detect anion by naphthalimide based sensors involve, uses of metal complexes containing naphthalimide units as a part of its ligand that serves as template for anion binding. While an anion interacts directly or indirectly with the metal ions, fluorescence properties of naphthalimide group changes leading to transducer signals. Based on such principle, both naphthalimide and naphthalenediimide based metal complexes or coordination polymers have been utilised to sense different anions. Ruthenium (II) based polypyridyl conjugate **1.30** was used as sensor for F^- ion in CH_3CN.[79]

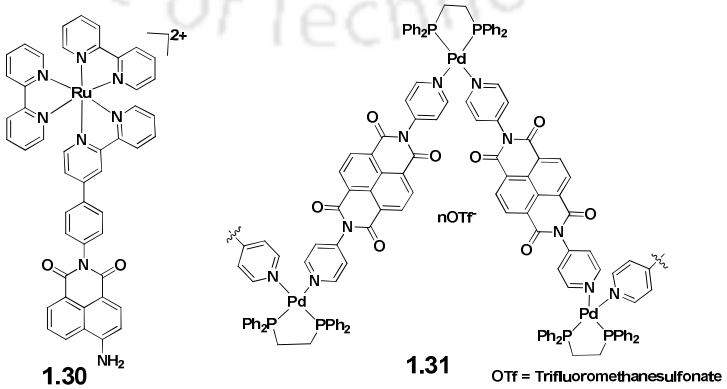

In this example, a metal to ligand charge transfer luminescence process is made use of in detection process. This complex can effectively sense fluoride ion in presence of other anions such as acetate, phosphate and chloride. Palladium (II) coordination polymer **1.31** detects fluoride ions through anion-π interactions. Electrochemical studies showed that trifluoromethanesulfonate anions suppressed π-acidity of dipyridyl naphthalenediimide whereas in a palladium (II) coordination complex π-acidity of dipyridyl naphthalenediimide gets enhanced. Thus, enhanced ability of F^- ions to cause electron transfer to dipyridyl naphthalenediimide of the palladium (II) dipyridyl naphthalenediimide coordination polymer led to colorimetric sensing of F^- ions.[80]

Anion-π interactions of naphthalenediimide have also relevance in ion-transport in biological systems. Important applications of anion-π interaction of such molecules are developed to study transport of anions across lipid bilayer membranes.[81-83] These kinds of studies are important as variety of diseases or channelopathies, most notably cystic fibrosis, arises when anion transport across biological membranes gets disrupted.[84] A range of compounds that function as discrete molecular carriers or as synthetic channels allowing anions to pass through a lipid bilayer are developed. Such molecules also provide an approach for modelling synthetic ion transporter which can mimic different biological activities such as trans-membrane anion transport and also to photosynthetic activity in system having anion-π interactions[85] for selectivity and multi-ion hopping across lipid bilayer membranes.[86] Naphthalenediimide (NDI) group were derivatized to generate hydrophobic rigid-rod like structural backbones. Such rods were designed such that they are long enough to span width of phospholipids bilayer. Matile *et al.* correlated theoretical

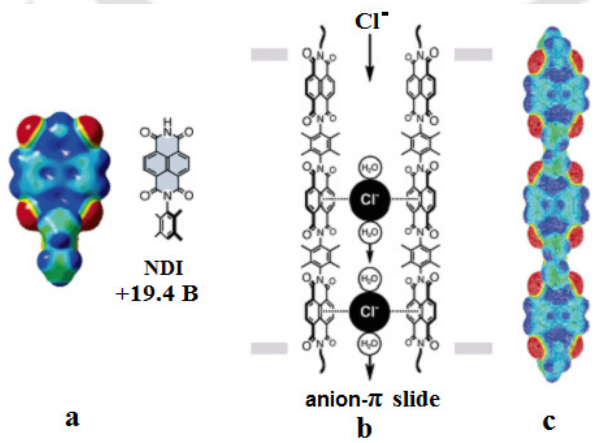

***Figure 1.4**: (a) Solis surfaces for the model NDI and its DFT computed ESP map, (b) Concept of anion- π slide in lipid bilayers and (c) DFT-computed ESP map. Blue areas: electron poor, red areas: electron rich.*

and experimental findings of anion-π slides for chloride-selective multi ion hopping across lipid bilayer by synthesizing shape-persistent oligo-p-phenylene-*N,N'*-naphthalenediimide (O-NDI) as π-rods. The concept of anion-π slide in lipid bilayer with DFT computed electrostatic potential maps (ESP) for this compound is shown in Figure **1.4**.[87] They have shown spectroscopic assays for measuring pH and ion concentrations inside phospholipid vesicles. It was also found that these hydrophobic and π-acidic rods can selectively transport anions across the lipid membrane. Matile *et al.* have shown experimentally that anion-π interactions control transmembrane transport of anions using some simple naphthalenediimide molecule and measured their anion binding in phospholipids liposome by a variety of fluorescence techniques.[88] From their experiment it was found that a compound with higher affinity for binding anions, showed better anion transport activity.

1.4 Cyclic imides as sensors for cations:

Design of chemo-sensors for transition metal ion is actively investigated, as this metal ion is a significant environmental pollutant and an essential trace element in biological systems. Cyclic imides are also frequently used for colorimetric and ratiometric chemosensors for metal ions. Depending on design principles, absorption and emission spectra of imide can be highly modulated by binding to cations. To recognize metal cations, the receptors should have some pre-organized binding sites. This criterion is fulfilled easily by functionalization with different units which has metal binding sites. Imide functional group contributes to supramolecular architecture of metal complexes, as well as they may be fluorescent or electroactive, such properties can be easily modulated and studied to design cation sensors. These compounds exhibit fluorescence responses to an analyte via PET,[89] ICT,[90] FRET (fluorescence resonance energy transfer)[91] and exciplex[92] mechanisms.

4-amino-1,8-naphthalimide derivatives have been reported by various group as a colorimetric and ratiometric sensors for different transition metal ions. In these classes of compounds addition of metal ion changes in both UV-visible spectra and fluorescence spectra are observed due to the binding of receptor to the metal ion through N and O atom. In some cases deprotonation of secondary amine also takes place which facilitate the formation of metal conjugate and as a result of which internal charge transfer takes place from metal complex to fluorophore. The proposed mechanism for the detection of M^{2+} is

generally based on the binding of donor atoms to metal ions or M^{2+}-induced deprotonation of the secondary amine directly conjugating with the 4-amino-1,8- naphthalimide

***Table 1.2**: A few Cu^{2+} and Zn^{2+} ion sensors based on naphthalimide.*

M^{2+}	Sensor				
Cu^{2+}	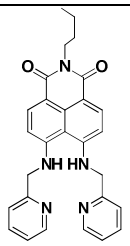 **1.28** Ref. 93	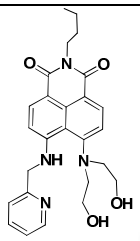 **1.29** Ref. 94	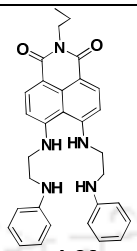 **1.30** Ref. 95	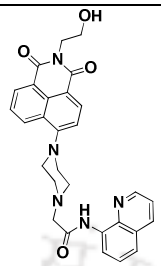 **1.31** Ref. 96	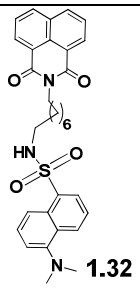 **1.32** Ref. 97
Zn^{2+}	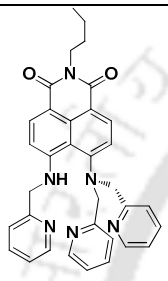 **1.33** Ref. 98	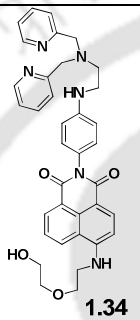 **1.34** Ref. 99	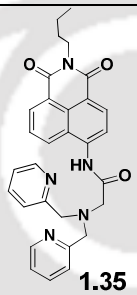 **1.35** Ref 100	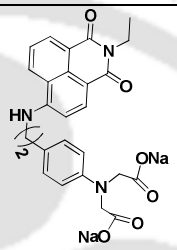 **1.36** Ref. 101-102	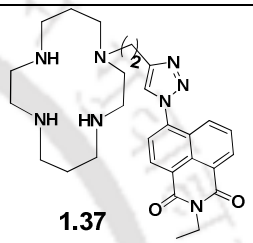 **1.37** Ref. 103

chromophore and changes in fluorescence spectra are due to photo-electron transfer or internal charge transfer mechanism. A few common metal ion sensors (**1.28-1.37**) for Cu^{2+} and Zn^{2+} ions have been shown in the Table **1.2** [93-103]

Naphthalimide based fluorescence ratiometric probes **1.38-1.41** were reported for selective detection of trivalent ions such as Cr^{3+}, Fe^{3+} and Al^{3+} over other metal ions (Table **1.3**). In

***Table 1.3**: A few sensors for trivalent metal ions developed based on naphthalimide unit.*

M^{3+}	Sensor	M^{3+}	Sensor	M^{3+}	Sensor	M^{3+}	Sensor
Cr^{3+}	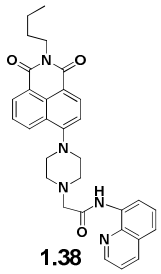 **1.38** Ref. 104	Fe^{3+}	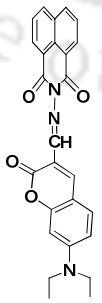 **1.39** Ref. 105	Cr^{3+} Fe^{3+} Al^{3+}	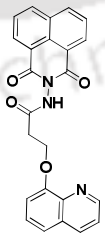 **1.40** Ref. 106	Cr^{3+} Fe^{3+}	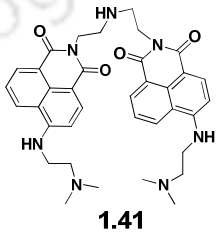 **1.41** Ref. 107

case of sensor **1.39,** it can specifically recognizes Fe^{3+} over other monovalent, divalent and trivalent metal ions through changing the conformation of naphthalimide moiety.[104-107]

Heavy metal ions and first row transition-metal ions usually play important roles in various biological systems or have toxic impacts on the environment. In particular, cadmium and mercury ions are considered to be very dangerous environmental pollutants by bio-accumulating through the food chain when they are ingested or inhaled by human

***Table 1.4**: A few naphthalimide based sensors for cadmium and mercury ion.*

M^{2+}	Sensor		
Cd^{2+}	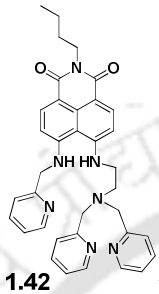 **1.42** Ref. 108	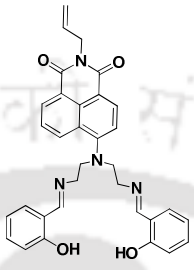 **1.43** Ref. 109	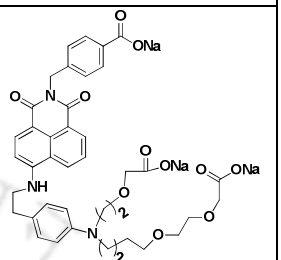 **1.44** Ref. 110
Hg^{2+}	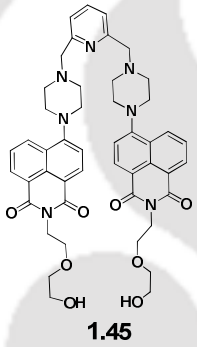 **1.45** Ref. 111	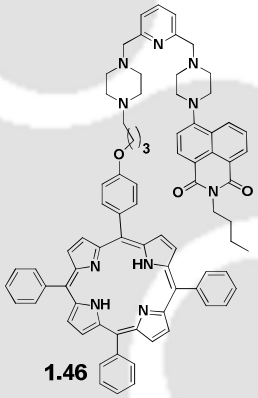 **1.46** Ref. 112	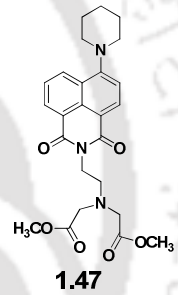 **1.47** Ref. 113

beings. Due to issues of environmental health hazard, a large numbers of chemo sensors for detection of cadmium and mercury have been reported till date. A few naphthalimide based ratiometric and highly fluorescence sensors for cadmium (II) and mercury (II) ions are shown in Table **1.4**.[108-113]

Thiourea based naphthalimide derivative **1.48** was used for detection of mercury (II) ions. Addition of mercury (II) ion to a solution of **1.48** causes quenching of fluorescence; quenching occurs through photo electron transfer mechanism present in a chemically transformed species. Mercury (II) ion facilitates desulfurization cum cyclization to form a phenyl imidazole derivative **1.49** (Scheme **1.3**). The chemical transformation generates a species which has the aniline part at a closer proximity than the parent compound, thus facilitates photo electron transfer in this case much efficiently. The receptor is highly selective in detecting mercury (II) ion in presence of other divalent metal ions. In order to improve practical applicability of such sensors in aqueous environment, gold-nanoparticle

are also used to immobilize naphthalimide receptor to generate characteristic optical signals.[114]

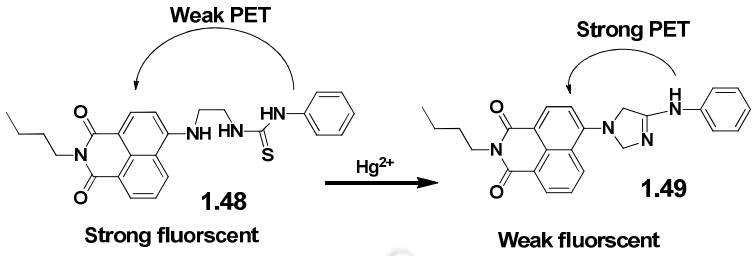

Scheme 1.3

Crown effect of cyclic ethers tethered to naphthalimide leading to molecules such as 15-crown-5 (**1.50a**) and 18-crown-6 (**1.51b**) receptor for Na^+ and K^+ ions were reported. This class of molecules are highly soluble in water act as OFF-ON, dual fluorescent probes for

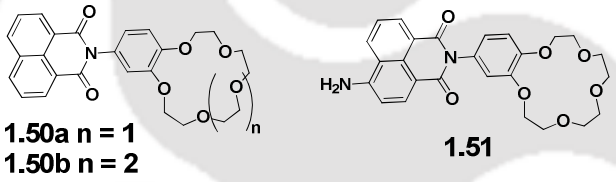

alkali metal ions. Depending upon the size of cations **1.50a** selectively binds Na^+ over K^+, whether **1.50b** displays higher sensitivity to K^+ relative to Na^+ ions.[115] Introduction of amine group at 4 position of **1.50a,** receptor **1.51** show specific binding towards Ba^{2+} ions.[116]

1.5 Coordination chemistry/polymers with cyclic imides and related compounds:

Cyclic imides derivatives containing different functional groups having suitable binding sites have been used to synthesize different metal complexes with diverse structures. Such ligands are extensively used in ion detections and are discussed partially in earlier section. Imides can be deprotonated to form metal complexes in which N-M bond prevails. In another class of reactions they may be used as precursors to result in amide or carboxylate ligands through ring opening reactions. This class of compounds are useful for synthesis of coordination polymers.[117] N-substituted cyclic imide derivatives are often used to construct highly organized structures with different metal ions. These organized structures are formed especially from 1,8-naphthalimide or naphthalenediimide derivatives through a

large range of bonding forces like classic M-donor atom bonds, to strong halogen or hydrogen bonds to much weaker forces such as weak hydrogen bonds and π···π stacking of small aromatics leading to various supramolecular architectures. Naphthalimide derivatives have been utilized as building blocks in metal based supramolecular architectures due to their π-deficient nature and ability to be readily functionalized. This nature has been exploited giving rise to systems in which extension of the structures occur through π-stacked interactions giving rise to new structures with new material properties. This type of work has largely been pioneered by Reger and co-workers over last decade, where they functionalized 1,8-naphthalimide moiety with various functional groups such as carboxylates, pyrazoles and other coordinating groups at the imide nitrogen site.[118] These functionalities have been used to construct various MOFs by reacting with transition metal ions as well as group 1 and group 2 metal ions and studied their structural aspects.

1,8-naphthalimide group incorporated into a bis(pyrazolyl)methane ligand system (**1.52-1.53**) are useful in the formation of silver complexes. In these complexes depending on the compositions and substituents, different supramolecular structures formed through π···π stacking interactions were observed.

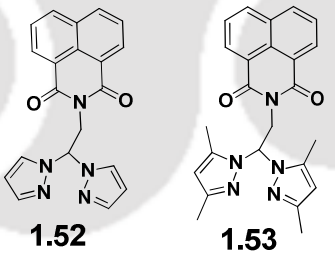

1.52 **1.53**

These examples provides viable means for studying interplay of weak interactions that contribute to the organization of the basic building blocks into higher dimensionality architectures.[119]

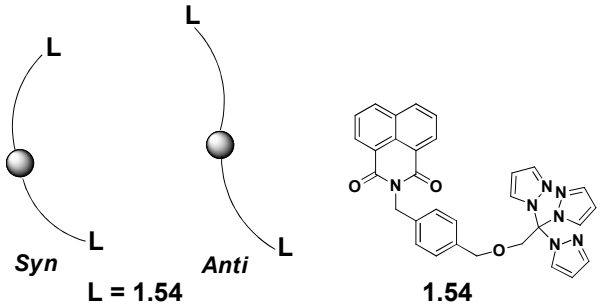

Scheme 1.04

Hetero-bifunctional ligand, **1.54** forms *syn* and *anti* conformations (Scheme **1.04**) by complexing with copper (II), iron (II) and cadmium (II) metal ions. Strong π···π stacking of the 1,8-naphthalimide functional groups dominates noncovalent structures of these four complexes.[120]

Naphthalimide containing aliphatic carboxylic acids (**1.55-1.56)** formed dimeric copper (II) complexes in the presence of either pyridine or 4,4´-bipyridine having dimeric cores of paddlewheel type structure. Strong π-stacking interactions of 1,8-naphthalimide groups organize these structures into sheets and 3D structures.[121]

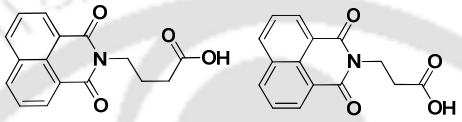

1.55 **1.56**

Trifunctional ligand, **1.57** contains a carboxylate donor group, a homochiral center which are derived from L-alanine and a strong π-stacking, 1,8-naphthalimide synthon. This ligand has been used to form copper (II) complexes in which packing patterns are guided by strong π···π stacking interactions. Such interactions lead to the formation of homochiral, helical, 3D supramolecular metal-organic framework. These complexes show conventional paramagnetic properties of copper (II) complexes in temperature range 20 K to 300 K. Possibility of intermolecular magnetic couplings below 20 K was suggested.[122] A tetrameric copper (II) metallacycle, $[Cu_4(\mathbf{1.58})_8(py)(MeOH)]$ was formed from L-aspargine containing naphthalimide, **1.58** that shows optical activity**.** The methanol ligand

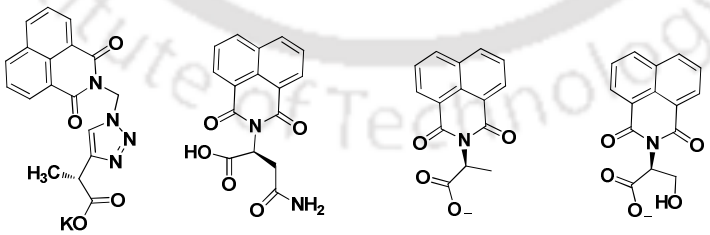

1.57 **1.58** **1.59** **1.60**

in this complex is located in a chiral pocket. This molecule can be replaced by exposing it to racemic ethyl-lactate vapour to form enantioselective optical isomer $[Cu_4(\mathbf{1.58})_8(py)((S)\text{-ethyl-lactate})]$. This change can occur in a single-crystal to single crystal transformation.[123] Chiral amino acids tethered naphthalimide ligands of L-alanine and L-serine (**1.59-1.60**) were found to form homochiral metal-organic frameworks of

group 1 and group 2 metal ions.[124] Ligand **1.59** forms tetrameric zinc (II) $[Zn_4(\mathbf{1.59})_6(OH)_2(MeOH)_4]\cdot 3(CH_2Cl_2)\cdot 2(MeOH)$ whereas a dimeric cadmium (II) complex ($[Cd_2(\mathbf{1.59})_4(DMF)_3(MeOH)]$ was formed on reaction with cadmium ions. Strong π-stacking 1,8-naphthalimide organize tetramers into a 3D architecture that contains linked, homochiral helical chains. Same ligand formed a dimeric cadmium complex with a 2D sheet structure. Both these complexes show luminescent properties in solid state.[125]

A series of enantiopure metal complexes of calcium (II) and strontium (II) with optically active ligands **1.59** and **1.60** were reported. In these complexes π-stacking interactions between 1,8-naphthalimide rings link adjacent rod like units of secondary building blocks into two and three-dimensional structures.[126] Interestingly, group 1 and group 2 metal ions bound to the carbonyl oxygen atoms of naphthalimide unit contribute to formation of complex structures. In all such cases, strong π···π interactions dominates in constructions of supramolecular architechture.

Zaworotko *et al*. reported imide ligand formed by condensation of nicotinic acid trimellitic anhydride **1.61**. This ligand generates a series of isostructural porous metal-organic complexes when coordinated to cobalt (II), nickel (II), copper (II), and cadmium (II) ions. These isostructural metal-organic materials were found to exhibit a porous structure having square channels. They are capable to efficiently store hydrogen gas.[127] Another phthalimide derivative of benzene-1,3-dicarboxylic acid **1.62** forms two supramolecular isomers with $[Cu_2(\mathbf{1.62})_4]$. Distinctions in their structures are very prominent; although in both cases paddlewheel dimeric copper carboxylate units are reflected as repeat units, but the final patterns in one case is Kagomé lattice and in other is NbO net topology.[128] Formation of these supramolecular isomers are guided by solvents used during synthesis.

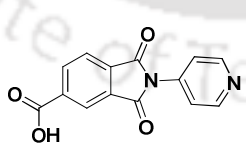

1.61

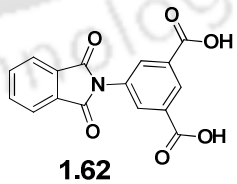

1.62

Su *et al* have reported a series of manganese (II), cadmium (II), and cobalt (II) complexes with semi-rigid ligands **1.63-1.66.** Characteristic feature of these ligands is that they have two relatively flexible pyridyl arms at two ends of diimides. Thus various conformations across imide are possible depending on the orientation of the pyridyl groups. These ligands generate discrete zero-dimensional to polymeric three-dimensional coordination

polymers though self assemblies. In solid state the packing patterns of these coordination polymers are guided by hydrogen bonds and π-interactions. Some of these coordination polymers are used as photoactive materials.[129]

A series of complexes of mercury (II), cadmium (II), zinc (II) and cobalt (II) with ligand **1.65**, were synthesized. Due to flexibility of the ligand, they adopt different conformations

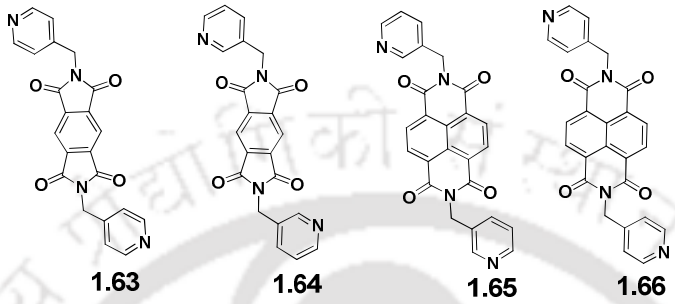

to generate discrete zero-dimensional to polymeric two-dimensional coordination structures. These structures are further stabilized by hydrogen bonds and π···π interactions in the crystal lattice. Different coordination assemblies such as metallacycle, herrringbone network, grid network and 1D chain formed by different metal salts with **1.66** are shown in the Scheme **1.5**. Synergistic effects of metal ions and anions in self-assemblies formation were observed in these polymers, thus conformation of the assemblies are tuned with the aid of ditopic ligands.[130]

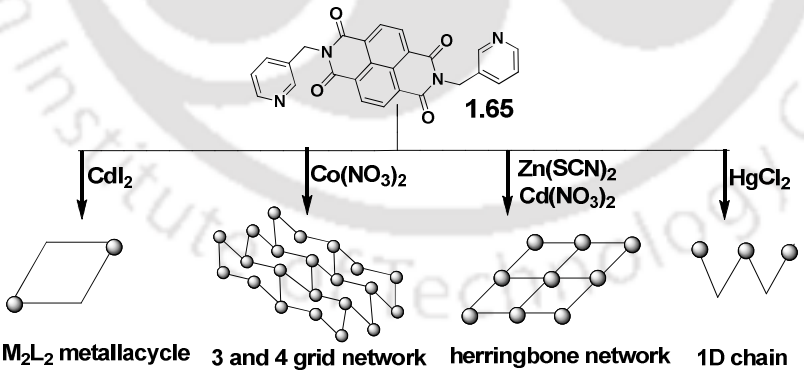

Scheme 1.5

On the other hand, ligand **1.66** forms one dimensional coordination polymer through different reactions involving the C-H activation, C-Cl bond cleavage, C-C bond coupling, and pyridyl N-methylation of ligand occur.[131] Ligand, **1.66** react with manganese trifluoro-acetate dihydrate and sodium thiocyanate under solvothermal conditions results in formation of one-dimensional coordination polymer namely,

$\{[Mn(NCS)_4(\mathbf{1.67})]\cdot 2.5H_2O\}_n$. This coordination polymer comprises of in situ generated new ligand (**1.67**) via a metal/ligand in situ reaction (Scheme **1.6**).

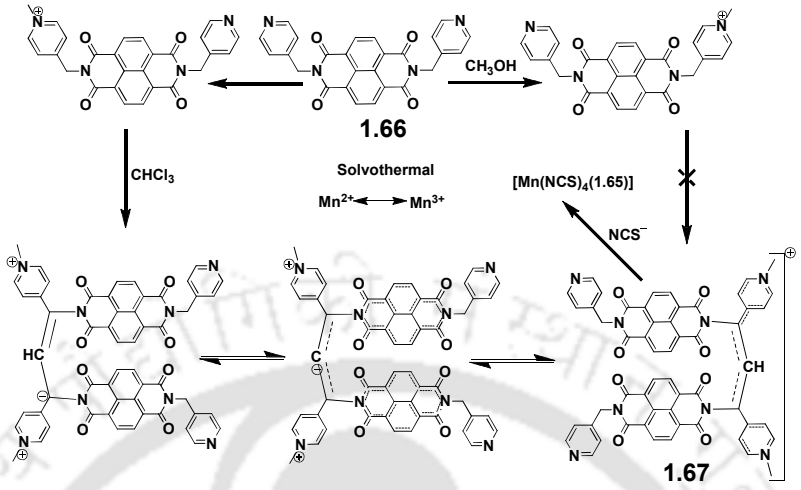

***Scheme 1.6**: Formation of **1.67** from reaction of **1.66** with manganese (II) ions.*

Several mononuclear and dinuclear copper complexes with ligands **1.68**-**1.71** have interesting packing features.[132] In these complexes weak interactions such as π···π, anion···π, solvent···π and C=O···π interactions give rise to extended structures.

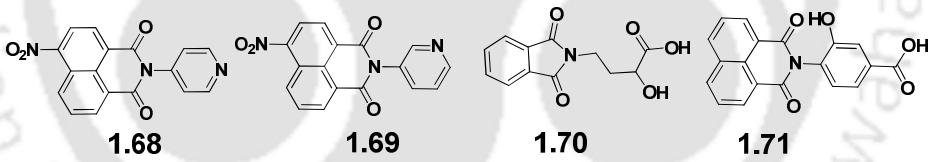

Trifunctional ligands **1.70** and **1.71** containing hydroxy group, carboxylic acid group show interesting supramolecular assemblies on formation of metal complexes. Flexible nature of ligand helps **1.70** to form coordination polymer by reacting with manganese (II) or zinc (II) salts. In case of the manganese coordination polymer competition between self assembling versus aquation at the metal ion site while forming assemblies, results in inclusion of neutral metal complexes as guest in assemblies of chains of coordination polymer. On the hand, introducing the hydroxy group on a rigid aromatic unit away such as skeleton of **1.71**, form mononuclear metal complex rather than a coordination polymer.[133]

1.6 Biological probe as DNA binding and photo cleavage:

Imides are planar and have scope to either intercalate between helical coil of DNA or stacks between the folds of the DNA coil. 1,8-Naphthalimide derivatives thus have been used for DNA binding, anticancer and also used as cellular imaging agents,. Generally being π···π deficient aromatic system[134] they bind to DNA[135] by insertion between the base pairs of double helix.[136] They exhibit good antitumor[137-138] activity, because their intercalation causes base pairs to separate vertically, thereby distorting sugar phosphate backbone and ability to change degree of rotation between successive base pairs.[139] Introducing nitro or amine group at 3 or 4 position of a naphthalimide ring, not only makes the molecule to act as a targeting agent for biomolecules,[140-141] but also affects significantly the electronic properties. As a consequence of such interactions chemical, photochemical and spectroscopic properties of DNA-bound to a naphthalimide changes. On the other hand, bromo derivative 1,8-Naphthalimides having bromine atom at 3 and 4 positions of the ring have been proposed as good candidates for photo-chemotherapeutic inhibition of enveloped viruses in blood and in blood products.[142-143] Moreover, 1,8-naphthalimides are powerful photo-reagents which can induce lesions in DNA molecules and as such possess the ability to kill cells when photoactivate.[144] Thus it is possible that binding mode of naphthalimide may depend on the DNA sequence.

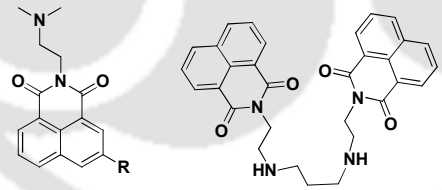

1.72a R = NH_2
1.72b R = NO_2

1.73

1,8-Naphthalimide derivatives as a DNA binding agent was initially developed by Brana and co-workers.[145] Two leading naphthalimide derivatives amonafide, **1.72a** and mitonafide, **1.72b** was tested for clinical trials. Compound **1.72a** was found to stabilize double stranded DNA against heat denaturation.[146-147] Bis-naphthimides such as **1.73** have been developed for enhancement of DNA binding and antitumour activity.[148-149] These compounds acts as a bis-intercalator and binds to DNA along the major groves and found to minimize the toxic side effect to healthy cells.[150-151] Gunnlaugsson *et al*. developed a series of bis-naphthalimides linked by the Troger's base (TB) moiety for DNA targeting.[152-154] These molecules are soluble in water that favour electrostatic interactions

with the negatively charged phosphate backbone of DNA. Photophysical measurements showed that they bind to DNA with similar affinity and display dual mode of binding with one naphthalimide ring intercalated between DNA base pairs while the second one is groove-bound.

Introduction of chiral amino acids into naphthalimide moieties (**1.74-1.76**) that overcome low aqueous solubility and achieve enhanced cellular uptake. Naphthalimide derivatives having derived chiral side chain at the imide position such as leucine,[155] L-lysine,[156] and α-amino acid derived naphthalimide[157] have been reported to show DNA intercalating and photocleaving properties.

Imperiali *et al.* have given a explicit elucidation on biomolecular interactions of 4-*N,N'*-dimethylamino-1,8-naphthalimide.[158-159] Recently solvatochromic chiral amino acid based fluorophore (**1.77**) that can detect dynamic protein-protein interactions through fluorescence resonance electron transfer process in water medium.[160]

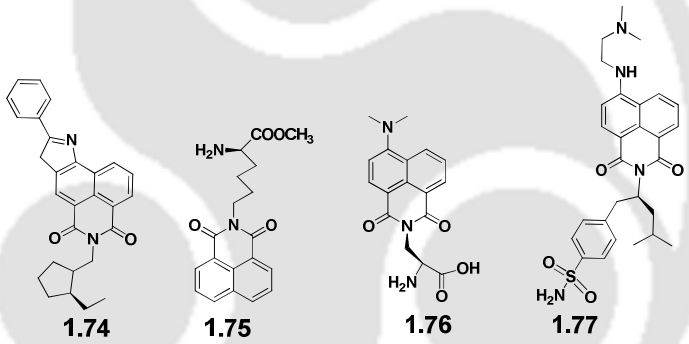

Imidazole based naphthalimides **1.78-1.79** show cyctotoxic activity against human colon carcinoma cell and they have higher affinity towards DNA due to additional heterocyclic ring attached to the naphthalimide unit. Such heterocyles have better stacking interactions as compared to parent naphthalimide derivative.[161] Anchoring pyridine through flexible connector at imide site of 1,8-naphthalimide such as in molecule **1.80** makes such molecules conducive for binding with DNA.[162-163]

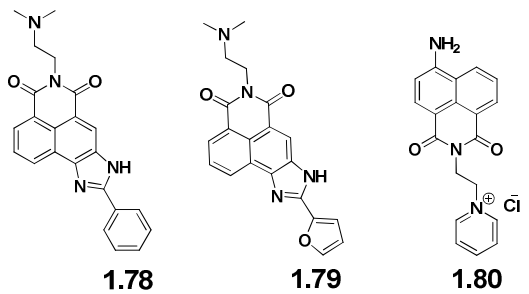

Cationic side chain interacts with phosphate backbone of DNA or with guanine.[164] Spectroscopic titrations show that side chain gets bound to DNA and remains in the major groove.

Naphthalimide based transition metal complexes are found to be chemotherapeutic agents for cancer.[165-167] Platinum complexes such as **1.81-1.82** overcome cellular resistance to cis-platin, which is a common problem encountered in cis-platin based chemotherapeutic complexes.[168] These complexes also show enhanced DNA binding affinity and cytotoxicity.[169]

Cobalt (II) complexes based naphthalimide derivatives **1.83** are found to induce DNA cleavage. They exhibit high cytotoxicity against HeLa cervical cancer cells upon UV-irradiation.[170] Several ruthenium (II)-naphthalimide complexes are identified as potential

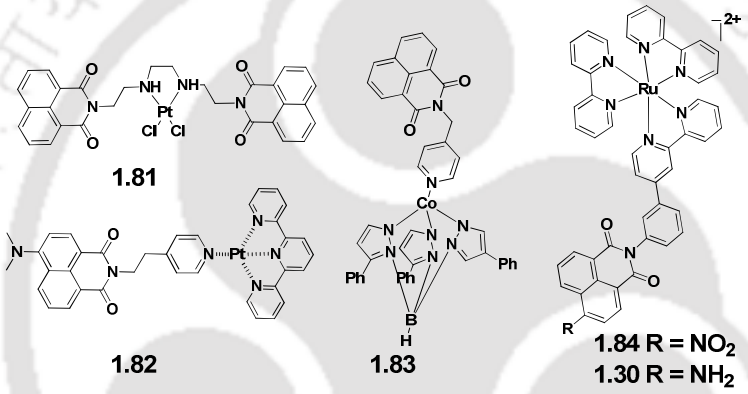

DNA binders as well as photocleaving agents. Complexes **1.84** and **1.30** show hypochromism and a red shift in absorption spectra in the presence of DNA.[171]

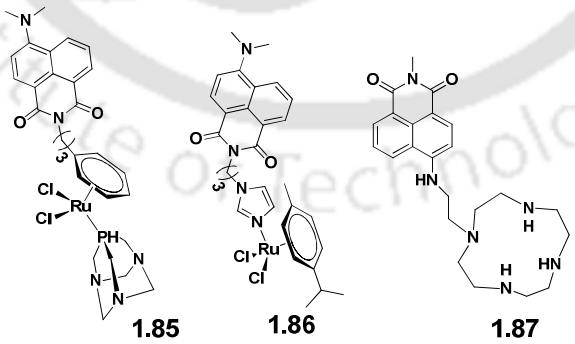

Ruthenium (II) arene complexes **1.85-1.86** which have naphthalimide derivative as additional part of ligand get intercalated by DNA.[172] Intercalation of naphthalimide unit within DNA and binding of ruthenium (II) arene unit with proteins enhance anticancer selectivity. Metal complexes of naphthalimide-cyclam conjugates show in-vitro antitumor

activities.[173] Zinc (II) complex **1.87** is a potential antiproliferative agent found to be active in cancer cell lines.

1.7 Scope of the present work:

From the above discussions it is clear that supramolecular assemblies of naphthalimides are guided not only by substituent present, but also on solvent and ions interacting with naphthalimides. More importantly pi-stacking interactions help the self-assembling properties to make definite impact on molecular and ion recognition. Stacking interactions make different types of assemblies contributing to their properties. It may be noted that π-interactions in a simple arene substituent may occur in different ways and two major structural features are identified as end···face (**1.88a**) and edge···face C-H···π (arene) (**1.88b**) interactions; and lateral off-set (**1.88c**) and face···face (**1.88d**) as shown below.[174]

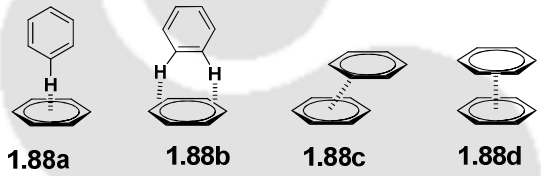

Such π-stacking interactions are of the magnitude of interaction energy in the range of 0.5 kcal/mol to 2.46 kcal/mol and valid at a distance 3.3-4.8Å.[175-176] We have shown in the beginning of this chapter some arrangements of naphthalimides to show π-stacking interactions. However, a pure naphthalimide derivative can have show π-stacking interactions and may result in interesting packing patterns. Besides all these several organic π-ligands such as 1,10-phenanthroline, 2,2'-bipyridine has ability to show stacking effect in metal complexes. Thus it would be interesting to develop selective synthetic methods to form multinuclear metal complexes guided by combing such effects. In this regard the naphthalene or benzene dicarboxylic acids which can be easily derived from their corresponding anhydride coupled with chelating nitrogen aromatic ligand would be of interest to generate selective synthetic methodologies.

The dipolar natures of cyclic imides make them versatile for supramolecular host-guest chemistry. They are useful materials for anion and cation sensing as well as for molecular recognition. Metal-organic frameworks have been recognized as photoluminescent material and useful materials for selective gas adsorption. Self assemblies leading to supramolecular architectures for guest binding of aromatic guest molecules widens their

applications. These derivatives are thus useful for bottom up approach to make assemblies for molecular recognitions. Although a vast literature on cyclic imide derivatives exists, yet ease of fictionalization makes large scope to study host-guest chemistry of functionalized imide derivatives. Presence of optical or electrochemical signalling unit makes avenues for development of naphthalimide based molecular devices such as molecular switch and molecular machines.

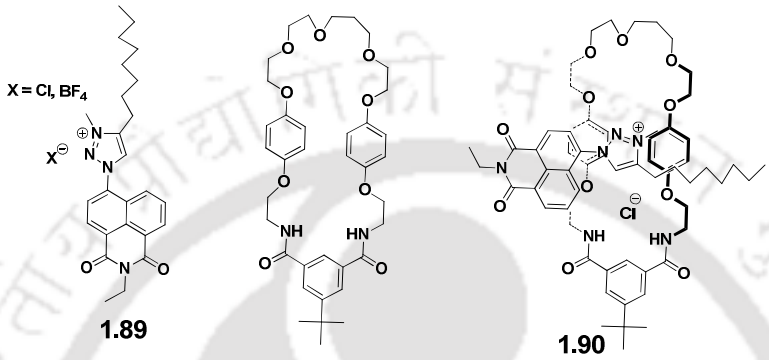

Scheme 1.7

For example anion-templated rotaxane structure **1.90**, incorporating naphthalimide triazolium motif, **1.89** (Scheme **1.7**) exhibit selective, uni-directional, anion-induced shuttling. Ability of a naphthalimide triazolium threading component are shown to form interpenetrated assemblies with counter-anion-dependent co-conformations.[177]

Operational mechanism another naphthalimide based molecular machine is based on time-resolved vibrational spectroscopy in which departure and arrival of a macrocycles were independently observed (Scheme 1**.8**) through formation of radical anion of naphthalimide moiety.[178]

Generally imides form different supramolecular motifs of hydrogen bonds or other weak interactions in solid state. Among all interactions $\pi\cdots\pi$ stacking interactions are more dominant which guides the overall supramolecular structure with different material properties such as fluorescence, optical and magnetic properties. Thus there is definite scope to design suitable to stack in different manners influencing physical properties. Based on the versatility and diverse possibilities to bind ions and guest molecules we have chosen to perform a systematic study on naphthalimide and phthalimide derivatives by attaching heterocyclic components. Heterocyclic components such as imidazole, pyridine and carboxylic acid unit are connected to naphthalimide or diimide to understand their

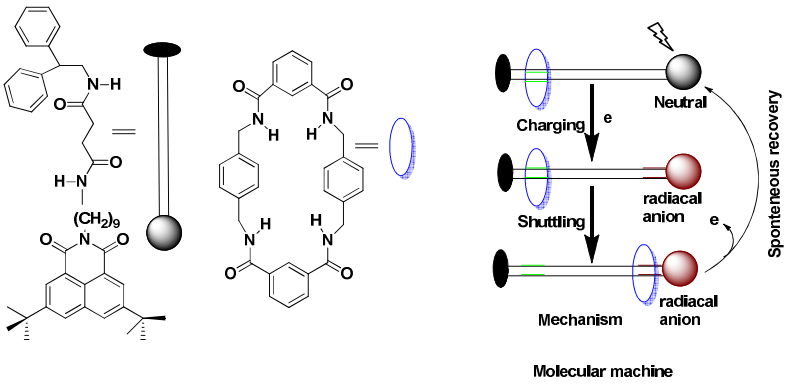

Scheme 1.8

assemblies and substrate binding. Use of a flexible or rigid group for construction of coordination complexes has been explored. Such complexes would have many degrees of freedom and few conformational restraints, which can give various topologies. It would be also of interest to functionalize naphthalimide with flexible nitrogen containing group and design to synthesize coordination polymers for various utilities. Thus, focus of the thesis work is to design and synthesize (a) stable fluorogenic molecules for fluorescence and optical detection of ionic analyte and understand their solid state supramolecular assemblies, (b) Design of supramolecular host containing both basic and acidic functionality to bind different guest and influence of solvent molecules, (c) To synthesize and characterize transition metal complexes, metallacycle and coordination polymer exhibiting interesting magnetic and fluorescence properties.

1.8 References:

1. Chen, X.; Guo, Y.; Tan, L.; Yang, G.; Li, Y.; Zhang, G.; Liu, Z.; Xu W.; Zhang, D. *J. Mater. Chem. C* **2013**, *1*, 1087-1092.
2. Kolosov, D.; Adamovich, V.; Djurovich, P.; Thompson, M. E.; Adachi, C. *J. Am. Chem. Soc.* **2002**, *124*, 9945-9954.
3. Tu,G.; Mei,C.; Zhou, Q.; Cheng,Y.; Geng, Y.; Wang, L.; Ma, D.; Jing, X.; Wang, F. *Adv. Funct. Mater.* **2006**, *16*, 101-106.
4. Jin, R.-F.; Tang, S.-S.; Sun, W.-D. *Tetrahedron* **2014**, *70*, 47-53.
5. Grabchev, I.; Moneva, I.; Bojinov, V.; Guittonneau, S. *J. Mater. Chem.* **2000**, *10*, 1291-1296.
6. Grabchev, I.; Chovelon, J.-M. *Polym. Adv.Technol*. **2003**, *14*, 601-608.
7. Pogozhev, D. V.; Bezdek, M. T.; Schauer, P. A.; Berlinguette, C. P. *Inorg. Chem*. **2013**, *52*, 3001-3006.

8. Qian, X.; Zhu, K.; Chen, K. *Dyes Pigm.* **1989**, *11*, 13-20.

9. Song, Z.; Zhan, H.; Zhou, Y. *Angew. Chem. Int. Ed*. **2010**, *49*, 8444-8448.

10. Chinapang, P.; Ruangpornvisuti, V.; Sukwattanasinitt, M.; Rashatasakhon, P. *Dyes Pigm.* **2015**, *112*, 236-238.

11. Bamesberger, A.; Schwartz, C.; Song, Q.; Han, W.; Wang, Z.; Cao, H. *New J. Chem*. **2014**, *38*, 884-888.

12. Gravchev, I.; Konstantinova, T. *Dyes Pigm.* **1997**, *33*, 197-203.

13. Bojinov, V.; Grabchev, I. *Dyes Pigm.* **2003**, *59*, 277-283.

14. Nawimanage, R. R.; Prasai, B.; Hettiarachchi, S. U.; McCarley, R. L. *Anal. Chem.* **2014**, *86*, 12266-12271.

15. Pischel, U.; Uzunova, V. D.; Remon, P.; Nau, W. M. *Chem. Commun.* **2010**, *46*, 2635-2637.

16. Yin, H.; Xu, Y.; Qian, X.; Li Y.; Liu, J. *Bioorg. Med. Chem. Lett.* **2007**, *17*, 2166-2170.

17. Wang, K.-R.; Wang, Y.-Q.; Yan, X.-H.; Chen, H.; Ma, G.; Zhang, P.-Z.; Li, J.-M.; Li, X.-L.; Zhang, J.-C. *Bioorg. Med. Chem. Lett.* **2012,** *22*, 937-941.

18. Reger, D. L.; Debreczeni, A.; Reinecke, B.; Rassolov, V.; Smith, M. D. *Inorg. Chem.* **2009**, *48*, 8911-8924.

19. Janiak, C. *J. Chem. Soc. Dalton Trans.* **2000**, 3885-3896.

20. Chin, D. L.; Zerkowshi, J. A.; Macdonald, G. M.; Whitesides, G. M. *Organised Molecular Assemblies in solid state* (Ed. J. K. Whitesell), John willey & Sons, Newyork, **1999**.

21. Desiraju, G. R. **2003**, *In Crystal Design: Structure and Functions* (Perspectives in Supramolecular Chemistry) (England: John Wiley).

22. Claessens, C. G.; Stoddart, J. F. *J. Phys. Org. Chem*. **1997**, *10*, 254-272.

23. Desiraju, G. R., Steiner, T. *The weak hydrogen bond*, IUCr Monographs on Crystallography 9, Oxford University Press, Oxford **1999**.

24. Jeffrey, G. A. *An Introduction to Hydrogen Bonding*, Oxford University Press, London, **1997**.

25. Dahl, T. *Acta Chem. Scand*. **1994**, *48*, 95-106.

26. Meyer, E. A.; Castellano, R. K.; Deiderich, F. *Angew. Chem. Int. Ed.* **2003**, *42*, 1210-1250.

27. Mooibroek, T. J.; Gamez, P. *Inorg. Chim. Acta* **2007**, *360*, 381-404.

28. Fyfe, M. C. T.; Stoddart, J. F. *Acc. Chem. Res*. **1997**, *30*, 393-401.

29. Pantos, G. D.; Pengo, P.; Sanders, J. K. M. *Angew. Chem. Int. Ed.* **2007**, *46*, 194-197.

30. Pantos, G. D.; Wietor, J.-L.; Sanders, J. K. M. *Angew. Chem. Int. Ed.* **2007**, *46*, 2238-2240.

31. Blacker, A. J.; Jazwinski, J.; Lehn, J.-M.; Cesario, M.; Guilhem, J.; Pascard, C. *Tetrahedron Lett.* **1987**, *28*, 6057-6060.

32. Iwanaga, T.; Nakamoto, R.; Yasutake, M.; Shinmyozu, T. *Angew. Chem., Int. Ed.* **2006**, *45*, 3643-3647.

33. Esteban-Gomez, D.; Fabbrizzi, L.; Licchelli, M.; Sacchi, D.; *J. Mater. Chem.* **2005**, *15*, 2670-2675.

34. Johnstone, K.; Bampos, N.; Gunter, M. J.; Sanders, J. K. M. *Chem. Commun*. **2003**, 1396-1397.

35. Kaiser, G.; Jarrosson, T.; Otto, S.; Ng, Y.-F.; Sanders, J. K. M. *Angew. Chem., Int. Ed.* **2004**, *43*, 1959-1962.

36. Pascu, S. I.; Jarrosson, T.; Naumann, C.; Otto, S.; Kaiser, G.; Sanders, J. K. M. *New J. Chem.* **2005**, *29*, 80-89.

37. Vignon, S. A.; Jarrosson, T.; Iijima, T.; Tseng, H.-R.; Sanders, J. K. M. Stoddart, J. F. *J. Am. Chem. Soc.* **2004**, *126*, 9884-9885.

38. Barooah, N.; Sarma, R. J.; Baruah, J. B. *Cryst. Growth Des.* **2003**, *3*, 639-641.

39. Harvey, R. G. *Polycyclic Aromatic Hydrocarbons*; John Wiley &Sons: New York, 1997.

40. Barooah, N.; Sarma, R. J.; Baruah, J. B. *CrystEngComm* **2006**, *8*, 608-615.

41. Barooah, N.; Baruah, J. B. *J. Mol. Struct.* **2008**, *872*, 205-211.

42. Deans, R.; Niemz, A.; Breinlinger, E. C.; Rotello, V. M. *J. Am. Chem. Soc*. **1997**, *119*, 10863-10864.

43. Tamanini, E.; Ponnuswamy, N.; Pantosx, G. D.; Sanders, J. K. M. *Faraday Discuss.* **2010**, *145*, 205-218.

44. Rasberry, R. D.; Smith, M. D.; Shimizu, K. D. *Org. Lett.* **2008**, *10*, 2889-2892.

45. Rathore, R.; Lindeman, S. V.; Kochi, J. K. *J. Am. Chem. Soc.* **1997**, *119*, 9393-9404.

46. Colquhoun, H. M.; Williams, D. J.; Zhu, Z. *J. Am. Chem. Soc.* **2002**, *124*, 13346-13347.

47. Iwanaga, T.; Nakamoto, R.; Yasutake, M.; Takemura, H.; Sako, K.; Shinmyozu, T. *Angew. Chem., Int. Ed*. **2006**, *45*, 3643-3647.

48. Bandela, A. K.; Chinta, J. P.; Hinge, V. K.; Dikundwar, A. G.; Row, T. N. G.; Rao, C. P. *J. Org. Chem.* **2011**, *76*, 1742-1750.

49. Singh, D.; Bhattacharyya, P. K.; Baruah, J. B. *Cryst. Growth Des*. **2010**, *10*, 348-356.

50. Carvalho, C. P.; Ferreira, R.; Silva, J. P. D.; Pischel, U. *Supramol. Chem.* **2013**, *25*, 92-100.

51. Bianchi, E.; BowmanJames, K.; Gracıa-Espana, E. *Supramolecular Chemistry of Anions*; Eds. Wiley-VCH: New York, **1997**.

52. Gale, P. A. *Coord. Chem. Rev.* **2003**, *240*, 1-226.

53. Martınez-Manez, R.; Sancenon, F. *Chem. Rev.* **2003**, 103, 4419-4476.

54. Beer, P. D.; Gale, P. A. *Angew. Chem., Int. Ed.* **2001**, *40*, 486-516.

55. Kluciar, M.; Ferreira, R.; Castro de, B.; Pischel, U. *J. Org. Chem.* **2008**, *73*, 6079-6085

56. Pfeffer, F. M.; Seter, M.; Lewcenko N.; Barnett, N. W. *Tetrahedron Lett*. **2006**, *47*, 5241-5242.

57. Tian, H.; Liu, B. *J. Mater. Chem*. **2005**, *15*, 3026-3033.

58. Liu, B.; Tian, H. *Chem. Lett.* **2005**, *34*, 686-687.

59. Veale, E. B.; Gunnlaugsson, T. Eur. Pat. Appl. EP09159892.0, **2009.**

60. Pischel, U.; Remon, P.; Ferreira, R. *J. Phys. Chem. C* **2009**, *113*, 5805-5811.

61. Bamesberger, A.; Schwartz, C.; Song, Q.; Han, W.; Wang, Z.; Cao, H. *New J. Chem*. **2014**, *38*,

884-888.

62. de Silva, A. P.; Rupasinghe, R. A. D. D. *J. Chem. Soc. Chem.Commun*.**1985**, 1669-1670.
63. de Silva, A. P.; de Silva, S. A. *J. Chem. Soc. Chem. Commun*. **1986**, 1709-1710.
64. Gomez, D. E.; Fabbrizzi, L.; Liechelli, M. *J. Org. Chem*. **2005**, *70*, 5717-5720.
65. Zhang, J. F.; Lim, C. S.; Bhuniya, S.; Cho, B. R. Kim, J. S. *Org. Lett.* **2011**, *13*, 1190-8893.
66. Gunnlaugsson, T.; Kruger, P. E.; Jenson, P.; Pfeffer, F. M.; Hussey, G. M. *Tetrahedron Lett.* **2003**, *44*, 8909-8913.
67. Wang, J.; Yang, L.; Hou, C.; Cao, H. *Org. Biomol. Chem.* **2012**, ***10***, 6271-6274.
68. Gunnlaugsson, T.; Kruger, P. E.; Lee, T. C.; Parkesh, R.; Pfeffer, F. M.; Hussey, G. M. *Tetrahedron Lett.* **2003**, *44*, 6575-6578.
69. Pfeffer, F. M.; Buschgens, A. M.; Barnett, N. W.; Gunnlaugsson, T.; Kruger, P. E. *Tetrahedron Lett.* **2005**, *46*, 6579-6584.
70. Bao, X.-P.; Wang, L.; Li, Wu,L.; Li, Z.-Y. *Supramol. Chem.* **2008**, *20*, 467-472.
71. Esteban-Gomez, D.; Fabbrizzi L.; Liechelli, M. *J. Org. Chem*. **2005**, *70*, 5717-5720.
72. Misra, A.; Shahid, M.; Dwivedi, P.; Srivastava, P.; Ali, R.; Razi, S. S. *ARKIVOC* **2013**, *2*, 133-145.
73. McDonald, K. P.; Ramabhadran, R. O.; Lee, S.; Raghavachari, K.; Flood, A. H. *Org. Lett.* **2011**, *13*, 6260-6263.
74. Yoon, J.; Qian, X.; Kim, J. S.; Lee, C.; Han, S. J.; Kim, N. H.; Kim, S.; Xu, Z. *Tetrahedron Lett.* **2007**, *48*, 9151-9154.
75. Zhao, L. Y.; Wang, G. K.; Chen, J. H.; Zhang, L. M.; Liu, B.; Zhang, J. F.; Zhao, Q. H.; Zhou, Y. *J. Fluorine Chem.* **2014**, *158*, 53-59.
76. Gorteau, V.; Bollot, G.; Mareda, J.; Matile, S. *Org. Biomol. Chem.* **2007**, *5*, 3000-3012
77. Samit Guha, Flynt S. Goodson, Lucas J. Corson, and Sourav Saha, *J. Am. Chem. Soc.* **2012**, *134*, 13679-13691.
78. Guha, S.; Saha, S. *J. Am. Chem. Soc.* **2010**, *132*, 17675-17677.
79. Elmes, R. B. P.; Gunnlaugsson, T. *Tetrahedron Letters* **2010**, *51,* 4082-4087.
80. Guha, S.; Goodson, F. S.; Clark, R. J.; Saha, S. *CrystEngComm.* **2012**, *14*, 1213-1215.
81. Davis, A. P.; Sheppard, D. N.; Smith, B. D. *Chem. Soc. Rev*. **2007**, *36*, 348-357.
82. Davis, J. T.; Okunola, O.; Quesada, R. *Chem. Soc. Rev*. **2010**, *39*, 3843-3862.
83. Gokel, G. W.; Barkey, N. *New J. Chem*. **2009**, *33*, 947-963.
84. Ashcroft, F. M. *Ion Channels and Disease*; Academic Press: San Diego, **2000**.
85. Mascal, M.; Armstrong, A.; Bartberger, M. D. *J. Am. Chem. Soc*. **2002**, *124*, 6274-6276.
86. Perez-Velasco, A.; Gorteau, V.; Matile, S. *Angew. Chem. Int. Ed*. **2008**, *47*, 921-923.
87. Gorteau, V.; Bollot, G.; Mareda, J.; Perez-Velasco, A.; Matile, S. *J. Am. Chem. Soc*. **2006**, *128*, 14788-14789.
88. Gorteau, V.; Bollot, G.; Mareda, J.; Perez-Velasco, A.; Matile, S. *J. Am. Chem. Soc*. **2006**, *128*,

14788-14789.

89. Veale, E. B.; Kitchen, J. A.; Gunnlaugsson, T. *Supramol. Chem.* **2013**, *25*, 101-108.
90. Hanaoka, K.; Muramatsu,Y.; Urano,Y.; Terai, T.; Nagano, T. *Chem. Eur. J.* **2010**, *16*, 568-572.
91. Mahato, P.; Saha, S.; Suresh, E.; Liddo, R. D.; Parnigotto, P. P.; Conconi, M. T.; Kesharwani, M. K.; Ganguly, B.; Das, A. *Inorg. Chem.* **2012**, *51*, 1769-1777.
92. Park, H. J.; Sung, N. K.; Kim, S. R.; Ahn, S. H.; Yoon, U. C.; Cho, D. W.; Mariano, P. S. *Bull. Korean Chem. Soc*. **2013**, *34*, 3681-3689.
93. Xu, Z.; Xiao, Y.; Qian, X.; Cui, J.; Cui, D. *Org. Lett.* **2005**, *7*, 889-892.
94. Huang, J.; Xu, Y.; Qian, X. Org. *Biomol. Chem.* **2009**, *7*, 1299-1303.
95. Xu, Z.; Qian, X.; Cui, J. *Org. Lett*. **2005**, *7*, 3029-3032.
96. Liu, Z.; Zhang, C.; Wang, X.; He, W.; Guo, Z. *Org. Lett*. **2012**, *17*, 4378-4381.
97. Jisha, V. S.; Thomas, A. J.; Ramaiah, D. *J. Org. Chem*. **2009**, *74*, 6667-6673.
98. Xu, Z.; Qian, X.; Cui, J.; Zhang, R. *Tetrahedron* **2006,** *62*, 10117-10122
99. Wang, J.; Xiao, Y.; Zhang, Z.; Qian, X.; Yang, Y.; Xu, Q. *J. Mater. Chem*. **2005**, *15*, 2836-2839.
100. Xu, Z.; Baek, K.-H.; Kim, H. N.; Cui, J.; Qian, X.; Spring, D. R.; Shin, I.; Yoon, J. *J. Am. Chem. Soc.* **2010**, *132*, 601-610.
101. Gunnlaugsson, T.; Lee, T. C.; Parkesh, R. *Org. Biomol. Chem*. **2003**, *1*, 3265-3267.
102. Parkesh, R.; Lee, T. C.; Gunnlaugsson, T. *Org. Biomol. Chem*. **2007**, *5*, 310-317.
103. Ast, S.; Rutledge, P. J.; Todd, M. H. *Eur. J. Inorg. Chem*. **2012**, 5611-5615.
104. Chen, Z.; Wang, L.; Zou, G.; Teng, M.; Yu, J. *Chin. J. Chem*. **2012**, *30*, 2844-2848.
105. Li, Z.; Zhou, Y.; Yin, K.; Yu, Z.; Li, Y.; Ren, J. *Dyes Pigm.* **2014**, *105*, 7-11.
106. Goswami, S.; Aich, K.; Das, A. K.; Manna, A.; Das, S. *RSC Adv.* **2013**, *3*, 2412-2416
107. Staneva, D.; Grabchev, I.; Soumillion, J.-P.; Bojinov, V. *J. Photochem. Photobiol. A*: *Chem.* **2007,** *189*, 192-197.
108. Lu, C.; Xu, Z.; Cui, J.; Zhang, R.; Qian, X. *J. Org. Chem*. **2007**, *72*, 3554-3557.
109. Wang, W.; Wen, Q.; Zhang, Y.; Fei, X.; Li, Y.; Yang, Q.; Xu, X. *Dalton Trans.* **2013**, *42*, 1827-1833.
110. Liu, D.; Qia, J.; Liu, X.; Cui, Z.; Chang, H.; Chen, J.; Yang, G. *Sens. Actuators B* **2014**, *204*, 655-658.
111. Guo, X.; Qian, X.; Jia, L. *J. Am. Chem. Soc*. **2004**, *126*, 2272-2273.
112. Li, C.-Y.; Zhang, X.-B.; Qiao, L.; Zhao, Y.; He, C.-M.; Huan, S.-Y.; Lu, L.-M.; Jian, L.-X.; Shen, G.-L.; Yu, R.-Q. *Anal. Chem*. **2009**, *81*, 9993-10001.
113. Dai, H.; Yan, Y.; Guo, Y.; Fan, L.; Che, Z.; Xu, H. *Chem. Eur. J*. **2012**, *18*, 11188-11191.
114. Leng, B.; Zou, L.; Jiang, J.; Tian, H. *Sens. Actuators B*, **2009**, *140*, 162-169.
115. Panchenko, P. A.; Fedorov, Y. V.; Perevalov, V. P.; Jonusauskas, G.; Fedorova, O. A. *J. Phys. Chem. A* **2010**, *114*, 4118-4122.

116. Nandhikonda, P.; Begaye, M. P.; Heagy, M. D. *Tetrahedron Lett.* **2009**, *50*, 2459-2461.

117. Baruah, A. M.; Karmakar, A.; Baruah, J. B. *Polyhedron* **2007**, *26*, 4479-4488.

118. Reger, D. L.; Leitner, A.; Smith, M. D.; *Inorg. Chem.* **2013**, *52*, 10041-10051.

119. Reger, D. L.; Semeniuc, R. F.; Elgin, J. D.; Rassolov, V.; Smith, M. D. *Cryst. Growth Des.* **2006**, *6*, 2758-2768.

120. Reger, D. L.; Sirianni, E.; Horger, J. J.; Smith, M. D. *Cryst. Growth Des*. **2010**, *10*, 386-393.

121. Reger, D. L.; Debreczeni, A.; Reinecke, B.; Rassolov, V.; Smith, M. D. *Inorg. Chem.* **2009**, *48*, 8911-8924.

122. Reger, D. L.; Horger, J. J.; Smith, M. D.; Long, G. J. *Chem. Commun.* **2009**, 6219-6221.

123. Reger, D. L.; Horger, J. J.; Smith, M. D. *Chem. Commun.* **2011**, *47*, 2805-2807.

124. Reger, D. L.; Leitner, A. P.; Smith, M. D. *Inorg. Chem*. **2012**, *51*, 10071-10073.

125. Reger, D. L.; Debreczeni, A.; Smith, M. D. *Eur. J. Inorg. Chem.* **2012**, 712-719.

126. Reger, D. L.; Leitner, A.; Pellechia, P. J.; Smith, M. D. *Inorg. Chem.* **2014**, *53*, 9932-9945.

127. Perman, A. J.; Dubois, K.; Nouar, F.; Zoccali, S.; Woltas, L.; Eddaoudi, M.; Larsen, R. W.; Zaworotko, M. J. *Cryst. Growth Des.* **2009**, *9*, 5021-5023.

128. Zhang, Z.; Wojtas, L.; Zaworotko, M. J. *Cryst. Growth Des.* **2011**, *11*, 1441-1445.

129. Li, G-B.; Liu, J-M.; Cai, Y-P.; Su, C-Y. *Cryst. Growth Des.* **2011**, *11*, 2763-2772.

130. Deng, H.-Y.; He, J.-R.; Pan, M.; Li, L.; Su, C.-Y. *Cryst.EngComm*. **2009**, *11*, 909-917.

131. Li, G.-B.; Liu, J.-M.; Yu, Z.-Q.; Wang, W.; Su, C.-Y. *Inorg. Chem.* **2009**, *48*, 8659-8661.

132. Kitchen, J. A.; Martinho, P. N.; Morgan, G. G.; Gunnlaugsson, T. *Dalton Trans.* **2014**, *43*, 6468-6479.

133. Singh, D.; Baruah, J. B. *Inorg. Chim. Acta*. **2013**, *394*, 703-709.

134. Brana, M. F.; Cacho, M.; Gradillas, A.; Pascual-Teresa, B.; Ramos, A. *Curr. Pharm. Des*. **2001**, *7*, 1745-1780.

135. Zee-Cheng, R. K. Y.; Cheng, C. C. *J. Med. Chem.* **1985**, *28*, 1216-1222.

136. Pasternack, R.F.; Gibbs, E.J.; Villafranca, J. J. *Biochemistry* **1983**, *22*, 2406-2414.

137. Kamal, A.; Reddy, B. S. N.; Reddy, G. S. K.; Ramesh, G. *Bioorg. Med. Chem. Lett.* **2002**, *12*, 1933-1935.

138. Li, Z.; Yang, Qi.; Qian, X. *Bioorg. Med. Chem.* **2005**, *13*, 4864-4870.

139. Chen, Z.; Liang, X.; Zhang, H.-Y.; Xie, H.; Liu, J.-W.; Xu, Y.-F.; Zhu, W.-P.; Wang, Y.; Wang, X.; Tan, S.-Y.; Kuang, D.; Qian, X.-H. *J. Med. Chem.* **2010**, *53*, 2589-2600

140. Stevenson, K. A.; Yen, S. F.; Yang, N. C.; Boykin D. W.; Wilson, W. D. *J. Med. Chem.* **1984**, *27*, 1677-1682.

141. Nitiss, J. L.; Zhou, J.; Rose, A.; Hsiung, Y.; Gale K. C.; Osheroff, N. *Biochemistry* **1998**, *37*, 3078-3085.

142. Chanh,T. C.; Lewis, D. E.; Allan, J. S.; Sogandares-Bernal, F.; Judy, M. M.; Utecht, R. E.; Matthews, J. L. *AIDS Res. Hum. Retroviruses* **1993**, *9*, 891-896.

143. Chanh, T. C.; Archer, B. J.; Utecht, R. E.; Lewis, D. E.; Judy M. M.; Matthews, J. L. *BioMed. Chem. Lett.* **1993**, *3*, 555-556.

144. Bailly, C.; Brana M.; Waring, M. J. *Eur. J. Biochem*. **1996**, 240,195-208.

145. Brana, M. F.; Berlanga, J. M. C.; Roldan, C. M.; DE patent 2, 318, 136 (**1973**), C.A. 86; 106, 236 (**1977**).

146. Brana, M. F.; Castellano, J. M.; Roldan, C. M.; Santos, A.; Vazquez, D.; Jimenez, A. *Cancer Chemother. Pharmacol.* **1980**, 4, 61.

147. Brana, M. F.; Sanz, A. M.; Castellano, J. M.; Roldan, C. M.; Roldan, C. *Eur. J. Med. Chem*. **1981**, *16*, 207-212.

148. Brana, M. F.; Castellano, J. M.; Moran, M. *Anti-CancerDrug Des*. **1993**, *8*, 257-268. 149. Brana, M. F.; Castellano, J. M.; Perron, D.; Maher, C.; Conlon, D.; Bousquet, P. F.; George, J.; Qian, X. D.; Robinson, S. P. *J. Med. Chem.* **1997**, *40*, 449-454.

150. McRipley, R. J.; Burns-Horwitz, P. E.; Czerniak, P. M.; Diamond, R. J.; Diamond, M. A.; Miller, J. L. D.; Page, R. J.; Dexter, D. L.; Chen, S.-F.; Sun, J.-H.; Behrens, C. H.; Seitz S. P.; Gross, J. L. *Cancer Res*. **1994**, *54*, 159-164.

151. Lin, P. K. T.; Pavlov, V. A. *Bioorg. Med. Chem. Lett.* **2000**, *10*, 1609-1612.

152. Veale, E. B.; Frimannsson, D. O.; Lawler M.; Gunnlaugsson, T. *Org. Lett.* **2009**, *11*, 4040-4043.

153. Veale, E. B.; Gunnlaugsson, T. *J. Org. Chem.* **2010**, *75*, 5513-5525.

154. Banerjee, S.; Ban, S. B.; Bright, S. A.; Smith, J. A.; Burgeat, J.; Martinez-Calvo, M.; Williams, D. C.; Kelly, J. M.; Gunnlaugsson, T. *J. Org. Chem.* 2014, 79, 9272-9283.

155. Wu, A.; Xu Y.; Qian, X. *Bioorg. Med. Chem.* **2009**, 17, 592-599.

156. Saito, I.; Takayama, M.; Sugiyama, H.; Nakatani, K.; Tsuchida, A.; Yamamoto, M. *J. Am. Chem. Soc*. **1995**, *117*, 6406-6407.

157. Yang, Q.; Yang, P.; Qian X.; Tong, L. *Bioorg. Med. Chem. Lett*. **2008**, *18*, 6210-6213.

158. Loving, G.; Imperiali, B.; *J. Am. Chem. Soc*. **2008**, *130*, 13630-13638.

159. Loving, G.; Imperiali, B. *Bioconjugate Chem.* **2009**, *20*, 2133-2141.

160. Socher, E.; Imperiali, B. *ChemBioChem*. **2013**, *14*, 53-57.

161. Li, F.; Cui, J.; Guo, L.; Qian, X.; Ren, W.; Wang K.; Liu, F. *Bioorg. Med. Chem*. **2007**, *15*, 5114-5121.

162. Banerjee, S.; Kitchen, J. A.; Gunnlaugsson T.; Kelly, J. M. *Org. Biomol. Chem*. 2**012**, *10*, 3033-3043.

163. Banerjee, S.; Kitchen, J. A.; Gunnlaugsson, T.; Kelly, J. M. *Org. Biomol. Chem.* **2013**, *11*, 5642-5655.

164. Thiagarajan, V.; Rajendran, A.; Satake, H.; Nishizawa S.; Teramae, N. *ChemBioChem*. **2010**, *11*, 94-100.

165. Reedijk, J. *Eur. J. Inorg. Chem*. **2009**, 1303-1312.

166. Farrer, N. J.; Salassa, L.; Sadler, P. J. *Dalton Trans.* **2009**, 10690-10701.

167. Elmes, R. B. P.; Erby, M.; Bright, S. A.; Williams, D. C.; Gunnlaugsson, T. *Chem. Commun.* **2012**, *48*, 2588-2590.

168. Perez, J. M.; Lopez-Solera, I.; Montero, E. I.; Brana, M. F.; Alonso, C.; Robinson, S. P.; Navarro-Ranninger, C. *J. Med. Chem.* **1999**, *42*, 5482-5486.

169. Banerjee, S.; Kitchen, J. A.; Bright, S. A.; Williams, D. C.; Kelly J. M.; Gunnlaugsson, T. *Chem. Commun*. **2013**, *49*, 8522-8524.

170. Roy, S.; Saha, S.; Majumdar, R.; Dighe, R. R.; Chakravarty, A. R. *Inorg. Chem*. **2009**, *48*, 9501-9509.

171. Ryan, G. J.; Quinn S.; Gunnlaugsson, T. *Inorg. Chem.* **2007**, *47*, 401-403.

172. Kilpin, K. J.; Clavel, C. M.; Edafe, F.; Dyson, P. J. *Organometallics* **2012**, *31*, 7031-7039.

173. Tan, S.; Han, K.; Li, Q.; Tong, L.; Yang, Y.; Chen, Z.; Xie, H.; Ding, J.; Qian, X.; Xu, Y. *Eur. J. Med. Chem.* **2014**, *85*, 207-214.

174. Hunter, C. A.; Sanders, J. K. M. *J. Am. Chem. Soc*. **1990**, 112, 5525-5534.

175. Lee, E. C.; Kim, D.; Jurecka, P.; Tarakeshwar, P.; Hobza, P.; Kim,K. S. *J. Phys. Chem. A* **2007**, *111*, 3446-3457.

176. Smith, T.; Slipchenko, L. V.; Gordon, M. S. *J. Phys. Chem. A* **2008**, *112*, 5286-5294.

177. Spence, G. T.; Pitak, M. B.; Beer, P. D. *Chem. Eur. J.* **2012**, *18*, 7100-7108.

178. Panman, M. R.; Bodis, P.; Shaw, D. J.; Bakker, B. H.; Newton, A. C.; Kay, E. R.; Brouwer, A. M.; Buma, W. J.; Leigh, D. A.; Woutersen, S. *Science* **2010**, *328*, 1255-1258.

CHAPTER 2

Metal carboxylate complexes formed through hydrolysis of cyclic anhydrides and imide

Selective guest binding properties of metallacycles are well known.[1] Metallacycles serve as precursor for nanochemistry[2-4] and some of them finds applications in magnetochemistry,[5-7] in cancer research[8] and in various organometallic transformations.[10] Transition metal based metallacycles have generated special interest as certain metallacycles behave as single molecular magnets.[9] Polydentate ligands having appropriate geometry are generally used to prepare metallacycles. Thus geometry favoring stabilization of cyclic compound of a polydentate ligand is a prime factor to successfully synthesize metallacycles. As polydentate ligand has multiple possibilities to form metal complexes which include formation of coordination polymer. A rigid ligand having two dicarboxylate groups at appropriate positions, such as 1,2 or 1,3 position of a benzene and 1,8 positions of naphthalene ring are suitable for the formation of metallacycles. However formation of cyclic or linear complexes or coordination polymers competes in such reactions. In order to have a control on synthetic pathways control on the reactivity of dicarboxylic acids required. Changes on the reaction condition such as by using dilution method may be helpful in the synthesis of macrocyclic ligands. Cyclic anhydrides such as phthalic anhydride or naphthalic anhydride are less reactive towards metal ions than parent dicarboxylic acids. They are also precursor for dicarboxylic acids hence we have studied their reactivity towards various metal salts under hydrolytic conditions. The results of such reactions are described in this chapter.

Moreover aromatic cyclic anhydrides are also precursor of cyclic aromatic imides. Hydrolysis reactions of cyclic anhydrides undergo ring opening of anhydrides leading to interesting supramolecular synthons[11] and polymers.[12-14] An oxynucleophile (eg. water or alcohol) opened ring of phthalic anhydride through either to form a dicarboxylic acid or a mono-ester of dicarboxylic acid.[15]

It is important to note that isolation and characterization of intermediate metal complexes formed during hydrolysis of esters would provide understanding on active sites of metallohydrolases.[16-18] On the other hand copper complexes are widely used in the hydrolysis reactions of esters,[19-24] anhydrides,[25] lactones[26] and imides.[27-28] Enantioselective hydrolysis of ester of α-amino acids are catalyzed by copper complexes.[29] So there is a

challenge to make model intermediate copper complexes to study such catalytic reactions.[30] Earlier it was shown that copper (II) ions cause methanolysis of amides[31-32] in which tetrahedral copper (II) complex exist as intermediate species.[33]

It was earlier shown that in copper complex catalyzed ester hydrolysis, coordination of copper ion facilitates intramolecular nucleophilic attack on the C=O group and subsequently it assists departure of leaving group.[34] Catalytic hydrolysis of phosphate esters by copper ions find use in DNA cleavage reactions,[35-38] phosphodiesterases[39] and in artificial nucleases.[40-42] There are also examples of Cu-catalyzed hydrolysis operating simultaneously with molecular recognition.[43] Copper containing metallosurfactants are useful in ester hydrolysis[44-46] while some copper complexes can hydrolyze polyester-based hydrogels.[47] Cyclic imides are important due to their abilities to generate amino acids through ring opening reactions.[48-49] Ring opening reactions of polyimide polymer results in the formation of metal ion containing polymers[50] as well as nano-dimensional materials.[51]

With the above points in mind we also discuss hydrolytic abilities of copper (II) and cadmium (II) salts towards aromatic 2-(3-(1H-imidazol-1-yl)propyl)isoindoline-1,3-dione (**2.3**). While studying such reactions we isolate an intermediate ester containg copper (II) carboxylate complexes and their solvent mediated solid state transformation either to coodination polymers or metallacycles.

2.1 Polynuclear metallacycles of cobalt, nickel and zinc:

It is observed that reaction of naphthalic anhydride with metal ions such as cobalt (II), nickel (II), zinc (II) ions are highly dependent on chelating π-aromatic N-hetreocycle such as 1,10-phenanthroline (*phn*) and 2,2'-bipyridine (*bpy*) (Scheme **2.1**). These reactions are highly specific to the ancillary ligands and product specificities are guided by reaction conditions.

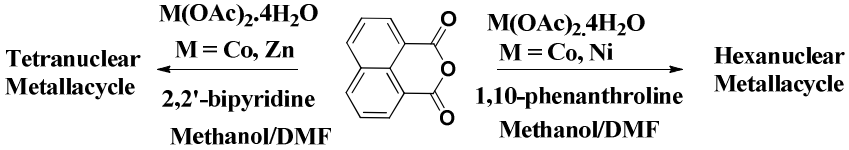

Scheme 2.1

Reaction of 1,8-naphthalic anhydride with cobalt (II) acetate and *bpy* exclusively yielded tetranuclear metallacycle $[Co_4(bpy)_4(naphDA)_4(H_2O)_4]\cdot 12H_2O$ (**2.1a**). Whereas, a similar reaction using *phn* resulted in the formation of a hexanuclear metallacycle $[Co_6(phn)_6(naphDA)_6(H_2O)_{12}]\cdot 6H_2O$ (**2.1b**) (where naphDA = naphthalene-1,8-dicarboxylic acid). These complexes were characterized from their elemental analysis, magnetic properties and X-ray crystal structures. The crystals structures of these two metallacycles were determined which are shown in Figure **2.1a** and **2.1b**. Metallacycle **2.1a** has cobalt (II) ions in hexacoordinate environments. Two coordination sites of each cobalt (II) ion are occupied by a *bpy* ligand, other three sites are occupied by one chelating carboxylate and one monodentate carboxylate and sixth site is occupied by a water molecule. Each naphDA acts as a bridging ligand by anchoring two cobalt (II) ions. Metallacycle **2.1b** also has hexacoordinate environments around the cobalt (II) ions. The coordination environments around each cobalt (II) ion is constituted by two water molecules, one *phn* and two oxygen atoms of two carboxylate groups from two independent naphDA. Structures of the two metallacycles are shown in Figure **2.1.**

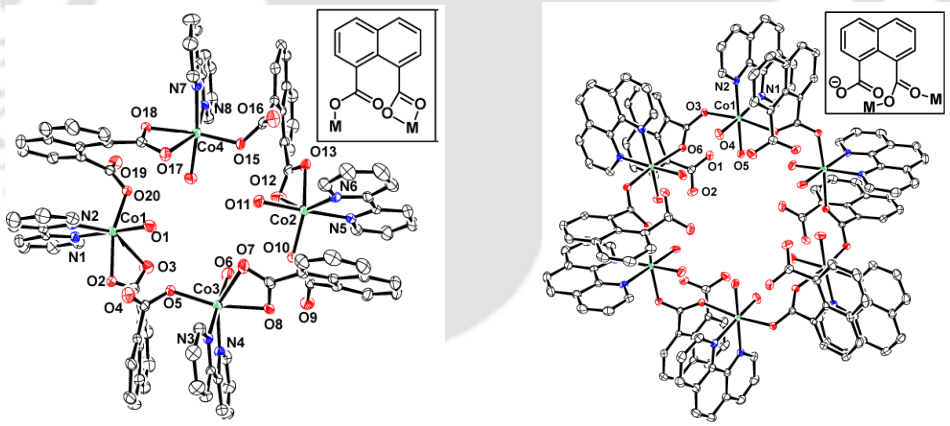

(a) (b)

Figure 2.1*: ORTEP view of metallacycle (a)* ***2.1a*** *and (b)* ***2.1b*** *(30% thermal ellipsoid probability, hydrogen atoms and water molecules are omitted for clarity); (inset are the different binding mode of dicarboxylate in the respective metallacycles.*

Bridging modes of carboxylates are different in both the metallacycles (which are shown in Figure **2.1**). Tetranuclear metallacycle **2.1a** use both the carboxylate anions of the naphthalene dicarboxylate to construct bridges connecting metal ions independently but in the case of hexanuclear metallacycle **2.1b** one carboxylate group remains uncoordinated and other carboxylate serves as a bridging ligand through two oxygen atoms. The chelating mode of carboxylate in **2.1a** is reflected in the carbonyl stretching frequency in

FT-IR spectrum which is observed at 1544 cm^{-1}. The stretching frequency at 1618 cm^{-1} in the FT-IR spectrum of **2.1b** signifies the bridging mode of carboxylate. The powder X-ray diffraction patterns of the two metallacycles **2.1a** and **2.1b** show similarities between the simulated and experimental patterns that confirms single components in the products. PXRD pattern of **2.1a** is shown in Figure **2.2c.**

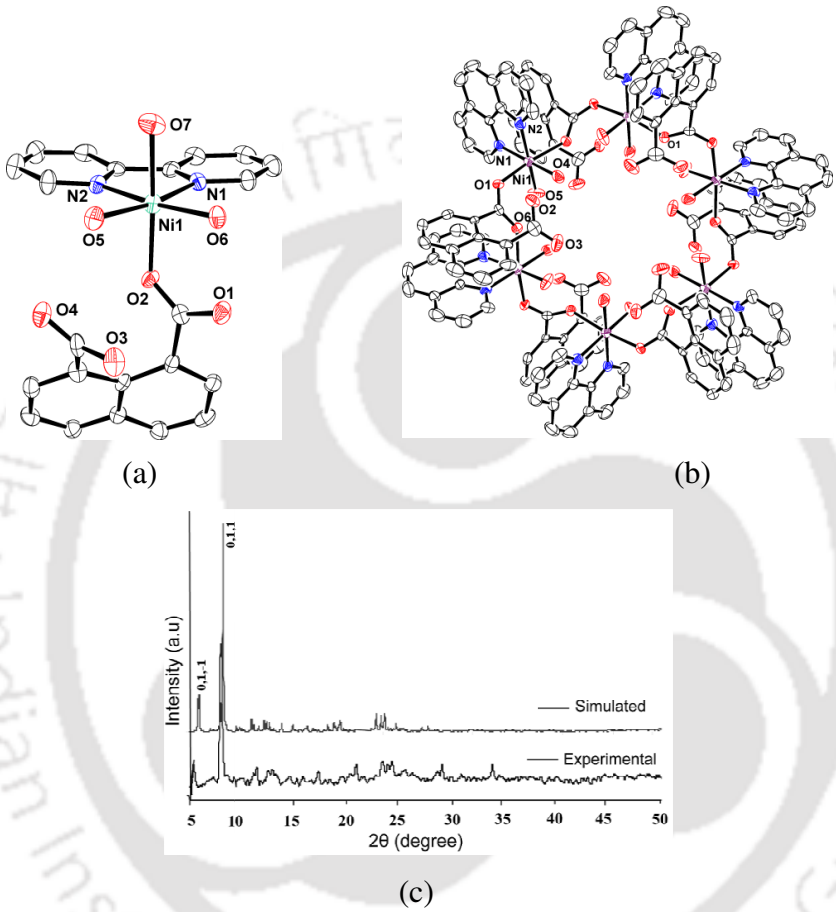

***Figure 2.2**: ORTEP view of (a) Complex **2.1c,** (b) Metallacycle **2.1d** (30% thermal ellipsoid probability, hydrogen atoms and lattice water molecules are omitted for clarity); (c) Comparison of the simulated (top) and the experimental (bottom) PXRD of the metallacycle **2.1a**.*

It may be noted that hydrogen bonds and other weak interactions such as π···π interactions play key role in the construction of supramolecular architechture.[52-56] Comparison of structure of the two cobalt metallacycles show that in case of *phn* their exist a strong π···π interactions between naphthalene ring with *phn* ring. Such interactions between naphthalene rings are less dominant. Ligands *bpy* and *phn* have different numbers of aromatic rings in their skeleton, but have similar bite angles to bind to metal ions; for example, in the case of **2.1a**, angle ∠N1-Co1-N2 is 77.44(18)° whereas in **2.1b** the angle

∠N1-Co1-N2 is 77.98(8)°. Metal-ligand bond parameters of the metallacycle **2.1a** are listed in the Table **2.1**.

***Table 2.1**: Metal-ligand bond parametres of the metallacycle **2.1a**:*

Compd. No.	M-L	d_{M-L}(Å)	∠L-M-L	Angle (°)	∠L-M-L	Angle (°)	∠L-M-L	Angle (°)
2.1a	Co1-O1	2.092(4)	O1-Co1-N2	176.48(18)	N2-Co1-O3	95.49(16)	O18-Co4-O17	59.31(14)
	Co1-O2	2.052(3)	O1-Co1-O3	87.11(15)	N5-Co2-O11	99.41(18)	N3-Co3-N4	77.29(17)
	Co1-O3	2.493(4)	O2-Co1-O3	56.58(14)	N5-Co2-N6	77.89(17)	N3-Co3-O7	153.77(15)
	Co1-O20	1.997(3)	O2-Co1-N2	88.05(14)	N5-Co2-O12	148.92(14)	N3-Co3-O8	95.25(14)
	Co1-N1	2.083(5)	O2-Co1-O1	91.42(14)	N5-Co2-O13	91.41(15)	N4-Co3-O7	94.09(15)
	Co1-N2	2.125(4)	O2-Co1-N1	92.90(15)	N6-Co2-O12	93.90(17)	N4-Co3-O8	83.76(14)
	Co2-O10	1.992(3)	O10-Co2-N5	110.78(15)	O5-Co3-O6	93.39(16)	N7-Co4-O16	102.33(18)
	Co2-O11	2.097(4)	O10-Co2-O13	91.97(15)	O5-Co3-N3	106.95(15)	N7-Co4-O18	89.01(15)
	Co2-O12	2.346(4)	O10-Co2-N6	157.54(15)	O5-Co3-N4	94.24(16)	N7-Co4-N8	77.37(16)
	Co2-O13	2.088(3)	O10-Co2-O12	99.31(14)	O5-Co3-O8	156.74(14)	N7-Co4-O17	147.21(16)
	Co2-N5	2.083(5)	O10-Co2-O11	89.13(14)	O5-Co3-O7	98.29(13)	N8-Co4-O17	92.95(16)
	Co2-N6	2.117(4)	O11-Co2-N6	177.30(18)	O6-Co-N3	101.18(17)		
	Co3-O5	1.996(3)	O11-Co2-O12	88.35(16)	O6-Co3-N4	172.33(16)		
	Co3-O6	2.079(4)	O13-Co2-O11	90.62(14)	O6-Co3-O6	88.92(14)		
	Co3-O7	2.325(4)	O13-Co2-N6	89.31(14)	O6-Co3-O7	84.04(15)		
	Co3-O8	2.127(3)	O13-Co2-O12	58.24(13)	O8-Co3-O7	58.91(13)		
	Co3-N3	2.088(4)	O20-Co1-O1	89.52(15)	O15-Co4-N7	108.48(15)		
	Co3-N4	2.119(4)	O20-Co1-O2	149.42(15)	O15-Co4-O16	90.59(15)		
	Co4-O15	2.006(3)	O20-Co1-N1	117.10(14)	O15-Co4-O18	162.34(14)		
	Co4-O16	2.089(4)	O20-Co1-N2	92.71(15)	O15-Co4-N8	91.95(14)		
	Co4-O17	2.306(4)	O20-Co1-O3	92.97(14)	O15-Co4-O17	103.03(15)		
	Co4-O18	2.131(3)	N1-Co1-O1	99.30(18)	O16-Co4-N8	177.40(16)		
	Co4-N7	2.089(4)	N1-Co1-N2	77.25(18)	O16-Co4-O17	85.94(18)		
	Co4-N8	2.131(4)	N1-Co1-O3	149.12(14)	O18-Co4-N8	89.50(14)		

The numbers of water molecules in the two metallacycles are different and this affects the binding modes of carboxylates significantly. Distances of separation between the two adjacent cobalt (II) ions in complexes **2.1a** and **2.1b** are 5.40 Å and 5.20 Å, respectively. Metal ligand bond parameters of the metallacycles are listed in the Table **2.2**.

Both the metallacycles have lattice water molecules and from the thermogravimetric analyses it is observed that both metallacycles release water molecules below 125 °C on heating. Thermogram of the metallacycle **2.1a** is shown in Figure **2.3a**. In the metallacycle **2.1a** twelve lattice water molecules are lost in the temperature range of 40-80 °C (calcd. and experimental weight losses are 9.5 % and 10.0 % respectively). Loss of four coordinated water and four *bpy* molecules are observed in the temperature range of 180-340 °C (calcd. and experimental losses are 59.9 % and 61.1 %, respectively). It thermochemically degrades in the range of 360-420 °C to form CoO (calcd. 86.1 %, experimental 87.3 %). On the other hand, **2.1b** shows weight loss in the temperature region of 46-460 °C showing formation of CoO as the decomposed product (calcd. 85.7 %, experimental 86.3 %). Formation of CoO in each case is confirmed by independently heating the metallacycles **2.1a** and **2.1b** at 460 °C and recording the IR and powder XRD patterns of the residues obtained after heating (Figure **2.20** in the experimental section). A reaction of cobalt (II) salt with cynnamic acid and *bpy* as ancillary ligand was reported to

form trinuclear metallacycle. This metallacycle also formed CoO as a residue after heating to 650 °C, which was established through thermogravimetric analysis and further confirmed by powder XRD study.[57]

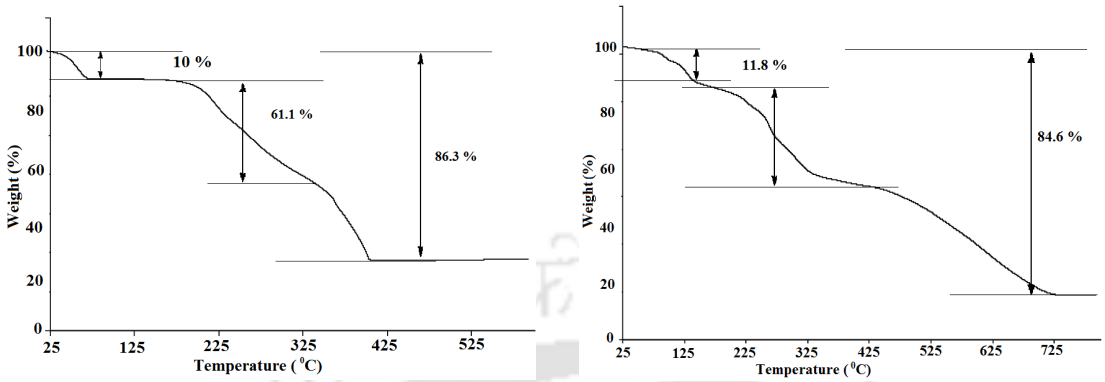

(a) (b)

***Figure 2.3**: Thermogram (heating rate 5 °C/min) of the metallacycle (a) **2.1a** and (b) **2.1d**.*

On the other hand cobalt propionate dinuclear complex containing pyridine N-oxide on heating resulted in the formation of Co_3O_4 as residue after heating it to 575 °C.[58] It is clear that formation of CoO from the metallacycle **2.1a** and **2.1b** is at relatively low temperature than that of the reported cobalt metallacycles.

Similar reaction of 1,8-naphthalic anhydride with nickel (II) acetate in presence of *bpy* was attempted to prepare tetranuclear complex but instead of getting tetranuclear metallacycle we got a mononuclear complex having compositions [Ni(*bpy*)(naphDA)$(H_2O)_3]\cdot H_2O$ (**2.1c**). The hexacoordinate structure of this complex comprises of a monodentate carboxylate and one free carboxylate bearing dicarboxylate ligand and one chelating *bpy* along with three water molecules coordinating to the nickel ion (Figure **2.2**). On the other hand reacting nickel (II) acetate in presence of *phn* and 1,8-naphthalic anhydride, a hexanuclear nickel (II) metallacycle $[Ni_6(phn)_6(naphDA)_6(H_2O)_{12}].20H_2O$ (**2.1d**) was formed which is isostructural with **2.1a** (Figure **2.2a**)**.** In this metallacycle distance between two neighbouring nickel (II) ions is 5.174 Å. Each naphDA bridges two nickel (II) ions by one carboxylate group of the ligand and the other carboxylate remains uncoordinated. The other carboxylate anion contributes to the overall charge of the metallacycle. Each nickel (II) ion has a hexacoordinate environment of which two sites are occupied by two water molecules, two sites by one *phn* ligand and two sites by two oxygen atoms of two different carboxylate. Metal ligand bond parameters of the metallacycle **2.1c** and complex **2.1d** are listed in Table **2.2**. In earlier work it was found that nickel (II) acetate forms mononuclear complex on reaction

with *bpy* in methanol whereas nickel (II) salts with propionic acid and pyridine N-oxide leads to the formation of dinuclear complex.[58,59] The presence of water molecules in the metallacycles are confirmed by thermogravimetric analysis. In thermogravimetric analyses

Table 2.2**: Metal-ligand bond parametres of the metallacycles **2.1b-2.1f.

Compd. No.	M-L	d_{M-L}(Å)	∠L-M-L	Angle (°)	∠L-M-L	Angle (°)	∠L-M-L	Angle (°)
2.1b	Co1-O4	2.070(2)	O3-Co1-N2	90.82(8)	O4-Co1-O5	94.35(11)	N2-Co1-N1	77.82(9)
	Co1-O3	2.0944(18)	O3-Co1-O5	86.28(8)	O4-Co1-N1	166.26(10)	N2-Co1-O6	84.96(8)
	Co1-O5	2.129(2)	O3-Co1-N1	112.63(7)	O4-Co1-O6	90.01(8)	N2-Co1-O5	174.27(10)
	Co1-O6	2.1545(18)	O3-Co1-O6	167.64(8)	O5-Co1-N1	97.52(10)		
	Co1-N2	2.123(2)	O4-Co1-O3	92.11(8)	O5-Co1-O6	81.43(7)		
	Co1-N1	2.144(2)	O4-Co1-N2	90.69(10)	N1-Co1-O6	101.33(8)		
2.1c	Ni1-O2	2.043(6)	O2-Ni1-N2	91.3(3)	O6-Ni1-O7	85.9(2)	N2-Ni1-O6	173.3(3)
	Ni1-O5	2.077(7)	O2-Ni1-N1	93.7(3)	O6-Ni1-O5	95.1(3)	N2-Ni1-O5	90.4(3)
	Ni1-O6	2.070(6)	O2-Ni1-O6	92.6(3)	N1-Ni1-O6	94.0(3)	N2-Ni1-O7	90.8(3)
	Ni1-O7	2.158(7)	O2-Ni1-O5	90.6(3)	N1-Ni1-O5	169.7(3)		
	Ni1-N1	2.067(8)	O2-Ni1-O7	174.1(3)	N1-Ni1-O7	92.1(3)		
	Ni1-N2	2.057(8)	O5-Ni1-O7	83.8(3)	N2-Ni1-N1	80.2(4)		
2.1d	Ni1-O1	2.065(3)	O1-Ni1-N1	90.49(15)	O4-Ni1-N2	167.44(16)	N1-Ni1-O5	175.23(17)
	Ni1-O4	2.034(4)	O1-Ni1-N2	94.74(15)	O4-Ni1-O5	94.18(17)	N1-Ni1-O6	101.09(14)
	Ni1-O5	2.087(4)	O1-Ni1-O5	87.23(14)	O4-Ni1-O6	89.36(15)	N2-Ni1-O6	85.50(15)
	Ni1-O6	2.147(4)	O1-Ni1-O6	168.25(14)	O5-Ni1-O6	81.08(13)		
	Ni1-N1	2.073(4)	O4-Ni1-O1	92.63(15)	N1-Ni1-N2	79.68(19)		
	Ni1-N2	2.079(5)	O4-Ni1-N1	90.11(18)	N2-Ni1-O5	96.32(18)		
2.1e	Zn1-O1	1.979(3)	O1-Zn1-O4	133.20(11)	O3-Zn1-N1	91.41(11)		
	Zn1-O3	2.078(3)	O1-Zn1-O3	92.52(12)	O4-Zn1-N1	168.17(14)		
	Zn1-O4	1.987(3)	O1-Zn1-N2	123.90(12)	O4-Zn1-O3	90.97(11)		
	Zn1-N1	2.146(3)	O1-Zn1-N1	94.28(12)	O4-Zn1-N2	102.63(11)		
	Zn1-N2	2.111(3)	O3-Zn1-N2	91.42(14)	N2-Zn1-N1	76.75(13)		
2.1f	Zn1-O1	1.984(4)	O1-Zn1-O5	126.96(16)	O3-Zn2-O10	94.60(18)	N3-Zn2-O4	91.51(18)
	Zn2-O3	2.064(4)	O1-Zn1-O9	94.57(17)	O3-Zn2-N3	148.2(2)	N3-Zn2-N4	77.6(2)
	Zn2-O4	2.454(5)	O1-Zn1-N1	110.27(16)	O3-Zn2-N4	91.34(17)	N4-Zn2-O4	85.24(18)
	Zn1-O5	2.034(4)	O1-Zn1-N2	95.82(18)	O8-Zn2-O3	106.14(16)		
	Zn2-O8	2.000(4)	O5-Zn1-O9	90.04(16)	O8-Zn2-O4	163.69(15)		
	Zn2-O10	2.097(5)	O5-Zn1-N1	122.08(17)	O8-Zn2-O10	95.2(2)		
	Zn1-O9	2.085(4)	O5-Zn1-N2	87.33(17)	O8-Zn2-N3	104.53(19)		
	Zn1-N1	2.108(4)	O9-Zn1-N1	94.04(17)	O8-Zn2-N4	95.16(19)		
	Zn1-N2	2.137(5)	O9-Zn1-N2	168.66(18)	O10-Zn2-O4	87.4(2)		
	Zn2-N3	2.109(5)	N1-Zn1-N2	78.10(19)	O10-Zn2-N3	90.8(2)		
	Zn2-N4	2.131(5)	O3-Zn2-O4	57.56(15)	O10-Zn2-N4	166.1(2)		

it is observed that the lattice water molecules are lost in the temperature range 70-146°C (calcd. % wt. loss 10.9; experimental % wt. loss 11.8). Twelve coordinated water and six *phn* molecules are lost in the range of 158-470 °C (calcd. wt. loss 44.15 % and experimental wt. loss 43.07 %); whereas, it thermochemically degrades in the temperature range of 475-740 °C to form NiO as the decomposed product (theoretical 86.4 %, experimental 84.6 %). These results suggest that formation of nickel (II) carboxylate complexes is very sensitive to ancillary ligand and reaction conditions.

Reaction of zinc (II) acetate with naphthalic anhydride in presence of *bpy* formed a tetranuclear zinc metallacycle. Structure of metallacycle $[Zn_4(bpy)_4(naphDA)_4(H_2O)_4]\cdot 2H_2O$ (**2.1e**) is shown in Figure **2.4a**. In this metallacycle zinc (II) ions are in five coordinated environment where the two carboxylate ions bind to two metal ions through monodentate fashion.

Zinc (II) ions are five coordinated in metallacycle **2.1e**, and it has very close structural resemblance to the tetranuclear cobalt (II) metallacycle **2.1a**. The basic difference between these two structures arises from the coordination environment of the metal ions. In case of cobalt (II) metallacycle **2.1a**, a hexacoordinate environment is observed whereas in zinc (II) metallacycle, pentacoordinated environment is observed. This difference provides slightly different orientations of carbonyl groups of carboxylate in each case. The distance of uncoordinated carbonyl oxygen atom from metal ion is 2.887 Å which is not suitable to have M-L interaction to call a dative bond. Hence zinc (II) centre is pentacoordinated rather than hexacoodinated in metallacycle **2.1e**. Metal-ligand bond distances and bond angles of the metallacycles are tabulated in Table **2.1** and Table **2.2**. Thermogravimetric analysis of the metallacycle **2.1e** shows that the lattice water molecules and coordinated water molecules are lost in the temperature range 86-140°C (% wt. loss of calcd. is 5.8 and that of experimental is 5.0).

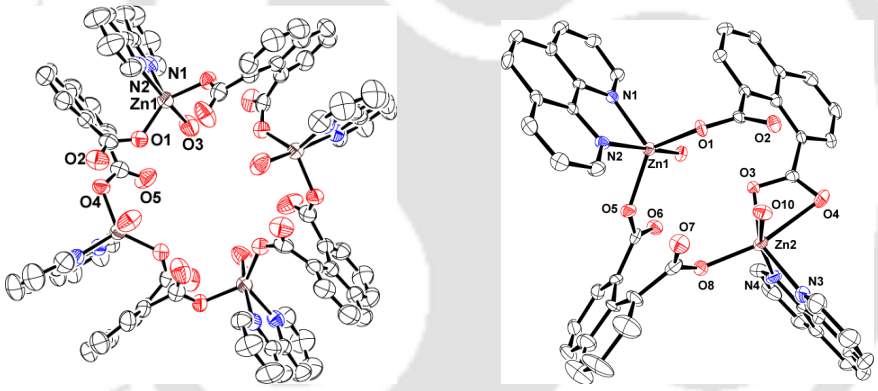

(a) (b)

***Figure 2.4**: ORTEP view of metallacycle (a) **2.1e**, (b) **2.1f** (30 % thermal ellipsoid probability, hydrogen atoms and water molecules are omitted for clarity).*

The reaction of zinc (II) acetate with 1,8-naphthalic anhydride and *phn* may be considered as an exceptionally case among the *phn* containing complexes described above. When zinc (II) acetate was reacted with *phn* a dinuclear metallacycle $[Zn_2(phn)_2(naphDA)_2(H_2O)_2]\cdot H_2O$ (**2.1f**) was formed. The compound is structurally very interesting. In case of complex **2.1e**, Zn ions are in two different coordination environments; it has one hexacordinated zinc (II) and another pentacoordinated zinc (II) ion. The hexacoordinated environment around zinc (II) ion has a chelating carboxylate, a monodentate carboxylate, a *phn* and a water molecule as ligand (Figure **2.4b**). The other zinc (II) ion has a five coordinate environment having two monodentate carboxylate, a *phn* chelate and a water molecule. Different type of environments around two zinc (II) ions

occur due to the puckering of the bridging naphthalate ring in the metallacycle. One of the carbonyl oxygen of bridging carboxylate projects away from the zinc (II) metal ion. This end binds to zinc (II) in a mono-dentate fashion. The metal-ligand bond distances and bond angles of metallacycle **2.1e** are listed in Table **2.2**. The zinc (II) complexes with pentacoordinated geometry in a highly geometrically strained condition were observed in dinuclear complex.[60] Recently, from our group it was shown that depending upon the nature of π-aromatic heterocylces, nuclearity of zinc hydroxyl carboxylate differs. In such examples, ancillary ligand *phn* provided a mononuclear complex and *bpy* resulted in the formation of dinuclear zinc metallacycle.[61]

From the thermogravimetric analysis it is observed that the lattice water molecules and the coordinated water molecules are lost below 90-136 °C in case of **2.1f** (calcd. % wt. loss 5.5 and experimental % wt. loss 6.4).

In an earlier study we showed that the hydrolysis of pyromellitic dianhydride led to dinuclear metallacycles with *phn* whereas use of *bpy* led to mononuclear carboxylate salts.[62-63] Depending on ancillary ligands phthalate forms polymeric or mononuclear complexes,[64] but in such cases tetra or hexanuclear metallacycles were not observed.

In all the metallacycles have π···π interactions between the naphthalene ring and ancillary ligands with different centroid to centroid distance. In case of **2.1a,** this distance is found to be in the range of 3.479-3.711 Å, whether in case of **2.1b, 2.1d** and **2.1e,** this distance are 3.389 Å, 3.368 Å and 3.762 Å respectively. These π···π interactions between the naphthalene and ancillary ligands contribute to the stability of these metallacycles.

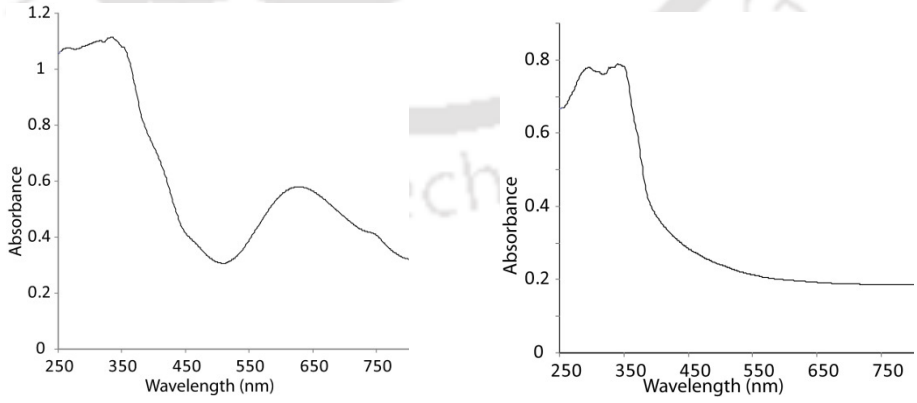

(a) (b)

Figure 2.5*: Diffused reflectance spectra of (a) metallacycle* ***2.2c*** *and (b) metallacycle* ***2.2e****.*

Diffuse reflectance spectra of these metallacycles have characteristic absorptions in the UV-region originates from the ligands and Visible-region originates from d-d transitions

in the case of nickel and cobalt complexes. For example, the cobalt (II) metallacycle **2.1a** absorbs at 459 nm and 617 nm whereas **2.1b** absorbs at 467 nm and 507 nm. Nickel (II) mononuclear complex **2.1c** and metallacycle **2.1d** show absorption at 626 nm. The zinc (II) ion has d^{10} electronic configuration, thus the zinc (II) metallacycles do not show absorption in visible region. Two representative diagrams are shown in Figure **2.5b**.

2.2 Magnetic studies of cobalt and nickel metallacycles:

Low temperature magnetic susceptibility measurements were studied for cobalt and nickel metallacycles. Plots of product of susceptibility and temperature value (χT) against temperature in the 1.8-300 K temperature range and the plots of magnetization *vs.* field at different temperatures with an applied magnetic field of 1000 Oe are shown in Figure **2.6.** The monotonic decrease of the χT product with lowering temperature suggests that both cobalt (II) metallacycle **2.1a** and **2.1b** have antiferromagnetic interactions. Low-temperature field dependence of the magnetization for **2.1a** and **2.1b** (Figure **2.6a,b** inset) shows that magnetization increases steadily to reach 9.5 and 14.2 μB at 2K and 70 kOe, which is comparable to a system consisting of four and six high-spin cobalt (II) ions (2.1 μB for each ion).[65] Experimental χT products of metallacycles **2.1a** and **2.1b** at room temperature are 11.3 cm^3 K mol^{-1} for **2.1a** and 19.0 cm^3 K mol^{-1} for **2.1b** which are much higher than the expected values for four (7.5 cm^3 K mol^{-1}) and six (11.25 cm^3 K mol^{-1}) non-interacting S = 3/2 spin-only cobalt (II) ions, respectively. Metallacycles **2.1a** and **2.1b** have $^4T_{1g}$ ground states due to octahedral arrangements around central cobalt (II) ions, so they show orbital contributions to magnetic moment.

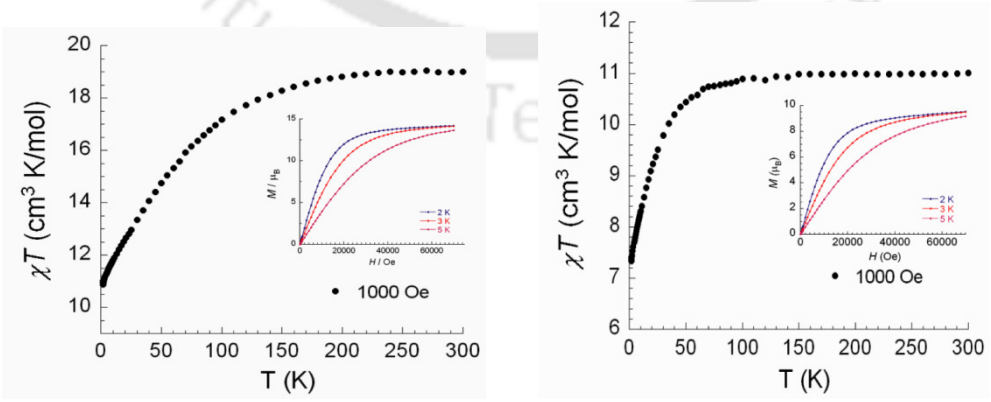

(a) (b)

***Figure 2.6**: Plots of χT vs. T for (a) **2.1a,** (b) **2.1b** under a dc field of 1000 Oe, the plots of magnetization vs. field at different temperatures are shown in the inset of the respective Figure.*

Lack of saturation in the magnetization curves indicates the presence of magnetic anisotropy and/or the lack of a well-defined ground state suggesting the presence of low-lying excited states that might be populated when a field is applied. It may be noted that the cobalt (II) hexanuclear metallacycle of 6-chloro-2-hydroxypyridine shows antiferromagnetic interactions.[66]

Magnetic relaxations of both the metallacycles **2.1a** and **2.1b** were tested using ac susceptibility measurements under zero dc field, no out-of-phase components were detected in both cases (Figure **2.7**). This behaviour is attributed to the fast zero-field tunnelling of the magnetization between sub levels of cobalt (II) ions.

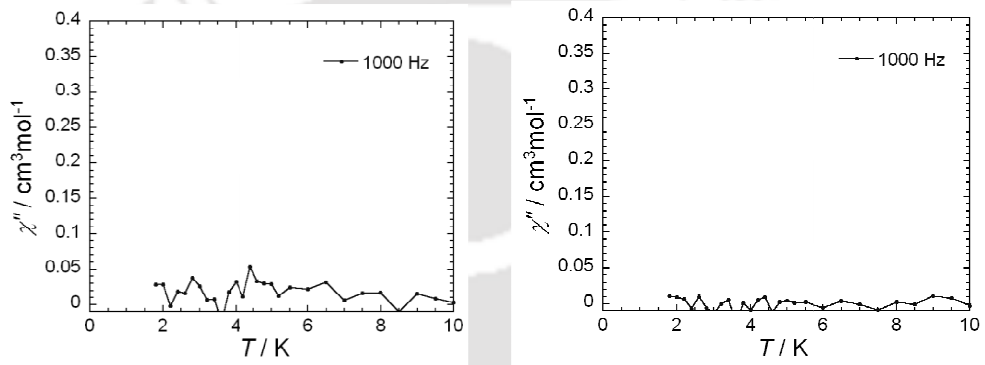

(a) (b)

Figure 2.7: *Plots of out-of-phase ac susceptibility vs. temperature at a constant frequency of 1000Hz for the metallacycles (a)* ***2.1a*** *and (b)* ***2.1b.***

With the application of an external dc field, the relaxation process is suppressed and then the out-of-phase component of ac susceptibility was detected. Tetranuclear-cluster-containing cobalt (II) complexes based on pendent-arm macrocyclic ligand with different carboxylates also exhibit antiferromagnetic interactions.[67] Dinuclear cobalt (II) metallacycle containing pyrazol ligand known to show paramagnetic behaviour at higher temperature and intramolecular antiferromagnetic interactions at low temperature.[68] For nickel (II) metallacycle **2.1c,** the value of χT increases and reach a maximum at 9.0 K and then rapidly drops on lowering the temperature (Figure **2.8**). This type of behaviour suggests the presence of dominant intramolecular ferromagnetic interactions. Maximum value of χT is 8.45 cm^3 K mol^{-1} at 9.0 K suggests a defined spin ground state of S = 3 with g = 2.37. Rapid decrease of χT below 10 K resulted from intermolecular antiferromagnetic interactions and/or the magnetic anisotropy of nickel (II) ions. In line with the structure, the magnetic susceptibility product is modelled using single J-model based on the spin Hamiltonian of H = 2J (S1·S2+S2·S3+S3·S4+S4·S5+S5·S6+S6·S1). J stands for the

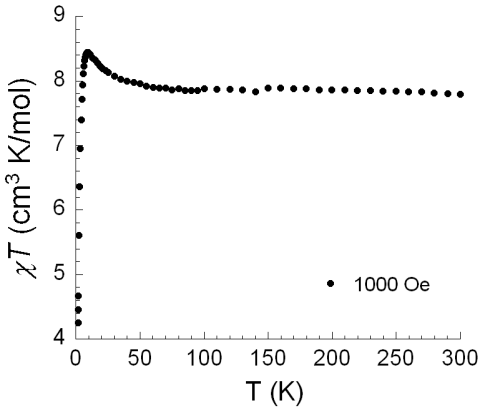

***Figure 2.8**: Plots of χT vs. T for **2.1c** under a dc field of 1000 Oe.*

interactions between the neighbouring nickel (II) ions (with S = 1) which are equalized within the metallacycle. In earlier study it was shown for nickel (II) hexanuclear dicubane type structures show a sudden drop in the χT below 6 K. This drop in χT is attributed to zero-field splitting and molecular effect of crystals.[69-70] Magnetic properties of tetranuclear nickel (II) metallacycles formed by pyridine based ligand shows dominant ferromagnetic interactions resulting in high-spin S = 4 ground state at low temperature.[71] In our case also similar interpretation is valid as the π systems may slightly reorganize to provide the π electrons to facilitate the intermolecular antiferromagnetic interactions contributing to the sharp decrease in the χT product. No out-of-phase signal was detected above 1.8 K, indicating the absence of slow relaxation of magnetization. From these studies it is observed that cobalt (II) tetranuclear and hexanuclear metallacycles show dominant antiferromagnetic interactions, whereas the nickel (II) metallacycle behaves as intramolecular ferromagnetic interactions.

2.3: Solvent mediated solid state transformation of copper (II) complexes:

In this section, reactions of phthalic anhydride, naphthalic anhydride, diphenic anhydride in presence of imidazole to prepare mononuclear and polymeric complexes are discussed. A series of copper (II) complexes $[Cu(cmb)_2(im)_2]$ (**2.2a**), $[Cu(cmn)_2(im)_4]$ (**2.2c**) and $[Cu(cmp)_2(im)_2]$ (**2.2e**) bearing various dicarboxylate monoester derivatives [cmb = 2-carbomethoxy-benzoate; cmn = 8-carbomethoxy-naphthalene-1-carboxylate; cmp=2-carbomethoxy-phenyl-2-benzoate] were generated from reaction of copper (II) acetate, imidazole (im) and an aromatic anhydride [phthalic, 1,8-naphthalic or biphenic anhydride for **2.2a**, **2.2c** or **2.2e**, respectively]. Formations of these complexes are shown in Scheme

2.2. Unusual solvent-mediated transformations of the crystals of two copper dicarboxylate monoester complexes to new crystals of corresponding dicarboxylate derivatives by hydrolysis of ester groups were observed.

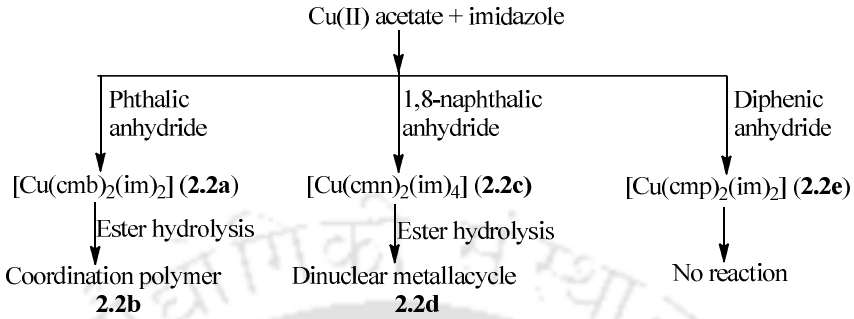

Scheme 2.2

Mononuclear complex **2.2a** was obtained from a reaction of phthalic anhydride with copper (II) acetate in methanol. From its elemental analysis, spectroscopic properties and structure determination confirmed it to be a mononuclear ester complex. When this complex was kept in contact with aqueous methanol it transformed to a copper (II) phthalate coordination polymer $\{[Cu_2(pht)_2(im)_4(H_2O)]\cdot H_2O\}_n$ (pht = phthalate anion) (**2.2b**). The transformation was also observed when crystals of **2.2a** were moistened with methanol and kept undisturbed. The crystals transformed to yield new type of crystals which were found to be the complex **2.2b**. The reaction involved in this transformation is shown in Scheme **2.3**. The crystals of **2.2b** have a visible absorption at 723 nm and are generally smaller in size than that of **2.2a**. In the complex **2.1a**, copper (II) ion is in octahedral coordination environment and is comprised of two chelating carboxylate groups and two imidazole ligands.

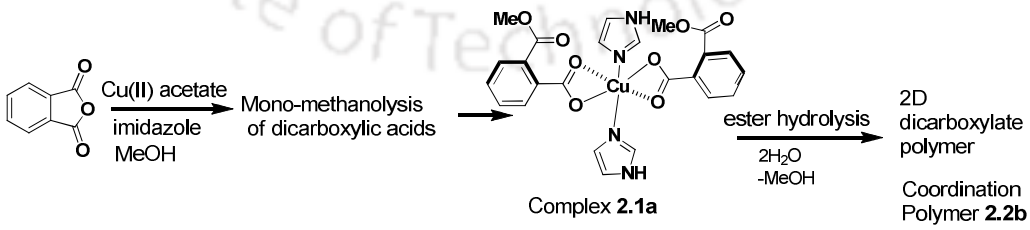

Scheme 2.3

Two imidazole ligands are in a mutually trans position of the octahedron. Morphology of crystals of the complex **2.2a** and dicarboxylate coordination polymer **2.2b** are quite

distinguishable. Their transformations were confirmed by microscopic views monitored with time after a crystal was moistened with a minimal amount of methanol (Figure **2.9**).

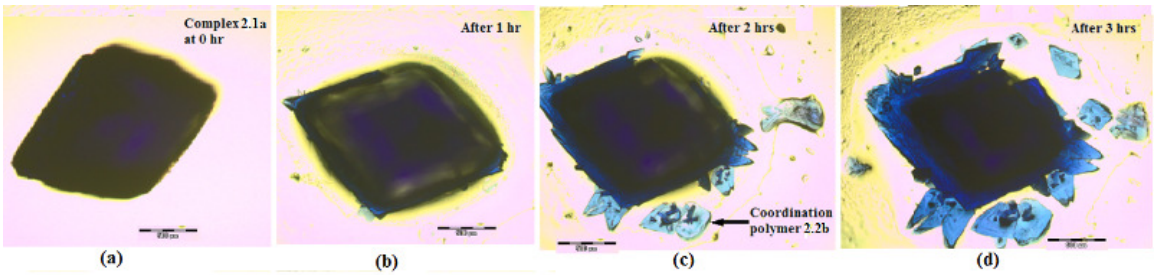

***Figure 2.9**: (a) Photograph of a crystal of complex **2.1a**. (b-d) Photograph of partially transformed crystal of the complex **2.1a** wetted by methanol under ambient conditions after (b) 1 h, (c) 2 h and (d) 3 h that leads to the formation of **2.2b**.*

From the above Figure it is seen that with time the crystal of **2.2a** breaks down with concomitant formation of new crystals. New crystals were picked up and characterized which were confirmed to be coordination polymer **2.2b.**

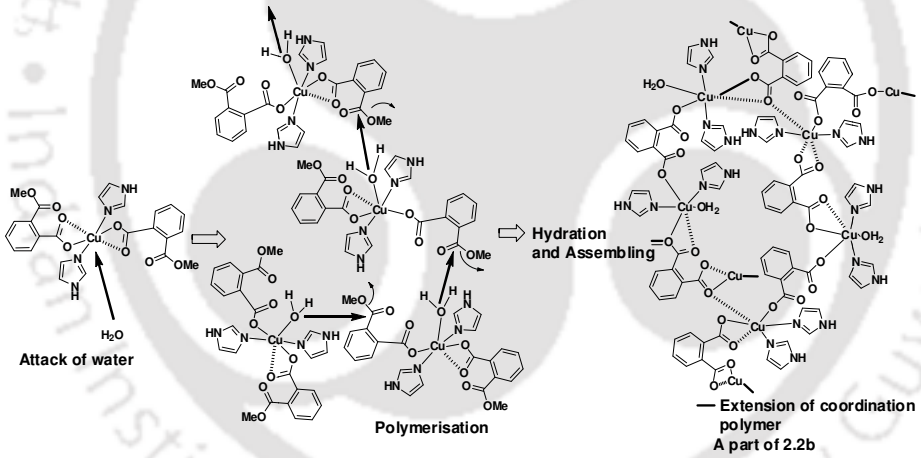

Scheme 2.4

Complete conversion of **2.2a** to **2.2b** took place within a day. These observations clearly show that during hydrolysis one form of crystal gradually transforms to another form of crystal. A proposed mechanism for chemical reactions involved in such transformation is shown in Scheme **2.4.**

An ester functional group present in the complex **2.2a** has a strong stretching vibration at 1730 cm^{-1}. This band is absent in IR spectrum of the crystals of coordination polymer **2.2d**. For comparison, overlaid IR spectra of the bulk samples before and after the transformation are shown in Figure **2.10a**. Solid state UV-visible (Figure **2.10b**) absorbance spectra of the complex **2.2a** and the coordination polymer **2.2b** are clearly

distinguishable. Complex **2.2a** shows absorption at 651 nm whereas coordination polymer **2.2b** absorbs at 723 nm due to the d-d transition of d^9 copper (II) ion. Although model intermediate tetrahedral copper complexes have been reported earlier for methanolysis reactions.[72-73]

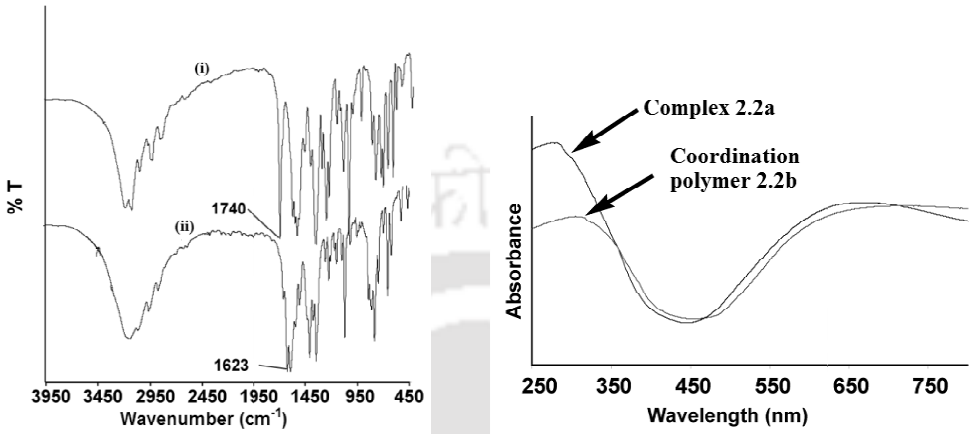

(a) (b)

Figure 2.10: *(a) Comparison of FT-IR spectra of (i)* ***2.2a*** *and (ii)* ***2.2b;*** *(b) solid state UV-visible spectra of the complex* ***2.2a*** *and the coordination polymer* ***2.2b.***

Crystal structure of **2.2a** is highly symmetrical with copper ions lying on a two fold axis and only half of the molecule is observed in its asymmetric unit. It contains a copper (II) ion that is coordinated with one 2-carbomethoxybenzoate and an imidazole ligand with two weak bonds. Complex **2.2a** has a copper (II) ion with a distorted octahedral geometry (Figure **2.11a**), filled by two bis-chelating carboxylate ligands and two imidazole. The Cu1-O1 and Cu1-N1 bond distances of 1.9637(14) and 1.9788(17)° respectively, support that these are strong dative bonds. On the other hand, the Cu1-O2 distance of 2.74 Å is indicative of a rather weak interaction of O2 with a copper ion. It may be suggested that steric congestion arising from the presence of the carbomethoxy groups twists the carboxylate ligands to reduce their chelation ability. It is interesting to note that the N1-Cu1-N1 bond angle of 164.63(11)° deviates by about 15° from 180° to allow it to adapt an octahedral geometry; thus, showing that the two imidazole moieties are not exactly at the mutual trans positions. These ligands are positioned in such a manner that the copper ion is slightly exposed from one direction for the approach of an external ligand. Such geometry provides more open space on one side of the distorted octahedron and helps the approach of water molecules to coordinate to a copper ion; thus, facilitating the hydrolysis of the ester groups to form polymer **2.2b**. In addition, the discrete monocopper (II)

$[Cu(cmb)_2(im)_2]$ blocks in the structure of **2.2a** are assembled, via the repeating N2-H2A/O2 hydrogen bonds, into a 2D H-bonded network (Figure **2.11b**).

We have taken topological analysis of all the complexes to find out any structural correlation among them. Generally topological analysis provides the convenient way of describing and predicting periodic 3D structure depending upon the chemical bonding and chemical properties. It has been analyzed from the topological viewpoint following the concept of the simplified underlying net.[74-77]

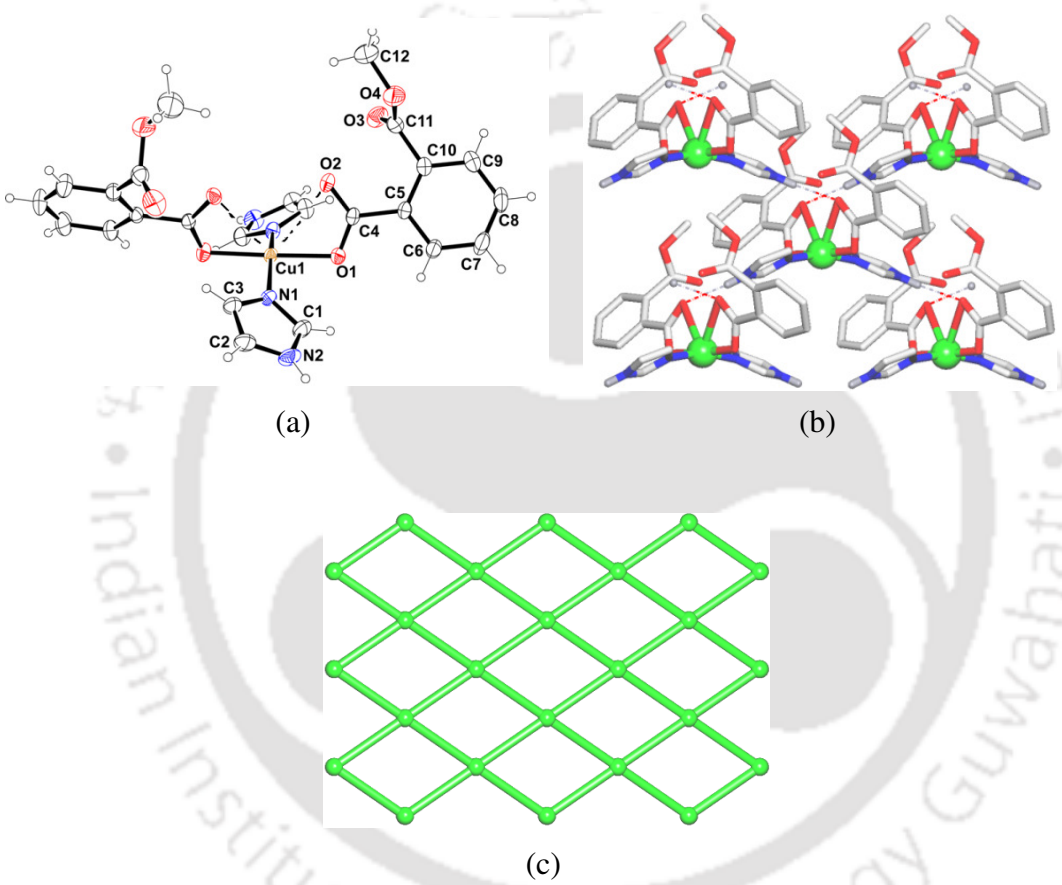

***Figure 2.11**: Structure of the complex **2.2a:** (a) ORTEP view (50% thermal ellipsoid probability). (b) H-bonding pattern showing inter linkage of monocopper (II) units into a 2D H-bonded layer; H atoms apart from those of H-bonds are omitted for clarity; color codes: Cu green balls, O red, N blue, C gray, H dark gray. (c) Topological representation of the simplified uninodal 4-connected 2D net with the **sql** topology and the point symbol of $(4^4 \cdot 6^2)$; green balls are the centroids of 4-connected $[Cu(cmb)_2(im)_2]$ nodes.*

After contracting the molecular $[Cu(cmb)_2(im)_2]$ units to the respective centroids, an underlying network has been obtained and is shown in above Figure **2.11c**. It is topologically described as a uninodal 4-connected net with a **sql**[Shubnikov tetragonal plane net] topology at the point symbol of $(4^4.6^2)$.[76, 78]

Asymmetric unit and the 2D metal-organic network of coordination polymer **2.2b** are shown in Figures **2.12a** and **2.12b**, respectively. The 2D corrugated layer can be visualized as assemblies of $[Cu_5(pht)_5]$ cyclic motifs driven by μ_2- and μ_3-phthalate moieties. The structure bears two different hexacoordinate copper ions, of which Cu1 is coordinated by two imidazole ligands and three independent phthalate moieties (two μ_3-pht and one μ_2-pht) with the carboxylate groups adapting monodentate $\eta^1:\eta^0$ and bidentate

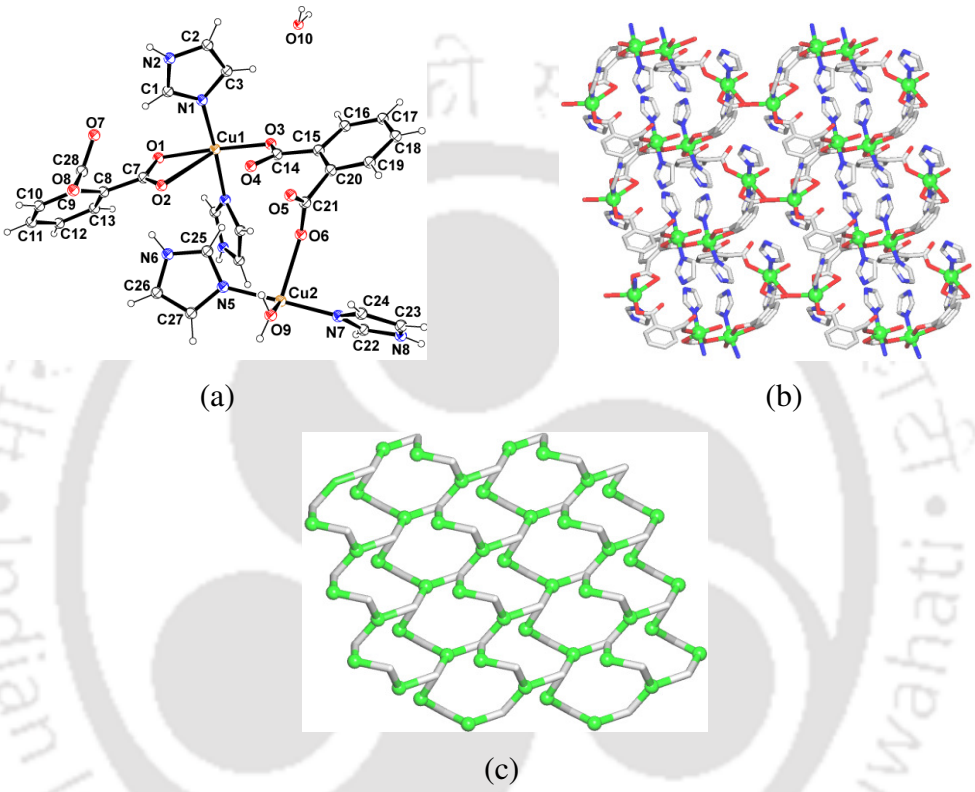

Figure 2.12: *(a) ORTEP view of asymmetric unit* ***2.2b*** *(30 % thermal ellipsoid probability) of the. (b) 2D metal-organic layer; the H atoms and solvent molecules are omitted for clarity; color codes: Cu green balls, O red, N blue, C gray. (c) Topological representation of the simplified uninodal 3-connected 2D net with the* ***hcb*** *topology and the point symbol of (6^3); color codes: 3-connected Cu1 nodes and 2-connected Cu2 linkers (green balls), centroids of 3-connected μ_3-pht nodes and 2-connected μ_2-pht linkers (gray).*

$\eta^1:\eta^1$ and μ_2-$\eta^2:\eta^1$ coordination modes. The other Cu2 ion is coordinated to a water molecule and two imidazole ligands, as well as to two independent μ_2- and μ_3-bridging phthalate dianions. Their carboxylate groups that are connected to the Cu2 atom exhibit the $\eta^1:\eta^0$ and μ_2-$\eta^2:\eta^1$ coordination modes. Thus, by virtue of monodentate, bidentate and bifurcated coordination of the phthalate dianions, they act as linkers to copper ions in the 2D coordination polymer **2.2b**. The Cu-N bond lengths vary from 1.965(3) to 1.981(3) Å, whereas the Cu-O bond distances are within the 2.007(3)-2.073(3) Å range, except the Cu2-O6 [2.309(3) Å], Cu1-O8 [2.499(3) Å] and Cu2-O8 [2.739(3) Å] bonds. The

relatively higher bond length of the two later bonds is due to side on (μ-η^2-O type) bridging mode with copper (II). These distances are within the admissible range reported for similar coordination modes in other copper complexes[79-81] and sum of the Vander Waals radii of the Cu and O atoms is found to be [2.92 Å].[82] The metal-ligand bond parameters of the complexes **2.2a** and **2.2b** are listed in the Table **2.3**.

Table 2.3**: Metal-ligand bond parameters of the complexes **2.2a-2.2e.

Compd. No.	M-L	d_{M-L}(Å)	∠L-M-L	Angle (°)	∠L-M-L	Angle (°)
2.2a	Cu1-O1	1.9637(14)	O1-Cu1-N1	89.09(7)		
	Cu1-O2	2.740	O1-Cu1-O2	53.23		
	Cu1-N1	1.978(17)	O2-Cu1-N2	106.22		
2.2b	Cu1-O1	2.073(3)	O3-Cu1-O1	175.81(12)	N5-Cu2-O6	92.94(13)
	Cu1-O3	2.007(3)	N1-Cu1-O1	172.59(15)	N5-Cu2-O7	89.72(13)
	Cu1-N1	1.981(3)	N1-Cu1-O3	89.97(13)	N5-Cu2-O9	89.27(14)
	Cu1-N4	1.965(3)	N4-Cu1-O1	87.96(13)	N5-Cu2-N7	176.76(15)
	Cu2-O6	2.309(3)	N4-Cu1-O3	90.13(14)	N7-Cu2-O7	93.14(13)
	Cu2-O7	2.022(3)	N4-Cu1-N1	91.45(13)	N7-Cu2-O9	87.50(14)
	Cu2-O9	2.056(3)	O7-Cu2-O6	102.83(11)	N7-Cu2-O6	87.94(13)
	Cu2-N5	1.962(3)	O7-Cu2-O9	148.95(14)		
	Cu2-N7	1.970(3)	O9-Cu2-O6	108.21(13)		
2.2c	Cu1-N1	2.006(10)	N1-Cu1-N3	90.9(5)	N3-Cu1-O2	90.0(4)
	Cu1-N3	2.014(12)	N1-Cu1-O2	91.6(4)		
2.2d	Cu1-O2	1.965(3)	O2-Cu1-O4	172.43(10)	O5-Cu1-O4	86.46(11)
	Cu1-O4	1.993(2)	O2-Cu1-O5	85.98(11)	O5-Cu1-O6	95.24(11)
	Cu1-O5	1.982(3)	O2-Cu1-O6	93.18(11)	N1-Cu1-O4	95.17(11)
	Cu1-O6	2.275(3)	O2-Cu1-N1	92.35(11)	N1-Cu1-O5	171.50(11)
	Cu1-N1	1.977(3)	O4-Cu1-O6	87.30(11)	N1-Cu1-O6	93.17(12)
2.2e	Cu1-N1	1.9799(19)	O1-Cu1-O2	55.19		
	Cu1-O1	1.9943(12)	O2-Cu1-N2	96.63		
	Cu1-O2	2.622	N1-Cu1-O1	90.84(6)		

Topological analysis of **2.2b** revealed a uninodal 3-connected network with the point symbol of (6^3) and **hcb**[Shubnikov hexagonal plane net (6, 3)] topology, which is different from the **sql** net encountered in **2.2a** (Figure **2.12c).** In **2.2b**, both the crystallization and coordinated water molecules are anchored to the O atoms of the phthalate ligands through different O-H/O hydrogen bonds, whereas N-H/O interactions between the imidazole moieties and COO^- or H_2O groups provide further stabilization of the structure. As a result, these multiple intermolecular H-bonding interactions are responsible for the extension of 2D metal-organic layers to a very complex 3D supramolecular architecture. After simplification,[72] topological analysis disclosed an intricate hexanodal 3,4,5,5,5,6-connected net with a unique topology described by the point symbol of $(4.5.6)(4^2.5^2.6.7)(4^3.5^2.6^4.7)(4^3.5^4.6.7.8)(4^5.5^2.6^3)$-$(4^6.5^2.6^4.7^2.8)$.

The powder-XRD patterns of **2.2a** and **2.2b** were recorded and compared with the simulated patterns which indicated a rational correlation between the two and it confirmed the phase purity of the complexes.

Crystals of complex **2.2a** belong to C2/c space group with a unit cell volume of 2568.0(3) $Å^3$, whereas the crystals of the coordination polymer **2.2b** crystallized in $P2_1/n$ space

group with a unit cell volume of 3101.33(19) Å^3. A helical 1D copper (II) phthalate imidazole coordination polymer [82] was prepared earlier from the reaction of copper (II) carbonate with phthalic acid in solution but this is structurally different from the one generated via the solid state transformation of **2.2a.**

We also examined the reaction of copper (II) acetate with 1,8-naphthalic anhydride in the presence of imidazole in DMF-methanol, which resulted in a mononuclear tetra imidazole di-(8-carbomethoxy-naphthalene-1-carboxylato) copper (II) complex, $[Cu(cmn)_2(im)_4]$ (**2.2c**). The complex has four coordinated nitrogen atoms of imidazole ligands in one plane around the copper (II) ion, while two monodentate 8-carbomethoxy-naphthalene-1-carboxylate ligand are in the axial positions; thus, forming the distorted octahedral geometry around the copper (II) center (Figure **2.13a**).

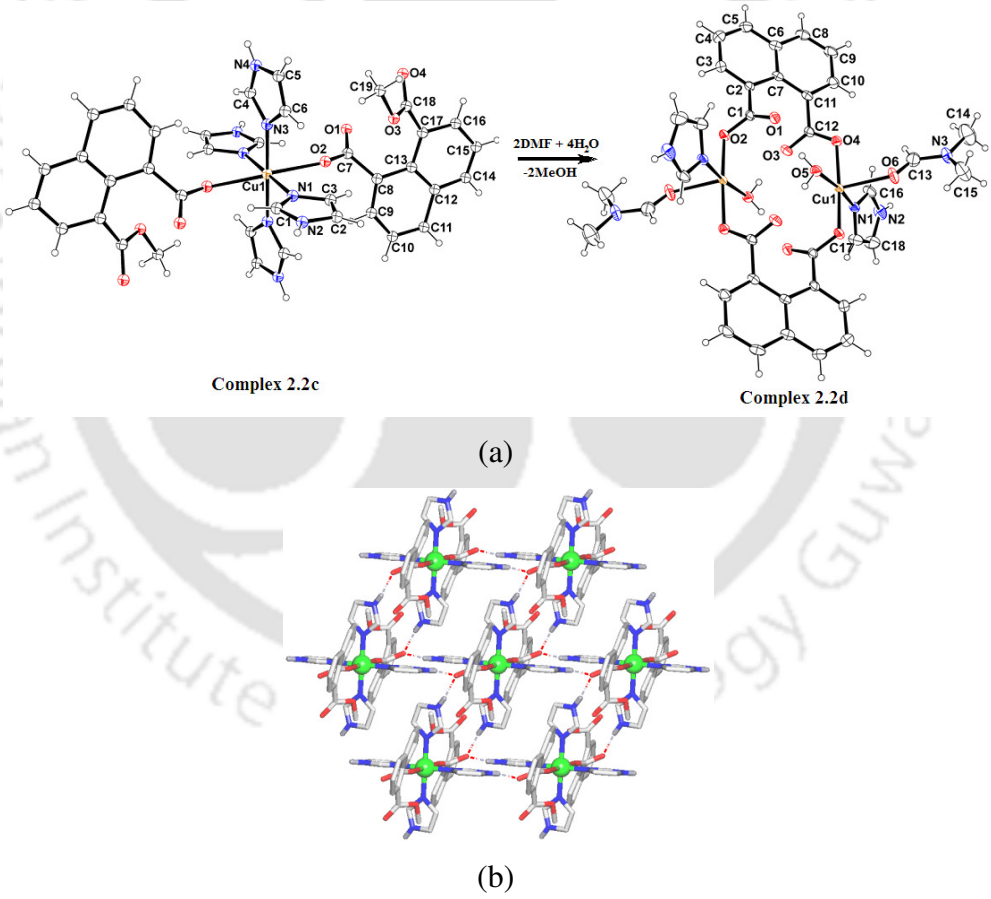

Figure 2.13: *(a) ORTEP view (30 % thermal ellipsoid probability) showing transformation of* ***2.2c*** *to* ***2.2d.*** *(b) $[Cu(cmn)_2(im)_4]$ units are held together through the intermolecular N2-H2A/O1 and N4-H4A/O1 hydrogen bonds, generating a 2D H-bonded network in* ***2.2c****.*

The molecule of complex **2.2c** has a Cu1 atom on an inversion centre. Asymmetric unit is constituted by one 8-carbomethoxynaphthalene-1-carboxylate anion and an imidazole molecule coordinated to copper ion. The observed lengths of the Cu1-N1, Cu1-N3 and

Cu1-O2 bonds are 2.006(10), 2.014(12) and 2.468(8) Å, respectively. The metal ligand bond parameters are listed in Table **2.3**. Chemical transformation of **2.2c** converting to **2.2d** occurred when moistened with DMF. Crystals of complex **2.2c** upon moistening with aqueous DMF transformed to another form of crystals. New sets of crystals were formed by hydrolysis of crystals of **2.2c** with simultaneous crystallization of a new dinuclear metallacycle (Figure **2.13**). From the figure it is clear that the rod shaped crystals of **2.2b** were gradually transformed to small crystals. These small crystals were characterized and found to be complex **2.2d** and it took four days for complete conversion. Changes in the crystals of complex **2.2c** that are transformed to metallacycle **2.2d** were monitored by using microscope and the micrographs are shown in Figure **2.14**. Structure of metallacycle $[Cu(nap)(im)(DMF)(H_2O)]_2$ (**2.2d**) (where nap = 1,8- naphthalenedicarboxylate) (Figure **2.13a**) has two copper (II) ions in an identical environment, which are interconnected by two independent μ_2-1,8- naphthalenedicarboxylate blocks with both COO groups acting in $\eta^1:\eta^0$-mode. Apart from two carboxylate oxygen atoms, the square pyramidal environment of each copper ion is filled by H_2O, DMF and imidazole ligands.

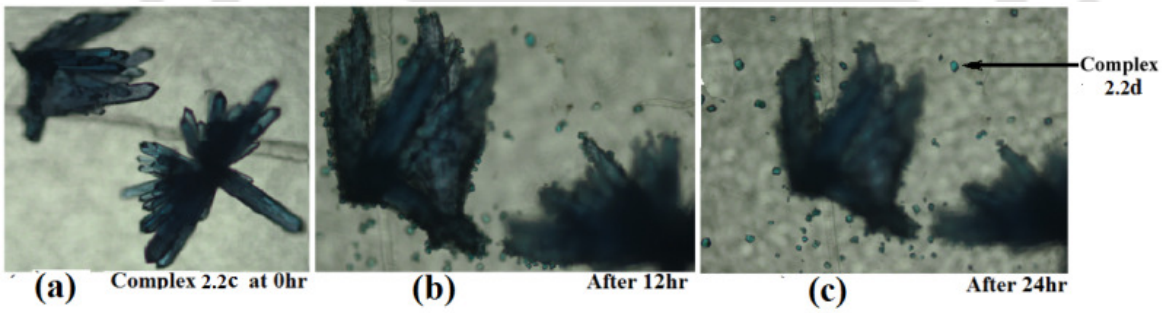

***Figure 2.14**: Transformation of the complex **2.2c** to the complex **2.2d** (a) at initial time (b) after 12 hours, (c) after 24 hours.*

The dimeric complex lies about an inversion centre. Such a transformation occurred as a consequence of the ease in the hydrolysis of ester group in the copper complex **2.2c** to form a dicarboxylate derivative. This conversion was observed through the naked eye because the blue colored crystals turned green once the crystals of **2.2c** were suspended in aqueous DMF. Solid state complex **2.2c** exhibits visible absorption at 553 nm, whereas the metallacycle **2.2d** absorbs at 711 nm. This absorption arises from d-d transition of d^9-copper ions. The complex **2.2c** has an IR stretching band at 1740 cm^{-1} due to the ester functional group, while this band is absent in **2.2d.** Although in contrast to the monocopper (II) units of **2.2c**, discrete structure of **2.2d** is composed of dicopper (II)

blocks which are also arranged by intermolecular H-bonds into a 2D hydrogen bonded network.

Powder-XRD pattern of the metallacycle **2.2d** was recorded and compared with the simulated patterns and found to be similar, which indicates the bulk purity of the crystalline form of **2.2d**.

Topological analysis of **2.2d** revealed the same **sql** topology as in **2.2c**. Therefore, conversion of **2.2c** to **2.2d** does not lead to a change in network topology which was observed during the transformation of **2.2a** to **2.2b**.

In addition to the above reactions, a similar reaction of diphenic anhydride with copper (II) acetate in DMF-methanol was investigated to prepare ester containing copper (II) complex. In an earlier work on ring opening reaction of diphenic anhydride by cystine derivatives it was shown that corresponding acid formed transforms to helical ester derivative via a reaction with diazomethane.[82] In the present case, reaction of diphenic anhydride with copper (II) acetate, followed by a treatment with imidazole, resulted in the formation of an ester group containing copper complex $[Cu(cmp)_2(im)_2]$ (**2.2e**). This compound has a distorted octahedral geometry around the copper (II) ion (Figure **2.15**), filled by two chelating $\eta^1:\eta^1$ -carboxylates in one plane and two imidazole ligands in mutually trans position.

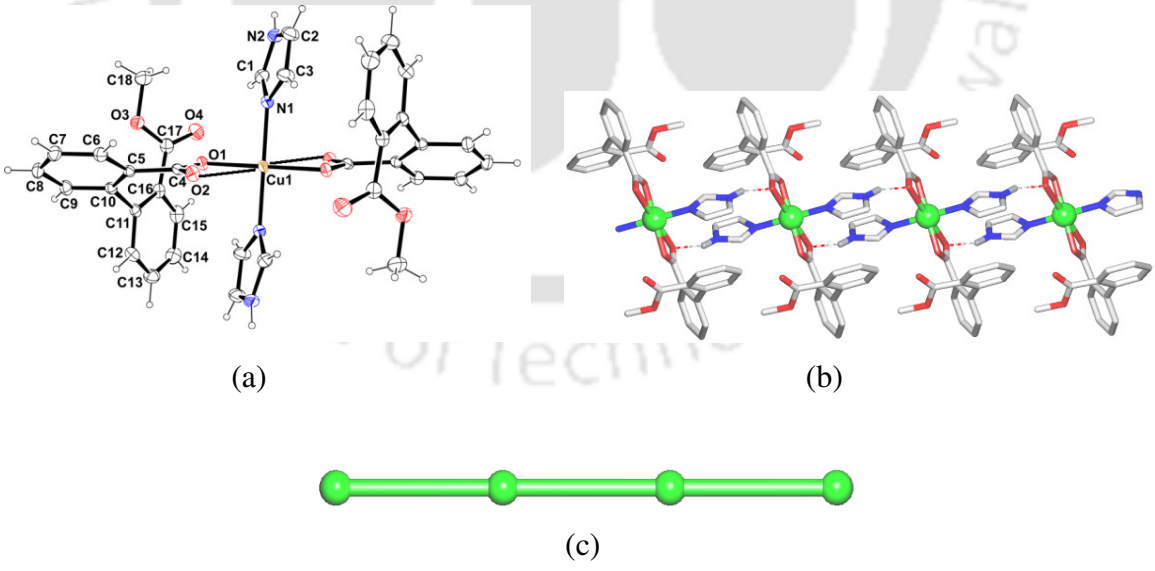

***Figure 2.15**: Structure of **2.2e**: (a) ORTEP view (30% thermal ellipsoid probability). (b) H-bonding pattern showing the inter linkage of monocopper (II) units into a 1D H-bonded chain; H atoms apart from those of H-bonds are omitted for clarity; color codes: Cu green balls, O red, N blue, C gray, H dark gray. (c) Topological representation of the simplified uninodal 2-connected 1D net with the 2C1 topology; green balls are the centroids of 2-connected $[Cu(cmp)_2(im)_2]$ nodes.*

In the crystal structure, the copper ion of complex **2.2c** lies on an inversion center.

The monocopper (II) units in **2.2e** are interlinked via the N2-H2A/O2 hydrogen bonds, forming a 1D H-bonded chain motif (Figure **2.15b**) that can be described as a uninodal 2-connected net with the **2C1** topology (Figure **2.15c**).[72] The complex **2.2e** is stable under ambient conditions and it can be easily recrystallized from a methanol solution. A comparison of structures of the complexes **2.2e** and **2.2a** shows that both compounds have six-coordinate copper (II) centre with a similar $\{CuN_2O_4\}$ environment but different geometries. For comparison, the ∠N1-Cu1-N1 bond angles are 164.63(11) and 180.00(6)° in **2.2a** and **2.2b**, respectively, whereas the ∠O1-Cu1-O1 bond angles are 177.97(10)° in **2.2a** and 180.00(7)° in **2.2e**. Therefore, there is relatively more space exposed on one side of the copper ion in the complex **2.2a** that facilitates the approach of a water molecule and eases the hydrolysis reaction. In **2.2a**, the ester groups are positioned on the same side across a plane, whereas in **2.2e** they are on the opposite side. Hence, the hydrophobic part in complex **2.2a** adapts a pincer type of arrangement that would have helped its facile hydrolysis in crystalline state. In the case of complex **2.2e**, the location of the two hydrophobic ester groups in opposite sides makes the approach of water less favorable from two directions providing extra stability toward hydrolysis. The metal-ligand bond parameters are listed in Table **2.3**.

From the above transformations the sequential formation of monoester intermediate is established in copper complexes through the hydrolysis of cyclic anhydrides. This is a unique observation in which we showed solid state transformations of an ester to carboxylate complexes.

2.4. Copper (II) acetate catalysed hydrolysis of cyclic imide:

Analogous to study on metal mediated hydrolysis reaction of cyclic anhydrides, we extended our study to mediated hydrolysis of a cyclic imide. For this purpose we chose the simple phthalimide based ligand, 2-(3-(1H-imidazol-1-yl)propyl)isoindoline-1,3-dione (**L = 2.3**) by condensation of phthalic anhydride with 3-(1H-imidazol-1-yl)propan-1-amine. The ligand was characterized by recording its ^{1}H-NMR, ^{13}C-NMR, IR and mass spectrometry and finally by determining its X-ray structure. Ligand shows ^{1}H-NMR signals at 4.07 ppm, 3.56 ppm and 2.07 ppm due to the three different methylene groups; the ring protons of the imidazole appear as three singlets at 8.00 ppm, 7.35 ppm and 7.07

ppm. The signals for benzene protons appear at 8.06 ppm, 7.84 ppm and 7.51 ppm with appropriate integrations.

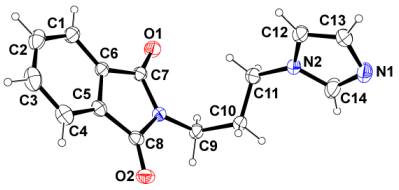

***Figure 2.16**: ORTEP view of **L** (35 % thermal ellipsoid probability).*

L shows carbonyl stretching frequency at 1712 cm^{-1} in its IR spectrum. Crystal structure of **L** is shown in Figure **2.16**. By reacting **L** with different copper (II) salts it was found that ligand formed copper (II) complexes with different compositions and is shown in Scheme **2.5**. The compositions were dependent on the counter ion used.

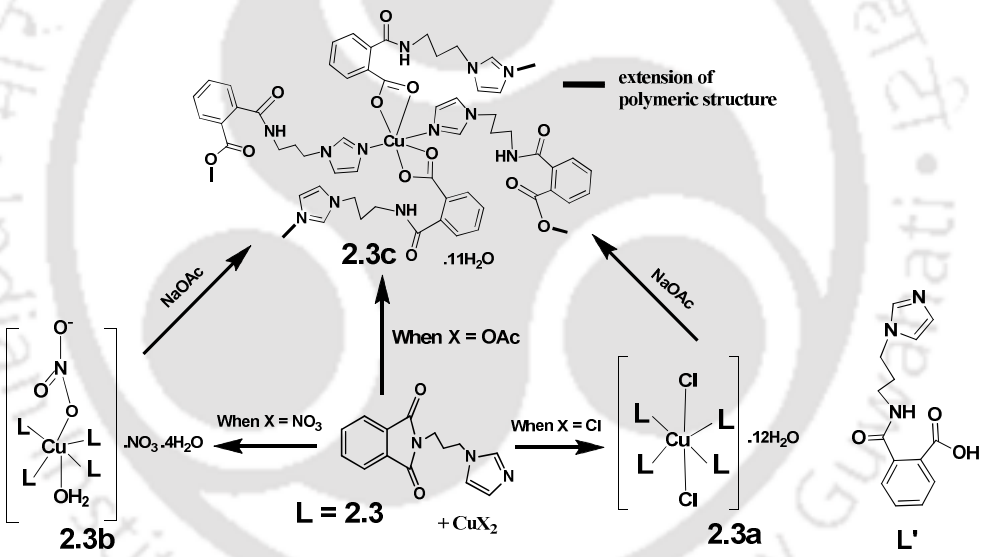

Scheme 2.5

Thus the reactions of **L** with copper (II) chloride or copper (II) nitrate resulted in the formation of the complexes $[CuL_4Cl_2]\cdot 12H_2O$ (**2.3a**) or $[CuL_4(H_2O)(NO_3)]\ NO_3\cdot 4H_2O$ (**2.3b**) respectively. Whereas, copper (II) acetate reacted with **L** to give a three dimensional coordination polymer $\{2[Cu(L')_2]\cdot 11H_2O\}_n$ (**2.3c**), (where **L′**=2-(3-(1H-imidazol-1-yl)propylcarbamoyl)benzoate anion). The coordination polymer **2.3c** was also obtained by reacting complex **2.3a** and **2.3b** with sodium acetate.

Common feature in the two mononuclear copper complexes **2.3a** and **2.3b** is that the complexes have 1:4 metal to ligand (**L**) ratio. The complexes **2.3a** and **2.3b** differ in their ionic nature. The complex **2.3a** is a hexacoordinated neutral complex in which the two

chlorides are coordinating. On the other hand, nitro-complex is a six-coordinated complex but it has an ionic nitrate anion outside the coordination sphere. This ionic nature is confirmed by the molar conductance values. For complex **2.3a** the molar conductance (in methanol) was found to be 20.4 S cm^2 mol^{-1} whereas in case of complex **2.3b** this value was found to be 110 S cm^2 mol^{-1}. Copper ion in **2.3b** is attached to four ligands (**L**), one nitrate and one water molecule. It has a nitrate anion outside the coordination sphere. The crystal structures of the complexes **2.3a** and **2.3b** are shown in Figure **2.17**. Complex **2.3a** has a highly symmetric structure with a centre of inversion passing through the copper ion. Thus, only symmetric half of the complex is observed in its asymmetric unit.

From thermogravimetric analysis (Figure **2.23a** in the experimental section) it is observed that there is a weight loss below 155 °C which can be corroborated the loss of lattice water molecules (% wt. loss, calcd.14.0 and experimental 13.6) in case of **2.3a**; whereas in case of **2.3b,** four lattice water molecules were lost at the temperature below 112 °C (% wt. loss, experimental 5.1 and calcd. 5.5).

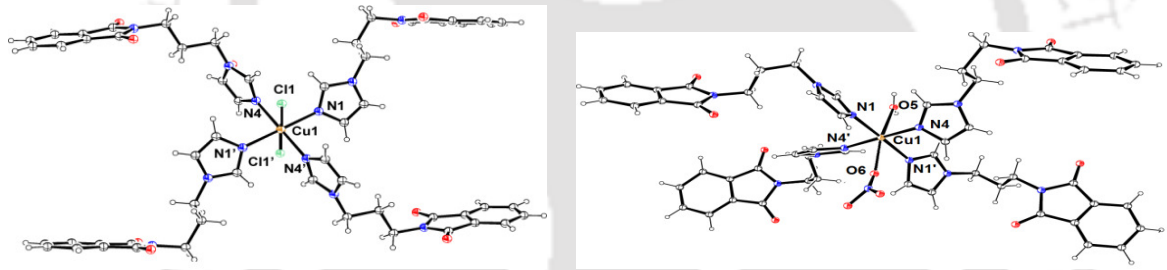

(a) (b)

Figure 2.17*: ORTEP view of (a) complex* ***2.3a****, (b) complex* ***2.3b*** *(35 % thermal ellipsoid probability; counter anions and lattice water molecules are omitted).*

In IR spectrum, nitrate-complex **2.3b** showed weak absorption at 1436 cm^{-1} and a strong absorption at 1401 cm^{-1} due to nitrates (Figure **2.23** in the experimental section). Although, nitrate complex adapts hexacoordinated geometry in solid state, the nitrate ion very weakly binds to copper ion. This is reflected in the Cu1-O6 distance, which is 2.815(11) Å, larger than the commonly observed Cu-O bonds (< 2.5 Å). So this may be considered to lie on the Jahn-Teller axis of this complex. The coordinated water molecule also binds in relatively weak manner apparent from its bond distance {Cu1-O5, 2.407(5) Å}. The metal-ligand bond parameters of the complexes **2.3a-d** are listed in Table **2.4**.

Coordination polymer $\{[Cu(\mathbf{L'})_2].4H_2O\}_n$ (**2.3c**) was formed from in situ ring opening of **L** to form **L′** by hydrolytic process. Thus the coordination polymer **2.3c** is comprised of a

new ligand which is of 2-(3-(1H-imidazol-1-yl)propylcarbamoyl) benzoic acid (H**L′**) coordinating to copper (II) ion.

***Table 2.4**: Metal-ligand bond parameters of the complexes **2.3a-2.3d**.*

Compd. No.	M-L	d_{M-L}(Å)	∠L-M-L	Angle (°)	∠L-M-L	Angle (°)
2.3a	Cu1-N1	2.022(7)	N1-Cu1-N4	91.7(3)		
	Cu1-N4	2.006(7)	N1-Cu1-Cl1	91.6(2)		
	Cu1-Cl1	2.909(3)	N4-Cu1-Cl1	91.0(2)		
2.3b	Cu1-O5	2.406(5)	O5-Cu1-O6	180(2)	N4-Cu1-O5	90.81(10)
	Cu1-O6	2.733(10)	N1-Cu1-O5	90.93(11)	N4-Cu1-O6	89.19(10)
	Cu1-N1	1.979(3)	N1-Cu1-O6	89.07(11)		
	Cu1-N4	2.002(3)	N1-Cu1-N4	90.57(13)		
2.3c	Cu1-O1	1.957(3)	O1-Cu1-O2	51.75		
	Cu1-O2	2.798	O1-Cu1-N2	90.57(14)		
	Cu1-N2	1.996(4)	O2-Cu1-N2	93.65		
2.3d	Cd1-O7	2.526(7)	O7-Cd1-O9	130.7(3)	N1-Cd1-O8	138.0(3)
	Cd1-O8	2.475(7)	O8-Cd1-O7	50.3(3)	N1-Cd1-O9	140.3(2)
	Cd1-O9	2.548(6)	O8-Cd1-O9	81.6(3)	N1-Cd1-O10	90.8(2)
	Cd1-O10	2.468(6)	O10-Cd1-O7	175.3(2)	N4-Cd1-O7	87.4(3)
	Cd1-N1	2.289(6)	O10-Cd1-O8	131.1(3)	N4-Cd1-O8	89.3(2)
	Cd1-N4	2.271(7)	O10-Cd1-O9	49.8(2)	N4-Cd1-O9	81.2(2)
	Cd1-N7	2.262(7)	N1-Cd1-O7	88.1(3)	N4-Cd1-O10	88.1(2)

The imidazole unit on one side is attached to a copper (II) ion whereas carboxylate end is anchored to another copper (II) ion. Thus ligand **L′** acts as a connector among the copper (II) ions to form a coordination polymer **2.3c**.

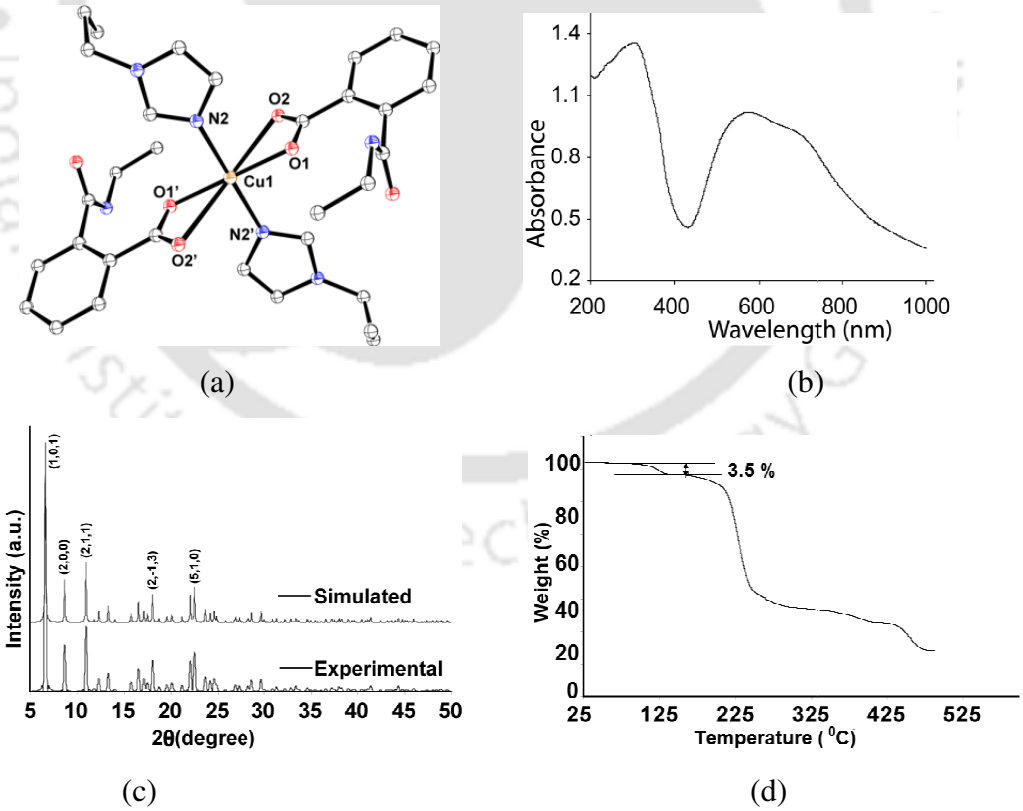

***Figure 2.18**: (a) ORTEP view of **2.3c** (30 % thermal ellipsoid probability) showing coordination environment around copper (hydrogen atoms and lattice waters are omitted), (b) Solid state UV-visible spectrum, (c) Comparison of simulated (top) as experimental (bottom) PXRD of **2.3c** and (d) Thermogram of **2.3c** (heating rate 7 °C/min).*

The interesting feature of this coordination polymer is its structure and route of formation through ring opening of imide bond by hydrolysis at ambient condition. The coordination polymer **2.3c** is a three dimensional structure and the coordination environments around copper is shown in Figure **2.18**. In solid state the complexes **2.3a**, **2.3b** and **2.3c** have visible absorptions at 599 nm, 584 nm and 574 nm respectively, due to d-d transition (in ^2E to ^2T) arising from d^9-electronic configurations and the copper (II) ions in each case are in distorted octahedral environment. The solid state UV-visible spectrum of **2.3c** is shown in Figure **2.18b**.

Thermogram of **2.3c,** shows that there is a weight loss of below 105 °C (calcd. wt. loss 4.7 % and experimental wt. loss 3.5 %) which can be corroborated to the loss of lattice water molecules (Figure **2.18d**).

By comparing the simulated and experimental powder XRD patterns of coordination polymer **2.3c** it is found that there is a similarity between the two which confirms the phase purity. The comparison spectrum is shown in Figure **2.18c**.

A ligand template copper (II) acetate intermediate complex could be responsible for the ring opening reaction. From the present results on the isolated complexes, it suggests that the role of acetate ion is to facilitate the attack by a water molecule on the imide bond to open the ring. This occurs due to the intrinsic basicity associated with acetate ion.

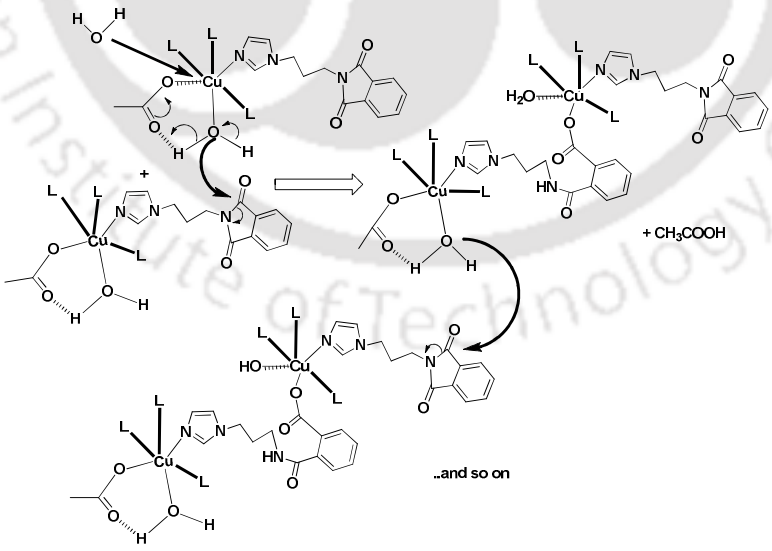

Scheme 2.6: *Plausible mechanism of formation of the coordination polymer* ***2.3c****.*

It also helps to bind the hydrolyzed part to copper by abstracting a liberated proton and it is well known that a benzoate can easily replace an acetate ligand from metal acetates and

this process paves way to form the coordination polymer. A plausible mechanism of formation of the coordination polymer **2.3c** is shown in the Scheme **2.6**. Since several copper (II) and zinc (II) ions are active sites in hydrolytic enzymes.[83] We studied the reaction of **L** in presence of zinc (II) salts. We did not obtained the complex formed from such reaction and also neither we obtained hydrolysis of the ligand. However the reaction of cadmium (II) acetate with ligand **L** led to the formation of a cadmium complex $[Cd\mathbf{L}_3(O_2CCH_3)_2]\cdot 2H_2O$ (**2.3d**). The complex **2.3d** is a mononuclear complex, it has three ligands anchored to the cadmium ion and it has also two chelating acetates.

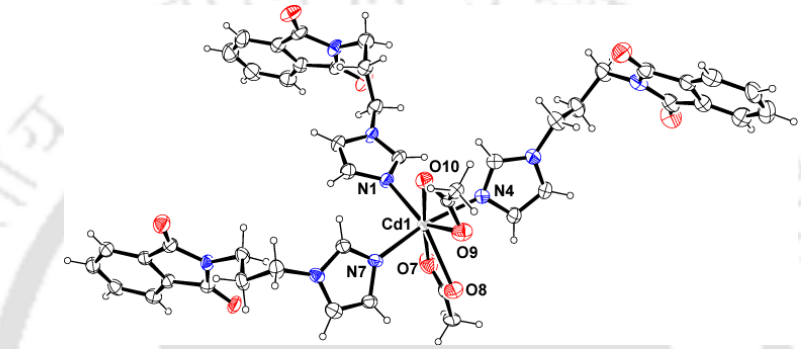

(a)

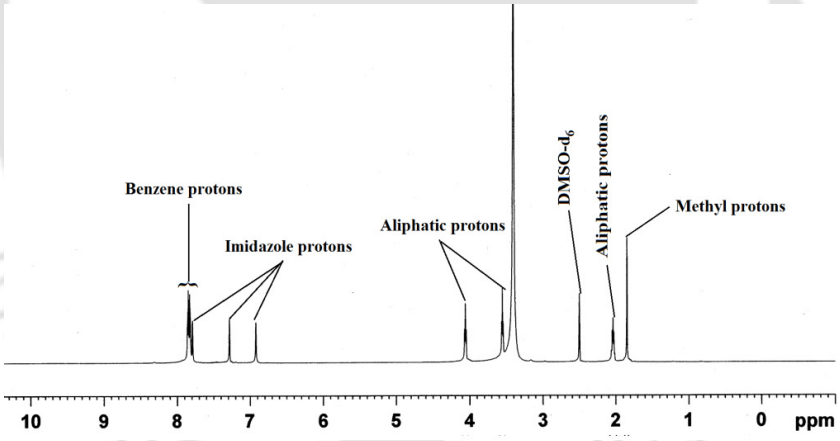

(b)

Figure 2.19: *(a) ORTEP view (50% thermal ellipsoid probability) (lattice water molecules are omitted) and (b) ^{1}H-NMR spectrum (600 MHz, DMSO-d_6) of complex* ***2.3d****.*

The crystal structure was determined and the structure is shown in Figure **2.19a**. It has a seven coordinated geometry around cadmium ion. The metal-ligand bond parameters are listed in Table **2.5**. The complex has two water molecules as solvent of crystallization.

By observing the ^{1}H-NMR spectrum of the complex **2.3d** with **L** show that there is slight shifting of chemical shift values for the protons. Signals for benzene protons merged and appeared as multiplet at 7.83 ppm; whereas imidazole protons appeared as singlet at 7.28,

7.79 and 6.92 ppm. Three aliphatic -CH_2- protons appeared at 4.05, 3.55 and at 2.03 ppm. Methyl protons of acetate groups appeared as a singlet at 1.84 ppm. This confirms that the complex is stable in solution.

By comparing the experimental PXRD pattern with simulated pattern it was found the similarities between the two patterns confirming the phase purity of the complexes **2.3a-2.3d**. In some cases slight deviation may be due to the loss of solvent molecules.

2.5 Conclusion:

Taking advantage of π-stacking effect of ligand we prepared metallacycles of cobalt (II), nickel (II) and zinc (II) with specific nuclearity. The π-stacking effect such as the one observed in hexanuclear metallacycles controls orientation of carboxylate thereby guiding the coordination mode of carboxylate which resulted in heaxnuclear cluster. Cobalt and nickel showed similar reactivity but zinc showed difference yet selective reactivity to form a pentacoordinated metallacycle. Cobalt (II) tetranuclear and hexanuclear metallacycle shows dominant antiferromagnetic interactions, whereas the nickel (II) metallacycle showed as intramolecular ferromagnetic interactions.

Solvent mediated solid state transformation from a mononuclear complex to dicarboxylate coordination polymer or dinuclear metallacycle via the fast hydrolysis of an ester group in copper (II) precursors is shown. This novel solid state transformation provides new avenues to explore solvent mediated solid state transformations. Topological analysis revealed that in the case of a **2.2a** to **2.2b** transformation, the overall 2D network topology changed from the 4-connected **sql** net to the 3-connected **hcb** net, while no topology modification was observed during the **2.2c** to **2.2d** transformation. Steric factor plays a crucial role to provide hydrophobic effect deterring hydrolysis of ester complex **2.2e**. This study also contributes to an understanding of the metal ion template transformations in the solid state, providing a useful methodology to prepare new compounds that are different from those obtained during conventional synthesis in solution.

We have also observed copper (II) acetate catalysed hydrolytic cleavage of imide at an ambient condition to form amide and carboxylic acid and in situ formation of a coordination polymer from the new ligand formed as a result of hydrolysis.

2.6 Experimental section:

The detailed synthetic methodologies for synthesis of metal complexes are described. Analytical data as well as spectroscopic data are listed along with each compound. The instrumental details and the crystallographic parameters are provided in Appendix.

Metallacycle 2.1a: To a methanol solution (20 ml) of $[Co(O_2CCH_3)_2]\cdot 4H_2O$ (0.125 g, 0.5 mmol), *bpy* (0.156 g, 1 mmol) was added and stirred for 30 min. Then 1,8-naphthalic anhydride (0.10 g, 0.5 mmol) was added to the reaction mixture and refluxed at 100 °C for 12 hours. Red colored solution thus obtained was kept for crystallization. Seven days later red crystals were observed. Isolated yield 70 % (based on Co). Elemental analysis (%) for $C_{88}H_{88}O_{32}N_8Co_4$: calcd. C 52.66, H 4.38, N 5.58; found C 52.68, H 4.31, N 6.20. IR (KBr, cm^{-1}): 3410 (br), 1577 (w), 1544 (m), 1456 (m), 1440 (s), 1347 (s), 1325 (m), 1218 (s), 1149 (m), 1080 (m), 1020 (w), 846 (w), 820 (w), 784 (s), 766 (s), 735 (m), 647(w), 617 (w), 573 (w). UV-vis (λ_{max}, solid) 286 nm, 459 nm, 617 nm.

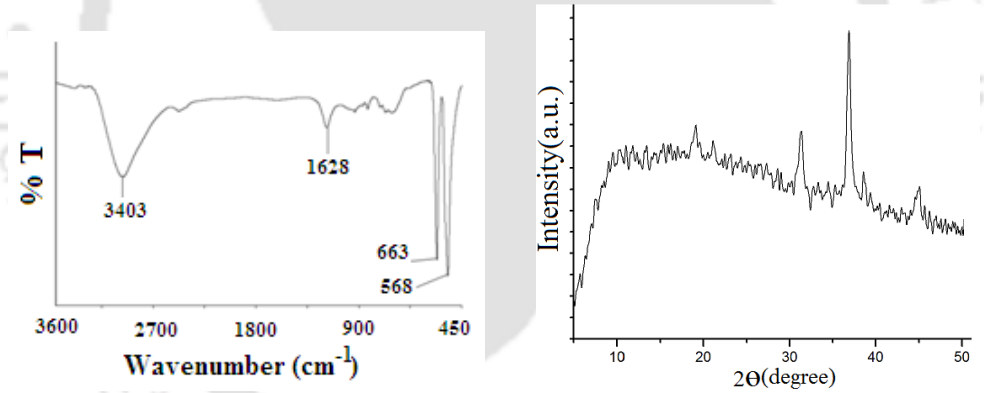

(a) (b)

Figure 2.20: *(a) IR spectrum and (b) PXRD pattern of the residue obtained after heating the metallacycle* ***2.1a*** *up to 420 °C.*

Metallacycle 2.1b: Metallacycle **2.1b** was synthesized in a similar procedure to that of **2.1a**, using $[Co(O_2CCH_3)_2]\cdot 4H_2O$ (0.125 g, 0.5 mmol) in methanol (20 mL), 1,8-naphthalic anhydride (0.10 g, 0.5 mmol), and *phn* (0.180 g, 1 mmol). Isolated yield (based on Co) 69 %. Elemental analysis (%) for $C_{144}H_{120}O_{56}N_{12}Co_6$: calcd. C 52.87, H 3.67, N 6.14; found C 52.66, H 3.68, N 5.60. IR (KBr, cm^{-1}): 3387 (br), 1669 (s), 1618 (s), 1563 (s), 1423 (w), 1407 (s), 1385(w), 1347 (s), 1253 (w), 1220 (m), 1143 (m), 1104 (s), 852 (m), 814 (m), 777 (s), 729 (s), 625 (m). UV-vis (λ_{max}, solid) 263 nm, 467 nm, and 507 nm.

Complex 2.1c: Metallacycle **2.1c** was synthesized by a similar procedure as that of the metallacycle **2.1a**, except nickel (II) acetate tetrahydrate in methanol (20 mL) was used instead of $[Co(O_2CCH_3)_2]\cdot 4H_2O$. Moreover, the molar ratio of 1,8-naphthalic anhydride (0.10 g, 0.5 mmol), nickel (II) acetate (0.124 g, 0.5 mmol), and *bpy* (0.078 g, 0.5 mmol) was taken as 1:1:1. Isolated yield of the green crystals of **2.1c** was 65 % (based on Ni). Elemental analysis (%) for $C_{22}H_{22}N_2NiO_8$: calcd. C 52.73, H 4.43, N 5.59; found C 53.47, H 3.9, N 5.89. IR (KBr, Cm^{-1}): 3431 (br), 1638 (w), 1564 (s), 1429 (m), 1416 (m), 1346 (s), 1228 (m), 1153 (m), 857 (m), 810 (w), 776 (s), 736 (s), 638 (w) cm^{-1}. UV/Visible (solid): λ_{max}= 626 nm and 330 nm.

Metallacycle 2.1d: Metallacycle **2.1d** was synthesized by a similar procedure as that of the metallacycle **2.1b**, except nickel (II) acetate tetrahydrate (0.124 g, 0.5 mmol) in methanol (20 mL) was used instead of $[Co(O_2CCH_3)_2]\cdot 4H_2O$. Moreover, the molar ratio of 1,8-naphthalic anhydride (0.20 g, 1 mmol), nickel (II) acetate (0.124 g, 0.5 mmol), and *phn* (0.180 g, 1 mmol) was taken as 1:2:2. Such ratios in the preparation of the metallacycles **2.1a** and **2.1b** were 1:1:2. Isolated yield of the green crystals of **2.1c** was 72 % (based on Ni). Elemental analysis (%) for $C_{144}H_{148}O_{56}N_{12}Ni_6$: calcd. C 52.49, H 4.53, N 5.10; found C 53.97, H 4.0, N 5.49. IR (KBr, Cm^{-1}): 3447 (br), 1615 (w), 1553 (s), 1427 (m), 1407 (m), 1350 (s), 1223 (m), 1146 (m), 854 (m), 818 (w), 783 (s), 729 (s), 631 (w) cm^{-1}. UV/Visible (solid): λ_{max}= 626 nm and 326 nm.

Metallacycle 2.1e: Metallacycle **2.1e** was prepared in a similar manner that of the compound **2.1d** except (0.156 g, 1 mmol) and 1,8-naphthalic anhydride (0.20 g, 1 mmol in 20 mL DMF) was used with zinc (II) acetate dehydrate (0.110 g, 0.5 mmol, in 10 mL methanol). Colorless crystals were obtained from DMF/methanol solution (1:1), yield 54 % (based on Zn). Elemental analysis (%) for $C_{88}H_{68}O_{22}N_8Zn_4$: calcd. C 57.11, H 3.70, N 6.05; found C 57.04, H 3.87, N 6.02. IR (KBr): 3439 (m), 3195 (br), 1559 (m), 1474 (m), 1432 (s), 1399 (s), 1349 (s), 1220 (s), 1159 (w), 1025 (s), 842 (m), 811 (w), 783 (s), 631 (w), 469 (w) cm^{-1}. UV/Visible (solid): λ_{max}(nm) = 281 and 334.

Metallacycle 2.1f: Metallacycle **2.1f** was synthesized in a similar procedure as that of the metallacycle **2.1e** using 1,8-naphthalic anhydride (0.20 g, 1 mmol in 20 mL DMF) with zinc (II) acetate dehydrate (0.110 g, 0.5 mmol, in 10 mL methanol) and *phn* (0.180 g, 1 mmol). Colorless crystals were obtained after 10-12 d. Yield 61 %. Elemental analysis (%) for $C_{48}H_{34}O_{11}N_4Zn_2$: calcd. C 59.21, H 3.52, N 5.75; found C 59.23, H 3.48, N 5.80. IR (KBr cm^{-1}.): 3435(m), 3157 (br), 1619 (br), 1428(s), 1397 (s), 1347 (s), 1217 (s), 1146 (m), 1104 (m), 867 (w), 843 (s), 810 (m), 782 (s), 725 (s), 627 (m), 470 (m).

Complex 2.2a: Phthalic anhydride (0.29 g, 2 mmol) was added to a methanolic solution (10 mL) of copper (II) acetate monohydrate (0.2 g, 1 mmol) and the reaction mixture was stirred for 30 min. To this reaction mixture, imidazole (0.15 g, 2 mmol) was added, followed by refluxing for 4 h. The reaction mixture was cooled to room temperature, filtered and kept undisturbed for crystallization. Dark-blue crystals of **2.2a** were obtained in one week. Yield, 62 % (based on Cu). For $C_{24}H_{22}CuN_4O_8$: % copper calcd. 11.38; found 11.42. IR (KBr, cm^{-1}): 3214 (br), 1730 (s), 1569 (m), 1390 (s), 1332 (m), 1288 (s), 1265 (s), 1123 (s), 1070 (s), 854 (m), 818 (s), 769 (s), 745 (s), 708 (m), 654 (s), 474 (m). Solid state UV-visible (nm): 275, 651.

Coordination polymer (2.2b): Dark-blue crystals of complex **2.2a** were moistened with a minimal amount of aqueous methanol and kept on a watch glass in an open atmosphere. Their gradual change to light-blue colored crystals of **2.2d** was completed in 2 days. Elemental analysis (%) for $[C_{28}H_{28}Cu_2N_8O_{10}]_n$: calcd. C 44.00, H 3.67, N 14.67; found C 45.10, H 3.49, N 15.03. IR (KBr, cm^{-1}): 3139 (w), 1616 (w), 1549 (br), 1443 (w), 1379 (s), 1329 (w), 1075 (s), 862 (w), 749 (s), 659 (s), 621 (m). Solid state UV-visible (nm): 298, 723.

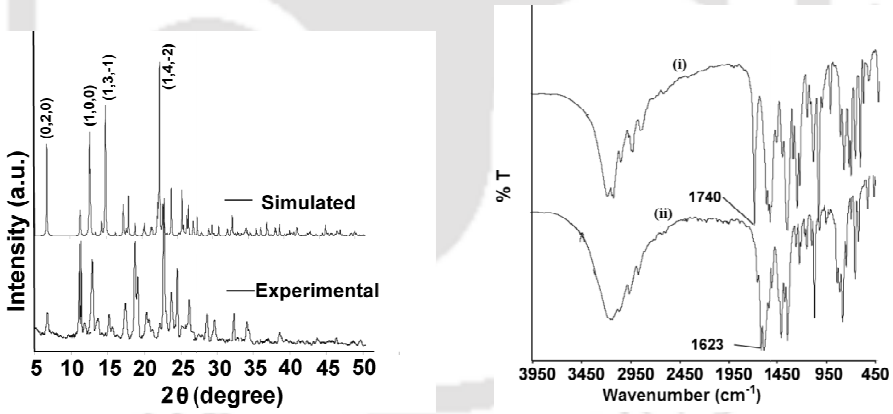

Figure 2.21*: (a) The experimental (bottom) and simulated (top) PXRD of complex* ***2.2c*** *and (b) FT-IR spectra of (i) complex* ***2.2c****; (ii) complex* ***2.2d****.*

Complex (2.2c): This compound was synthesized using a similar procedure used for **2.2a**, except applying 1,8-naphthalic anhydride (0.4 g, 2 mmol) in DMF-methanol solvent (1:1, v/v) instead of phthalic anhydride in methanol. In this case, a 1:2:4 ratio of Cu, 1,8-naphthalic anhydride and imidazole was used. Blue crystals appeared after one week. Yield, 67 % (based on Cu). For $C_{38}H_{34}CuN_8O_8$: % of copper calcd. 7.99, found 8.10. IR (KBr, cm^{-1}): 3129 (br), 1740 (s), 1598 (w), 1577 (s), 1541 (s), 1442 (s), 1395 (s), 1303 (s),

1125 (s), 1074 (s), 1014 (s), 849 (m), 759 (m), 659 (s), 455 (m). Solid state UV-visible (nm): 280, 553.

Complex 2.2d: Blue crystals of **2.2c** were moistened with a minimal amount of aqueous DMF and kept on a watch glass in an open atmosphere. Their gradual change to green crystals of **2.2d** was complete within 1-2 d. Elemental analysis (%) for $C_{36}H_{38}Cu_2N_6O_{12}$: calcd. C 49.44, H 4.35, N 10.99; found C 50.01, H 4.58, N 10.96. IR (KBr, cm^{-1}): 3141 (br), 1662 (w), 1623 (m), 1596 (m), 1409 (s), 1345 (s), 1223 (m), 1071 (s), 843 (w), 784 (s), 657 (s), 623 (s), 465 (m). Solid state UV-visible (nm): 297, 711.

Complex 2.2e: This compound was synthesized by reacting diphenic anhydride (0.45 g, 2 mmol) with copper (II) acetate monohydrate and imidazole in a DMF-methanol solvent (1:1, v/v) using a similar procedure to that used for the synthesis of complex **2.2c**. Blue colored crystals were formed after one week. Yield, 64 % (based on Cu). Elemental analysis (%) for $C_{36}H_{30}CuN_4O_8$: calcd. C 60.88, H 4.26, N 7.89; found C 60.53, H 4.32, N 7.96. IR (KBr, cm^{-1}): 3214 (br), 1730 (s), 1610 (w), 1567(m), 1391 (s), 1289 (s), 1263 (m), 1124(s), 1074(s), 818(s), 768(s), 703 (s), 654 (s), 474 (m). Solid state UV-visible (nm): 276, 574.

Synthesis of 2-(3-(1H-imidazol-1-yl)propyl)isoindoline-1,3-dione, L (2.3): Phthalic anhydride (0.45 g, 3 mmol) was dissolved in warm acetic acid (20 mL) and to this warm solution, 3-(1H-imidazol-1-yl)propan-1-amine (0.360 g, 3 mmol) was added. The reaction mixture was refluxed for 12 h. It resulted in formation of a clear solution which was cooled and diluted with 10 mL of water. Upon standing for about 20 d white crystals were obtained. Yield, 46 % (based on Cu). M. P. = 103 °C. IR (KBr, cm^{-1}): 3116 (w), 2941 (w), 1712 (s), 1466 (w), 1432 (m), 1239 (m), 1078 (w), 1030 (m), 896 (m), 828 (m), 720 (s), 662 (m), 530 (s). Elemental analysis (%) for $C_{14}H_{13}N_3O_2$: calcd. C 65.87, H 5.13, N 16.46; found C 65.89, H 5.11, N 16.47. ^{1}H-NMR (400MHz, DMSO-d_6): 8.06 (*t*, 1H, 5.2Hz), 8.00 (*s*, 1H), 7.84 (*s*, 2H), 7.51 (*t*, 1H, 4.8Hz), 7.35 (*s*, 1H), 7.07 (*s*, 1H), 4.07 (*t*, 2H, 6.8Hz), 3.56 (*t*, 2H, 6.4Hz), 2.07 (*m*, 2H, 6.8Hz). ESI (mass, m/e) 255.9912 (calcd. 255.1008) which correspond to (M) peak.

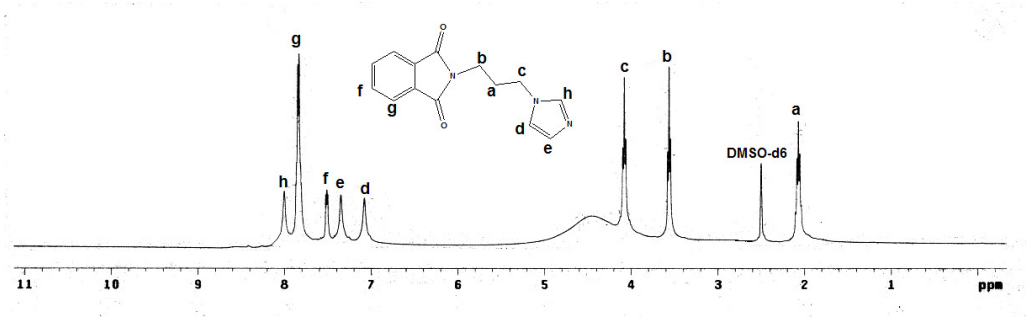

(a)

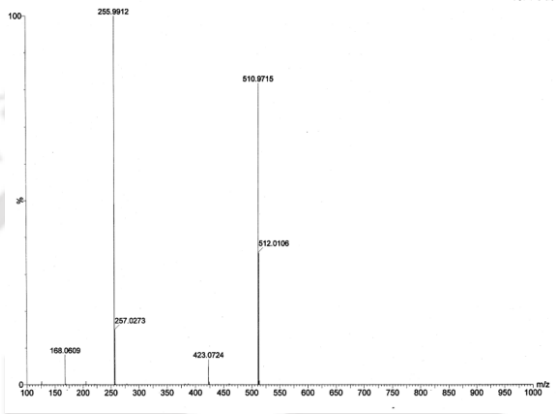

(b)

Figure 2.22**: (a) ^{1}H-NMR spectrum (DMSO-d_6) and (b) ESI mass spectrum of **L.

Complex 2.3a: To a well stirred methanolic (25 mL) solution of the ligand (**L**) (1.02 g, 4 mmol), $CuCl_2 \cdot 2H_2O$ (0.17 g, 1 mmol) was added and stirred for 12 h at room temperature. A blue colored clear solution was obtained. The solution was filtered and allowed to evaporate at room temperature. After 7-8 d blue needle like crystals appeared. Yield, 59 % (based on Cu). Elemental analysis (%) for $C_{56}H_{76}Cl_2CuN_{12}O_{20}$: calcd. C 48.99, H 5.54, N 12.25; found C 48.10, H 5.29, N 11.83. IR (KBr, cm^{-1}): 3457 (br), 3139 (w), 2943(w), 1770 (s), 1708 (s), 1526 (s), 1400 (w), 1384 (s), 1299 (m), 1238 (s), 1102 (s), 1028 (m), 892 (m), 722 (s), 657 (s), 531 (s). UV-visible (solid, λ_{max}): 306 nm and 599 nm.

Complex 2.3b: An identical procedure as for complex **2.3a** was adapted but copper (II) nitrate hexahydrate was used. In this case rod shaped blue crystals were obtained. Yield, 54 % (based on Cu). Elemental analysis (%) for $C_{56}H_{57}CuN_{14}O_{19}$: calcd. C 51.94, H 4.41, N 15.15; found C 50.65, H 4.32, N 14.33. IR (KBr, cm^{-1}): 3456 (br), 1771 (s), 1708 (s), 1579 (s), 1527 (s), 1436 (w), 1401 (s), 1335 (w), 1238 (s), 1112 (s), 1096 (s), 1025 (s), 891 (m), 772 (m), 721 (s), 658 (s), 624 (w), 528 (m). UV-visible (solid, λ_{max}): 304 nm and 584 nm.

Coordination polymer 2.3c: To a solution of **L** (1.02 g, 4 mmol) in methanol, copper (II) acetate monohydrate (0.2g, 1mmol) was added at room temperature and stirred for 12 hours. A clear solution was obtained. The solution was filtered and allowed to evaporate at room temperature. After one week blue prism-like crystals of complex **2.3c** obtained. Yield = 48 % (based on Cu). Elemental analysis (%) for $C_{56}H_{60}Cu_2N_{12}O_{23}$: calcd. C 48.13, H 4.30, N 12.03; found C 47.26, H 4.19, N 11.82. IR (KBr, cm^{-1}): 3460 (br), 1714 (w), 1633 (s), 1566 (s), 1441 (m), 1381 (s), 1322 (s), 1245 (s), 1097 (s), 953 (w), 879 (m), 755 (s), 699 (s), 567 (m), 473 (s). UV-visible (solid, λ_{max}): 301 nm and 574 nm.

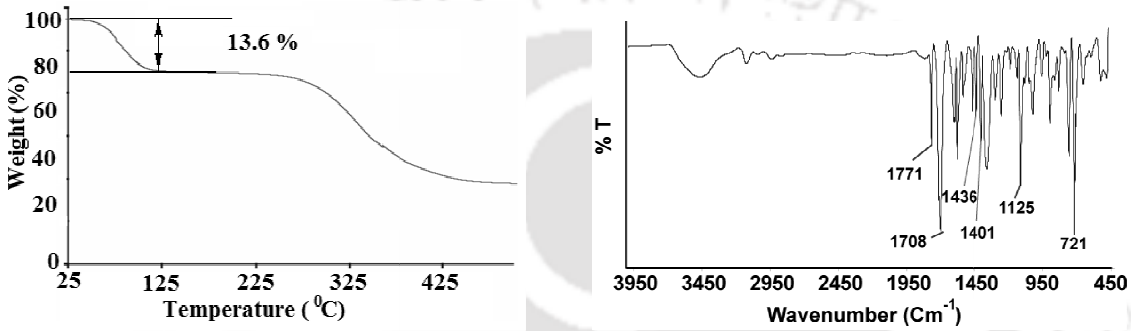

(a) (b)

Figure 2.23: *(a) Thermogram (heating rate 7 °C/min) diagram of* ***2.3a*** *and (b) FT-IR spectrum of the complex* ***2.3b.***

Complex 2.3d: A similar procedure as used for **2.3c** using cadmium acetate as the metal salt resulted in formation of **2.3d**. After 10-12 days, needle shaped colorless crystals were obtained. Yield = 52 % (based on Cu). Elemental analysis (%) for $C_{46}H_{49}CdN_9O_{12}$: calcd. C 53.47, H 4.74, N 12.20; found C 43.01, H 4.62, N 11.68. IR (KBr, cm-1) 3520 (br), 3122 (m), 2944 (w), 1772 (s), 1708 (s), 1610 (m), 1523 (s), 1389 (s), 1234 (s), 1093 (s), 1024 (s), 937 (s), 896 (m), 822 (w), 760 (m), 718(s), 655 (s), 623 (m), 529 (s). ^{1}H-NMR (600MHz, DMSO-d_6): 7.83 (*m*, benzene ring protons), 7.79 (*s*, 1H), 7.28 (*s*, 1H), 6.92 (*s*, 1H), 4.05 (*t*, 2H, 7.2 Hz), 3.55 (*t*, 2H, 6.6 Hz), 2.03 (*t*, 2H, 6.6 Hz), 1.84 (*s*, 3H).

2.7 References:

1. Fish, R. H. *Coord. Chem. Rev.***1999**, *185*, 569-584.
2. Therrien, B. *Eur. J. Inorg. Chem*. **2009**, 2445-2453.
3. Han, Y. F.; Jia, W. G.; Yu, W. B.; Jin, G. X.; *Chem. Soc. Rev*. **2009**, *38*, 3419-3434.
4. Northrop, B. H.; Yang, H. B.; Stang, P. J. *Chem. Commun*. **2008**, 5896-5908.
5. Oshio, H.; Hoshino, N.; Ito, T.; Nakano, M. *J. Am. Chem. Soc*. **2004**, *126*, 8805-8812.

6. Langley, S.; Helliwell, M.; Sessoli, R.; Teat, S. J.; Winpenny, R. E. P. *Dalton Trans*. **2009**, *38*, 3102-3110.
7. Ma, Y.-S.; Song, Y.; Tang, X.-Y.; Yuan, R.-X. *Dalton Trans*. **2010**, *39*, 6262-6265.
8. Barry, N. P. E.; Edafe, F.; Therrien, B. *Dalton Trans*. **2011**, *40*, 7172-7180.
9. Wakatsuki, Y.; Yamazaki, H. *J. Chem. Soc. Dalton Trans*. **1978**, 1278-1282.
10. Ma, Y.; Xue, F.; Tang, X.; Chen, B.; Yuan, R. *Inorg. Chem. Commun*. **2012**, *15*, 285-287.
11. Barooah, N.; Sarma, R.J.; Baruah, J. B. *CrystEngCommun*. **2006**, *8*, 608-615.
12. Chen, Y.; Deng, L. *J. Am. Chem. Soc*. **2001**, *123*, 11302-11303.
13. Rodrignez, B.; Rantanen, T.; Bolm, C. *Angew. Chem., Int. Ed. Engl*. **2006**, *45*, 6924-6926.
14. Atiken, R.A.; Gopal, J.; Hirst, J. A. *J. Chem. Soc. Chem. Commun*. **1988**, 632-634.
15. Baruah, A. M.; Karmakar, A.; Baruah, J. B. *Polyhedron* **2007,** *26,* 4518-4524.
16. Chin, J. *Acc. Chem. Res.* **1991**, *24*, 145-152.
17. Wilcox, D. E. *Chem. Rev*. **1996**, *96*, 2435-2458.
18. Williams, N. H.; Takasaki, B.; Wall M.; Chin, J. *Acc. Chem. Res*. **1999**, *32*, 485-493.
19. Wood, R. D.; Nakon, R.; Angelici, R. J. *Inorg. Chem.* **1978**, *17*, 1088-1090.
20. Nakon, R.; Angelici, R. J. *J. Am. Chem. Soc.* **1973**, *95*, 3170-3174.
21. Mortellaro, M. A.; Bleisch, T. J.; Duerr, B. F.; Kang, M. S.; Huang, H.; Czamik, A. W. *J. Org. Chem.* **1995**, *60***,** 7238-7246.
22. Duerr, B. F.; Czarnik, A.W. *Tetrahedron Lett.* **1989**, *30***,** 6951-6954.
23. Suh, J.; Chung, S.; Lee, S. H. *Bioorg. Chem.* **1987**, *15,* 383-408.
24. Hay, R.W.; You-Quan, C. *Polyhedron* **1995**, ***14***, 869-872.
25. Baruah, J. B. *J. Chem. Sci.* **2011**, *123*, 123-129.
26. Baruah, A. M.; Karmakar, A.; Baruah, J. B. *Polyhedron* **2007**, *26***,** 4479-4488.
27. King, S. A. *J. Org. Chem.* **1994**, *59***,** 2253-2256.
28. Ranadive, V. B.; Samant, S. D. *Indian J. Chem. Sect. B* **1995**, *34B*, 102-106.
29. Yamskov, I. A.; Berezin, B. B.; Belchich, L. A.; Davankov, V. A. *Die Makromolekulare Chemie* **1979**, *180***,** 799-802.
30. Raycroft, M. A. R.; Cimpean, L.; Neverov, A. A.; Brown, R. S. *Inorg. Chem*. **2014**, *53***,** 2211-2221.
31. Brohmer, M. C.; Bannwarth, W. *Eur. J. Org. Chem.* **2008**, 4412-4415.
32. Brohmer, M. C.; Mundinger, S.; Brase, S.; Bannwarth, W. *Angew. Chem., Int. Ed.* **2011**, *50***,** 6175-6177.
33. Barrera, I. F.; Maxwell, C. I.; Neverov, A. A.; Brown, R. S. *J. Org. Chem.* **2012**, *77*, 4156-4160.
34. Raycroft, M. A. R.; Maxwell, C. I.; Oldham, R. A. A.; Saffouri Andrea, A.; Neverov, A. A.; Brown, R. S. *Inorg. Chem.* **2012**, *51*, 10325-10333.
35. Morrow, J. R.; Trogler, W. C. *Inorg. Chem.* **1988**, *27***,** 3387-3394.

36. Deal, K. A.; Burstyn, J. N. *Inorg. Chem.* **1996**, *35*, 2792-2798.
37. Menger, F. M.; Can, L. H.; Johnson, E.; Durst, D. H. *J. Am. Chem. Soc.* **1987**, *109*, 2800-2803.
38. Serpersu, E. H.; Shortle, D.; Mildvan, A. S. *Biochemistry* **1987**, *26,* 1289-1300.
39. Williams, N. H.; Takasaki, B.; Wall, M.; Chin, J. *Acc. Chem. Res.* **1999**, *32*, 485-493.
40. Shell, T. A.; Mohler, D. L. *Curr. Org. Chem.* **2007,** *11,* 1525-*1542.*
41. Sumaoka, J.; Yamamoto, Y.; Kitamura, Y.; Komiyama, M. *Curr. Org. Chem.* **2007**, *11,* 463-475.
42. Morrow, J. R.; Iranzo, O. *Curr. Opin. Chem. Biol.* **2004***, 8,* 192-200.
43. Reichenbach-Klinke, R.; Konig, B. *J. Chem. Soc. Dalton Trans.* **2002**, 121-130.
44. Weijnen, J. G. J.; Koudijs, A.; Engbersen, J. F. G. *J. Chem. Soc. Perkin Trans*. **1991**, *2*, 1121-1126.
45. Bunton, C. A.; Savelli, G. *Adv. Phys. Org. Chem.* **1986**, *22*, 213-309.
46. Fendler, J. H.; *Membrane Mimetic Chemistry*, Wiley & Sons, New York, **1982.**
47. Wang, D. K.; Rasoul, F.; Hill, D. J. T.; Hanson, G. R.; Noble, C. J.; Whittaker, A. K. *Soft Matter* **2012**, *8*, 435-445.
48. *Ogawa*, *J.*; *Shimizu*, *S.*; In *Stereoselective Biocatalysis*, *Patel*, *R. N. Ed. Marcel Dekker Publ. New York*, ***2000***, 1-21.
49. Ong, B. L.; Jackson, J. F. *Biochem. J.* **1972**, *129*, 583-593.
50. Kim, H.; Jang, J. *Polymer* **2000**, *41*, 6553-6561.
51. Li, Y.; Lu, Q.; Qian, X.; Zhu, Z.; Yin, J. *Appl. Surf. Sci.* **2004**, *233*, 299-306.
52. Desiraju, G. R. *Acc. Chem. Res.* **2002**, *35*, 565-573.
53. Zaman, M. B.; Udachin, K. A.; Ripmeester, J. A. *Cryst. Growth Des.* **2004**, *4*, 585-589.
54. Desiraju, G. R. *Angew. Chem., Int. Ed. Engl.* **1995**, *34*, 2311-2327.
55. Desiraju, G. R. *Angew. Chem., Int. Ed.* **2011**, *50*, 52-59.
56. Blake, A. J.; Champness, N. R.; Cooke, P. A.; Nicolson, J. E. B. *Chem. Commun.* **2000**, 665-666.
57. Wang, X.-W.; Chen, Y.; Chen, J.-Z.; Liu, J.-H.; Han, L. *Z. Naturforsch* **2008**, *63b*, 129-133.
58. Kumar, N.; Kachroo, P. L.; Kant, R. *J. Therm. Anal. Calorim*. **1979**, *17*, 81-85.
59. Ye, B.-H.; Chen, X.-M.; Xue, F.; Ji, L.-N.; Mak, T. C. W. *Inorg. Chim. Acta* **2000**, *299*, 1-8.
60. Klower, F.; Lan, Y.; Nehrkorn, J.; Waldmann, O.; Anson, C. E.; Powell, A. K. *Chem. Eur. J.* **2009**, *15*, 7413-7422.
61. Phukan, N.; Baruah, J. B. *RSC Adv*. **2013**, *3*, 1151-1157.
62. Klower, F.; Lan, Y.; Nehrkorn, J.; Waldmann, O.; Anson, C. E.; Powell, A. K.; *Chem. Eur. J.* **2009**, *15*, 7413-7422.

63. Baruah, A. M.; Karmakar, A.; Baruah, J. B. *Polyhedron* **2007**, *26,* 4479-4488;
64. Baca, S. G.; Filippova, I. G.; Gerbeleu, N. V.; Simonov, Y. A.; Gdaniec, M.; Timco, G. A.; Gherco, O. A.; Malaestean, Y. L. *Inorg. Chim. Acta* **2003**, *344*, 109-116;
65. Simonov, Y. A.; Baca, S. G.; Filippova, I. G.; Gdaniec, M.; Gherco, O. A.; Gerbeleu, N. V. *Russ. J. Coord. Chem.* **2004**, *30*, 727-732.
66. Fondo, M.; Deibe, A. M. G.; Ocampo, N.; Bermejo, M. R.; Sanmartin, J. *Z. Anorg. Allg. Chem*. **2005**, *631*, 2041-2045.
67. Chen, H.-H.; Yang, J.; Liu, Y.-Y.; Ma, J.-F. *CrystEngComm* **2013**, *15*, 5168-5178.
68. Reger, D. L.; Pascui, A. E.; Foley, E. A.; Smith, M. D.; Jezierska, J.; Ozarowski, A. *Inorg. Chem.* **2014**, *53*, 1975-1988.
69. Worl, S.; Pritzkow, H.; Fritsky, I. O.; Kramer, R. *Dalton Trans*. **2005**, 27-29.
70. Moubaraki, B.; Murray, K. S.; Hudson, T. A.; Robson, R. *Eur. J. Inorg. Chem*. **2008**, 4525-4529
71. *Katsenis, A. D.; Kessler,* V. *G.; Papaefstathiou, G. S. Dalton Trans*. **2011**, *40*, 4590-4598.
72. Brohmer M. C.; Bannwarth, W. *Eur. J. Org. Chem*. **2008**, *26*, 4412-4415.
73. Barrera, I. F.; Maxwell, C. I.; Neverov A. A.; Brown, R. S. *J. Org. Chem*. **2012**, *77*, 4156-4160.
74. Blatov, V. A.; *IUCr Comp. Comm. Newsletter*, **2006**, *7*, 4-38.
75. Blatov, V. A.; Proserpio, D. M. *in Modern methods of crystal structure prediction*, ed. A. R. Oganov, Wiley, **2010**, 1-28.
76. Blatov, V. A.; O'Keeffe M.; Proserpio, D. M. *CrystEngComm* **2010**, *12*, 44-48.
77. Alexandrov, E. V.; Blatov, V. A.; Kochetkova A. V.; Proserpio, D. M. *CrystEngComm* **2011**, *13*, 3947-3958.
78. O'Keeffe, M.; Yaghi, O. M. *Chem. Rev*. **2012**, *112*, 675-702.
79. Delgado, F. S.; Sanchiz, J.; Ruiz-Perez, C.; Lloret F.; Julve, M. *Inorg. Chem*. **2003**, *42*, 5938-5948.
80. Bondi, A. *J. Phys. Chem*. **1964**, *68*, 441-451.
81. Baca, S. G.; Reetz, M. T.; Goddard, R.; Filippova, I. G.; Simonov, Y. A.; Gdaniec M.; Gerbeleu, N. *Polyhedron* **2006**, *25*, 1215-1222.
82. Karle, I. L.; Venkateshwarlu, P.; Nagaraj, R.; Sarma, A. V. S.; Vijay, D.; Sastry, N. G.; Ranganathan, S. *Chem. Eur. J.* **2007**, *13*, 4253-4263.
83. Bertini, I.; Gray, H. B.; Lippard, S. J.; Valentine, J. S. *Bioinorganic Chemistry*, First South Asian ed., **1998**.

CHAPTER 3

Divalent Manganese, Cobalt, Zinc, Cadmium and Mercury complexes of imidazole tethered to 1,8-naphthalimide

Naphthalimide derivatives are commonly used as fluorescence probes[1-5] and optical materials.[6] Study on chromogenic properties of naphthalimide derivatives help us to understand biological interactions.[7-8] Naphthalimides have vast photochemistry[9-10] and they are used to make bio-models for anion transport.[11-13] Solar cells are developed based on ruthenium complexes of naphthalimides.[14] Stacking interactions between naphthalimides generate interesting structures.[15-18] Naphthalimides have capability to bind with DNA[19-21] and act as anticancer agents.[22-26] Naphthalimide based dyads are potent inhibitors against human β-*N*-acetyl-D-hexosaminidase.[27] Furthermore, imide containing flexible ligands are useful in synthesis of metal complexes with diverse structural variations.[28-29] Naphthalimide itself is not a good ligand to bind to metal ions. By making N-substitutions with various functional groups, they can be used as fluorescence probes for different ions.[30-33] Imidazole is a ubiquitous and essential group in biology, especially as a metal-coordinating site.[34-35] Imidazole based naphthalimide have been shown to have interesting DNA binding ability and anticancer activity.[36] Naphthalimide derivatives shows interesting fluorescence properties depending on various metal salts.[37-38] Such studies are limited to understand the role of cations to change optical properties. Thus, we have chosen a ligand N-(3-imidazol-1-yl-propyl)-1,8-naphthalimide (**L^1**), which is a substituted naphthalimide with three intervening methylene groups, connected to an imidazole. This compound is chosen as it is expected to adapt different conformations such as linear or bent as illustrated in Figure **3.1**. Stabilization of any of such a structure would influence fluorescence properties of naphthalimide ring. On the other hand, some N-functionalized 1,8-naphthalimide compounds having a nitrogen-heterocyclic ring show dual fluorescence properties.[39] Dual fluorescence in such compounds originate from charge transfer through an excited state with extended conjugation (ESEC).[40-44] Ligand, **L^1** on complexation with metal ion can be organized in different ways such as linear or bend but having imidazole ring parallelly placed over naphthalimide ring or imidazole ring placed perpendicularly over naphthalimide ring as illustrated Figure **3.2**. When N-(3-imidazol-1-yl-propyl)-1,8-naphthalimide adapt a stretched geometry (Figure **3.2a),** lone pair of electrons present on imidazole nitrogen atom would less likely to contribute to the

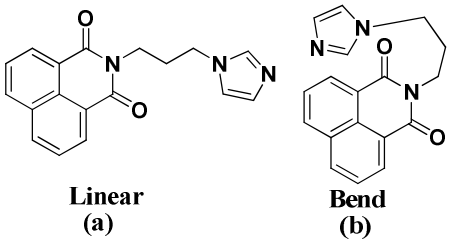

***Figure 3.1**: Different conformations of the ligand (a) linear and (b) bend.*

photo-induced electron transfer (PET) process as it will have a projection away from the naphthalimide ring whereas the geometry shown in Figure **3.2b** has a parallel orientation over an electron deficient naphthalimide ring which would favor an intramolecular charge transfer process. A geometry shown in Figure **3.2c** would help in formation of exciplex

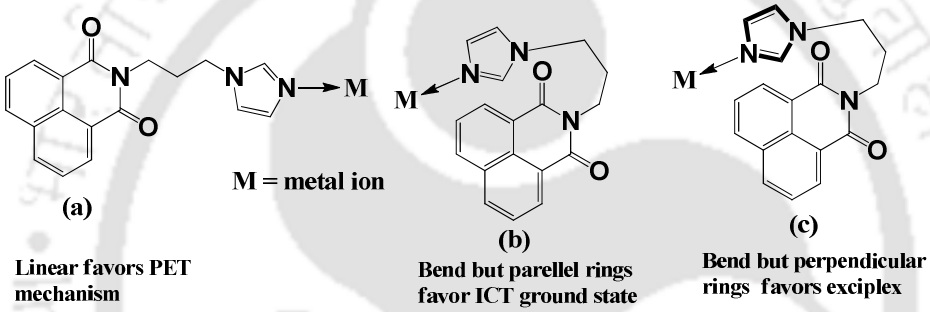

***Figure 3.2**: Geometries of L^1 attached to a metal ion (a) linear form; and bend forms having (b) parallel or (c) non-parallel orientation of the imidazole ring over the 1,8-naphthalimide ring.*

state. Because of these orientations, different kind of mechanism would be involved to cause drastic change in fluorescence spectra. On the other hand, a metal ion may have a role in stabilizing any of these conformations while forming a metal complex. For these reasons, we have choosen $\mathbf{L^1}$ to synthesize some transition metal complexes and to find out if there any correlation between structure and fluorescence property.

3.1 Synthesis and characterization of N-(3-imidazol-1-yl-propyl)-1,8-naphthalimide:

N-(3-imidazol-1-yl-propyl)-1,8-naphthalimide was reported earlier and we followed a synthetic procedure in which 1-(3-aminopropyl)imidazole and 1,8-naphthalic anhydride was condensed in dimethylformamide whereas in the reported procedure it was prepared in toluene.[36] Compound was characterized by various spectroscopic techniques such as FT-IR, NMR and ESI-Mass spectrometry. In IR spectrum, the carbonyl stretching frequencies of the compound are observed at 1689 cm^{-1} and 1650 cm^{-1}; whereas C-N and

C-H stretching frequencies are observed at 1236 cm^{-1} is 2941 cm^{-1} respectively. In ^{1}H-NMR of **L^1,** multiplet at 2.26 ppm, triplet at 4.06 ppm and triplet at 4.22 ppm are for the protons of three methylene groups. On the other hand, signals for the imidazole protons appear at 7.03 ppm and 7.56 ppm. Naphthalene protons appear at 8.58 ppm and at 8.21 ppm as doublet and one triplet at 7.78 ppm (Figure **3.15b** in the experimental section). ^{13}C-NMR shows peak at 29.1, 37.1 and 44.4 ppm due to methylene carbons; at 118.4, 127.6 and 133.9 ppm for imidazole carbons; at 121.8, 126.5, 128.9, 130.8 and 136.8 ppm due to carbons on naphthalene ring. Peak at 163.7 ppm (Figure **3.3**) is attributed to the carbonyl carbon.

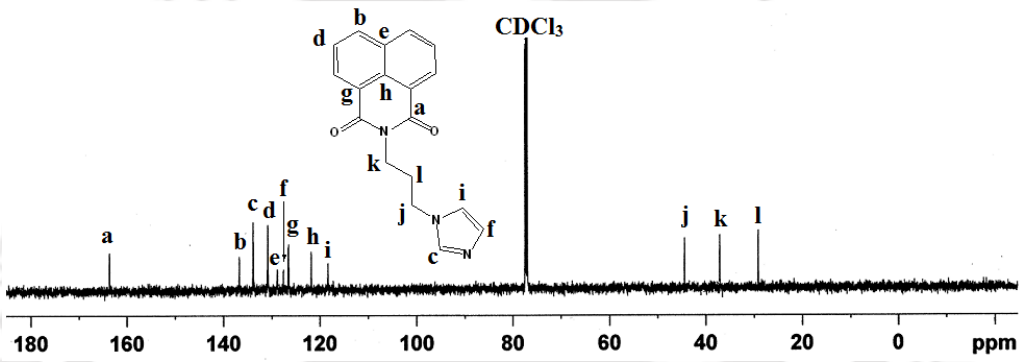

***Figure 3.3**: ^{13}C-NMR (150 MHz, $CDCl_3$) spectrum of the ligand, **L^1**.*

3.2. Metal complexes of N-(3-imidazol-1-yl-propyl)-1,8-naphthalimide:

Since N-(3-imidazol-1-yl-propyl)-1,8-naphthalimide is a neutral ligand, we took up a study to prepare metal thiocyanate complexes having **L^1,** as some metal thiocyanate complexes themselves show interesting photoluminescence properties.[14] Besides this, ruthenium thiocyanate complexes are extensively used in dye sensitized solar cell.[45-46] Hence, several thiocyanate complexes of manganese (II), cobalt (II), zinc (II) and cadmium (II) having N-(3-imidazol-1-yl-propyl)-1,8-naphthalimide were prepared by reacting different metal salts with potassium thiocyanate. When such reactions were carried out with manganese (II) chloride or cobalt (II) chloride corresponding thiocyanate complexes were obtained with metal to **L^1** ratio 1:4. On the other hand, reactions of zinc (II) nitrate and cadmium (II) nitrate yielded thiocyanate complexes but with metal to **L^1** ratio 1:2 and 1:4 respectively. Similar reaction of zinc (II) chloride or cadmium (II) chloride or mercury (II) chloride with or without potassium thiocyanate but in presence of **L^1** resulted in chloro complexes without incorporation of thiocyanate ligand having metal

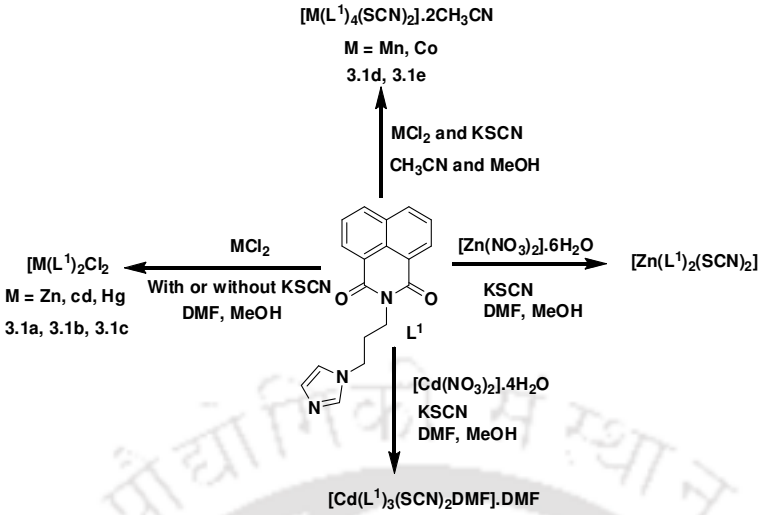

Scheme 3.1 *Reaction of* ***L*** ^{1} *with different metal salts (where DMF = N,N'-dimethylformamide; MeOH = methanol)*

to $\mathbf{L}^{1}$ in 1:2 ratios. The thiocyanate complexes were being sorted due to their interesting photoluminescence properties in different metal complexes.[43] Reaction of $\mathbf{L}^{1}$ with different metal salts are illustrated in Scheme **3.1**. All the complexes were characterized by their elemental analyses and further characterized by various spectroscopic techniques. The structures of the complexes were characterized by single crystal X-ray diffraction. To ascertain the bulk purity of the complexes, powder X-ray diffraction patterns of each sample was recorded. By comparing the experimental PXRD patterns with simulated patterns we found good agreement between them for all the complexes which confirmed the presence of single compound in each case.

Zinc, cadmium and mercury chloride complexes having formula [M$\mathbf{L}^{1}_{2}$Cl$_2$] were non ionic. They show molar conductance values in the range of 15-21 S cm^2 mol^{-1}.

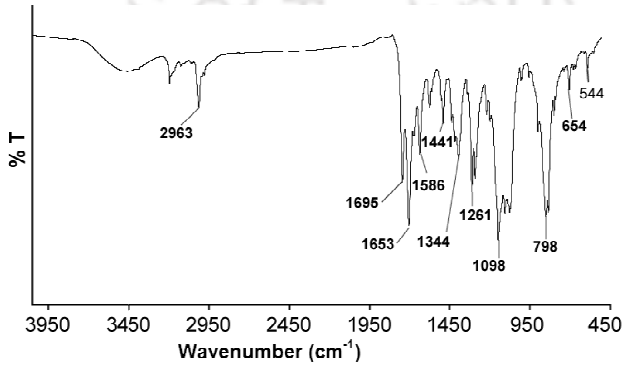

Figure 3.4*: FT-IR spectrum of the complex* ***3.1a****.*

These complexes show an additional stretching frequency in IR spectrum observed in the range 530-544 cm^{-1} in addition to naphthalimide ligand which is due to metal-nitrogen bond stretching vibrations. Carbonyls stretching frequencies of the naphthalimide rings are less significantly affected showing that they don't participate in coordination to metal ion. One representative IR spectrum of complex **3.1a** is shown in Figure **3.4.**

^{1}H-NMR spectra of complexes **3.1a-3.1c** are compared with that of the ligand, $\mathbf{L^1}$ which is shown in Figure **3.5**. From these spectra it is clear that signals appear for naphthalimide protons, imidazole ring protons and methylene protons are slightly shifted in each case. In complex **3.1a** the shift observed is nominal whereas complex **3.1b** and **3.1c** has considerable difference from the parent ligand.

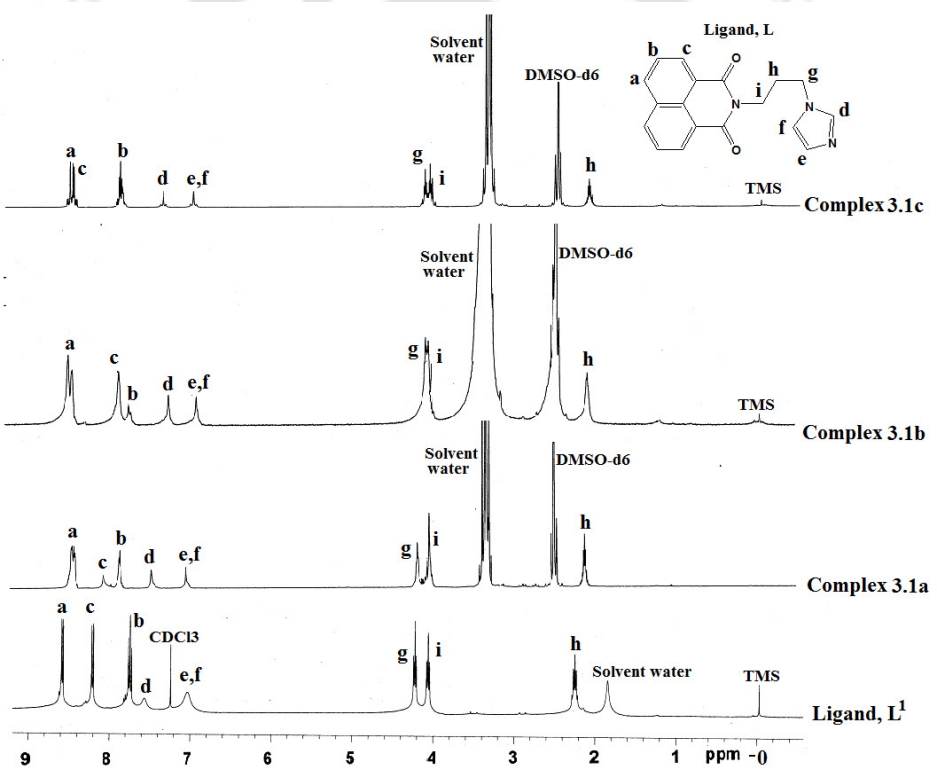

***Figure 3.5**: ^{1}H-NMR spectra of $\mathbf{L^1}$ ($CDCl_3$) and complex **3.1a-3.1c** (600MHz, DMSO-d_6).*

This difference is especially with respect to the signals of the methylene groups of $\mathbf{L^1}$ which appear as two distinct sets of triplets at 4.06 and 4.22 ppm. These two triplets merged to one multiple in **3.1b** and appear in very closely spaced chemical shift. Such merging of peaks is also observed in case of some other protons. From the spectra it is clear that the complexes are stable in solution. This clearly shows that there is some shielding contribution of the metal ions on the chemical shift of these peaks. Such shielding effects are observed in

imidazole protons assigned as d, e, f in Figure **3.5**. The chemical shift differences observed in the complexes suggest their stability in solution.

From the single crystal X-ray structure it was found that three complexes **3.1a**-**3.1c** were isomorphous. This means that crystals of the complexes belong to same space group having similar structure but differ in bond parameters. This is due to obvious reasons of having different metal ions. Single crystal X-ray analysis revealed that the complexes **3.1a**-**3.1c** crystallized in monoclinic C2/c space group and each metal ion lies on a two fold axis. Asymmetric unit in each case contains one ligand, one chloride ion and half of the metal ion. One illustrative example of the structure of complex **3.1a** is shown in Figure **3.6a**. The complex has symmetry related Cl1 and Cl1' related by two fold axis, same is to for atoms N1 and N1'. The symmetry operators are given in the figure caption.

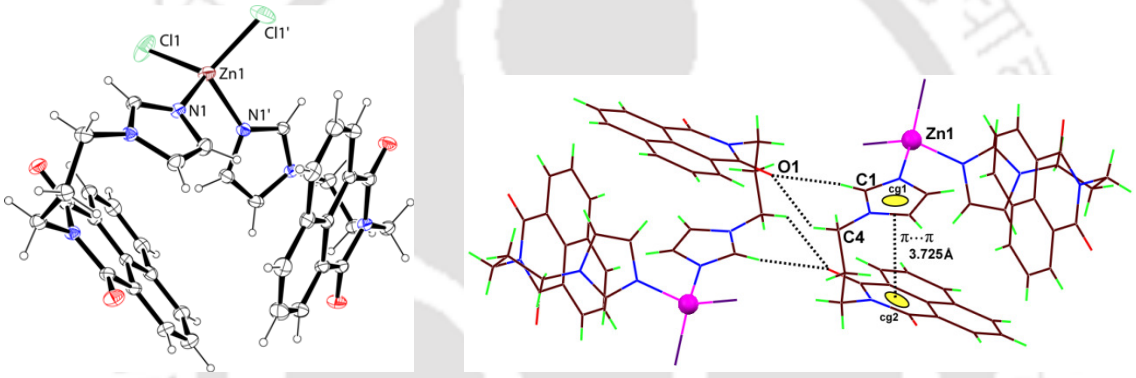

(a) (b)

Figure 3.6**: (a) ORTEP view of **3.1a** (30% thermal ellipsoid probability); symmetry of ' = [2-x, y, (1/2)-z]; selected bond distances are (Zn1-N1 = 2.028(2) Å; Zn1-Cl1 = 2.237(11) Å). (b) Weak interactions showing C-H···O and π···π stacking ($d_{cg1-cg2}$= 3.725 Å, where cg1 = centre of gravity of imidazole ring and cg2 = centre of gravity of imide ring) interactions in **3.1a.

Compound **3.1a** has a distorted tetrahedral geometry and it is a four coordinated zinc (II) complex. The coordination geometry around zinc ion comprises of two coordinating N atoms of imidazole of $\mathbf{L^1}$ and two chloride ligands. $\mathbf{L^1}$ in these cases adapts a bend structure. Bend form of the ligand is stabilized by weak C-H···O and π···π stacking interactions as shown in Figure **3.6b**. These weak interactions arise from intermolecular interactions between the carbonyl group of 1,8-naphthalimide with one imidazole C-H ($d_{C\cdots O}$ = 3.214 Å) and another C-H bond of the propylene group at the α-position next to the imidazole unit ($d_{C\cdots O}$ = 3.262 Å). The formation of intramolecular stacking interaction between imidazole and naphthalene ring is favored by the flexible propylene group. This π···π interaction distance between imidazole ring and imide ring is found to be 3.725 Å. Since the other two

complexes have similar geometries, these are not discussed here in details but the metal-ligand bond parameters are listed in Table **3.1**.

Table 3.1**: Metal-ligand bond parameters of the complexes **3.1a-3.1c.

Compd. No.	M-L	d_{M-L}(Å)	∠L-M-L	Angle (°)	∠ L-M-L	Angle (°)
3.1a	Zn1-N1	2.028(2)	N1-Zn1-N1	99.41(13)	N1-Zn1-Cl1	112.63(7)
	Zn1-Cl1	2.237(11)	N1-Zn1-Cl1	107.74(7)	Cl1-Zn1-Cl1	115.58(8)
3.1b	Cd1-N1	2.231(2)	N1-Cd1-N1	94.99(12)	N1-Cd1-Cl1	112.84(7)
	Cd1-Cl1	2.413(10)	N1-Cd1-Cl1	107.93(7)	Cl1-Cd1-Cl1	118.00(7)
3.1c	Hg1-N1	2.268(7)	N1 -Hg1-N1	92.3(4)	N1-Hg1-Cl1	111.5(2)
	Hg1-Cl1	2.451(5)	N1- Hg1-Cl1	106.3(2)	Cl1-Hg1-Cl1	124.2(3)

From Table **3.1,** it can be seen that metal-ligand bond distances are in the sequence Zn < Cd < Hg. The observed trend is due to the increase in the size of the metal ions. The π···π distance between imidazole and imide ring in case of cadmium (II) and mercury (II) complexes are observed to be 3.707 Å and 3.735 Å respectively. Powder XRD patterns of the complexes **3.1a**-**3.1c** recorded and compared with the simulated patterns and found similarity between the two patterns which confirmed the phase purity in these complexes.

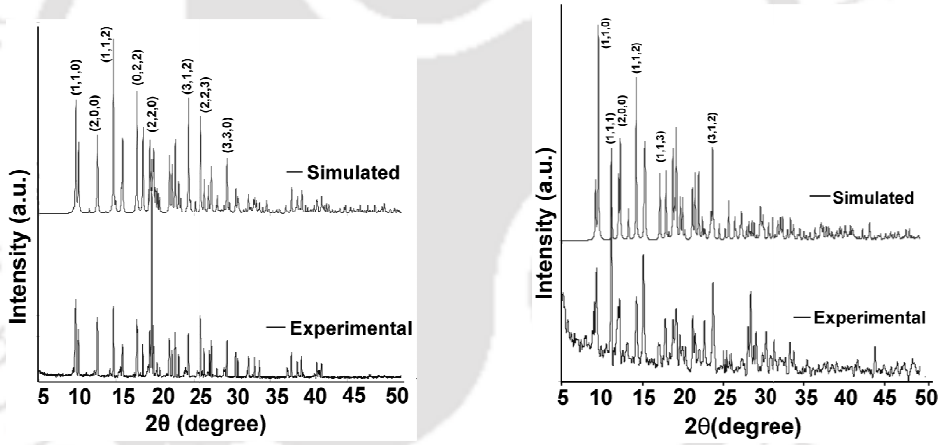

***Figure 3.7**: Comparison of the simulated (top) and the experimental (bottom) PXRD of the complex (a) **3.1a** and (b) **3.1c**.*

PXRD patterns of complex **3.1a** and **3.1c** are shown in Figure **3.7**. As mentioned in the Scheme **3.1,** the complexes **3.1d**-**3.1g** are metal thiocyanate complexes. Thiocyanate is an ambidentate ligand and it can form metal complex by coordinating through nitrogen atom or sulphur atom. FT-IR spectra of thiocyanate complexes **3.1d-3.1g** show the characteristic stretching frequencies of thiocyanate in the region of 2051-2075 cm^{-1}. These values show the presence of thiocyanate ions in complexes **3.1d**-**3.1g** where it binds through a nitrogen atom to the metal ion in each case.[47] The composition of complexes **3.1d**-**3.1g** differs in numbers of $\mathbf{L^1}$ present in each case.

In both manganese (II) and cobalt (II) complexes the metal to ligand ($\mathbf{L^1}$) ratio is 1:4. Zinc (II) complex **3.1f** of $\mathbf{L^1}$ having thiocyanate ligand has 1:2 Zn to $\mathbf{L^1}$ ratio whereas in case of cadmium (II) complex **3.1g** has 1:3 cadmium to $\mathbf{L^1}$ ratio. These values are ascertained on the basis of elemental analysis.

Manganese complex **3.1d** and cobalt complex **3.1e** have similar composition, namely $[M\mathbf{L^1}_4(SCN)_2]\cdot 2CH_3CN$ {M = Mn (**3.1d**) and M = Co (**3.1e**)}and these two complexes are isomorphous. Crystals of complexes **3.1d** as well as **3.1e** belong to triclicnic *P-1* space group. Structures of these two complexes are highly symmetric. Asymmetric unit of each of the two complexes contain two ligands ($\mathbf{L^1}$), one thiocyanate ligand, half of the metal ion and one lattice acetonitrile molecule outside the coordination sphere. The manganese atom in the complex **3.1d** and the cobalt atom in the complex **3.1e** lie on an inversion centre.

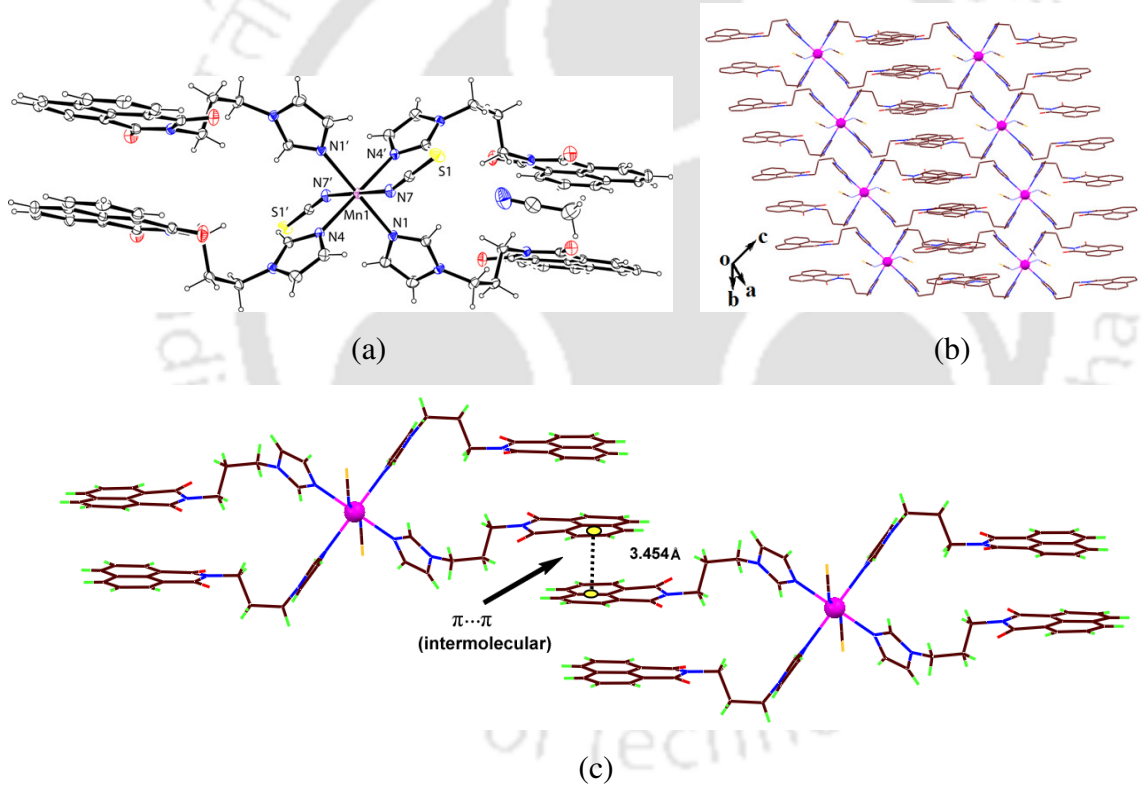

Figure 3.8: *(a) ORTEP view (30% thermal ellipsoid probability) of complex* ***3.1d;*** *symmetry of ' = (-x, 1-y, -z); (b) Supramolecular 3D layer structure and (c) diagram showing intermolecular π···π interactions of complex* ***3.1d****.*

Distorted octahedral geometry around manganese (II) or cobalt (II) centre of six coordinated complexes **3.1d** and **3.1e** are satisfied by two types four crystallographically equivalent nitrogen atoms of four imidazole groups of $\mathbf{L^1}$ (Mn1-N1 2.275(19) Å; Mn1-N4 2.260(19) Å; Co1-N1 2.169(4) Å; Co1-N4 2.161(4)) and two crystallographically equivalent nitrogen

atoms of two thiocyanate ligands (Mn1-N7 2.236(2) Å); Co1-N7 2.157(4) Å). Thus two thiocyanate ligands occupy the axial positions of a distorted octahedral geometry.

Crystal structure of the complex **3.1d** is shown in Figure **3.8a**. Metal-ligand bond parameters of these complexes are listed in the Table **3.2**. The interesting feature of these two structures is that the naphthalimide rings are π-stacked with another naphthalimide ring of neighbouring molecules on each side so that 3D supramolecular layered structures are formed (Figure **3.8b**). These stacking interactions favor between the naphthalene rings as the ligand $\mathbf{L^1}$ in the two complexes adapts a linear structure (Figure **3.8c**). While forming such structures the imidazole rings are not in one plane with respect to naphthalimide ring across the metal centres. This π···π interaction distances in these two complexes are 3.454 Å and 3.434 Å in case of manganese (II) and cobalt (II) complex respectively.

***Table 3.2**: Metal-ligand bond parameters of the complexes **3.1d-3.1g**.*

Compd. No.	M-L	d_{M-L} (Å)	∠ L-M-L	Angle (°)	∠ L-M-L	Angle (°)
3.1d	Mn1- N1	2.275(19)	N1- Mn1- N4	88.12		
	Mn1- N4	2.260(19)	N1- Mn1- N7	89.67		
	Mn1- N7	2.236(2)	N4- Mn1- N7	92.67		
3.1e	Co1- N1	2.169(4)	N1- Co1- N4	88.92		
	Co1- N4	2.161(4)	N1- Co1- N7	90.37		
	Co1- N7	2.157(4)	N4- Co1- N7	92.64		
3.1f	Zn1-N1	1.986(3)	N1-Zn1 -N4	114.52(10)	N4 -Zn1-N8	102.27(11)
	Zn1-N4	1.997(3)	N1-Zn1 -N7	103.77(11)	N7- Zn1-N8	111.58(12)
	Zn1-N7	1.972(3)	N1-Zn1 -N8	115.03(12)		
	Zn1-N8	1.940(3)	N4-Zn1 -N7	109.85(12)		
3.1g	Cd1-N1	2.327(2)	N1-Cd1-N4	178.09(7)	N4-Cd1-N11	90.36(8)
	Cd1-N4	2.335(2)	N1-Cd1-O7	88.72(8)	N4-Cd1-N7	87.37(7)
	Cd1-N7	2.339(2)	N1-Cd1-N11	91.18(9)	N4-Cd1-N10	90.92(8)
	Cd1-N10	2.340(3)	N1-Cd1-N7	93.77(7)	N7-Cd1-N10	92.63(9)
	Cd1-N11	2.343(3)	N1-Cd1-N10	87.50(9)	N11-Cd1-N10	177.69(9)
	Cd1-O7	2.337(2)	N4-Cd1-O7	90.20(8)	O7-Cd1-N7	176.79(8)
			O7-Cd1-N11	88.57(9)	O7-Cd1-N10	89.50(9)

The metal complexes bearing the thiocyanate ligand have gained special interest due to their ease of degradability and their labile nature.[48]

From the thermogravimetric analysis, it is seen that for the complex **3.1d**, one step weight loss due to the two solvent acetonitrile molecules take place in the temperature range 70-170 °C (observed weight loss of 5.1 %, calcd. weight loss of 5.6 %). The weight loss of coordinated thiocyanate molecules and decomposition of organic ligand started at 250 °C and ended at about 460 °C (Figure **3.17a** in experimental section). Similar trends in weight loss of the isomorphous complex **3.1e** to that of the complex **3.1d** are observed. The two solvent acetonitrile molecules are lost in the range 88-200 °C (observed weight loss of 5.4 %, calcd. 5.5 %) and the weight loss of the coordinated thiocyanate molecules started from 260 °C and ends at 460 °C. Powder X-ray diffraction patterns of these two complexes **3.1d**-**3.1e** recorded and compared with the simulated patterns which show similarity between

experimental and simulated patterns. This confirms the bulk purity of the complexes. One representative PXRD pattern is shown in Figure **3.17b** in the experimental section.

Zinc thiocyanate complex having a composition [Zn$\mathbf{L^1}_2(SCN)_2$] (**3.1f**) crystallized in monoclinic $P2_1/c$ space group. In FT-IR spectrums, it shows stretching frequency of C=N bond at 2075 cm^{-1} for thiocyanate ligand which is shown in Figure **3.9a**. Besides this, it has signals from naphthalimide ligand at 1691, 1651 cm^{-1} due to the carbonyl stretching. Metal-nitrogen bond vibration appeared at 530 cm^{-1}. Structure of the complex determined by X-ray crystallography is shown in Figure **3.9b**. The asymmetric unit of the complex contains one metal ion, two ligands ($\mathbf{L^1}$) and two coordinated thiocyanate molecules. It is a four coordinated zinc complex with a distorted tetrahedral geometry.

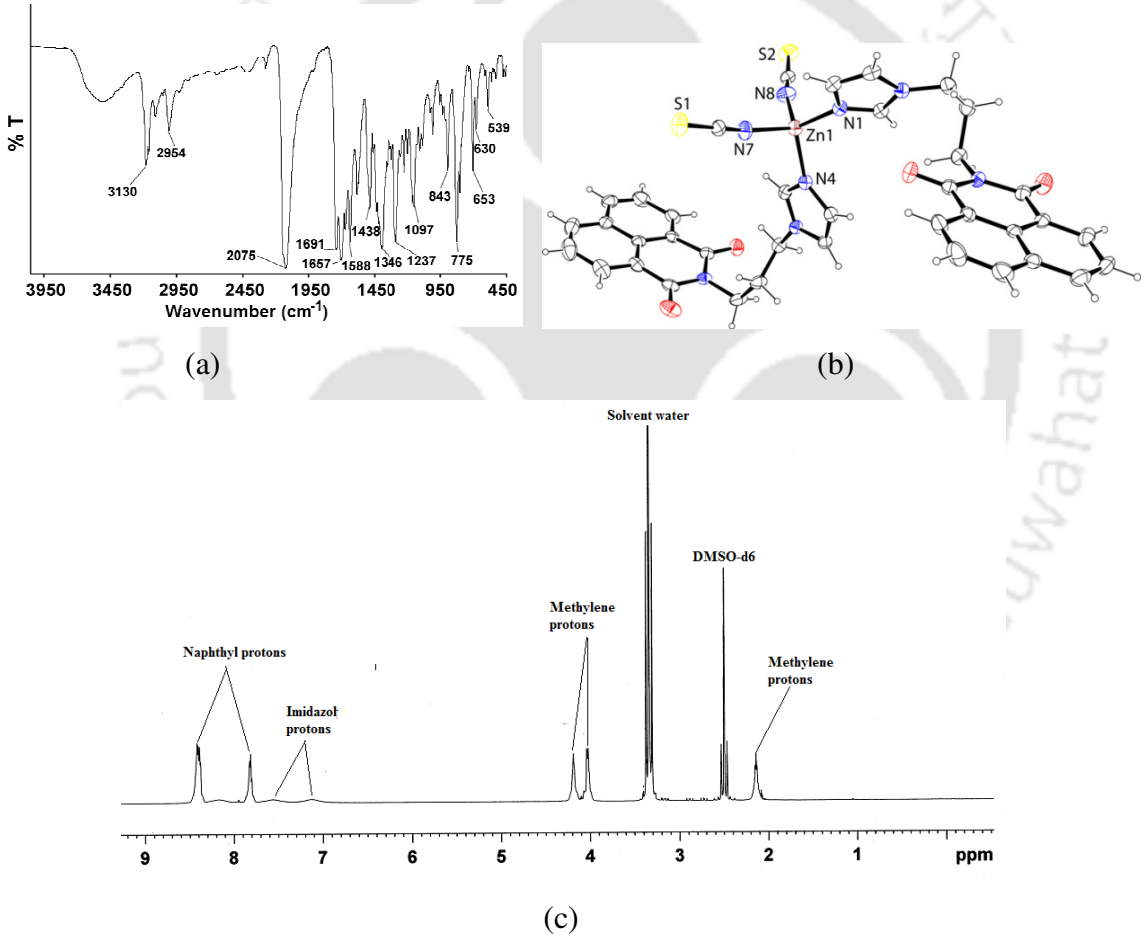

***Figure 3.9**: (a) FT-IR spectrum, (b) ORTEP view (30% thermal ellipsoid probability) and (c) ^{1}H-NMR spectrum (600 MHz, DMSO-d_6) of the complex **3.1f**.*

The coordination around Zn ion is satisfied by four nitrogen atoms; two nitrogen atoms are from imidazole of the ligand (Zn1-N1 1.986(3) Å, Zn1-N4 1.997(3) Å) and two other nitrogen atoms are from thiocyanate molecules (Zn1-N7 1.972(3) Å, Zn1-N8 1.940(3) Å). ^{1}H-NMR spectrum of the complex **3.1f** in DMSO-d_6 is shown in Figure **3.9c**. It shows

signals at 2.15 ppm, 4.04 ppm and at 4.19 ppm corresponds to the methylene protons; two broad signals at 7.15 ppm and 7.56 ppm correspond to the imidazole protons. Whereas chemical shift value for naphthalene protons appears in the range 8.39-8.42 ppm. ^{1}H-NMR spectrum of the complex shows slight shift from the parent ligand which suggests that the complex is stable in solution.

Similarly, cadmium complex with thiocyanate ligand has a composition [Cd**L**$^{1}_{3}$(SCN)$_2$DMF]·DMF (**3.1g**). The complex **3.1g** was characterized by its IR, ^{1}H-NMR and finally by X-ray crystal structure. ^{1}H-NMR spectrum of the complex shows methyl signals for two DMF molecules, one corresponding to coordinated DMF and the other to free DMF molecule which shows at 2.88 and 2.72 ppm respectively. The integration of the complex showed the presence of two molecules of DMF per molecule. Signal at 7.9 ppm observed which is due to CH protons of DMF. Besides these, the complex shows signals arising from **L**^{1} which are marked in Figure **3.9c**.

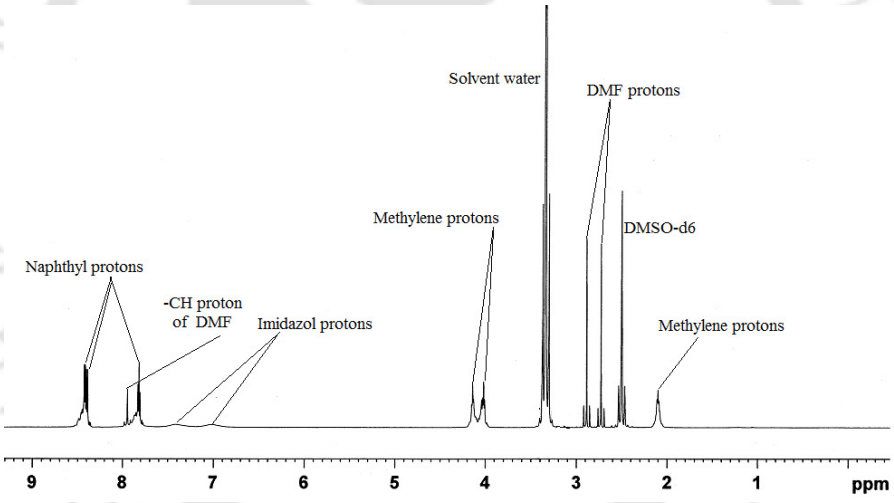

(a)

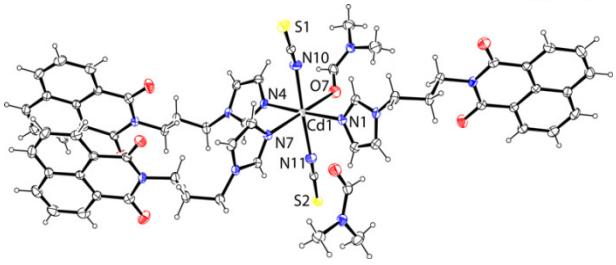

(b)

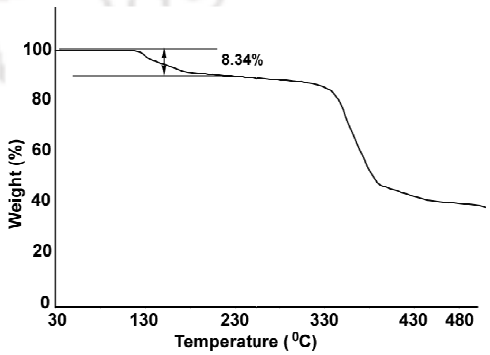

(c)

***Figure 3.10**: (a) ^{1}H-NMR spectrum (600 MHz, DMSO-d_6) of the complex **3.1g**, (b) ORTEP view (30% thermal ellipsoid probability) and (c) Thermogram of the complex **3.1g** (heating rate 7 °C/min).*

Cadmium (II) complex is a hexacoordinate complex which has three ligands ($\mathbf{L^1}$) and one DMF molecule occupying one plane of a distorted octahedral geometry whereas two thiocyanate occupying the axial positions of a distorted octahedron (Figure **3.10b**). In addition, there is a DMF molecule outside the coordination sphere. Although DMF was used as a solvent in the synthesis of the complexes **3.1a**-**3.1c**, **3.1f**-**3.1g**, it was not observed as solvent of crystallization nor as ligand in the complexes other than **3.1g**. A hexacoordinate environment of cadmium (II) ion is satisfied by three ligands, $\mathbf{L^1}$ (Cd1-N1 2.327(2) Å; Cd1-N4 2.335(2) Å and Cd1-N7 2.339(2) Å), two thiocyanate ligands (Cd1-N10 2.340(3) Å and Cd1-N11 2.343(3) Å) and one DMF molecule (Cd1-O7 2.337(2) Å). Metal-ligand bond parameters of the complexes **3.1f** and **3.1g** are listed in Table **3.2**.

Table **3.2** shows that in case **3.1f,** thiocyanate ligands are coordinated to metal with slightly different Zn-N bond length to that of the imidazole coordinating to Zn ion. This is probably due to the bulky naphthalimide group with a flexible methylene unit affecting the packing patterns. Table **3.2** also clearly indicates hexacoordination of cadmium despite of having a DMF molecule as a solvent of crystallization. Cadmium is known to form seven or eight coordinated metal complex but in this case the synergic effect of weak interactions in stabilizing π-stacked systems probably inhibits one of the DMF molecules to coordinate to cadmium ion.

To confirm that there are two DMF molecules in the complex, thermogram of the complex **3.1g** (Figure **3.10c**) was recorded which shows a weight loss of 8.34 % in the region 120-182 °C which corresponds to loss of one lattice DMF molecule and one coordinated DMF molecule (calcd. loss 8.98 wt. %).

From the above discussion it is clear that the compositions of complexes are guided by metal ion and the anionic ligand.

3.3. UV-visible and photoluminescence properties of the complexes:

UV-visible absorption and fluorescence properties of the ligand and all the complexes were carried out in solid state as well as in solution. Ligand, $\mathbf{L^1}$ showed absorption at 360 nm. The complexes have UV-visible absorptions in the range of 315-360 nm which originates mainly from the ligand. By comparing with analogous compounds, absorptions in this region originate from the n→π* transition.[49] UV-visible absorption in both solid and in solution of the ligand and also of all the complexes are shown in Figure **3.11**. From the

figure it is clear that the absorption features in solid and solutions differ but the pattern of change in intensity of the metal complexes are similar with respect to ligand.

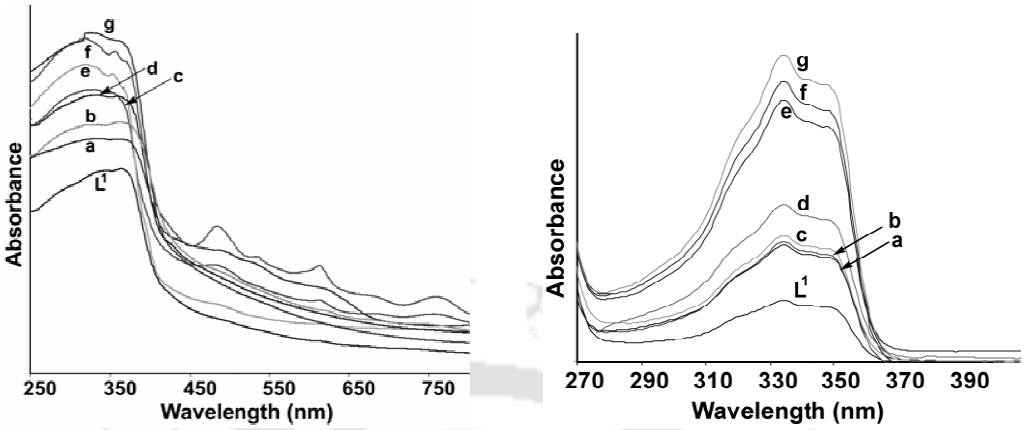

(i) (ii)

Figure 3.11*: UV-Visible spectra of the ligand and the complexes (i) (a)* ***3.1e****, (b)* ***3.1g****, (c)* ***3.1f****, (d)* ***3.1b****, (e)* ***3.1c****, (f)* ***3.1a*** *and (g)* ***3.1d*** *(in solid state); (ii) (a)* ***3.1b****, (b)* ***3.1a****, (c)* ***3.1c*** *, (d)* ***3.1f*** *, (e)* ***3.1e****, (f)* ***3.1d****, (g)* ***3.1g*** *in DMF (concentration of* 10^{-6} *M each).*

In the solid state, $\mathbf{L^1}$ shows a strong emission at 461 nm on excitation at 350 nm. Similar excitation of solid samples of the complexes **3.1a**-**3.1e** also shows emissions in the range of 425-481 nm (Figure **3.12**). From the figure, it is observed that complexes **3.1c**, **3.1f** or **3.1g** show fluorescence enhancement with respect to the ligand ($\mathbf{L^1}$). On the other hand, the complexes **3.1d** and **3.1e** show quenching of fluorescence with a small shift towards longer wavelength. The central metal ions in complex **3.1d** and complex **3.1e** are manganese (d^5, high-spin) and cobalt (d^7) in (+2) oxidation state respectively which are paramagnetic. Both complexes show lower fluorescence intensity than the parent ligand due to the paramagnetic nature of the metal ions.[50] These complexes have stretched conformations of the ligand and hence follow conventional fluorescence emission resembling the emission of the parent ligand. The fluorescence emission spectra of solid samples of these tetrahedral complexes are interesting; they show a characteristic emission on variation of anions and cations. The increase and decrease in intensity of fluorescence emission shown by these complexes are schematically presented in Scheme **3.2**. The complexes **3.1a**-**3.1c** have chloride ions, among them the complexes **3.1a** and **3.1b** show fluorescence emissions at 428 nm and 425 nm respectively, which are lower than the fluorescence emission of the ligand at 461 nm. The emission peak of mercury complex **3.1c** has higher intensity than that of the free ligand, $\mathbf{L^1}$ that occurs at 430 nm which is 31 nm less than the fluorescence emission of the ligand in the solid state.

On the other hand, complexes **3.1f** and **3.1g** have fluorescence emissions at longer wavelength than that of the parent ligand. A close examination of the structures of **3.1a**, **3.1b** and **3.1f** show that the orientation of 1,8-naphthalimide rings are similar in **3.1a** and **3.1b** but different from **3.1f** and **3.1g**. The complex **3.1f** has a non-parallel bent orientation whereas the complex **3.1g** has a stretched orientation of the ligand.

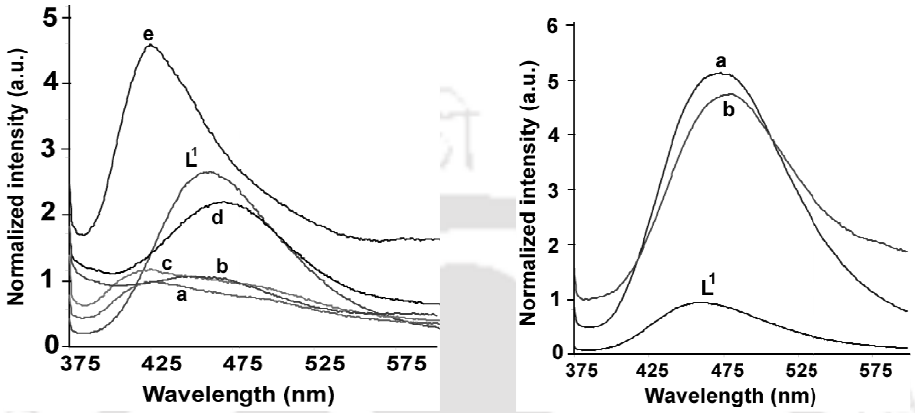

(i) (ii)

***Figure 3.12**: Solid state fluorescence emission of ligand **L**[1] and complexes (i) (a) **3.1a**, (b) **3.1e,** (c) **3.1b**, (d) **3.1d,** (e) **3.1c** and (ii) (a) **3.1f**, (b) **3.1g** at room temperature (λ_{ex} = 350 nm).*

Thus, twisting of the ligand to adapt near parallel orientation between the imidazole ring and 1,8-naphthalimide rings favors shorter wavelength emission due to stabilization of the ground state by intramolecular charge transfer. A stretched orientation or an orientation not favoring stabilization of the ground state of **L**[1] would help in stabilization of the inter-molecular charge transfer excited state, taking the emission to a longer wavelength.

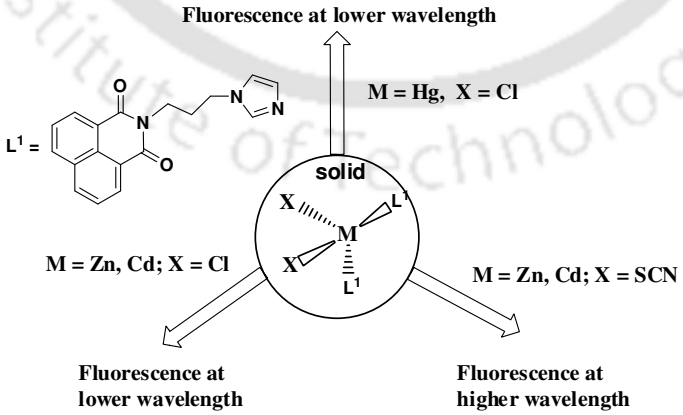

Scheme 3.2

The mercury being large and having a more diffused charge shows intra-molecular interaction between imidazole and the naphthalimide ring helps in the stabilization of the

ground state and accordingly emits at shorter wavelengths. The enhanced fluorescence intensity of mercury (II) complex may be attributed to the coordination of the ligands to the mercury (II) ions which effectively increases the rigidity of the ligands and reduces the loss of energy via radiationless thermal vibrations. Fluorescence emission of $\mathbf{L^1}$ in DMF solution by titrating an aqueous solution of chloride salts of zinc, cadmium or mercury was independently studied (Figure **3.13).** As anticipated, addition of mercury ions showed enhancement of fluorescence whereas the addition of zinc chloride or cadmium chloride quenched the emission intensity causing emission at a new wavelength (Figure **3.13a** and **3.13b**).

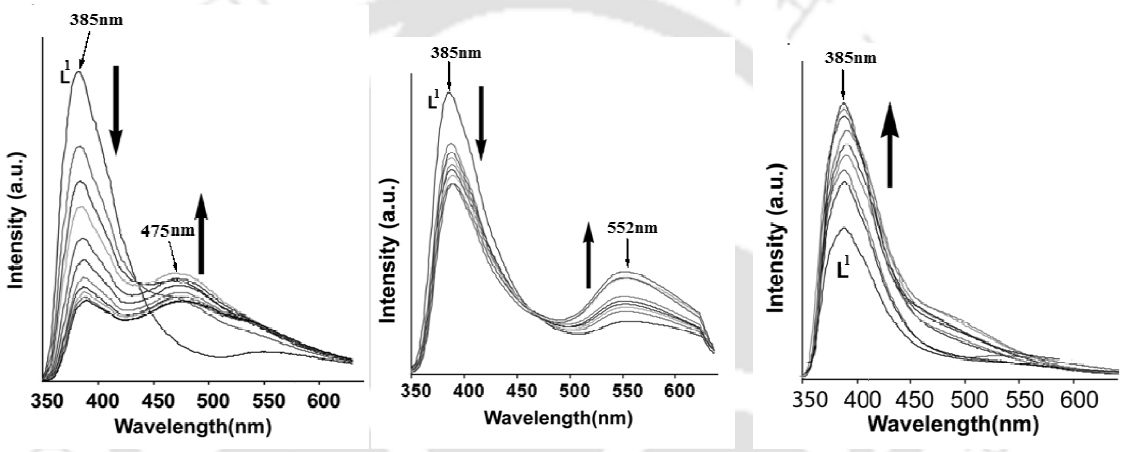

Figure 3.13*: The changes in fluorescence emission intensity of (λ_{ex} = 340 nm) of ligand, $\mathbf{L^1}$ (2 ml of 10^{-4} M solution in DMF) on addition of (a) zinc (II) chloride, (b) cadmium (II) chloride and (c) mercury (II) chloride (5µl aliquots of a 10^{-2} M solution in water).*

We find an analogy between solution and solid state fluorescence emission from the observed changes. The single emission peak of the ligand changes on titration with zinc chloride and at the end of titration, emission at 385 nm and 475 nm wavelengths are observed; whereas similar titration with cadmium chloride yielded emissions at 385 nm and 552 nm, respectively. The role of anions in the fluorescence emission of naphthalimide fluorophores interacting with various anions is well established.[51] Heagy and co-workers have shown that depending on the orientations of pyridine over a naphthalimide ring causes fluorescence shift to either a shorter wavelength (SW) or to a longer wavelength (LW).[40-44] Thus in solution, addition of zinc ions facilitated the stretching of the ligand leading to emission at longer wavelength to occur from stabilization of exciplex through intermolecular $\pi\cdots\pi$ interactions.[52]

The fluorescence emission spectra of the complexes in solutions were determined and are shown in Figure **3.14**. It is clear from the figure that the fluorescence quenching with respect to the ligand occurred in solution in each metal complex.

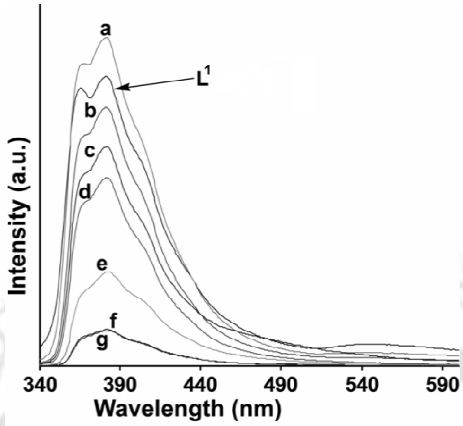

Figure 3.14 : *Fluorescence emission spectra (λ_{ex} 330 nm) of the complex (a)* ***3.1c****, (b)* ***3.1b****; (c)* ***3.1f****; (d)* ***3.1a****; (e)* ***3.1g****; (f)* ***3.1e****; (g)* ***3.1d*** *and ligand (**L**^{1}) in DMF (concentration of 10^{-4} M each).*

However, the exception was the mercury complex **3.1c** which showed fluorescence enhancement. There are multiple components of fluorescence in each case, pointing out a number of orientations present in solutions. This makes a clear distinction between mercury and other ions. There are terpyridine ligands distinguishing mercury[53-54] in aqueous medium; but our system can distinguish mercury in aqueous solution containing cadmium and zinc ions. The quantum yields of the ligand as well as all the complexes were determined from their respective solution in DMF. Quantum yield of the ligand **L**^{1} is 0.36 and the complexes lie in the range of 0.37-0.50 and are shown in Table **3.3**.

Table 3.3*: Quantum yield of the ligand and the complexes* ***3.1a****-****3.1g****.*

Compd.	Quantum yield	Compd.	Quantum yield
Ligand, **L**^{1}	0.36	Complex **3.1d**	0.38
Complex **3.1a**	0.37	Complex **3.1e**	0.41
Complex **3.1b**	0.35	Complex **3.1f**	0.50
Complex **3.1c**	0.40	Complex **3.1g**	0.46

To understand the effect of temperature on the fluorescence changes, we recorded temperature dependent fluorescence emissions at different temperatures for the complexes **3.1a**-**3.1c**. This is carried out with the anticipation that as the thermal energy increases the ligand would open up from bend geometry which disfavors intramolecular charge transfer interaction. Three illustrative examples on the changes of fluorescence in solution with respect to temperature are shown in Figure **3.15**.

Slight decrease of fluorescence intensity in the case of complexes **3.1a** and **3.1b** are observed as the temperature is increased while mercury complex **3.1c** shows slight

increase of fluorescence emission as the temperature is increased. It may be mentioned that the nitrogen heterocyclic ring attached to 1,8-naphthalimides are important as some

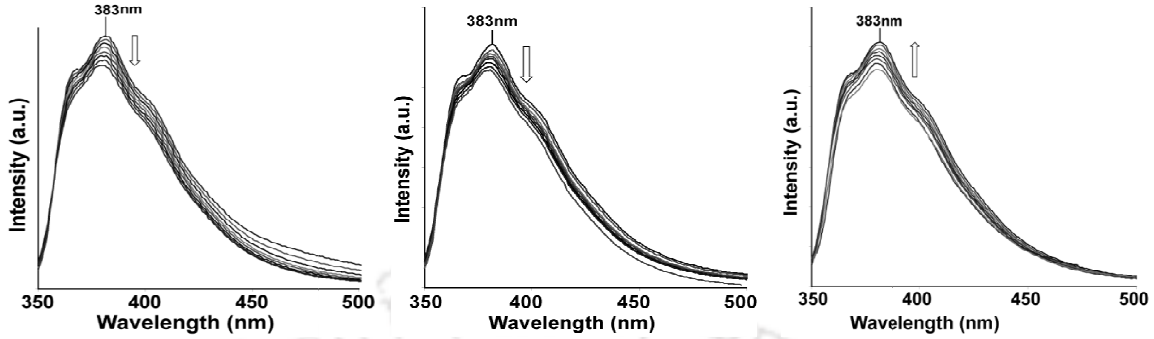

(a) (b) (c)

Figure 3.15*: Temperature dependent fluorescence spectra of the complex (a)* ***3.1a,*** *(b)* ***3.1b*** *and (c)* ***3.1c****. (30 °C to 100 °C at 10 °C interval of temperature; 0.1 mM solution each in DMF;* λ_{ex}*= 330 nm, downward arrow shows decease in intensity).*

of them show dual fluorescence. These are related to coplanar or orthogonal geometries of the 1,8-naphthalimide part with respect to the nitrogen containing heterocyclic units attached to them.[34,58] Thus, the complexes **3.1a** and **3.1b** show a decrease of fluorescence intensity on heating, suggesting the decrease in photo-electron energy transfer contribution to the emission process by change of orientation. On the other hand, mercury complex having a folded structure stretches out on heating that show an increase in the fluorescence intensity. When there is no metal ion to guide the orientation of the ligand $\mathbf{L^1}$, the lone pair of electrons present on the nitrogen atom of imidazole contributes to photo-electron energy transfer (PET) mechanism,[54] causing a partially quenched state at the start of heating; on heating, the orientation of $\mathbf{L^1}$ changes, and accordingly the intensity grows.

3.4. Conclusion:

In conclusion, it is shown that depending on the metal ion different mononuclear transition metal complexes are formed with $\mathbf{L^1}$. Difference in solid state structures are reflected in their fluorescence properties. Fluorescence behaviour of such complexes can be correlated with solid state structures. For example complex having bent geometry causes emission at shorter wavelength whereas complex having stretched geometry show emission at longer wavelength. The free ligand as well as the complexes in solution show fluorescence enhancement possibly due to change in orientation of flexible ligand. On heating, conformational changes disfavor participation of lone pairs in the nitrogen atom of

imidazole in such a process and hence enhancement of fluorescence intensity of the ligand was observed. Mercury (II) ion shows significant fluorescence enhancement with a shift towards shorter wavelength whereas cadmium (II) or zinc (II) ion quenches fluorescence in presence of chloride ions.

3.5 Experimental Section:

The detailed synthetic methodologies for synthesis of naphthalimide and the transition metal complexes are described. Analytical data as well as spectroscopic data are listed along with each compound. The instrumental details and the crystallographic parameters are provided in Appendix.

Synthesis of N-(3-imidazol-1-yl-propyl)-1,8-naphthalimide (L^1): It was synthesized by refluxing a mixture of 1,8-naphthalic anhydride (1.0 g, 5 mmol) and 3-(1H-imidazol-1-yl)propan-1-amine (0.60 g, 5 mmol) in DMF at 100 °C for 12 h. Then the reaction mixture was cooled and ice-cold water was added. The silky white precipitate of $\mathbf{L^1}$ formed was filtered and dried in air. IR (KBr, cm^{-1}): 3083 (s), 1689 (m), 1650 (s), 1589 (m), 1441 (s), 1386 (w), 1344 (s), 1236 (s), 1173 (w), 1082 (w), 908 (m), 779 (s), 671 (w). ^{1}H-NMR (400 MHz, DMSO-d_6): 8.58 (*d,* 1H, 6.4Hz), 8.21 (*d*, 1H, 8Hz), 7.78 (*t*, 1H, 7.6Hz), 7.56 (*s*, 1H), 7.03 (*s*, 1H), 4.22 (*t*, 2H, 6.4Hz), 4.06 (*t*, 2H, 7.2Hz), 2.26 (*m*, 2H) (Figure **3.16a**). ^{13}C-NMR (150 MHz, DMSO-d_6): 163.7 ppm (carbonyl carbon), 136.8 pm (naphthalene carbon), 133.9 ppm (imidazole carbon), 130.8, 128.9 ppm (naphthalene carbon), 127.6 ppm (imidazole carbon), 126.5, 121.8 ppm (naphthalene carbon), 118.4 ppm (imidazole carbon), 44.4, 37.1, 29.1 ppm (aliphatic carbon). HR-ESI MS (mass, m/e) 306.1247 (calcd. 306.1164) and it correspond to (M+1) peak (Figure **3.16b**). M.P = 165 °C.

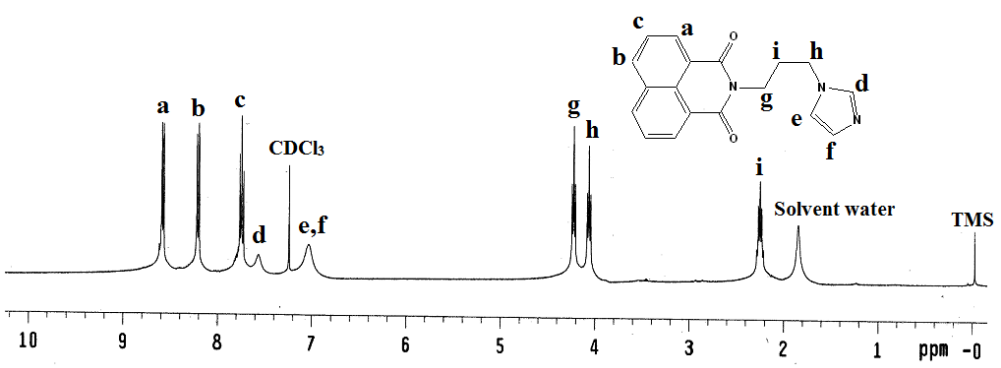

(a)

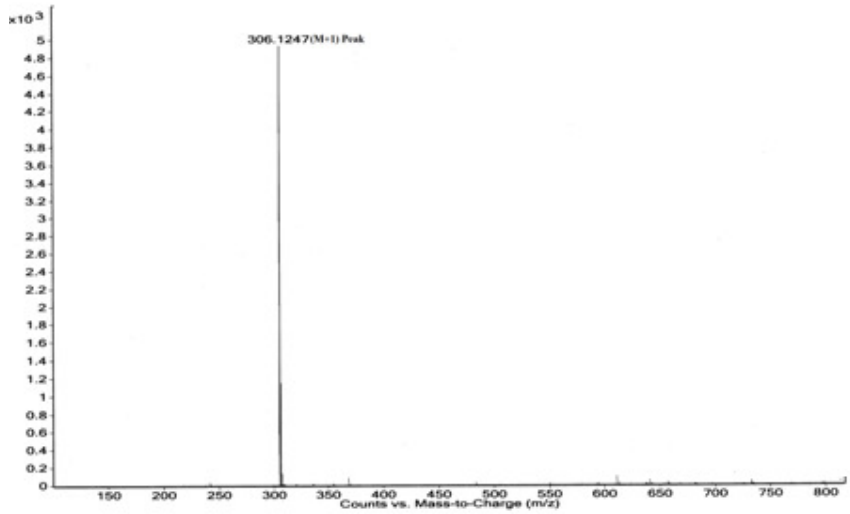

(b)

Figure 3.16: *(a) ^{1}H-NMR spectrum and (b) HR-ESI MS (M+1) spectrum of* ***L^1*****.**

Complex 3.1a: Ligand **L^1** (0.61 g, 2 mmol) was dissolved in warmed DMF and added to a methanolic solution of zinc chloride (0.136 g, 1 mmol). The reaction mixture was refluxed for 4 h and was cooled to room temperature. The filtered solution was kept undisturbed for crystallization. After one week white crystals appeared. Yield, 51 % (based on Zn). Elemental analysis (%) for $C_{36}H_{30}C_{l2}N_6O_4Zn$: calcd. C 57.89, H 4.05, N 11.25; found C 57.95, H 4.07, N 11.45. IR (KBr, cm^{-1}): 3414 (br), 2963 (s), 1695 (s), 1653 (s), 1586 (s), 1441 (m), 1344 (m), 1261 (s), 1242 (m), 1170 (w), 1098 (s), 1057 (w), 1026 (w), 850 (w), 801 (m), 785 (m), 654 (w), 544 (w). ^{1}H-NMR (600 MHz, DMSO-d$_6$): 8.48 (*d*, 1H, 6.6 Hz), 8.42 (*br*, 1H), 7.84 (*t*, 1H, 7.8 Hz), 7.44 (*s*, 1H), 7.02 (*s*, 1H), 4.17 (*t*, 2H, 6.6 Hz), 4.10 (*t*, 2H, 5.4 Hz), 2.12 (*m*, 2H).

Complex 3.1b: Complex **3.1b** was prepared by a procedure similar to that for complex **3.1a** but cadmium chloride was used instead of zinc chloride. One-week later colorless crystals of **3.1b** were obtained. Yield, 39 % (based on Cd). Elemental analysis (%) for $C_{36}H_{30}Cl_2N_6O_4Cd$: calcd. C 54.46, H 3.81, N 10.58; found C 54.51, H 3.82, N 10.61. IR (KBr, cm^{-1}): 3140 (m), 1694 (m), 1653 (s), 1586 (m), 1440 (w), 1342 (m), 1242 (s), 1170 (w), 1097 (m), 849 (m), 783 (s), 750 (w), 544 (w). ^{1}H-NMR (600 MHz, DMSO-d$_6$): 8.51 (*d*, 1H, 24 Hz), 7.87 (*bs*, 1H), 7.71 (*br*, 1H), 7.22 (*s*, 1H), 6.88 (*s*, 1H), 4.08 (*t*, 2H, 6 Hz), 4.05 (*t*, 2H, 7.2 Hz), 2.08 (*bs*, 2H).

Complex 3.1c: This complex was prepared by a procedure similar to that for complex **3.1a** but mercuric chloride was used instead of zinc chloride. On standing for 6-7 d, colorless crystals were observed. Isolated yield, 41 % (based on Hg). Elemental analysis (%) for

$C_{36}H_{30}Cl_2N_6O_4Hg$: calcd. C 49.01, H 3.43, N 9.53; found C 49.10, H 3.44, N 9.61. IR (KBr, cm^{-1}): 3139 (s), 1693 (m), 1654 (m), 1625 (s), 1518 (m), 1440 (m), 1342 (m), 1241 (s), 1096 (m), 1170 (w), 1096 (m), 1056 (w), 848 (s), 782 (s), 543 (m). ^{1}H-NMR (600 MHz, DMSO-d_6): 8.47 (*d*, 1H, 7.2 Hz), 8.42 (*d*, 1H, 8.5 Hz), 7.83 (*t*, 1H, 7.8 Hz), 7.31 (*s*, 1H), 6.93 (*s*, 1H), 4.10 (*t*, 2H, 7.2 Hz), 4.03 (*t*, 2H, 7.2 Hz), 2.08 (*m*, 2H).

Complex 3.1d: To a binary mixture solution of acetonitrile and methanol of **L^1** (0.61 g, 2 mmol), manganese chloride tetrahydrate (0.10 g, 0.5 mmol) was added. After stirring the mixture for 5 min, potassium thiocyanate (0.10 g, 1 mmol) was added. The reaction mixture was refluxed for 4 h and then cooled, filtered and allowed to evaporate at room temperature. Brown colored crystals were observed after a week. Isolated yield, 54 % (based on Mn). Elemental analysis (%) for $C_{78}H_{66}N_{16}O_8S_2Mn$: calcd. C 63.53, H 4.51, N 15.20; found C 63.73, H 4.61, N 16.01. IR (KBr, cm^{-1}): 3466 (bs), 3121 (m), 2958 (w), 2059 (s), 1698 (m), 1661 (s), 1591 (s), 1515 (s), 1443 (s), 1349 (s), 1238 (s), 1174 (w), 1088 (w), 931 (m), 844 (s), 775 (s), 661 (m), 537 (w).

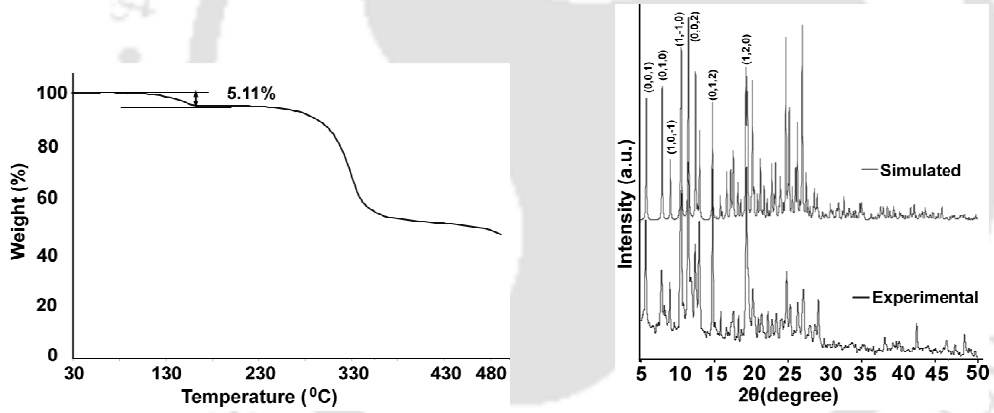

(a) (b)

***Figure 3.17**: (a) Thermogram (heating rate 7 °C/min) and (b) comparison of simulated (top) and experimental (bottom) PXRD pattern of the complex **3.1d**.*

Complex 3.1e: Complex **3.1e** was synthesized by the same procedure as that of **3.1d**, cobalt chloride hexahydrate (0.12 g, 0.5 mmol) was used instead of $MnCl_2{\cdot}4H_2O$. Yield, 51 % (based on Co). Elemental analysis (%) for $C_{78}H_{66}N_{16}O_8S_2Co$: calcd. C 63.36, H 4.50, N 15.16; found C 63.38, H 4.51, N 15.34. IR (KBr, cm^{-1}): 3444 (br), 3126 (w), 2071 (s), 1698 (s), 1660 (s), 1591 (s), 1515 (s), 1442 (s), 1349 (s), 1237 (s), 1174 (m), 1104 (w), 1089 (w), 935 (w), 844 (m), 775 (s), 661 (m), 537 (w).

Complex 3.1f: It was prepared by a similar procedure as that of the complex **3.1d** where zinc nitrate hexahydrate was used. Colorless crystals were obtained after 7-8 d. Isolated

yield, 39 % (based on Zn). Elemental analysis (%) for $C_{37}H_{30}N_8O_4S_2Zn$: calcd. C 56.96, H 3.88, N 14.36; found C 56.49, H 3.87, N 14.23. IR (KBr, cm^{-1}): 3130 (m), 2954 (w), 2075 (s), 1691 (w), 1657 (m), 1588 (m), 1535 (m), 1438 (s), 1346 (w), 1237 (s), 1173 (w), 844 (s), 755 (s), 653 (s), 630 (m), 539 (w), 409 (w). ^{1}H-NMR (600 MHz, DMSO-d_6): 8.42-8.39 (*m*, 6H, naphthalene protons), 7.81-7.56 (*bs*, 3H, imidazole protons), 4.19 (*m*, 2H, N-CH_2), 4.04 (*t*, 2H, 4.8 Hz, N-CH_2), 2.15 (*m*, 2H, -CH_2-).

Complex 3.1g: Complex **3.1g** was synthesized by a similar procedure as that of **3.1d** where cadmium nitrate tetrahydrate was used instead of zinc nitrate hexahydrate. Brown crystals were formed after 8 d. Isolated yield, 45 % (based on Cd). IR (KBr, cm^{-1}): 3112 (w), 2954 (w), 2062 (s), 1702 (m), 1661 (s), 1590 (m), 1513 (s), 1443 (s), 1236 (s), 1091 (m), 843 (m), 774 (s), 659 (s), 539 (m). ^{1}H-NMR (600 MHz, DMSO-d_6): 8.45-8.41 (*m*, 18H, naphthalene protons), 7.94 (*s*, 2H, OC-H of DMF), 7.83-7.43 (*bs*, 9H, imidazole protons), 4.15 (*t*, 6H, 6.6 Hz, NCH_2), 4.02 (*t*, 6H, 7.2 Hz, NCH_2), 2.88 (*s*, 6H, CH_3 of DMF), 2.72 (*s*, 6H, CH_3 of DMF), 2.10 (m, 6H, -CH_2-).

3.6 Quantum yield determination:

Quantum yields of $\mathbf{L^1}$ and all the complexes were measured by using the following formula in which quinine sulfate was used as a standard. The concentration of all the compounds was prepared in such a way that their absorption maxima should be around 0.1.

$$\text{Quantum Yield} = \frac{\text{Area of the compound}}{\text{Area of Q.S}} \times \frac{\text{Absorbance at 333nm (Q.S)}}{\text{Absorbance at 333nm (Compound)}} \times \frac{\text{R.I of DMF}}{\text{R.I of water}} \times 0.54$$

Where Q.S, and R.I are quinine sulfate and refractive index respectively. And area means the area covered by a fluorescence curve of the respective compound.

3.7 References:

1. Duke, R. M.; Veale, E. M.; Pfeffer, F. M.; Kruger P. E.; Gunnlaugsson, T. *Chem. Soc. Rev.* **2010**, *39*, 3936-3953.
2. Gunnlaugsson, T.; Kruger, P. E.; Jensen, P.; Pfeffer, F. M.; Hussey, G. M. *Tetrahedron Lett.* **2003**, *44*, 8909-8913.
3. Poteau, X.; Brown, A. I.; Brown, R. G.; Holmes, C.; Matthew, D. *Dyes Pigm.* **2000**, *47*, 91-105.

4. Silva, A. P. D.; Gunaratne, H. Q. N.; Gunnlaugsson, T.; Huxley, A. J. M.; McCoy, C. P.; Rademacher, J. T.; Rice, T. E. *Chem. Rev*. **1997**, *97*, 1515-1566.
5. Guha, S.; Goodson, F. S.; Corson L. J.; Saha, S. *J. Am. Chem. Soc*. **2012**, *134*, 13679-13691.
6. Lee, K.-Y. *Chem. Rev*. **1993**, *93*, 449-486.
7. Loving, G.; Imperiali, B. *Bioconjugate Chem*. **2009**, *20*, 2133-2141.
8. Loving, G.; Imperiali, B. *J. Am. Chem. Soc*. **2008**, *130*, 13630-13638.
9. Cho, D. W.; Fujisuka, M.; Choi, K. H.; Park, M. J.; Yoon, U. C.; Majima, T. *J. Phys. Chem. B* **2006**, *110*, 4576-4582.
10. Xu, Y.; Qian, X.; Yao, W.; Mao, P.; Cui, J. *Bioorg. Med. Chem*. **2003**, *11*, 5427-5433.
11. Gorteau, V.; Bollot, G.; Mareda, J.; Perez-valasco, A.; Matile, S. *J. Am. Chem. Soc.* **2005**, *128*, 14788-14789.
12. Davis, J. T. *Nat. Chem.* **2010**, *2*, 516-517.
13. Sawson, R. E.; Hennig, A.; Weimann, D. P.; Emery, D.; Ravikumar, V.; Montenegro, J.; Takeuchi, T.; Gabutti, S.; Mayor, M.; Mareda, J.; Schalley, C. A.; Matile, S. *Nat. Chem.* **2010**, *2*, 533-538.
14. Pogozhev, D. V.; Bezdek, M. J.; Schauer, P. A.; Berlinguette, C. P. *Inorg. Chem*. **2013**, *52*, 3001-3006.
15. Reger, D. L.; Debreczeni, A.; Smith, M. D. *Inorg. Chim. Acta* **2010**, *364*, 10-15.
16. Sarma, R. J.; Tamuly, C.; Barooah, N.; Baruah, J. B. *J. Mol. Struct*. **2007**, *829*, 29-36.
17. Singh, D.; Baruah, J. B. *Cryst. Growth Des*. **2012**, *12*, 2109-2121.
18. Singh, D.; Baruah, J. B. *Inorg. Chim. Acta* **2012**, *390*, 37-40.
19. Saito, I.; Takayama, M.; Sugiyama, H.; Nakatani, K. *J. Am. Chem. Soc*. **1995**, *117*, 6406-6407.
20. Brana, M. F.; Cacho, M.; Ramos, A.; Dominguez, M. T.; Pozuelo, J. M.; Abradelo, C.; Rey-Stolle, M. F.; Yuste, M.; Carrsco, C.; Bailly, C. *Org. Biomol. Chem*. **2003**, *1*, 648-654.
21. Veale, E. B.; Gunnlaugsson, T. *J. Org. Chem*. **2010**, *75*, 5513-5525.
22. Ingrassia, L.; Lefranc, F.; Kiss, R.; Mijatovic, T. *Curr. Med. Chem*. **2009**, *161*, 192-121.
23. Nitiss, J. L.; Zhou, J.; Rose, A.; Huiung, Y.; Gale, K. C.; Osheroff, N. *Biochemistry* **1998**, *37*, 3078-3085.
24. Banerjee, S.; Veale, E. B.; Phelan, C. M.; Murphy, S. A.; Tocci, G. M.; Gillespie, L. J.; Frimannsson, D. O.; Kelly, J. M.; Gunnlaugsson, T. *Chem. Soc. Rev*. **2013**, *42*, 1601-1618.
25. Wang, K.; Wang, Y.; Yan, X.; Chen, H.; Ma, G.; Zhang, P.; Li, J.; Li, X.; Zhang, J. *Bioorg. Med. Chem. Lett*. **2012**, *22*, 937-941.
26. Gasioski, P.; Danel, K. S.; Matusiewicz, M.; Uchacz, T.; Kuznik, W.; Kityk, A. V. *J. Fluoresc*. **2012**, 81-91.

27. Guo, P.; Chen, Q.; Liu, T.; Xu, L.; Yang, Q.; Qian, X. *Med. Chem. Lett*. **2013**, *4*, 527-531.
28. Reger, D. L.; Horger, J.; Smith, M. D.; Long, G. J. *Chem. Commun*. **2009**, 6219-6221.
29. Reger, D. L.; Leitner, A.; Smith, M. D. *Inorg. Chem*. **2013**, *52*, 10041-10051.
30. Xu, Z.; Xiao, Y.; Qian, X.; Cui, J.; Cui, D. *Org. Lett.* **2005**, *7*, 889-892.
31. Huang, J.; Xu, Y.; Qian, X. Org. *Biomol. Chem.* **2009**, *7*, 1299-1303.
32. Xu, Z.; Qian, X.; Cui, J. *Org. Lett*. **2005**, *7*, 3029-3032.
33. Liu, Z.; Zhang, C.; Wang, X.; He, W.; Guo, Z. *Org. Lett*. **2012**, *17*, 4378-4381.
34. Tagaki, W.; Ogino, K. *Top. Curr. Chem*. **1985**, *128*, 143-147.
35. Spiro, T. G. *Metal Ions in Biology*, Wiley: New York, **1981**.
36. Kilpin, K. J.; Clavel, C. M.; Edafe, F.; Dyson, P. J. *Organometallics* **2012**, *31*, 7031-7039.
37. Chovelon, J.-M.; Grabchev, I.; *Spectrochim. Acta A* **2007**, *67*, 7-91.
38. Okamoto, H.; Satake, K.; Kimura, M. *ARKIVOC* **2007**, *viii*, 112-123.
39. Nath, J. K.; Baruah, J.B. *J. Fluoresc.* **2014**, *24*, 649-655.
40. Paudel, S.; Nandhikonda, P.; Heagy, M. D. *J. Fluoresc*. **2009**, *19*, 681-691.
41. Nandhikonda, P.; Begaye, M. P.; Chao, Z.; Heagy, M. D. *Org. Biomol. Chem.* **2010**, *8*, 3195-3201.
42. Cao, C.; Chang, V.; Hernandez, R.; Heagy, M. D. *J. Org. Chem*. **2005**, *70*, 4929-4934.
43. Mello, J. V.; Finney, N. S. *Angew. Chem., Int. Ed*. **2001**, *40*, 1536-1538.
44. Biczok, L.; Valat, P.; Wintgens, V. *Phys. Chem. Chem. Phys*. **1999**, *1*, 4759-4766.
45. Nazeeruddin, M. K.; Kay, A.; Rodicio, I.; Humpbry-Baker, R.; Miiller, E.; Liska, P. *J. Am. Chem. Soc*. **1993**, *115*, 6382-6390.
46. Nazeeruddin, M. K.; Pechy, P.; Gratzel, M. *Chem. Commun*. **1997**, 1705-1706.
47. Mitchell, P. C. H.; Williams, R. J. P. *J. Chem. Soc.* **1960**, 1912-1918.
48. Abedi, A.; Amani, V.; Boca, R.; Dlhan, L.; Khavasi, H. K.; Safari, N. *Inorg. Chim. Acta* **2013**, *395*, 58-66.
49. Kucheryavy, P.; Li, G.; Vyas, S.; C.; Hadad and K. D. Glusac, *J. Phys. Chem. A* **2009**, *113*, 6453-6646.
50. Xu, Z.; Yoon, J.; Spring, D. R. *Chem. Commun*. **2010**, *46*, 2563-2565.
51. Ali, H. D. P.; Kruger, P. E.; Gunnlaugsson, T. *New J. Chem*. **2008**, *32*, 1153-1161.
52. Nath, J. K.; Baruah, J. B. *New J. Chem*. **2013**, *37*, 1509-1519.
53. Shunmugam, R.; Gabriel, G. J.; Smith, C. E.; Aamer, K. A.; Tew, G. N. *Chem. Eur. J.* **2008**, *14*, 3904-3907.
54. Kim, H. N.; Ren, W. X.; Kim, J. S. Yoon, J. *Chem. Soc. Rev*. **2012**, *41*, 3210-3244.
55. Cho, D. W.; Fujisuka, M.; Sugimoto, A.; Yoon, U. C.; Mariano, P. S.; Majima, T. *J. Phys. Chem. B* **2006**, *110*, 11062-11068.

CHAPTER 4

Transition metal based carboxylate coordination polymers of naphthalimide-tethered pyridine and their photoluminescence and magnetic properties

Rational design and synthesis of metal-organic framework (MOF) or coordination polymer with intriguing architectures and topologies still a long term challenge. Among the different MOFs, metal carboxylates have attracted much attention because of the versatile coordination binding modes of carboxylate groups along with hydrogen bond donor and acceptors properties in making complexes with various dimensionalities.[1-5] Metal carboxylates with flexible ligands have also been studied for the formation of coordination networks possessing permanent porosity and high thermal stability, which are useful for ionic exchange,[6] separation,[7]chemisorption,[8] gas storage,[9] catalysis,[10-12] magnetism,[13-14] optoelectronics,[15-18] photoactivations,[19] proton conductions[20] and luminescence properties.[21] Moreover, naphthalimide derivatives connected to carboxylic acids form strong π···π interactions. These interactions have been used as secondary building units (SBUs) to construct supramolecular architectures in naphthalimide based complexes.[22] Extension of structures occur through π···π stacking interactions that give rise to new structures with various material properties.[23-24] We have discussed earlier the role of weak interactions in the formation of supramolecular networks of N-phthaloylglycinato and 4-carboxy-N-phthaloylglycinato complexes of transition metals.
[25-27] Besides this, supramolecular aspects of transition metal complexes of cyclic imide tethered both carboxylic acids and hydroxy carboxylic acids were also discussed that led to different supramolecular architectures.[28-29] Reger *et al.* reported series of copper (II) carboxylate dimers with flexible carboxylate ligands derived from propionic acid and butanoic acid tethered by 1,8-naphthalimide unit.[30] The supramolecular networks in these dimers are sustained by strong π···π stacking interactions of electron deficient naphthalimide units. By using both carboxylates and pyridyl based naphthalimide as ligand, different structural diversity of coordination polymers or MOF or SMOFs (Supramolecular Metal-Organic Frameworks) can be constructed. These types of complexes are not more exploited and much work in this direction is required to have control over construction of void in a predictable manner. Besides these, π···π stacking

interaction are used in the construction of single chain magnet (SCM) in some cobalt (II) complexes.[31] SCM behavior was observed in cobalt (II) complexes due to pseudo-1D arrangement of the cations through π···π stacking interactions between pyridine rings of one of the dipyridylamine ligands.

These observations encouraged us to use modified pyridine based ancillary ligands containing naphthalimide unit for construction of supramolecular metal complexes to explore novel material properties. Another motivating factor for this study was ready references on fumarate,[32-33] malonate,[34]maleate,[35-36] adipate[37]. On the other hand, π-stacking interactions and supramolecular features of naphthalimide ligands provide impetus[38] to generate new structural patterns. We studied the reaction of different first row transition metal salts with N-(4-pyridylmethyl)-1,8-naphthalimide, **L²** as ancillary ligand and different dicarboxylic acids as shown in Chart **4.1**. Dicarboxylic acids which act as linker to form coordination polymer are malonic acid (H_2Mal), fumeric acid (H_2Fum) and

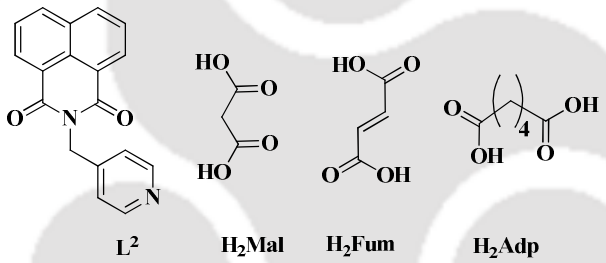

Chart 4.1

adipic acid (H_2Adp). This chapter deals with the syntheses, characterization, supramolecular structural features, photoluminescence and magnetic properties of transition metal coordination polymers of dicarboxylates and conformational flexible methyl pyridine that are tethered by naphthalimide units.

4.1 Synthesis of N-(4-pyridylmethyl)-1,8-naphthalimide (L^2):

N-(4-pyridylmethyl)-1,8-naphthalimide was prepared by a reported procedure[39] and characterized by FT-IR and ^{1}H-NMR spectroscopy. In ^{1}H-NMR spectrum, the pyridyl proton, 'a' appears as doublet at 8.61 ppm due to deshielding effect of nitrogen atoms whereas pyridyl proton 'e' appears at 7.37 ppm as doublet. The naphthalene protons 'b' and 'c' appear at 8.52 ppm and 8.24 ppm as doublet whereas 'd' protons shows a chemical

shift value at 7.76 ppm as tripet. Aliphatic proton 'f' appears as a singlet at 5.36 ppm (Figure **4.1**).

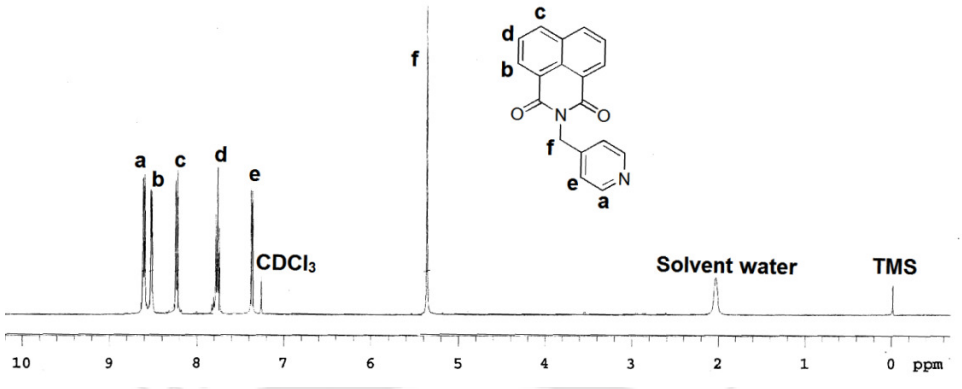

***Figure 4.1**: ^{1}H-NMR (400MHz, $CDCl_3$) spectrum of ligand, L^2.*

4.2 Coordination polymers of manganese (II), cobalt (II) and copper (II):

A series of one dimensional coordination polymers of manganese (II), cobalt (II) and copper (II) were prepared by reacting metal acetate with $\mathbf{L^2}$ and different dicarboxylic acids as shown in Scheme **4.1**.

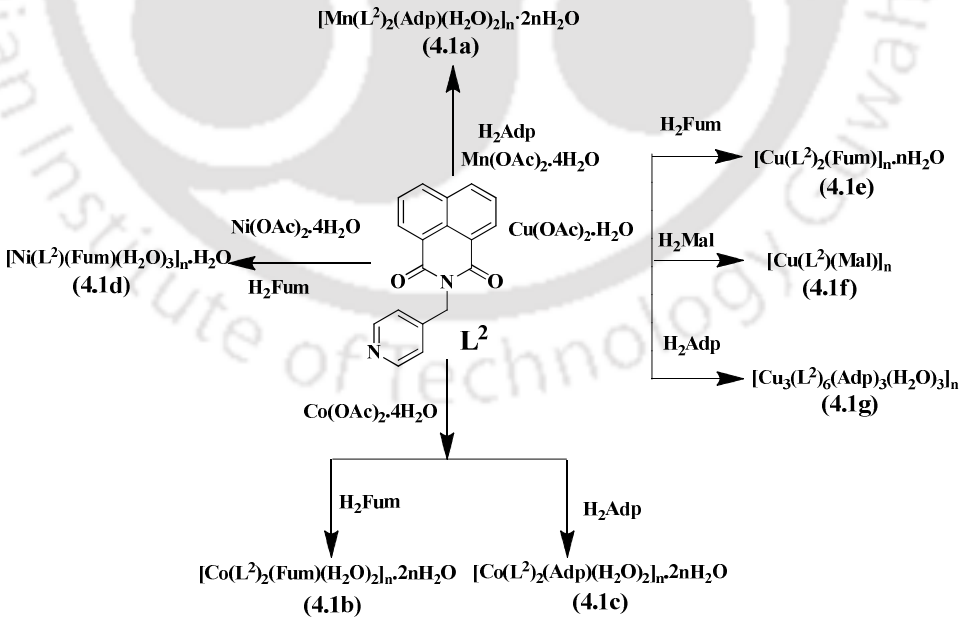

Scheme 4.1:** Syntheses of the coordination polymers **4.1a-4.1g.

The formation of a particular coordination polymer was found to be dependent on the ratio of metal /$\mathbf{L^2}$ / dicarboxylic acid used in the reaction. For example, 1:2:1 ratio was used for

the preparation of the coordination polymers **4.1a**, **4.1b**, **4.1c**, **4.1e**, and **4.1g**, whereas the rest of the coordination polymers were prepared from the reaction with 1:1:1 molar ratios. These coordination polymers were characterized by FT-IR, UV-Visible, thermogravimetric analyses and finally by X-ray crystal structure. Powder X-ray diffraction spectra were also recorded to check the phase purity of the coordination polymers.

Each manganese ion in manganese (II) adipate coordination polymer $[Mn(\mathbf{L^2})_2(Adp)(H_2O)_2]_n \cdot 2nH_2O$ **(4.1a)** is in an O_4N_2 environment with distorted octahedral coordination geometry. Two $\mathbf{L^2}$-ligands attached to each manganese ion having Mn1-N1= 2.302(5) Å distance are axially located trans to each other. There are two carboxylate ligands from two independent adipates (one carboxylate each) coordinated in a monodentate fashion to manganese ion (Mn1-O3 = 2.172(3) Å). Two water molecules

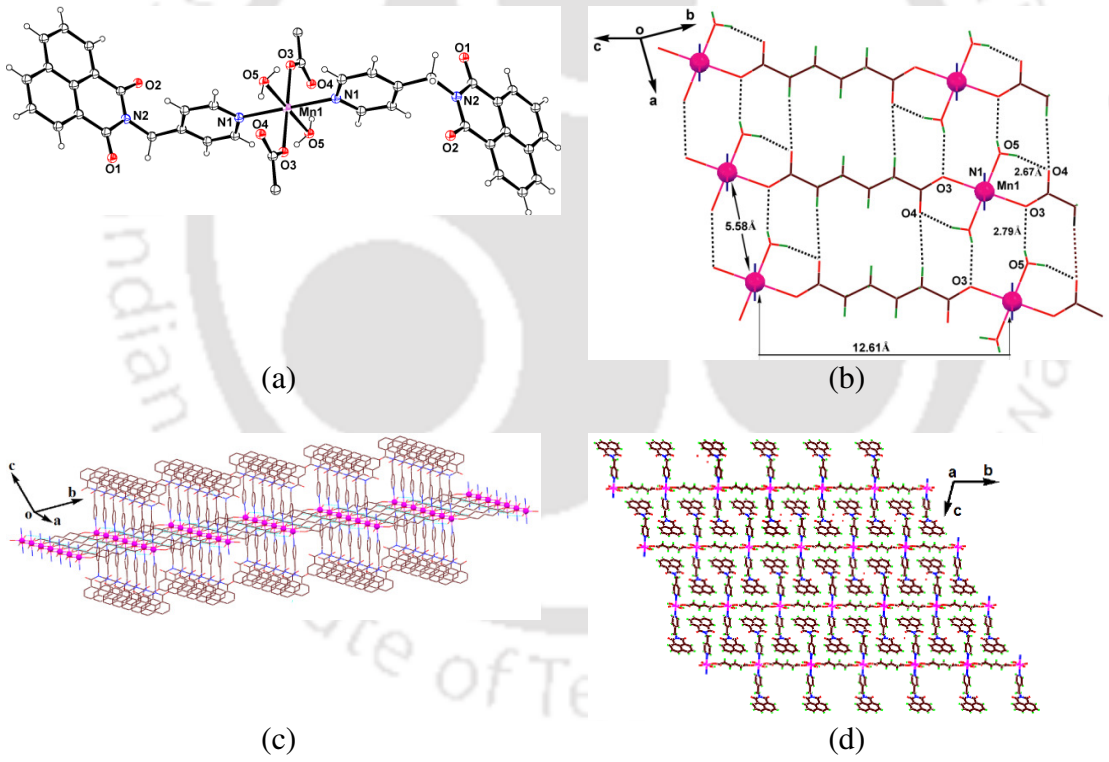

Figure 4.2: *(a) ORTEP view (30% thermal ellipsoid probability) of* ***4.1a*** *showing coordination environments around manganese (II) ions, (b) Hydrogen-bonded motif of coordinated water molecules, (c) Hydrogen-bonded structure of* ***4.1a*** *forming 2D sheet and (d) 3D supramolecular architecture along a-crystallographic axis.*

(Mn1-O5 = 2.196(4) Å) (Figure **4.2a**) coordinated to each manganese ion. Metal-ligand bond parameters of **4.1a** are listed in Table **4.1**. Carboxylate ligands are trans to each other facilitating formation of linear chain structure. Uncoordinated carbonyl oxygen atom of

carboxylate groups takes part in a bifurcated hydrogen bond, one part of which is intramolecular and other part being intermolecular. The intermolecular hydrogen bond involves one C-H of adipate molecule of an adjacent chain [C20-H20A···O4 (3.59 Å)], which helps in self-assembly formation between layers. There is bifurcated hydrogen bond between carbonyl oxygen of coordinated carboxylate groups with coordinated water molecules in which the O5-H5A···O4 distance is 2.64 Å, whereas a coordinated oxygen atom of carboxylate is involved in O5-H5B···O3 (O3-O5 = 2.79 Å) hydrogen-bond with a coordinated water molecule attached on cobalt (II) ions of the adjacent chain (Figure **4.2b**). Selected hydrogen bond parameters are listed in the Table **4.4**. Due to these hydrogen-bonds, one-dimensional polymeric chains form a hydrogen-bonded 2D sheet (Figure **4.2c**). With further weak interactions of lattice water molecules and naphthalimide ligands, a 3D supramolecular architecture is obtained (Figure **4.2d**).

Thermogram of the coordination polymer **4.1a** (Figure **4.3a**) shows 5.26 % weight loss from 80 to 170 °C. It corresponds to loss of two molecules of water of crystallization (calcd. wt. loss 4.3 %). Second weight loss of 21.8 % occurs from 190 to 320 °C due to two coordinated water molecules and one Adp linker (calcd. 22.17 %). At 475 °C, this coordination polymer transformed to MnO (calcd. 8.4 %, found 9.0 % residue).

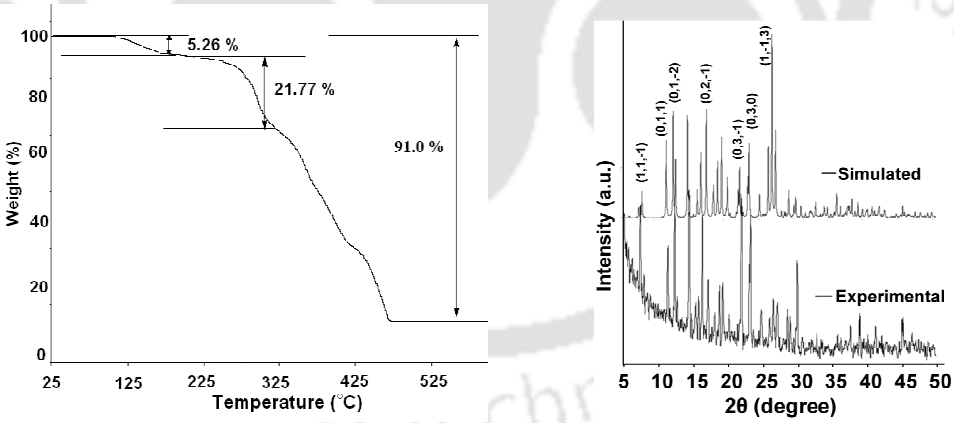

(a) (b)

Figure 4.3: *(a) Thermogram (heating rate 7 °C/min) and (b) Comparison of simulated (top) and experimental (bottom) PXRD patterns of the coordination polymer* ***4.1a****.*

Loss of coordinated water molecules at a higher temperature is attributed to their extra stability in the lattice due to intramolecular and intermolecular hydrogen-bonds.

By comparing the experimental powder X-ray diffraction patterns of **4.1a** with simulated patterns, similarity between the two is observed which confirms the bulk purity of the compound (Figure **4.3**).

Manganese (II) adipate complex occurring as $[Mn(Adp)]_n$ adapts interpenetrated layered structure having dinuclear manganese (II) units as nodes.[40] Aqua bridged dimeric manganese (II) adipate complex form a two-dimensional polymeric structure[40] which loses water molecules on heating to about 200 °C and annealed samples on exposure to moisture reabsorbs water;[41] however, at 600 °C it forms Mn_3O_4. Manganese adipate coordination polymer with dinuclear manganese-carboxylate units having chelating as well as a bridging carboxylate were reported earlier but coordination polymer **4.1a** has a linear structure. Formations of manganese adipate complexes are dependent on reaction conditions. For example, polymeric or dimeric manganese adipate complexes having a 1,10-phenanthroline ligand were formed under different reaction conditions. Dimeric $[Mn(phen)(H_2O)]^{2+}$ cations bridged by two tridentate adipate ligands adapt twisted conformer.[37] These comparisons show **4.1a** to be a very simple example of a linear coordination polymer with a sheet-like structure formed by stacking of naphthalimides in which chains are held by C-H···O interactions. Hence, in the coordination polymer **4.1a**, intermolecular C-H···O interactions along with the O-H···O interactions facilitated by stacking effects of naphthalimides bring manganese ions to close proximity to have antiferromagnetic interactions.

Aliphatic dicarboxylic acids such as adipic acid or fumaric acid forms wide varieties of cobalt (II) complexes either as monomer,[46] polymer,[47-48] or as complexes with dicarboxylate anions.[49] On the other hand, double bond geometry of cobalt (II) maleate complex can be modulated to form a fumarate complex by ligands such as pyridine or bipyridine.[50]

Coordination polymer of $\mathbf{L^2}$ and fumerate with cobalt (II), $[Co(\mathbf{L^2})_2(Fum)(H_2O)_2]_n \cdot 2nH_2O$ **(4.1b)** has distorted octahedral geometry around each cobalt (II) ion which are constructed by two nitrogen atoms as donors from two ligands ($\mathbf{L^2}$) { Co1-N1 2.184(5) Å; Co1-N3 2.169(5) Å}, two oxygens of monodentate bridging fumarate {Co1-O7 2.058(4) Å; Co1-O10 2.068(4) Å} and two water molecules {Co1-O5 2.162(5) Å; Co1-O6 2.112(5) Å} (Figure **4.4a**). Four oxygen atoms from ligands around each cobalt ion are in one plane of distorted octahedron and two nitrogen atoms are coordinated to cobalt centres are trans to each other. Metal-ligand bond parameters of the coordination polymer are listed in the Table **4.1**. Lattice water molecules of the coordination polymer **4.1b** interact with coordinated water molecules and also with carbonyl of carboxylate groups (Figure **4.4b**). In addition, there are C-H···π interactions among naphthalimide rings with hydrogen atom and centroid of interacting aromatic part ($d_{C\text{-}H\cdots\pi}$ = 3.70 Å). Coordination polymer shows

strong O···π interactions among the naphthalimide ring (O···$\pi_{centroid}$ distance 3.09 Å). There are also C-H···π interactions between hydrogen atom of one CH_2-group of $\mathbf{L^2}$ and pyridine moiety of another $\mathbf{L^2}$ (C···$\pi_{centroid}$ distance 3.67 Å shown in Figure **4.4c**).

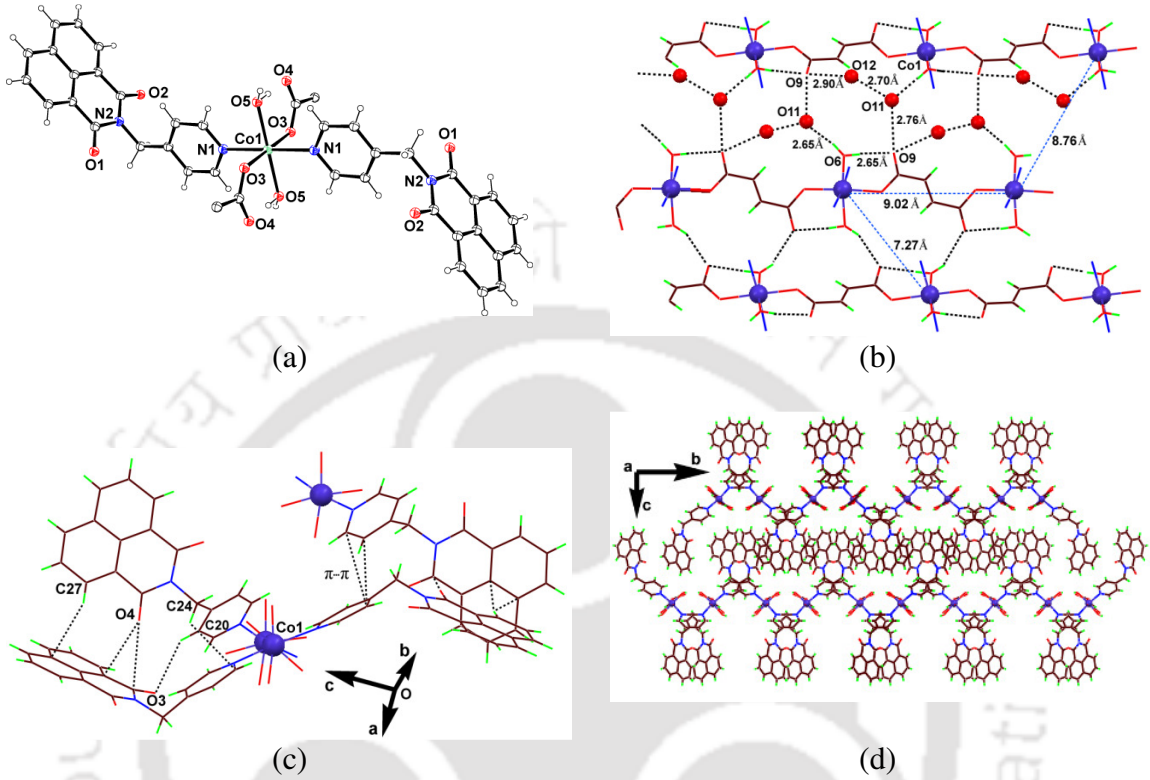

***Figure 4.4**: (a) ORTEP view (30% thermal ellipsoid probability) showing the coordination environment around cobalt ion in **3.1b**, (b) Assembling of chains with lattice water molecules, (c) Diagram showing C-H···π, C-H···O, O···π, and π···π interactions and (d) 2D-supramolecular network of **4.1b**.*

These interactions result in the formation of a 2D supramolecular network shown in Figure **4.4d.** Selected hydrogen bond parameters are listed in the Table **4.3** in the experimental section. From thermogravimetric analysis of **4.1b** (Figure **4.19a** in the experimental section) shows 4.9 % weight loss at 80-130 °C which corresponds to the loss of two water molecules of crystallization (calcd. wt. loss 4.4 %). A second weight loss of 17.8 % occurs from 135 to 330 °C that may be due to the loss of one fumerate linker (calcd. 19.1 wt. %). Further weight loss completes at 400 °C which leads to the formation of CoO (calcd. residue 9.2 %, experimental 9.8 %).

Coordination environment around cobalt (II) ions in coordination polymer $[Co(\mathbf{L^2})_2(Adp)(H_2O)_2]_n \cdot 2nH_2O$ (**4.1c**) are similar to that of the coordination polymer **4.1a** and they are isostructural. Supramolecular assembly of cobalt (II) adipate without ancillary ligand in complex $[(\mu\text{-}Adp)_2Co(\mu\text{-}H_2O)_2Co(H_2O)_4]$[48] was reported earlier which

do not directly have aqua bridges between cobalt ions. Thus, the difference between such structures with the coordination polymer **4.1c** is mainly due to the role of $\mathbf{L^2}$ in organizing assembly of coordination polymer. In the present case naphthalimide inhibits water molecules to bridge cobalt centres. Structure of **4.1c** depicting coordination environment is

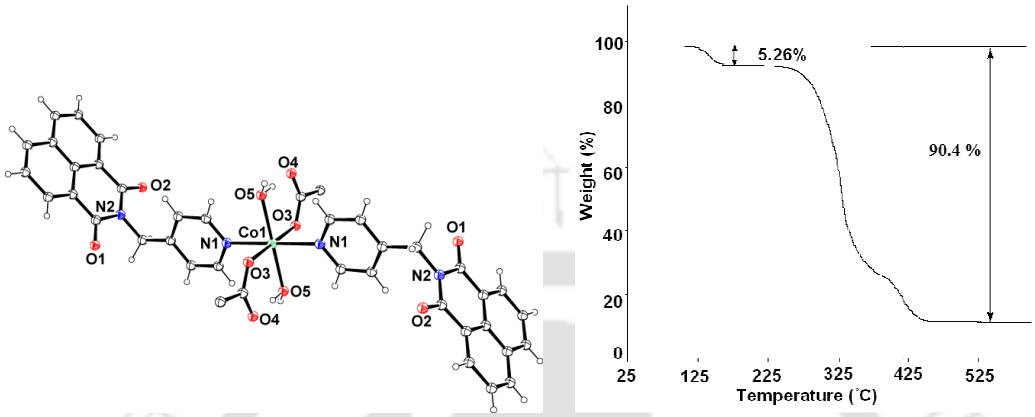

(a) (b)

Figure 4.5**: (a) ORTEP view (30% thermal ellipsoid probability) of showing the coordination environment around cobalt ion in **4.1c** and (b) Thermogram (heating rate 7 °C/min) of **4.1c.

shown in Figure **4.5a**. Thermogravimetric analysis of the coordination polymer **4.1c** (Figure **4.5b**) shows that 5.3 % weight loss takes place between 90 and 130 °C due to the loss of two water molecules of crystallization (calcd. 4.2 %). On further heating, it gives a residue of 9.6 % at 450 °C which corresponds to the formation of CoO (calcd. 9.9 %).

There are many aliphatic dicarboxylate nickel complexes which form mixed ligand complexes having oxo,[51-52] hydroxo,[53-54] and alkoxo ligands.[55] nickel (II) dicarboxylate bridges adapt syn-syn [56-57] or syn-anti geometry[58] among which the latter geometry is less preferred.

***Table 4.1**: Metal-ligand bond parameters of the coordination polymers **4.1a-4.1d**.*

Compd. No.	M-L	d_{M-L}(Å)	∠L-M-L	Angle (°)	∠ L-M-L	Angle (°)	∠ L-M-L	Angle (°)
4.1a	Mn1-N1	2.302(5)	N1-Mn1-O3	90.97(15)				
	Mn1-O3	2.172(3)	O3-Mn1-O5	90.56(15)				
	Mn1-O5	2.196(4)	N1-Mn1-O5	91.24(17				
4.1b	Co1- N1	2.184(5)	N3-Co1-N1	171.7(2)	O7-Co1-O10	172.32(19)	O10-Co1-O6	88.90(19)
	Co1- N3	2.169(5)	O5-Co1-N1	92.40(19)	O7-Co1-N3	90.05(18)	O10-Co1-N1	97.22(18)
	Co1- O5	2.162(5)	O6- Co1-N1	83.28(19)	O10-Co1-N3	85.78(18)		
	Co1- O6	2.112(5)	O7-Co1-N1	87.81(18)	O6-Co1-O5	172.4(2)		
	Co1- O7	2.058(4)	O5-Co1-N3	95.6(2)	O7-Co1-O5	88.57(18		
	Co1-O10	2.068(4)	O6-Co1-N3	89.0(2)	O7- Co1-O6	97.5(2)		
4.1c	Co1-N1	2.212(3)	O3-Co1-N1	91.21(10)				
	Co1-O3	2.112(2)	O5-Co1-N1	91.47(10)				
	Co1-O5	2.137(2)	O3-Co1-O5	91.86(9)				
4.1d	Ni1-N1	2.075(4)	O3-Ni1-N1	91.09(12)	O6-Ni1-O8	92.01(11)	O5-Ni1-O8	87.14(12)
	Ni1-O3	2.047(2)	O5-Ni1-N1	175.56(15)	O6-Ni1-O9	177.15(10)	O5-Ni1-O9	90.70(15)
	Ni1-O5	2.029(3)	O6-Ni1-N1	86.28(13)	O3-Ni1-O6	88.61(10)	O8-Ni1-O9	85.14(11)
	Ni1-O6	2.127(3)	O8-Ni1-N1	93.14(12)	O3-Ni1-O8	175.76(11)		
	Ni1-O8	2.060(3)	O9-Ni1-N1	93.74(13)	O3-Ni1-O9	94.24(10)		
	Ni1-O9	2.073(3)	O3-Ni1-O5	88.67(12)	O5-Ni1-O6	89.28(15)		

The coordination polymer $[Ni(\mathbf{L^2})(Fum)(H_2O)_3]_n \cdot H_2O$ (**4.1d**) has hexa-coordinated nickel ions and each has one $\mathbf{L^2}$ ligand coordinating (Figure **4.5a**) through pyridine [Ni-N1, 2.075(4) Å]. Other coordination sites are occupied by two monodentate carboxylates groups (Ni1-O3, 2.047(2) Å, Ni1-O8, 2.060(3) Å) and three water molecules (Ni1-O5, 2.047(2) Å, Ni1-O6, 2.127(3) Å, and Ni1-O9, 2.073(3) Å).

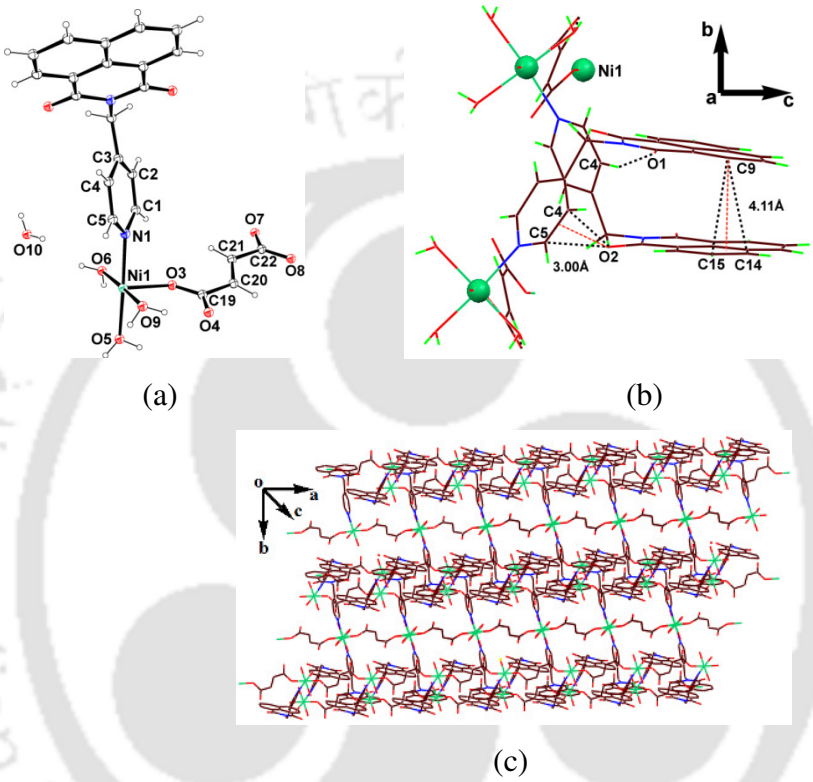

***Figure 4.6**: (a) ORTEP view of asymmetric unit of **4.1d**, (30% thermal ellipsoid probability), (b) Prominent C-H···O, π···π and O···π interactions in **4.1d** and (c) 3D-supramolecular chain present in lattice of **4.1d** (hydrogen atoms and lattice water molecules are omitted for clarity).*

Metal-ligand bond parameters are listed in Table **4.1**. Ligand $\mathbf{L^2}$ attached to alternate metal ions are trans to each other and have π···π interactions as shown in Figure **4.6b**. These interactions help to form 3D supramolecular chains as shown in Figure **4.6c**.

In thermogram (heating rate 7 °C/min) of coordination polymer **4.1d** (Figure **4.19b** in the experimental section), 3.2 % weight loss is observed between 50 and 85 °C which corresponds to the loss of one lattice water molecule (calcd. wt. loss 3.4 %). A second weight loss of 9.7 % at 90-175 °C corresponds to loss of three coordinated water (calcd. wt. loss 10.6 %) molecules and a third weight loss of 23.7 % occurs due the loss of one fumerate (calcd. wt. loss 24.7 %) in the temperature range of 194-320 °C. Coordination

polymer finally yielded NiO (residue obtained; experimental 12.95 % and calcd. 14.07 %) at 475 °C.

We found that naphthalimide tethered pyridine ligand provided new copper malonate, fumarate, and adipate coordination polymers. They have shown large structural difference among themselves. The dicarboxylate ligand plays a major role in the three coordination polymers.

Copper (II) centers in the coordination polymer $[Cu(\mathbf{L}^2)_2(Fum)]_n \cdot nH_2O$ (**4.1e**) have distorted octahedral geometries which are reflected in ∠O-Cu-O bond angle ranging from 51.2(2) to 76.6(2)°. The crystallographic asymmetric unit of **4.1e** comprises a copper (II) ion, one fumerate, two ligands ($\mathbf{L}^2$) and one lattice water molecule (Figure **4.7a**). Distortion around copper (II) ions in **4.1e** is due to Jahn-Teller distortion as well as from binding modes. Such binding modes of two ends of the fumarate to copper (II) ions are different (Figure **4.7b**). One end acts as a chelating bidentate whereas the other end acts as μ^1-O-carboxy bridge. One oxygen atom O8 of fumarate bridges two Cu atoms whereas O5 and O6 bind through a chelating manner to a copper ion. Cu-O bond distances of the chelating carboxylate group are unequal (Cu1-O5, 1.952(5) Å, Cu1-O6, 2.787(8) Å).

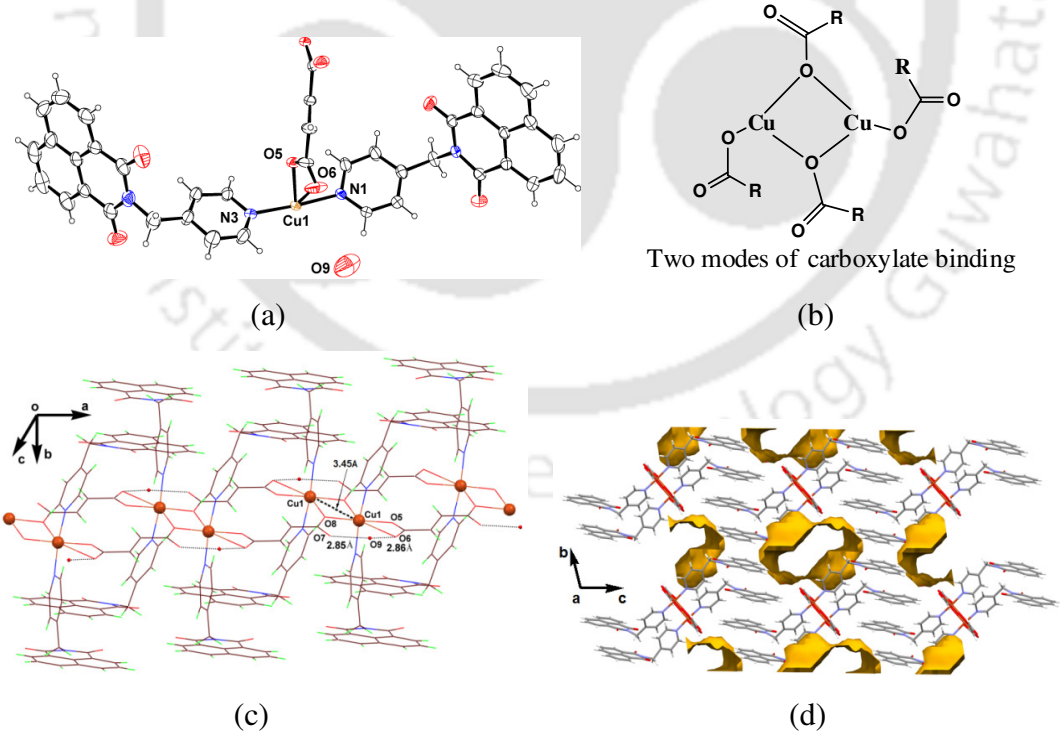

***Figure 4.7**: ORTEP view of asymmetric unit of **4.1e** (30% thermal ellipsoid probability), (b) Carboxylate bridge around two copper ions, (c) Coordination environment around copper (II) ion and (d) Porous structure of the coordination polymer **4.1e**.*

On the other hand, bridging O atoms also make a nonsymmetric bridge with different copper oxygen distances Cu1-O8, 1.974(5) Å and Cu1′-O8, 2.414 (6) Å. As a result of the μ^1-O bridge, copper ions come close to each other (Cu1 to Cu1 separation 3.45 Å) (Figure **4.7c**). Overall a 3D supramolecular sheet-like structure of coordination polymer is forms and it is guided by various weak interactions. The coordination polymer **4.1e** contains a solvent accessible void with a radius 1.2 Å running along a-crystallographic axis (Figure **4.7d**). The volume of these voids is 2085.7 $Å^3$ and they occupy 23.4 % of the unit cell volume.

Asymmetric unit of the coordination polymer $[Cu(\mathbf{L^2})(Mal)]_n$ (**4.1f**) contains one copper (II) ion, one $\mathbf{L^2}$, one malonate group and one water molecule as a ligand (Figure **4.8a**). Copper (II) centers are in a distorted square pyramidal geometry. Each copper ion is associated with one nitrogen of the pyridine part of $\mathbf{L^2}$ (Cu1-N1, 2.031(4) Å) and four oxygen atoms, two oxygen atoms from one Mal group (Cu1-O3, 1.918(3) Å and Cu1-O5, 1.982(3) Å), third oxygen dative site is from another Mal group (Cu1-O6, 1.969(3) Å) and fourth oxygen site is from a coordinated water molecule (Cu1-O7, 2.235(4) Å).

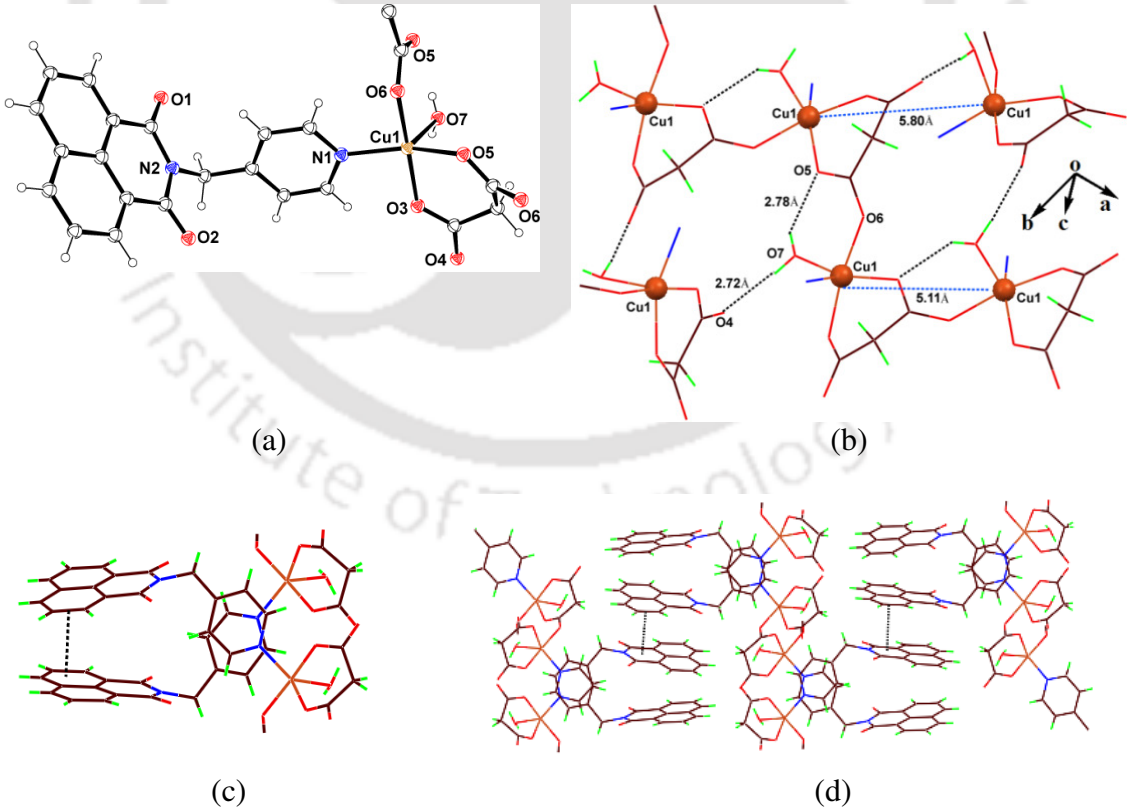

***Figure 4.8**: (a) ORTEP view (50% thermal ellipsoid probability) of asymmetric unit of **4.1f**, (b) Hydrogen-bonded motif formed by coordinated water molecule, (c) π···π interactions between naphthalimide rings in a chain and (d) π···π interactions between naphthalimide rings of neighbouring chains in the lattice of **4.1f**.*

One oxygen atom O4 of malonate group from adjacent chain and O5 of same chain forms acceptor hydrogen-bond with coordinated water molecule (O4···O7, 2.72 Å and O5···O7, 2.78 Å) as shown in Figure **4.8b**. There exist C-H···O interactions between naphthalene ring with malonate oxygen and O···π interaction between pyridyl ring and malonate oxygen. Although naphthalimide rings are positioned oblique to each other in a nonparallel manner, two different weak π···π stacked interactions exist among naphthalene rings (Figure **4.8c**). One of which is inter chain type (centroid to centroid distance 3.52 Å) and another is among naphthalimide rings on the same chain (centroid to centroid distance 4.15 Å) which leads to the formation of a sheet like structure and also helps in the formation of a chain that runs parallel to the bc-plane of the unit cell (Figure **4.8d**).

In case of copper (II) adipate coordination polymer $[Cu_3(\mathbf{L^2})_6(Adp)_3(H_2O)_3]_n$, asymmetric unit of (**4.1g**) contains three copper ions bridged by three Adp groups and each copper ion is ligated by two $\mathbf{L^2}$ and a water (Figure **4.9a**).

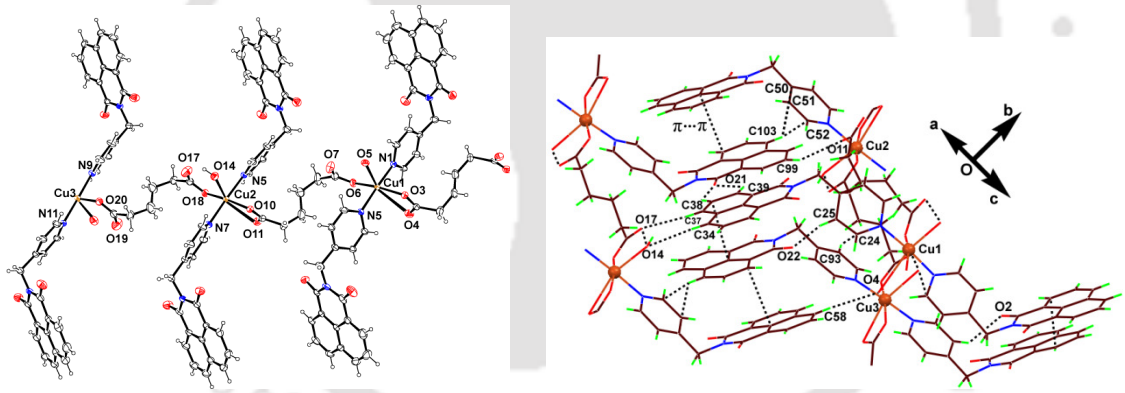

(a) (b)

***Figure 4.9**: (a) ORTEP view (30% thermal ellipsoid probability) of asymmetric unit of **4.1g**, (b) π···π interactions between naphthalimide rings and C-H···π interactions in the lattice of **4.1g**.*

Each copper (II) ion adapts a distorted octahedral geometry and it has one monodentate carboxylate (Cu1-O6, 1.9672(19) Å) and one bidentate chelating carboxylate (Cu1-O3, 1.977(17) Å, Cu1-O4, 2.793(2) Å) of Adp bound to copper ion. Metal-ligand bond parameters of the coordination polymers **4.1e**-**4.1g** are listed in Table **4.2**. Polymer **4.1g** exhibits face-to-face π···π interactions between naphthalene rings with a centroid-to-centroid distance of 3.67 Å (Figure **4.9b**). There are also C-H···π interactions between C-H of the naphthalene ring with the pyridyl ring (donor to π-centroid distance as 3.42 Å).

These weak interactions lead to the formation of a 2D lamellar structure. A few selected hydrogen bond parameters of **4.1e**-**4.1g** are listed in the Table **4.4.**

Thermogram of **4.1e** (Figure **4.19c** in the experimental section) shows 3.2 % weight loss at 70-90°C corresponding to the loss of one lattice water molecule. There is a loss of 14.5 % weight in the range of 115-196 °C which is due to the loss of one fumerate ligand (calcd. 15.1 wt. %). Coordination polymer **4.1f** has a weight loss of 20.3 % (calcd. wt. % 21.7) in the temperature range 100-230 °C due to the loss of one malonate group.

Table 4.2**: Metal-ligand bond parameters of the coordination polymers **4.1e-4.1g.

Compd. No.	M-L	d_{M-L}(Å)	∠L-M-L	Angle (°)	∠ L-M-L	Angle (°)
4.1e	Cu1-N1	2.014(7)	N3-Cu1-N1	173.4(3)	O8-Cu1-O8	76.6(2)
	Cu1-N3	2.006(7)	O5-Cu1-N1	87.0(3)	O5-Cu1-O8	176.9(3)
	Cu1-O5	1.952(5)	O8-Cu1-N1	92.0(2)	N1-Cu1-O8	90.2(2)
	Cu1-O8	1.974(5)	O5-Cu1-N3	87.3(3)	O5-Cu1-O6	51.4(2)
	Cu1-O8	2.414(6)	O8-Cu1-N3	94.0(2)		
	Cu1-O6	2.787(8)	O5-Cu1-O8	100.5(2)		
4.1f	Cu1-N1	2.031(4)	O3-Cu1-N1	89.59(14)	O3-Cu1-O6	170.78(16)
	Cu1-O3	1.918(3)	O5-Cu1-N1	151.69(15)	O3-Cu1-O7	88.84(16)
	Cu1-O5	1.982(3)	O6-Cu1-N1	91.13(14)	O5-Cu1-O6	84.45(14)
	Cu1-O6	1.969(3)	O7-Cu1-N1	108.35(15)	O5-Cu1-O7	99.96(15)
	Cu1-O7	2.235(4)	O3-Cu1-O5	90.57(14)	O6-Cu1-O7	99.65(15)
4.1g	Cu1-N1	2.016(2)	O3-Cu1-N1	88.36(8)	O18-Cu2-N7	89.19(9)
	Cu1-N3	2.040(2)	O6-Cu1-N1	89.31(8)	N7-Cu2-O14	95.92(9)
	Cu1-O3	1.977(17)	N1-Cu1-N3	174.38(10)	O18-Cu2-O10	169.06(10)
	Cu1-O5	2.349(2)	O3-Cu1-N3	92.11(8)	O10-Cu2-O14	89.24(8)
	Cu1-O6	1.967(19)	O6-Cu1-N3	88.88(8)	O18-Cu2-O14	101.70(8)
	Cu2-N5	2.022(2)	O6-Cu1-O3	165.82(9)	N11-Cu3-N9	177.80(12)
	Cu2-N7	2.021(2)	O3-Cu1-O5	96.23(8)	O25-Cu3-N9	92.61(9)
	Cu2-O10	1.990(18)	N1-Cu1-O5	93.54(9)	O20-Cu3-N9	89.44(9)
	Cu2-O14	2.408(2)	N3-Cu1-O5	91.98(8)	O25-Cu3-N11	87.63(9)
	Cu2-O18	1.960(19)	O6-Cu1-O5	97.87(8)	O20-Cu3-N11	89.93(9)
	Cu3-N9	2.014(2)	O10-Cu2-N5	89.63(8)	O20-Cu3-O25	169.70(12)
	Cu3-N11	2.010(2)	O18-Cu2-N5	90.96(8)		
	Cu3-O20	1.948(2)	O14-Cu2-N5	86.85(9)		
	Cu3-O25	1.987(2)	N5-Cu2-N7	177.14(11)		
	Cu1-O4	2.793(2)	O10-Cu2-N7	89.69(8)		

It was earlier shown that mono-deprotonated malonate complex $[Cu(HMal)_2 \cdot 2H_2O]$([Cu-Mal]) easily decarboxylates to form CuO.[60] The coordination polymer **4.1g** loses 19.6 % weight at 86-246°C due to loss of three coordinated water molecules and three adipate anions (calcd. wt. % 20.2) from each repeat unit.

Structural studies on **4.1e**-**4.1g** have revealed that bridging modes of carboxylic acids varies in these copper coordination polymers. Ligand $\mathbf{L^2}$ is dipolar with two carbonyl groups which have the ability to guide coordination modes through their participation in supramolecular interactions. A special feature of the coordination polymer **4.1e** is that it has Cu_2O_2 cores. On the other hand, the packing pattern of copper (II) malonate polymer **4.1f** is highly influenced by the π-interactions. In this polymer, naphthalimide rings are positioned in a head to head manner, which is interesting as in naphthalimide compounds stacking occurs as head to tail to account for dipolar interactions.

Different coordination modes and different nuclearities of copper (II) dicarboxylates are common in the literature.[56]

For example, copper (II) malonate complexes exist as hydrates[57] and polymers[58] and possesses different carboxylate bridging modes such as syn-syn, anti-syn or anti-anti mode.[59-63] Layered structures of copper (II) malonate to include organocationic species are well studied.[64] In our present case we find that stacking of naphthalimide group as well as pyridine coordination along with flexibility of dicarboxylate ligand guides the coordination environment of copper.

4.3. Magnetic studies of the coordination polymers 4.1a-4.1g:

Magnetic measurement of the coordination polymers **4.1a to 4.1g** were carried out at low temperature. For the coordination polymer **4.1a,** plot of $\chi_M T$ *vs.* T under 1000 Oe external field in temperature range of 300-2 K is shown in Figure **4.10a**. Room temperature $\chi_M T$ value for **4.1a** is 4.23 $cm^3\ mol^{-1}\ K$ which is close to the spin-only value 4.37 $cm^3\ mol^{-1}\ K$ for one isolated high spin manganese (II) ion (S = 5/2 state and g_{Mn} = 2.0). As the temperature is lowered, $\chi_M T$ value remains almost constant down to about 15 K, where value begins to decrease to a minimum value 3.37 $cm^3\ mol^{-1}\ K$ at 2 K. This type of magnetic behaviour indicates weak antiferromagnetic interactions between the chains. M *vs.* H plot of **4.1a** at a different temperature (2-5 K) shown in Figure **4.10b**. At 2 K, an increase of magnetization was observed with a value of 4.70 μB at 7 T which is closer to the saturation value of 5.0 μB that is expected for spin-only manganese (II) ion.

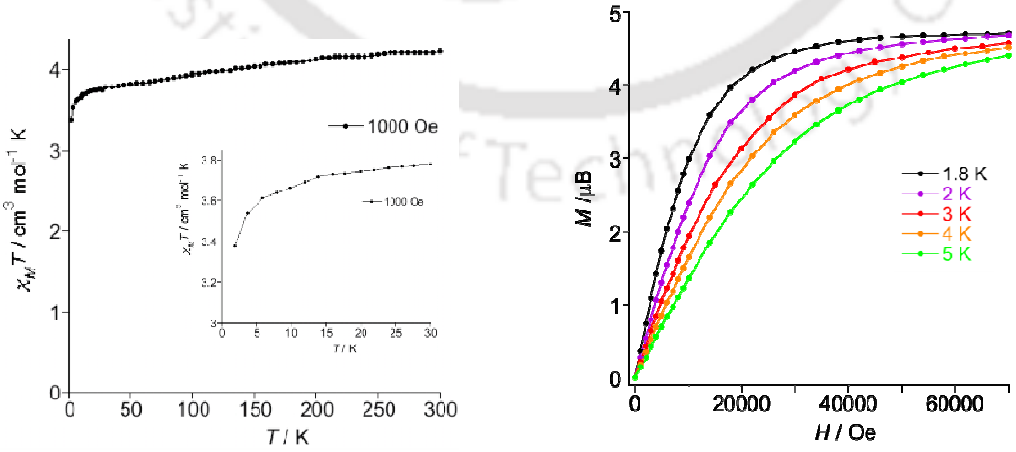

(a) (b)

Figure 4.10: *Plots of (a) $\chi_M T$ vs. T (inset is an expansion in the range of temperature range 2-30 K) and (b) M vs. H for the coordination polymer* ***4.1a****.*

Magnetization values at higher temperatures do not superimpose which indicates the presence of a low-lying excited state and zero-field splitting in this polymer. Magnetic susceptibility of **4.1a** measured in 3.5 Oe ac magnetic field and 1500 Oe dc magnetic field showed a strong frequency dependence of the in- and out-of-phase signals (χ' and χ''), (Figure **4.18** in the experimental section) which showed the presence of slow magnetization relaxation, typical of single chain magnetic (SCM) behaviour. Fitting to the $\log(1/2\pi\nu)$ *vs.* 1/T plot based on the Arrhenius relationship $1/\tau = (1/\tau_0)\exp(-\Delta_{eff}/kBT)$ showed a relaxation time $\tau_0 = 1.27\times10^{-6}$ s and large relaxation energy barrier $\Delta_{eff} = 16.98$ K (Figure **4.11**). This clearly showed single-chain magnetic properties of the coordination polymer **4.1a**.

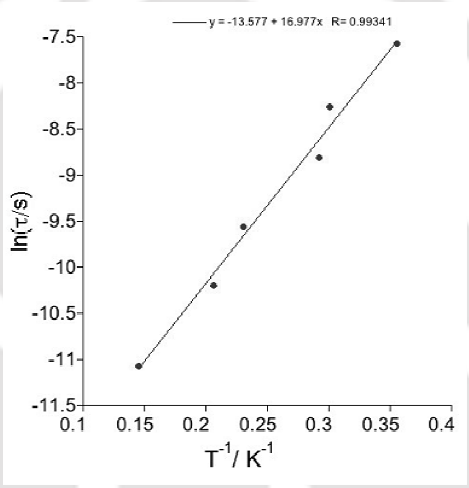

Figure 4.11*: Arrhenius plot for SCM of the coordination polymer* ***4.1a****.*

Observation of antiferromagnetic inter chain interactions is evident as the distance between two manganese ions of adjacent chains is 5.58 Å whereas along a chain the adjacent manganese ions are 12.61 Å apart from each other (Figure **4.1b**). Molecule-based magnetic materials such as single chain magnets have become an outstanding area of research because of their application in high-density storage device and molecular electronics.[65-69] Azido bridged manganese coordination polymer of *N,N'*-bis(5-chlorosalicylidene)-1,3-diaminopropane was reported to show single chain magnetic behaviour at low temperature where manganese atom is in +3 oxidation state.[70] Single chain magnet behaviour have also been observed in a chiral hetero-metallic cobalt (II)-copper (II) 1D polymer derived from a bis bidentate ligand.[71] Recently another pyrenylnitronylnitroxide based cobalt complex have been reported to show a single chain magnetic behaviour and they are strongly dependent on the structure of the chains and on

their supramolecular packing.[72] Manganese (II) polynuclear phthalate or terephthalate were shown to exhibit antiferromagnetic behavior.[73] Manganese phthalate 1D or 2D networks having phthalates as bridging ligands show antiferromagnetic properties.[74-75] Weak intra layer ferromagnetic interactions in manganese (III) malonate complexes were documented earlier.[76]

For **4.1b** and **4.1c**, $\chi_M T$ values at 300 K are 2.82 and 2.69 $cm^3\ mol^{-1}\ K$ respectively, which are close to the spin only value (S = 3/2 and g_{Co} = 2.1) of 2.5-3.1 $cm^3\ mol^{-1}\ K$ expected for the non interacting one high-spin cobalt (II) ion. This behavior is common for cobalt (II) complexes that can be attributed to orbital contribution of cobalt (II).[77]

The $\chi_M T$ values of **4.1b** and **4.1c** shows a continuous decrease to a minimum value of 1.45 and 1.25 $cm^3\ mol^{-1}\ K$ at 2K respectively (Figure **4.12**) which are in accordance with antiferromagnetic behavior of the cobalt (II) ions. Structures of two complexes have large differences in distances between the adjacent cobalt ions.

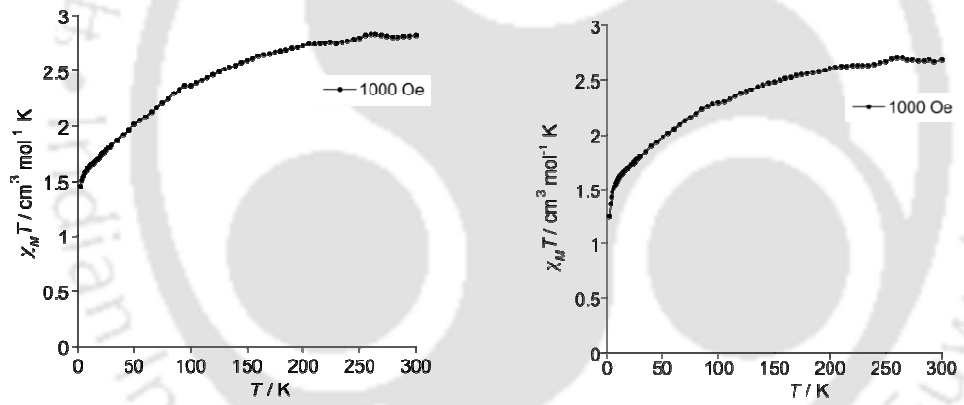

***Figure 4.12**: Plot of $\chi_M T$ vs. T for the coordination polymers (a) **4.1b** and (b) **4.1c**.*

Adjacent cobalt-to-cobalt distance in the same chain of cobalt (II) coordination polymer **4.1b** is 7.27 Å and similar distances between cobalt ions of adjacent chains are 9.02 Å. Thus, inter-chain interactions are not possible but coordination polymer has an olefinic double bond between carboxylates making an effective exchange through conjugation. On the other hand, the coordination polymer **4.1c** being isostructural to **4.1a**, an inter-chain interaction makes antiferromagnetic effect feasible. M *vs.* H plots of **4.1b** (Figure **4.18a** in the experimental section) and **4.1c** shows a saturation value 2.86 μB and 2.52 μB respectively per formula unit at 2 K and 7 T which is lower than saturation value of 3 μB

for spin-only cobalt (II) ion (S = 3/2 and g_{Co} = 2.1). This behaviour also supports an antiferromagnetic coupling between the cobalt (II) ions in **4.1b** and **4.1c**.

Room-temperature $\chi_M T$ value for the coordination polymer **4.1d** (Figure **4.13a**) is 1.07 $cm^3\ mol^{-1}\ K$ which is close to a spin-only value 1.10 $cm^3\ mol^{-1}\ K$ for one isolated high-spin nickel (II) ion (S=1 and g_{Ni} = 2.1). As the temperature is lowered, $\chi_M T$ value remains almost constant down to about 30 K, from where the value begins to decrease to a minimum value of 0.51 $cm^3\ mol^{-1}\ K$ at 2 K. An M *vs.* H plot of **4.1d** (Figure **4.18b** in the experimental section) shows almost a saturation value of 1.95 μB per formula unit at 2 K and 7 T, which is close to a saturation value of 2 μB for spin-only nickel (II) ion (S= 1 and g_{Ni}= 2.1). The open framework of nickel fumarate with hydroxy bridged nickel (II) complex $[Ni_3(OH)_2(Fum)(H_2O)_4]\cdot 2H_2O$ showed exceptional ferromagnetic properties.[78] Plot of the $\chi_M T$ *vs.* T under 1000 Oe external field in temperature range of 300-2 K for **4.1e** is shown in Figure **4.13b** and **4.1f-4.1g** are shown in Figure **4.14**.

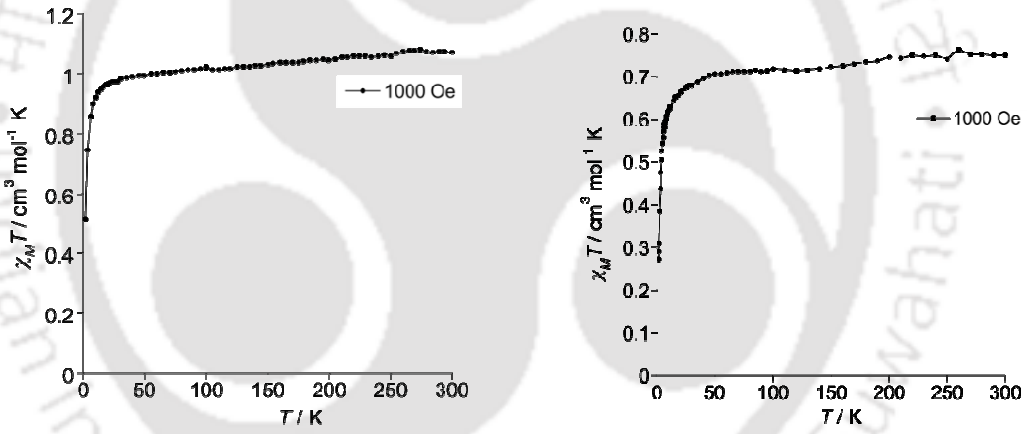

(a) (b)

***Figure 4.13**: Plot of $\chi_M T$ vs. T for the coordination polymers (a) **4.1d** and (b) **4.1e**.*

Room-temperature $\chi_M T$ value for **4.1e** is 0.75 $cm^3\ mol^{-1}\ K$, which is close to spin only value 0.8 $cm^3\ mol^{-1}\ K$ for two copper (II) ions (S = 1/2 and g_{Cu}= 2.1). As temperature is lowered, the $\chi_M T$ value remains constant to 35 K, where value decreases to 0.27 $cm^3\ mol^{-1}\ K$ at 2 K. M *vs.* H plot of **4.1e** show a saturation value of 1.87 μB per formula unit at 2 K and 7 T, which is close to saturation value 2 μB for spin-only value for two copper (II) ions (S = 1/2 and g_{Cu} = 2.1).

For the coordination polymer **4.1f,** the $\chi_M T$ value at room temperature is 0.48 $cm^3\ mol^{-1}\ K$ which is higher than the calculated value for one magnetically non interacting copper (II) ion (S = 1/2 and g_{Cu} = 2.1).[79-81] Upon cooling, $\chi_M T$ smoothly decreases to attain a quasi

plateau between 80 and 35 K (with $\chi_M T$ = 0.36 cm^3 mol^{-1} K) and it further sharply increases to 0.77 cm^3 mol^{-1} K at 2.0 K. M *vs.* H plot of **4.1f** (Figure **4.19d** in the experimental section) show near saturation value of 0.96 *B* per formula unit at 2 K and 7 T, which is closer of saturation value of **4.1f** μB for spin-only copper (II) ion (S = 1/2 and g_{Cu} = 2.1). Thus, **4.1f** shows ferromagnetic interaction between copper centres at low temperature. For the copper (II) grids, ferromagnetic interactions were reported especially in the case of single-atom linkages between the metal ions, Cu-O-Cu.[82] In our case the ferromagnetic interactions may arise due to triple atoms linkage between the adjacent metal ions, Cu-O=C-O-Cu.

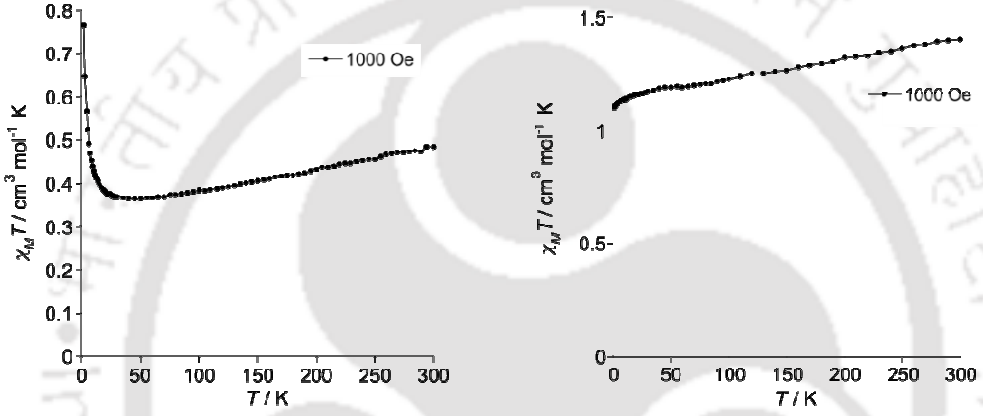

Figure 4.14: *Plot of $\chi_M T$ vs. T for the coordination polymer (a)* ***4.1f*** *and (b)* ***4.1g****.*

Another two copper (II) [2×2] grid-like complexes were reported to show for both the occurrence of intramolecular ferromagnetic interactions.[83]

On the other hand, $\chi_M T$ value of the coordination polymer **4.1g** at 300 K is 1.40 cm^3 mol^{-1} K which is higher than the spin-only value ($\chi_M T$ = 1.2 cm^3 mol^{-1} K) of three copper (II) ions (S =1/2 and g_{Cu} = 2.1). Upon cooling, $\chi_M T$ value decreases monotonically to 1.10 cm^3 mol^{-1} K at 2 K. M *vs.* H plot of **4.1g** show a saturation value of 2.79 μB per formula unit at 2 K and 7 T which is closer of saturation value of 3 μB for three spin-only copper (II) ions (S = 1/2 and g_{Cu} = 2.1).

Copper-malonate complexes show inter chain antiferromagnetic coupling.[84-85] Three-dimensional malonate bridged networks,[58] $[Cu(Mal)(DMF)]_n$, exhibits ferromagnetic ordering below 2.6 K, whereas $[Cu(Mal)(0.5pyz)]\cdot H_2On$ shows metamagnetic property. Aliphatic dicarboxylate with a rigid spacer such as fumarate forms bridges between copper ions. For example, copper (II) fumarate complex with phenanthroline ligands has a dimeric structure in which one fumarate dianion bridges two copper centers through

terminal carboxylate groups in a monodentate fashion, and another fumarate acts as anion, and the complex shows weak antiferromagnetic interactions between the copper ions.[86]

Adipic acid forms a copper (II) complex by connecting two copper ions through the two carboxylate groups.[87-88]

Polymeric trinuclear adipate $[Cu_3(Adp)_2(OH)_2(H_2O)_4]_n$ shows weak antiferromagnetic interactions.[87] Copper adipate metalloorganic framework with Cu(2,2′-bpyridine) node shows weak antiferromagnetic interactions.[88]

From the structural and magnetic study, we have found wide variations on structures and magnetic properties of these coordination polymers and summary of the results listed in a tabular form in Table **4.3**.

***Table 4.3**: Type of structures and magnetic behavior of the coordination polymers.*

Formulae	no.	type of structure	magnetic properties at low temperature	type of coordination
$[Mn(\mathbf{L^2})_2(Adp)(H_2O)_2]_n \bullet 2nH_2O$	**4.1a**	3D supramolecular layer-like structure	Weak antiferromagnetic interaction, single chain magnetic behaviour.	distorted octahedral
$[Co(\mathbf{L^2})_2(Fum)(H_2O)_2]_n \bullet 2nH_2O$	**4.1b**	2D supramolecular network	antiferromagnetic behaviour	distorted octahedral
$[Co(\mathbf{L^2})_2(Adp)(H_2O)_2]_n \bullet 2nH_2O$	**4.1c**	3D supramolecular layer-like structures	antiferromagnetic behaviour	distorted octahedral
$[Ni(\mathbf{L^2})(Fum)(H_2O)_3]_n \bullet H_2O$	**4.1d**	3D chain-like supramolecular architecture	antiferromagnetic behaviour	distorted octahedral
$[Cu(\mathbf{L^2})_2(Fum)]_n \bullet nH_2O$	**4.1e**	3D supramolecular sheet-like structure	antiferromagnetic behaviour	distorted octahedral
$[Cu(\mathbf{L^2})(Mal)]_n$	**4.1f**	2D sheet-like structure	ferromagnetic interaction between Cu(II) sites	distorted square pyramidal
$[Cu_3(\mathbf{L^2})_6(Adp)_3(H_2O)_3]_n$	**4.1g**	2D lamellar structure	weak antiferromagnetic coupling between Cu(II) sites	distorted octahedral

4.4 EPR studies of copper coordination polymers 4.1e-4.1g:

We recorded solid state X-band electron paramagnetic resonance (EPR) spectra of the copper coordination polymers **4.1e**-**4.1g** to confirm the oxidation state of copper in these polymers. Differences in coordination environment in **4.1e**-**4.1g** are reflected in electron paramagnetic resonance spectra shown in Figure **4.15**. From solid state X-band EPR spectra of three copper coordination polymers **4.1e**-**4.1g** calculated g average (g_{av}) values are 2.11, 2.04, and 2.03, respectively. EPR spectra of crystalline samples of **4.1f** and **4.1g** were recorded at room temperature showed a relatively simple pattern. They show g_{II} and

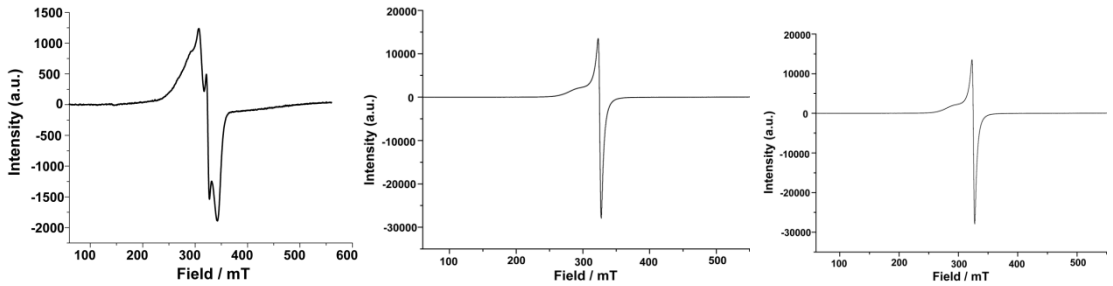

***Figure 4.15**: Solid state X-band EPR spectrum of (a) **4.1e,** (b) **4.1f** and (c) **4.1g**.*

$g_{\perp}$ for distorted octahedral geometry and are devoid of hyperfine splitting. On the other hand, **4.1e** showed a complex pattern in EPR spectra which could not be explained on the basis of our data from room temperature. Nonetheless, it could discern paramagnetic center to be copper ions. Thus, it is observed that coordination environment of polymer **4.1e** favors a Cu_2O_2 core which apparently could show different magnetic properties including diamagnetism [79-80] but shows antiferromagnetic properties at low temperature. It has a comparatively smaller Cu···Cu separation which is 3.454 Å between the copper metal ions, allowing them to have very weak interactions between them reflected in magnetic measurements. On the other hand, **4.1f** and **4.1g** have larger distances between neighbouring copper (II) ions and hence do not show magnetic coupling at ambient condition.

4.5 UV-Visible and photoluminescence properties:

The coordination polymers **4.1a-4.1g** are slightly soluble in common solvents and hence UV-visible spectra of the ligand $\mathbf{L^2}$ and the oordination polymers **4.1a-4.1g** were recorded in the solid state for a uniform comparison (Figure **16a**). Solid state UV-visible spectra of free $\mathbf{L^2}$ display two absorption bands at 330 and 359 nm. These absorptions are attributed to $\pi \rightarrow \pi^*$ and $n \rightarrow \pi^*$ transitions. Coordination polymer **4.1a** shows an absorption in UV-region due to ligand and it does not absorb in the visible region because of the A_{1g} ground state. UV-visible spectra of **4.1b-4.1g** have absorptions in the UV region as well as in the visible region; absorptions in the UV regions are due to ligand and in the visible regions are due to d-d transitions.

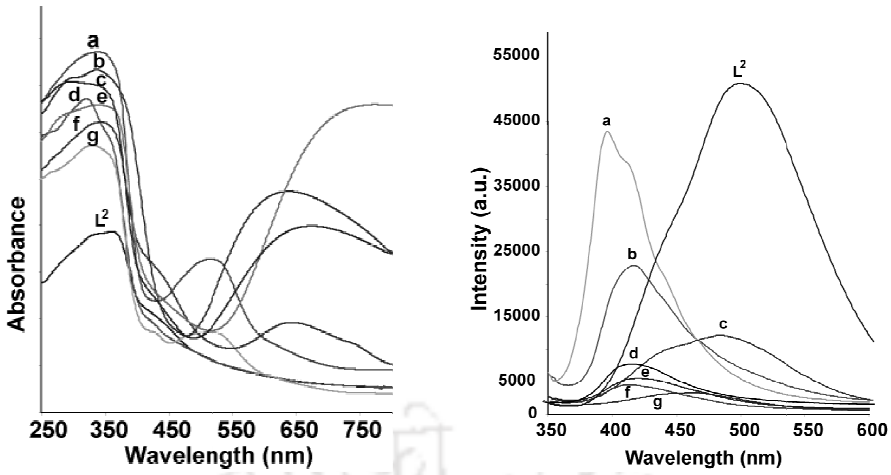

(i) (ii)

***Figure 4.16**: Solid state (i) UV-visible spectra of **L²** and the coordination polymers (a) **4.1b**, (b) **4.1e**, (c) **4.1g**, (d) **4.1a**, (e) **4.1f**, (f) **4.1d**, and (g) **4.1c.** (ii) Photoluminescence spectra of **L²** and coordination polymers (a) **4.1c**, (b) **4.1a**, (c) **4.1d**, (d) **4.1e**, (e) **4.1f**, (f) **4.1g**, and (g) **4.1b** at room temperature (λ_{ex} = 330 nm).*

Since ligand **L²** is fluorescent, we have investigated solid state photoluminescence properties of the coordination polymers **4.1b-4.1g** at room temperature. Ligand-based luminescence properties are useful in the detection of metal ions.[10-12] Due to enhanced stability of metal complexes compared to organic counterparts, coordination polymers are used as photoluminescent materials.[89] Generally d^{10}-metal coordination polymers exhibit photoluminescence properties.[90] Solid state fluorescence of **L²** shows a broad photoluminescence emission at 500 nm which is assigned to intermolecular charge transfer based on earlier observations on such emissions by metal complexes having fluorescent aromatic ligands.[91] In solid state, coordination polymers show the quenching of fluorescence with differing intensity and shift of emission maxima (λ_{ex} = 330 nm in each case) toward a shorter wavelength from the ligand takes place. Exceptions are **4.1b** and **4.1d** which show quenching of fluorescence intensities without a significant shift. Solid state emission spectra of powdered sample of ligand as well as coordination polymers are shown in Figure **16b**. Blue-shift observed is ascribed to ligand to metal charge transfer transitions[92] and different rigidity of the crystal packing in the solid state.[93] Difference in emission spectra are attributed to individual electronic configurations of the metal ions and stacking patterns. Coordination polymers **4.1d** and **4.1f** have one naphthalimide ring per metal centre whereas other coordination polymers have two each. Sequence of emission intensities shown by solid samples of the coordination polymers is **L² > 4.1c > 4.1a > 4.1d > 4.1e > 4.1f > 4.1g > 4.1b**.

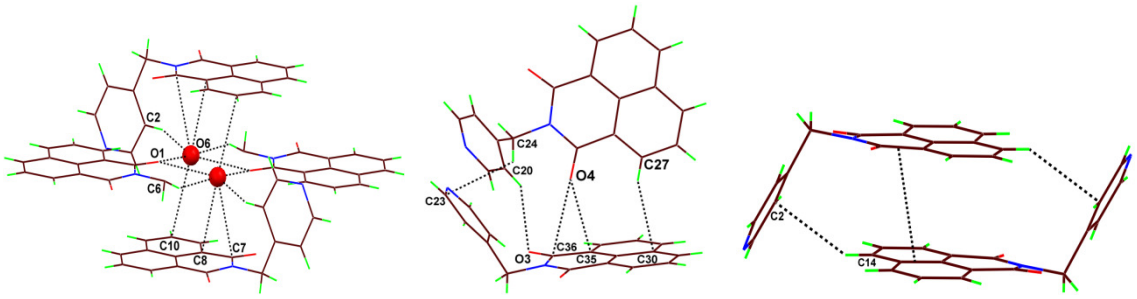

(a) (b) (c)

***Figure 4.17**: Assemblies of water molecules held through C-H···O with a CH of pyridine and oxygen-π interactions with naphthalimide in **4.1a**; (b) C-H···π interaction in **4.1b** between perpendicularly placed naphthalimide rings; (c) π-stacking of naphthalimide rings in **4.1e**.*

Thus, the metal ion as well as packing has a role in deciding fluorescence emissions. Analysis of packing patterns of these coordination polymers show some prominent interactions associated with naphthalimide rings. The packing pattern of the coordination polymer **4.1a** shows the presence of dimers of water molecules held in assemblies of naphthalimides (Figure **17a**). Water molecules are observed to be present above naphthalimide rings and are held by weak C-H···O interactions. The situation is similar to positioning of an anion over naphthalimide via C-H···anion interactions.[94] The coordination polymer **4.1b** has C-H···π and O···π interactions between naphthalimide rings (Figure **17b**). Coordination polymer **4.1c** has dimeric assemblies of water molecules which are held by a carbonyl group of the naphthalimide ring. In the crystal lattice of coordination polymer **4.1d** naphthalimide rings have very small portions which are parallel to each other. Naphthalimide rings in lattices of coordination polymer **4.1e** are parallel to each other and have π···π interactions (Figure **17c**). On the other hand, the crystal lattice of coordination polymer **4.1f** has naphthalimide rings in oblique positions, but their distance of separations suggests that they have π···π interactions. Naphthalimide rings of the oordination polymer **4.1g** are parallel in its lattice, and separating distance of the rings is suitable for π···π interactions. From the separation distance between the naphthalimide rings in lattice, it may be suggested that there is insignificant π-interactions among the naphthalimide rings in the in coordination polymer **4.1d** and **4.1f**.

4.6 Conclusion:

In conclusion, it is observed that supramolecular interactions associated with naphthalimide rings of $\mathbf{L^2}$ and the flexibility of the dicarboxylic acids guide the

coordination modes of different carboxylates. Changes in coordination and assembling properties caused by supramolecular interactions of naphthalimide group on these coordination polymers decide their photoluminescence and magnetic properties. At low temperature all the coordination polymers show weak antiferromagnetic behaviour other than copper malonate coordination polymer which show ferromagnetic coupling. Single chain magnetic property of manganese adipate coordination polymer **4.1a** is due to weak interactions between polymer chains. Frequency dependency of χ' and χ'' given in Figure **4.18a** and **4.18b** in the experimental section clearly shows that in χ'' there is a clear maximum at different fields, which is indicative of SCM behavior. In this polymer, the distance between neighbouring manganese ions of polymeric chain is 12.612 Å, but interchain hydrogen bonds bring two manganese ions of neighbouring chain to a distance of 5.584 Å. Such an orderly arrangement enables the polymer to show SCM properties at low temperature.

4.7 Experimental section:

The detailed synthetic methodologies for synthesis of naphthalimide and the coordination polymers are described. Analytical data as well as spectroscopic data are listed along with each compound. The instrumental details and the crystallographic parameters are provided in Appendix.

Synthesis of N-(4-pyridylmethyl)-1,8-naphthalimide (L^2): L^2 was synthesized by refluxing a mixture of 1,8-naphthalic anhydride (1.0 g, 5 mmol) and 4-picolylamine (0.54 g, 5 mmol) in DMF at 100 °C for 12 h. Then the reaction mixture was cooled and cold water was added. The brown precipitate of L^2 formed was filtered and dried in air. Yield 78%. IR (KBr, cm^{-1}): 3073 (w), 1660 (s), 1588 (s), 1506 (m), 1373 (s), 1347 (w), 1230 (s), 1178 (s), 1071 (w), 994 (w), 938 (m), 774 (s), 645 (w). ^{1}H-NMR (400 MHz, $CDCl_3$): 8.61 (*d,* 1H, 6.8Hz), 8.52 (*d*, 1H, 8Hz), 8.24 (*d*, 1H, 8.0Hz), 7.76 (*t*, 1H, 7.2Hz), 7.26 (*s*, 1H), 5.36 (*s*, 2H).

Coordination polymer 4.1a: To a solution of ligand, L^2 (0.58 g, 2 mmol) dissolved in warm methanol (10 mL), adipic acid (0.15g, 1mmol) was added. The resulting solution was stirred for 30 min. Manganese (II) acetate tetrahydrate (0.26 g, 1 mmol) was added to the above mixture and refluxed for 1 h. A white precipitate formed was dissolved in water, filtered and kept undisturbed for crystallization. White crystals of **4.1a** were obtained (isolated yield 51% based on Mn). Elemental analysis (%) for $C_{42}H_{40}MnN_4O_{12}$: calcd. C

59.51, H 4.76, N 6.61; found C 59.68, H 4.89, N 6.93. IR (KBr, cm^{-1}): 3559 (m), 1706 (s), 1659 (s), 1590 (w), 1407 (m), 1316 (w), 1240 (s), 960 (s), 701 (w), 478 (m).

Coordination polymer 4.1b: Coordination polymer **4.1b** was prepared by a similar procedure as that of coordination polymer **4.1a** by reacting cobalt (II) acetate tetrahydrate (0.25 g, 1 mmol), $\mathbf{L^2}$ (0.58 g, 2 mmol), and fumaric acid (0.12 g, 1 mmol) (ratio of Co/$\mathbf{L^2}$/H_2Fum = 1:2:1). A pink precipitate formed from the reaction mixture was dissolved in water and kept undisturbed. Pink crystals of **4.1b** were obtained after a few days (Isolated yield 49 % based on Co). Elemental analysis (%) for $C_{40}H_{34}CoN_4O_{12}$: calcd. C 58.47, H 4.17, N 6.82; found: C 58.70, H 4.39, N 7.02. IR (KBr, cm^{-1}): 3421 (br), 1716 (s), 1662 (s), 1549 (m), 1380 (s), 1236 (s), 1177 (m), 1054 (s), 781 (s), 679 (s), 536 (w).

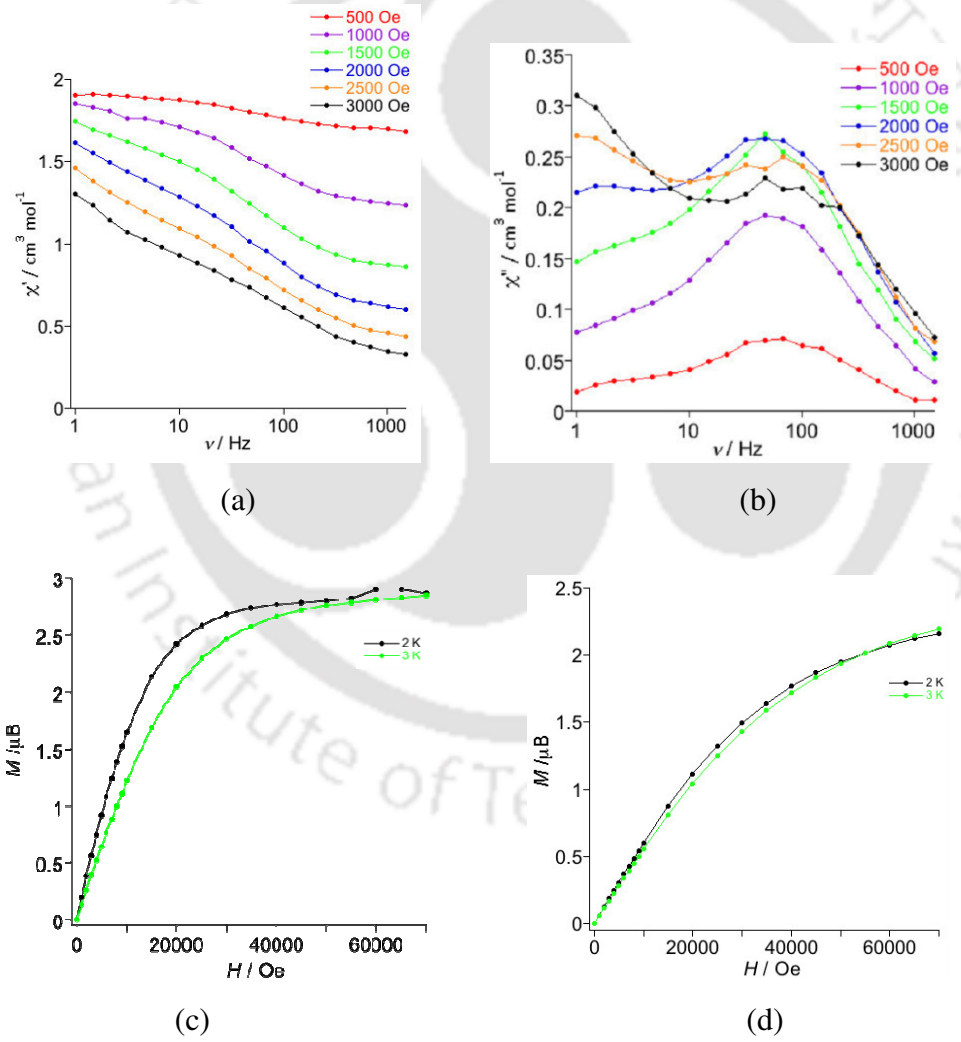

Figure 4.18: *Frequency dependency plot of* ***4.1a*** *(a) χ', (b) χ''; Plot of M vs. H at 2K and at 3K of (c)* ***4.1b*** *and (d)* ***4.1d.***

Coordination polymer 4.1c: Similar procedure as that of **4.1a** was employed to prepare **4.1c** by reacting cobalt (II) acetate tetrahydrate, $\mathbf{L^2}$ and adipic acid with a ratio of

Co/**L**^{2}/H_2adp = 1:2:1. Pink precipitate obtained was dissolved in DMF/water mixture. After 7 d pink crystals were isolated (isolated yield 50 % based on Co). Elemental analysis (%) for $C_{42}H_{40}CoN_4O_{12}$: calcd. C 59.23, H 4.73, N 6.58; found C 59.48, H 4.81, N 6.87. IR (KBr, cm^{-1}): 3557 (w), 1706 (s), 1659 (s), 1590(m), 1314 (m), 1239 (s), 1315 (m), 959 (s), 780 (s), 691 (m), 478 (m).

Coordination Polymer 4.1d: Green crystals of coordination polymer **4.1d** were obtained from a reaction of nickel (II) acetate tetrahydrate (0.25 g, 1 mmol), **L**^{2} (0.29 g, 1 mmol) and fumeric acid (0.12 g, 1 mmol) with a ratio of Ni/**L**^{2}/H_2Fum = 1:1:1 (isolated yield 49 % based on Ni). Elemental analysis (%) for $C_{22}H_{22}NiN_2O_{10}$: calcd. C 49.56, H 4.16, N 5.25; found C 49.73, H 4.31, N 5.56. IR (KBr, cm^{-1}): 3428 (br), 1700 (m), 1660 (s), 1548 (m), 1380 (s), 1234 (s), 1176 (m), 954 (m), 781 (s), 680 (m).

***Table 4.4**: Selected hydrogen bond parameters of the coordination polymers **4.1a-4.1d**.*

Compd .no.	D-H···A [symmetry]	$d_{D\text{-}H(Å)}$	$d_{H\cdots A(Å)}$	$d_{D\cdots A(Å)}$	∠D-H···A(°)
4.1a	O5-H5A···O4	0.86(5)	1.73(5)	2.563(6)	161(6)
	O5-H5B···O3 [1+x,y,z]	0.82	2.16	2.793(6)	134
	C1-H1···O5 [1-x,-y,-z]	0.93	2.48	3.126(8)	127
	C2-H2···O6	0.93	2.22	3.098(17)	157
	C6-H6A···O2 [2-x,-y,1-z]	0.97	2.34	3.210(9)	149
	C6 -H6B···O1 [1+x,y,z]	0.97	2.33	2.702(10)	102
	C6 -H6B···O6	0.97	2.51	3.406(18)	154
	C11-H11···O4 [x,1+y,1+z]	0.93	2.43	3.337(10)	164
4.1b	O5-H5A···O8 [1/2+x,1/2-y,z]	0.85(9)	2.09(10)	2.881(7)	155(9)
	O5-H5B···O7	0.84(4)	2.50(10)	2.947(6)	114(10)
	O5-H5B···O8	0.84(4)	1.89(4)	2.723(6)	168(13)
	O6-H6M···O9	0.85(3)	1.80(3)	2.654(6)	176(14)
	O6-H6M···O10	0.85(3)	2.43(8)	2.927(6)	118(7)
	O6-H6N···O11 [x,-1+y,z]	0.85(4)	1.83(4)	2.659(9)	166(5)
	C1-H1···O6	0.93	2.51	2.975(8)	111
	C20-H20···O4	0.93	2.47	3.119(8)	127
	C20-H20···O3 [1/2+x,-1/2-y,z]	0.93	2.52	3.286(9)	139
	C24-H24B···O3	0.97	2.35	2.706(9)	101
4.1c	O5 -H5A···O3 [2-x,1-y,1-z]	0.83(3)	2.01(3)	2.832(4)	171(5)
	O5 -H5B···O3 [1-x,1-y,1-z]	0.84(4)	2.58(5)	3.052(4)	117(4)
	O5- H5B···O4 [1-x,1-y,1-z]	0.84(4)	1.72(4)	2.553(4)	173(6)
	C1-H···O5	0.93	2.38	3.015(5)	126
	C2-H2···O6	0.93	2.21	3.091(16)	157
	C6 -H6A···O2	0.97	2.33	2.707(6)	102
	C6 -H6A···O6 [-1+x,y,z]	0.97	2.48	3.393(17)	156
	C6 -H6B···O1 [-x,1-y,-z]	0.97	2.33	3.211(6)	150
	C11-H11···O4 [x,-1+y,-1+z]	0.93	2.45	3.348(6)	164
4.1d	O5-H5A···O10 [-x,1-y,1-z]	0.82	2.03	2.769(5)	150
	O5-H5B···O10 [1/2-x,1/2+y,1-z]	0.82(5)	1.94(4)	2.720(4)	160(5)
	O6- H6M···O3 [-x,1-y,1-z]	0.83(4)	2.15(3)	2.901(4)	151(5)
	O6-H7N···O7	0.82	1.87	2.608(4)	149
	O9 -H9A···O4	0.82	1.97	2.709(4)	149
	O9 -H9B···O4 [1/2+x,3/2-y,z]	0.83(3)	2.10(3)	2.923(4)	173(4)
	O10 -H10A···O6	0.84(6)	2.16(5)	2.869(5)	141(5)
	O10 -H10B···O7 [-1/2+x,1/2-y,z]	0.84(4)	1.85(5)	2.655(5)	160(4)
	C4 -H4···O1 [1/2+x,1/2-y,z]	0.93	2.32	3.202(9)	158
	C6 -H6B···O2	0.97	2.23	2.622(11)	103
	C10 -H10···O4 [-1/2-x,-1/2+y,-z]	0.93	2.48	3.37(2)	162
	C14 - H14···O9 [1/2-x,-1/2+y,-z]	0.93	2.52	3.424(9)	165

Coordination Polymer 4.1e: Blue precipitate was obtained on addition of copper (II) acetate monohydrate (0.20 g, 1 mmol) to a solution of $\mathbf{L^2}$ and fumeric acid (0.12 g, 1 mmol) (ratio Cu/$\mathbf{L^2}$/H_2Fum = 1:2:1) in methanol on refluxing for 1 h. Precipitate obtained was dissolved in DMF and kept undisturbed for crystallization. After one week, blue crystals suitable for single crystal diffraction were obtained (isolated yield 60 % based on Cu). Elemental analysis (%) for $C_{40}H_{28}CuN_4O_9$: calcd. C 62.21, H 3.65, N 7.26; found C 62.30, H 3.79, N 7.42. IR (KBr, cm^{-1}): 3460 (br), 1700 (m), 1662 (s), 1587 (s), 1383 (s), 1242 (m), 955 (w), 780 (s), 657 (m), 523 (m).

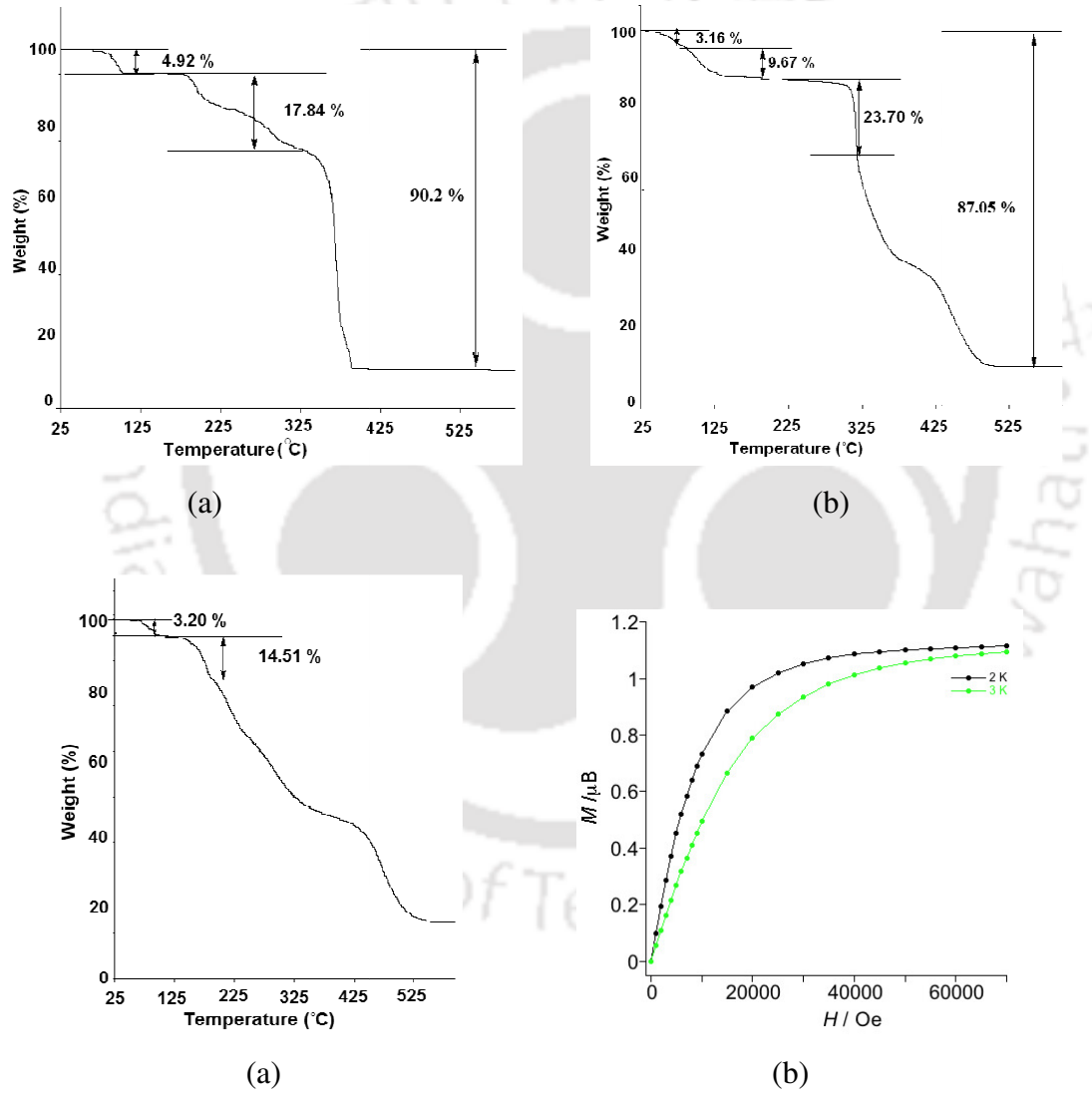

***Figure 4.19**: Thermogram (heating rate of 7 °C/min) of (a) **4.1b**, (b) **4.1d**, (c) **4.1e** and (d) Plot of M vs. H at 2K and at 3K of **4.1f**.*

Coordination Polymer 4.1f: Malonic acid (0.11 g, 1 mmol) was added to a solution of ligand $\mathbf{L^2}$ dissolved in warm methanol and stirred for 30 min. To this solution copper (II) acetate monohydrate was added (ratio of Cu/$\mathbf{L^2}$/H_2Mal = 1:1:1) and refluxed for 1 h. The

precipitate obtained was dissolved in DMF and kept for crystallization. Blue crystals were obtained (isolated yield 42 % based on Cu). Elemental analysis (%) for $C_{21}H_{16}CuN_2O_7$: calcd. C 53.45, H 3.42, N 5.94; found C 53.69, H 3.58, N 6.18. IR (KBr, cm^{-1}): 3505 (br), 3101 (br), 1708 (m), 1644 (br), 1536 (w), 1449 (m), 1344 (m), 1233 (s), 1176 (m), 961 (s), 782 (s), 726 (s), 575 (m), 501 (w).

***Table 4.5**: Selected hydrogen bond parameters of the coordination polymers **4.1e-4.1g**.*

Compd. no.	D-H···A [symmetry]	$d_{D-H(Å)}$	$d_{H\cdots A(Å)}$	$d_{D\cdots A(Å)}$	∠D-H···A(°)
4.1e	C5 -H5···O5	0.93	2.59	2.902(13)	100
	C6 -H6A···O1	0.97	2.31	2.693(11)	103
	C6 -H6A···O3 [2-x,1-y,-z]	0.97	2.30	3.195(12)	153
	C10- H10···O7 [2-x,1-y,1-z]	0.93	2.59	3.480(14)	160
	C15-H15···O1 [-1+x,y,z]	0.93	2.55	3.198(13)	127
	C19 -H19···O7	0.93	2.55	3.298(13)	138
	C22-H22···N4	0.93	2.62	2.931(12)	100
	C22- H22···O2	0.93	2.41	3.317(12)	165
	C27- H27···O1 [1-x,1-y,-z]	0.93	2.52	3.239(15)	135
	C39 -H39···O5 [2-x,1-y,-z]	0.93	2.59	3.414(11)	147
	C22-H22···N4 [1-x,1-y,-z]	0.93	2.62	2.931(12)	100
4.1f	O7-H7A···O5 [1-x,1/2+y,1/2-z]	0.70(5)	2.21(6)	2.786(5)	141(6)
	O7-H7B···O4 [3/2-x,1/2+y,z]	0.82	1.90	2.716(5)	176
	C1-H1···O6	0.93	2.37	2.932(6)	119
	C5-H5···O3	0.93	2.26	2.821(6)	118
	C6-H6A···O1	0.97	2.35	2.718(7)	102
	C14-H14···O4 [x,1/2-y,-1/2+z]	0.93	2.53	3.277(7)	138
4.1g	O14-H14···O17	0.82	2.02	2.6314	131
	C4 -H4···O15 [-x,2-y,-z]	0.93	2.33	3.14	146
	C5 -H5···O5	0.93	2.42	3.1029	130
	C6 -H6A···O1	0.97	2.35	2.7102	101
	C9-H9···O16 [-1+x,y,1+z]	0.93	2.38	3.0951	134
	C11-H11···O19 [-1+x,y,1+z]	0.93	2.57	3.4933	174
	C113- H11B···O24	0.97	2.33	2.6972	101
	C24 -H24···O4	0.93	2.51	3.2752	139
	C25- H25···O22 [-x,1-y,1-z]	0.93	2.36	3.1259	140
	C28- H28···O5	0.93	2.56	3.1787	124
	C29 -H29B···O9	0.97	2.33	2.6965	102
	C37 -H37···O17 [x,-1+y,z]	0.93	2.53	3.4208	161
	C38-H38···O21 [1+x,y,-1+z]	0.93	2.49	3.1498	128
	C52-H52···O14	0.93	2.43	3.0171	121

Coordination Polymer 4.1g: A similar procedure used in synthesis of **4.1e** was employed to prepare coordination polymer **4.1g**. Copper (II) acetate monohydrate (0.2 g, 1 mmol), $\mathbf{L^2}$ (0.58 g, 2 mmol) and adipic acid (0.17 g, 1 mmol) in a molar ratio of Cu/$\mathbf{L^2}$/Adp = 1:2:1 was used in this reaction. Precipitate obtained was dissolved in DMF solvent and kept undisturbed. Blue crystals were obtained from the solution after one week (isolated yield 56 % based on Cu). Elemental analysis (%) for $C_{126}H_{101}Cu_3N_{12}O_{27}$ (**4.1g**): calcd. C 62.90, H 4.23, N 6.99; found C 63.24, H 4.37, N 7.27. IR (KBr, cm^{-1}): 3454 (br), 1706 (s), 1660 (s), 1583 (s), 1385 (s), 1235 (s), 1175 (m), 955 (m), 781 (s), 653 (m), 520 (w).

4.8 References:

1. Noro, S.; Kitagawa, S.; Kondo, M.; Seki, K. *Angew. Chem. Int. Ed.* **2000**, *39*, 2081-2084.
2. Hagrman, P. J.; Hagrman, D.; Zubieta, J. *Angew. Chem., Int. Ed.* **1999**, *38*, 2638-2684.
3. Castro, S. L.; Sun, Z. M.; Grant, C. M.; Bollinger, J. C.; Hendrickson, D. N.; Christou, G. *J. Am. Chem. Soc.* **1998**, *120*, 2365-2375.
4. Seo, J. S.; Whang, D.; Lee, H.; Jun, S. I.; Oh, J.; Jeon, Y. J.; Kim, K. *Nature* **2000**, *404*, 982-986.
5. Fabelo, O.; Canadillas-Delgado, L.; Delgado, F. S.; Lorenzo-Luis, P.; Laz, M. M.; Julve, M.; Ruiz-Perez, C. *Cryst. Growth Des*. **2005**, *5*, 1163-1167.
6. Pan, L.; Woodlock, E. B.; Wang, X.; Lam, K. -C.; Rheingold, A. L. *Chem. Commun.* **2001**, 1762-1763.
7. Kuznicki, S. M.; Bell, V. A.; Nair, S.; Hillhouse, H. W.; Jacubinas, R. M.; Braunbarth, C. M.; Toby, B. H.; Tsapatsis, M. *Nature* **2001**, *412*, 720-724.
8. Yaghi, O. M.; Li, H.; Groy, T. L. *J. Am. Chem. Soc.* **1996**, *118*, 9096-9101.
9. Pan, L.; Liu, H.; Lei, X.; Huang, X.; Olson, D. H.; Turro, N. J.; Li, J. *Angew. Chem., Int. Ed.* **2003**, *42*, 542-546.
10. Kondo, M.; Okubo, T.; Asami, A.; Noro, S. -I.; Yoshitomi, T.; Kitagawa, S.; Ishii, T.; Matsuzaka, H.; Seki, K. *Angew. Chem., Int. Ed.* **1999**, *38*, 140-143.
11. Kitaura, R.; Onoyama, G.; Sakamoto, H.; Matsuda, R.; Noro, S.; Kitagawa, S. *Angew. Chem., Int. Ed*. **2004**, *43*, 2684-2687
12. Hasegawa, S.; Horike, S.; Matsuda, R.; Furukawa, S.; Mochizuki, K.; Kinoshita, Y.; Kitagawa, S. *J. Am. Chem. Soc*. **2007**, *129*, 2607-2614.
13. Halder, G. H.; Kepert, C. J.; Moubaraki, B.; Murray, K. S.; Cashion, J. D. *Science* **2002**, *298*, 1762-1765.
14. Kostakis, G. E.; Powell, A. K. *Coord. Chem. Rev*. **2009**, *253*, 2686-2697
15. Lin, W.; Wang, Z.; Ma, L. *J. Am. Chem. Soc.* **1999**, *121*, 11249-11250
16. Yaghi, O. M.; Li, H.; Davis, C.; Richardson, D.; Groy, T. L. *Acc. Chem. Res.***1998**, *31*, 474-484.
17. Kitagawa,S.; Kondo, M. *Bull. Chem. Soc. Jpn*. **1998**, *71*, 1739-1753.
18. Tzeng, B.-C.; Chiu, T.-H.; Chen, B.-S.; Lee, G.-H. *Chem. Eur. J*. **2008**, *14*, 5237-5245.
19. Maji, T. K.; Matsuda, R.; Kitagawa, S. *Nat. Mater*. **2007**, *6*, 142-148.
20. Nagao, Y.; Fujishima, M.; Ikeda, R.; Kanda, S.; Kitagawa, H. *Synth. Met*. **2003**, *431*, 133-134.
21. Tao, J.; Yin, X.; Wei, Z.; Huang, R.; Zheng, L. *Eur. J. Inorg. Chem.* **2004**, *1*, 125-133.
22. Reger, D. L.; Debreczeni, A.; Reinecke, B.; Rassolov, V.; Smith, M. D. *Inorg. Chem.* **2009**, *48*, 8911-8924.

23. Reger, D. L.; Horger, J. J.; Smith, M. D.; Long, G. J. *Chem. Commun.* **2009**, 6219-6221.
24. Reger, D. L.; Horger, J. J.; Smith, M. D. *Chem. Commun.* **2011**, *47*, 2805-2807.
25. Barooah, N.; Sarma, R. J.; Batsanov, A. S.; Baruah, J. B. *Polyhedron* **2006**, *25*, 17-24.
26. Deka, K.; Barooah, N.; Sarma, R. J.; Baruah, J. B. *J. Mol. Struct.* **2007**, *827*, 44-49.
27. Barooah, N.; Karmakar, A.; Sarma, R. J.; Baruah, J. B. *Inorg. Chem. Commun.* **2006**, *9*, 1251-1254.
28. Singh, D.; Baruah, J. B. *Cryst. Growth Des.* **2012**, *12*, 2109-2121.
29. Singh, D.; Baruah, J. B. *Inorg. Chim. Acta* **2013**, *394*, 703-709.
30. Reger, D. L.; Debreczeni, A.; Reinecke, B.; Rassolov, V.; Smith, M. D. *Inorg Chem.* **2009**, *48*, 8911-8924.
31. Tangoulis, V.; Lalia-Kantouri, M.; Gdaniec, M.; Papadopoulos, C.; Miletic, V.; Czapik, A. *Inorg. Chem*. **2013**, *52*, 6559-6569.
32. Mukherjee, P. S.; Dalai, S.; Mostafa, G.; Zangrando, E.; Lu, T.-H.; Rogez, G.; Mallah, T.; Chaudhuri, N. R. *Chem. Commun*. **2001**,1346-1347.
33. Konar, S.; Mukherjee, P. S.; Zangrando, E.; Lloret, F.; Chaudhuri, N. R. *Angew. Chem., Int. Ed*. **2002**, *41*, 1561-1563.
34. Sain, S.; Maji, T. K.; Mostafa, G.; Lu, T.-H.; Chaudhuri, N. R. *New J. Chem*. **2003**, *27*, 185-187.
35. Zheng, Y.; Xie, H.J. *Solid State Chem*. **2004**, *177*, 1352-1358.
36. Li, M.-X.; Xie, G.-Y.; Jin, S.-L.; Gu, Y.-D.; Li, M.-Q.; Liu, J.; Xu, Z.; You, X.-Z. *Polyhedron* **1996**, *15*, 535-539.
37. Zheng, Y.-Q.; Zheng, M. -F. Z. *Naturforsch*. **2003**, *58b*, 266-270.
38. Reger, D. L.; Debreczeni, A.; Smith, M. D. *Inorg. Chim. Acta* **2010**, *364*, 10-15.
39. Barooah, N.; Sarma, R. J.; Batsanov, A. S.; Baruah, J. B. *J. Mol. Struct.* **2006**, *791*, 122-130.
40. Batten, S. R.; Robson, R. *Angew. Chem., Int. Ed*. **1998**, *37*, 1460-1494.
41. Mukherjee, P. S.; Konar, S.; Zangrando, E.; Mallah, T.; Ribas, J.; Chaudhuri, N. R. *Inorg. Chem*. **2003**, *42*, 2695-2703.
42. Setifi, Z.; Setifi, F.; Smith, G.; El-Ghozzi, M.; Rouag, D.-A.; Avignant, D.; Merazig, H. *Acta Crystallogr*. **2013**, *69E*, m335-m336.
43. Beko, S. L.; Batts, J. W.; Schmidt, M. U. *Acta Crystallogr*. **2009**, *65C*, m347-m351.
44. Zheng, Y.-Q.; Lin, J.-L.; Pan, A.-Y. *Z. Anorg. Allg. Chem*. **2008**, *626*, 1718-1720.
45. Yang, M.-H. *Acta Crystallogr*. **2008**, *64E*, m1406.
46. Padmanabhan, M.; Joseph, J. C.; Thirumurugan, A.; Rao, C. N. R. *Dalton Trans*. **2008**, 2809-2811.
47. Ma, S.; Simmons, J. M.; Yuan, D.; Li, J.-R.; Weng, W.; Liu, D.-J.; Zhou, H.-C. *Chem. Commun*. **2009**, 4049-4051.

48. Wages, H. E.; Taft, K. L.; Lippard, S. J. *Inorg. Chem*. **1993**, *32*, 4985-4987.
49. Nikiforova, M. E.; Sidorov, A. A.; Aleksandrov, G.G.; Ikorskii, V. N.; Smolyaninov, I. V.; Okhlobystin, A. O.; Berberova, N. T.; Eremenko, I. L. *Russ. Chem. Bull. Int. Ed*. **2007**, *56*, 943-952.
50. Chaudhuri, P.; Kupers, H. J.; Wieghardt, K.; Gehring, S.; Haase, W.; Nuber, B.; Weiss, J.J. *Chem. Soc., Dalton Trans*. **1988**, 1367-1370.
51. Buchanan, R. M.; Mashuta, M. S.; Oberhausen, K. J.; Richardson, J. F. *J. Am. Chem. Soc.* **1989**, *111*, 4497-4498.
52. Zheng, Y.-Z.; Tong, M.-L.; Zhang, W.-X.; Chen, X.-M. *Angew. Chem., Int. Ed*. **2006**, *45*, 6310-6314.
53. Konar, S.; Zangrando, E.; Drew, M. G. B.; Ribas, J.;Chaudhuri, N. R. *Dalton Trans*. **2004**, 260-266.
54. Zhou, Z.-H.; Ye, J.-J.; Deng, Y.-F.; Wang, G.; Gao, J.-X.; Wao, H.-L. *Polyhedron* **2002**, *21*, 787-792.
55. Seguatni, A.; Fakhfakh, M.; Smiri, L. S.; Gressier, P.; Boucher, F.; Jouini, N. *J. Solid State Chem*. **2012**, *187*,7-14.
56. Ohata, N.; Masuda, H.; Yamauchi, O. *Angew. Chem., Int. Ed*. **1996**, *35*, 531-532.
57. Naumov, P.; Ristova, M.; Soptrajanov, B.; Drew, M. G. B.; Ng, S. W. *Croatica Chim. Acta* **2002**, *75*, 701-711.
58. Liu, T.-F.; Sun, H.-L.; Gao, S.; Zhang, S.-W.; Lau, T.-C. *Inorg. Chem*. **2003**, *42*, 4792-4794.
59. Slone, R. V.; Yoon, D. I.; Calhoun, R. M.; Hupp, J. T. *J. Am. Chem. Soc*.**1995**, *117*, 11813-11814.
60. Karipides, A.; Ault, J.; Reed, T. *Inorg. Chem*. **1977**, *16*, 3299-3302.
61. Chung, K. H.; Hong, E.; Do, Y.; Moon, C. H. J. *J. Chem. Soc., Chem. Commun*. **1995**, 2333-2334.
62. Chattopadhyay, D.; Chattopadhyay, S. K.; Lowe, P. R.; Schwalbe, C. H.; Mazumder, S. K.; Rana, A.; Ghosh, S. *J. Chem. Soc., Dalton Trans*.**1993**, 913-916.
63. Calogero, S.; Stievano, L.; Diamandescu, L.; Mihaila-Tarabasanu, D.; Valle, G. *Polyhedron* **1997**, *16*, 3953-3966.
64. Keene, T. D.; Zimmermann, I.;Neels, A.; Sereda, O.; Hauser, J.; Liu, S.-X.; Decurtins, S. *Cryst. Growth Des*. **2010**, *10*, 1854-1859.
65. O. Sato, *Acc. Chem. Res*. **2003**, *36*, 692-700
66. Halder, G. J.; Kepert, C. J.; Moubaraki, B. K.; Murray, S.; Cashion, J. D. *Science* **2002**, *298*, 1762-1765.
67. Coronado, E.; Galan-Mascaros, J. R.; Gomez-Garcia, C. J.; Laukhin, V. *Nature* **2000**, *408*, 447-449.

68. Train, C.; Gheorghe, R.; Krstic, V.; Chamoreau, L. M.; Ovanesyan, N. S.; Rikken, L. J. A.; Gruselle, M.; Verdaguer, M. *Nat. Mater*. **2008**, *7*, 729-734.
69. Turnbull, M. M.; Sugimoto, T.; Thompson, L. K. *Molecule-Based Magnetic Materials*, American Chemical Society, Washington, DC, **1996.**
70. Bhargavi, G.; Rajasekharan, M. V.; Costes J.-P.; Tuchagues, J.-P. *Dalton Trans*. **2013**, *42*, 8113-8123.
71. Pardo, E.; Train, C.; Lescouezec, R.; Journaux, Y.; Pasan, J.; Ruiz-Perez, C.; Delgado, F. S.; Ruiz-Garcia, R.; Lloret, F.; Paulsen, C. *Chem. Commun*. **2010**, *46*, 2322-2324.
72. Vaz, M. G. F.; Cassaro, R. A. A.; Akpinar, H.; Schlueter, J. A.; Lahti, P. M.; Novak, M. A. *Chem. Eur. J*. **2014**, *20*, 5460-5467.
73. Lloret, F.; Julve, M.; Cano, J.; Ruiz-Garcia, R.; Pardo, E. *Inorg. Chim. Acta* **2008**, *361*, 3432-3445
74. Ma, C.; Wang, W.; Zhang, X.; Chen, C.; Liu, Q.; Zhu, H.; Liao, D.; Li, L. *Eur. J. Inorg. Chem*. **2004**, 3522-3532.
75. Ma, C.; Chen, C.; Liu, Q.; Liao, D.; Li, L.; Sun, L. *New J. Chem*. **2003**, *27*, 890-894.
76. Delgado, F. S.; Kerbellec, N.; Ruiz-Perez, C.; Cano, J.; Lloret, F.; Julve, M. *Inorg. Chem*. **2006**, *45*, 1012-1020.
77. Mondal, A.; Durdevik, S.; Chamoreau, L. M.; Journaux, Y.; Julve, M.; Lisnard, L.; Lescouezec, R. *Chem. Commun*. **2013**, *49*, 1181-1183.
78. Guillou, N.; Pastre, S.; Livage, C.; Ferey, G. *Chem. Commun*. **2002**, 2358-2359.
79. Culpepper, M. A.; Cutsail, G. E.; Gunderson, W. A.; Hoffman, B. M.; Rosenzweig, A. C. *J. Am. Chem. Soc*. **2014**, *136*, 11767-11775.
80. Gherman, B. F.; Cramer, C. J. *Coord. Chem. Rev*. **2009**, *253*, 723-753.
81. Pavlova, S. V.; C. Chen, K. H. -C.; Chan, S. I. *Dalton Trans*. **2004**, 3261-3274.
82. Matthews, C. J.; Avery, K.; Xu, Z.; Thompson, L. K.; Zhao, L.; Miller, D. O.; Biradha, K.; Poirier, K.; Zaworotko, M. J.; Wilson, C.; Goeta, A. E.; Howard, A. K. *Inorg. Chem*. **1999**, *38*, 5266-5276.
83. Madalan, A. M.; Cao, X.-Y.; Rogez, G.; Lehn, J.-M. *Inorg. Chem*. **2014**, *53*, 4275-4277.
84. Li, B.; Wang, X.; Zhang, Y.; Gao, S.; Zhang, Y. *Inorg. Chim. Acta* **2005**, *358*,3519-3524
85. Zheng, Y.-Q.; Zhai, X.-S.; Jin, L.; Zhu, H.-L.; Lin, J.-L.; Xu, W. *Polyhedron* **2014**, *68*, 324-333.
86. Wang, Y. Y.; Wang, X.; Shi, Q. Z. *Transition Met. Chem*. **2002**, *27*, 481-484.
87. Bakalbassis, E. G.; Korabik, M.; Michailides, A.; Mrozinski, J.; Raptopoulou, C.; Skoulika, S.; Terzis, A.; Tsaousis, D. *J. Chem. Soc., Dalton Trans*. **2001**, 850-885.
88. Fatima, S.; Abdelaziz, B.; Jean, S.-P.; Jean-Yves, S.; Smail, T. *Inorg. Chim. Acta* **2006**, *359*, 3269-3274.

89. He, K. H.; Song, W. C.; Li, Y. W.; Chen, Y. Q.; Bu, X. H. *Cryst. Growth Des*. **2012**, *12*, 1064-1068.
90. Fang, H. C.; Zhu, J. Q.; Zhou, L. J.; Jia, H. Y.; Li, S. S.; Gong, X.; Li, S. B.; Cai, Y. P.; Thallapally, P. K.; Liu, J.; Exarhos, G. J. *Cryst. Growth Des*. **2010**, *10*, 3277-3284.
91. Fang, S.-M.; Zhang, Q.; Hu, M.; Yang, X.-G.; Zhou, L.-M.; Du,M.; Liu, C.-S. *Cryst. Growth Des*. **2010**, *10*, 4773-4785.
92. Valeur, B. *Molecular Fluorescence: Principles and Applications*; Wiley-VCH: Weinheim, Germany, **2002.**
93. Zhang, L. Y.; Liu, G. F.; Zheng, S. L.; Ye, B. H.; Zhang, X. M.; Chen, X. M. *Eur. J. Inorg. Chem*. **2003**, 2965-2971.
94. Nath, J. K.; Baruah, J. B. *New J. Chem*. **2013**, *37*, 1509-1519.

CHAPTER 5

Anion assisted assemblies of *N,N′*-bis(3-imidazol-1-ylpropyl)naphthalenediimide

Supramolecular chemistry of anions is important in biology,[1-11] medicines, catalysis, ion exchange processes and in environment.[12-15] Generally, neutral or cationic substrates interact with anions through hydrogen bonding. Many host system possesses selective anion binding site to act as host in which interactions are guided by weak dispersive forces.[16-27] Among various host molecules for anion binding, naphthalimide derivatives are often used as fluorophoric host.[28-29] Naphthalimides show good emissive properties and are able to selectively detect anions.[30-37] Dipolar nature of naphthalimide rings helps them to stack in orderly manners and such effects are utilised to recognise poly aromatic hydrocarbons.[38-39] Non-covalent forces between electron deficient aromatic systems and anions, namely anion-π interaction has important role in anion recognition. Involvement of π-rings in molecular anion recognition and anion transport [40] indicate that anion-π contacts could be a prominent tactor in such processes.[41] Pioneering observations on anion channels [42-43] and anion-π interactions [1-2,25-26] have generated studies on anion binding with naphthalenediimide and related systems. Anion-π interactions in naphthalenediimide based compounds showed important roles in various organic transformation.[44-45]

Functional groups present across naphthalenediimide ring, such as in *N,N′*-bis(3-imidazol-1-ylpropyl)naphthalenediimide (**L^3**) (Figure **5.1**), would provide cleft like geometry (Figure **5.1b**). On protonation of **L^3** will hold anions and binding of such anions to the functional unit may be influenced by the naphthalenediimide ring. Thus different orientations of imidazole across a rigid naphthalenediimide unit could turn out to be an important factor. This should be particularly effective with naphthalenediimide ring as they would interact through anion-π interactions. In literature structural studies focussing on projection of the units connected to imide nitrogen resulting in cisoid or transoid geometries (Figure **5.1a**) have been carried out.[46-55] Thus, the effects of orientations of an anion or acid binding site in distant places across a naphthalenediimide ring (Figure **5.1c**) would help to understand different arrangements of anions assisted by charge[42] and also help in understanding anion-π interactions.[1-2,40] There is also the possibility to design a replica of biological molecules, such as histamine receptors or metalloproteins, from

naphthalenediimides having imidazole units across the two ends.[56] Being ubiquitous in nature, imidazole functionality plays critical role in many structures within the human body, notably as histamine and histidine. Our observations on anion-π interactions and the

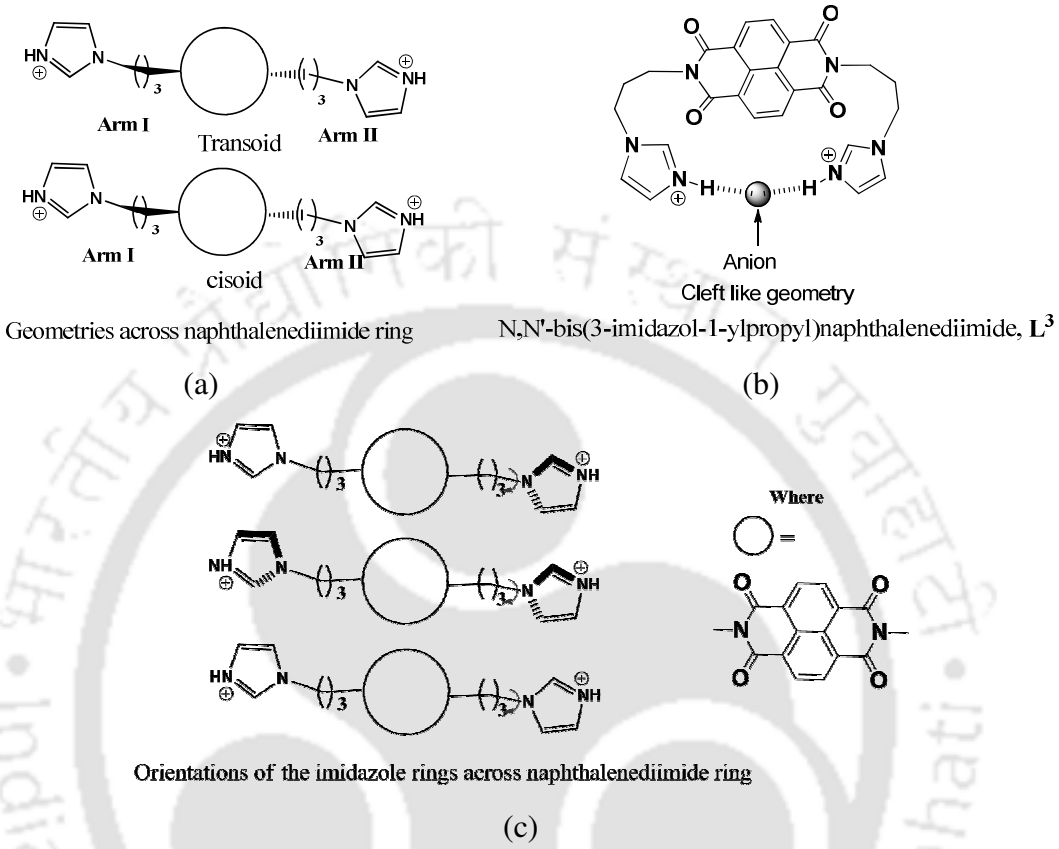

***Figure 5.1**: Some orientations of protonated **L**[3]; (a) geometries across naphthalenediimide ring, (b) cleft like geometry of **L**[3] to hold anion and (c) different orientaions of imidazole rings across naphthalenediimide rings.*

formation of anion chains by protonated *N,N'*-bis(3-imidazol-1-ylpropyl)naphthalenediimide and influence of fluorescence intensity are discussed in this chapter.

5.1 Synthesis of *N,N'*-bis(3-imidazol-1-ylpropyl)naphthalenediimide (L[3]):

N,N'-bis(3-imidazol-1-ylpropyl)naphthalenediimide was synthesised by condensation of 1,4,5,8-Naphthalenetetracarboxylic acid dianhydride with 3-(1H-imidazol-1-yl)propan-1-amine by following a similar procedure for the synthesis of analogous compounds reported earlier.[49] Ligand, **L**[3] was characterised by various spectroscopic techniques such as FT-IR, ^{1}H-NMR, ^{13}C-NMR and mass spectrometry. In FT-IR spectrum it shows carbonyl frequency of naphthalenediimide at 1699 cm^{-1} and 1650 cm^{-1}. ^{1}H-NMR shows one singlet at 8.60 ppm for naphthalene proton; three singlets at 7.66 ppm, 7.22 ppm and

6.87 ppm were respectively due to imidazole CH protons. Aliphatic protons 'e' and 'f' appeared as a multiplet in the range 3.9-4.2 ppm; whereas a multiplet for the protons 'g' appeared at 2.28 ppm (Figure **5.2**). ^{13}C-NMR for carbonyl carbon, attached to the imide ring appears at 162.7 ppm; naphthalene carbon bearing CH appears at 137.3 ppm whereas tertiary carbon merges with one of the imidazole carbon appearing at 119.3 ppm. In addition, carbon on naphthalene ring linked to imide appears at 128.3 ppm whereas imidazole ring protons appear at 130.4 and 126.0 ppm. There are three signals for aliphatic carbons at 44.0 ppm, 37.8 ppm and 29.0 ppm for the methylene carbons. The compound shows ESI- HR MS at 483.1772 (calcd. 483.1703) which correspond to M+1 peak.

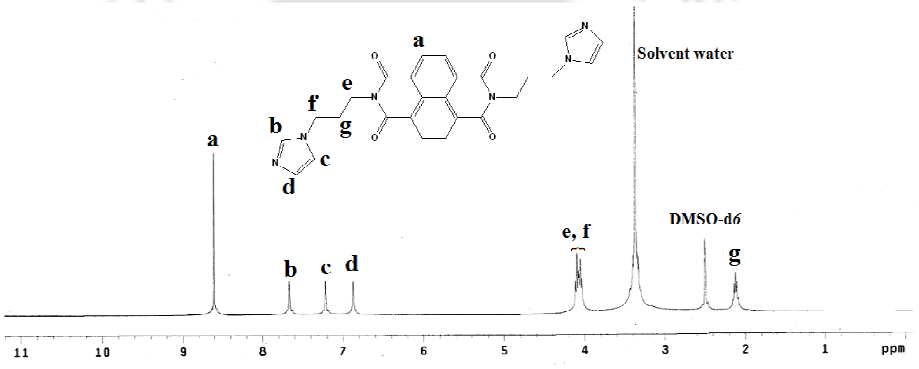

***Figure 5.2**: ^{1}H-NMR of the **L**^{3} (400MHz, DMSO-d_6).*

5.2: Salts of *N,N'*-bis(3-imidazol-1-ylpropyl)naphthalenediimide:

Different crystalline salts were prepared by reacting *N,N'*-bis(3-imidazol-1-ylpropyl)naphthalenediimide with different mineral acids. Crystalline salts of **L**^{3} namely $[H_2(\mathbf{L}^3)Cl_2].2H_2O$ (**5.1a**), $[H_2(\mathbf{L}^3)Br_2].2H_2O$ (**5.1b**), $[H_2(\mathbf{L}^3)(ClO_4)_2]$ (**5.1c**) were formed by reacting hydrochloric acid, hydrobromic acid and perchloric acid respectively. Reaction of sulfuric acid with **L**^{3} in aqueous methanol resulted in a bisulfate salt $[H_2(\mathbf{L}^3)(HSO_4)_2].H_2O$ (**5.1d**) whereas such a reaction in a binary solvent of methanol and dimethylformamide led to the formation of methyl sulfate salt $[H_2(\mathbf{L}^3)(MeSO_4)_2]$ (**5.1e**). Formation of esters by reaction of sulfuric acid is well known, but there are only few examples to isolate such species from solution.

Hydrogenphosphate, $[H_2\mathbf{L}^3(HPO_4)].H_2O$ (**5.1f**) and nitrate $[H_2\mathbf{L}^3(NO_3)_2]$ (**5.1g**) salts were obtained when phosphoric acid and nitric acid were reacted with **L**^{3} respectively. On the other hand the reaction of **L**^{3} with hydrofluoric acid in glass tube led to the formation of hexafluorosilicate salt $[H_2\mathbf{L}^3(SiF_6)].1.5H_2O$ (**5.1h**). The SiF_6^{2-} anion was formed by the reaction of hydrofluoric acid and silica. We did not obtain crystalline salt of **L**^{3} by reacting

with hydrofluoric acid in quartz tube. The whole results are summarized in the Scheme **5.1**.

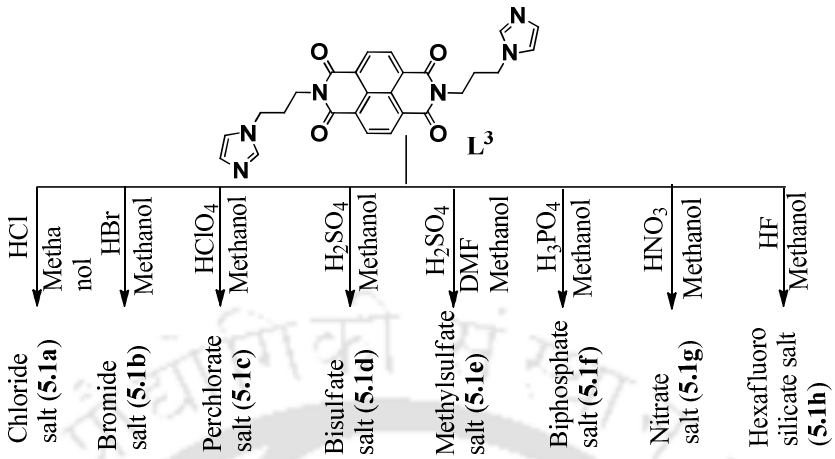

Scheme 5.1: *syntheses of different salts of* ***L*** ^{3}

All the salts were characterized by FT-IR, ^{1}H-NMR and finally by single crystal X-ray diffraction technique. Presence of solvent molecules was confirmed by thermogravimetric analyses. Powder X-ray diffraction (PXRD) patterns of the salts **5.1a-5.1h** were determined**.** By comparing experimental PXRD patterns with simulated patterns, similarities were found which suggested the uniformity of the structural features of the bulk materials confirming the formation of one type of species in each case.

^{1}H-NMR spectra of the ligand along with the salts **5.1a-5.1h** were recorded. ^{1}H-NMR of **L**^{3} and salts **5.1a**, **5.1d** and **5.1h** were compared and shown in Figure **5.3**. Significant shift of the signals was observed for imidazole protons.

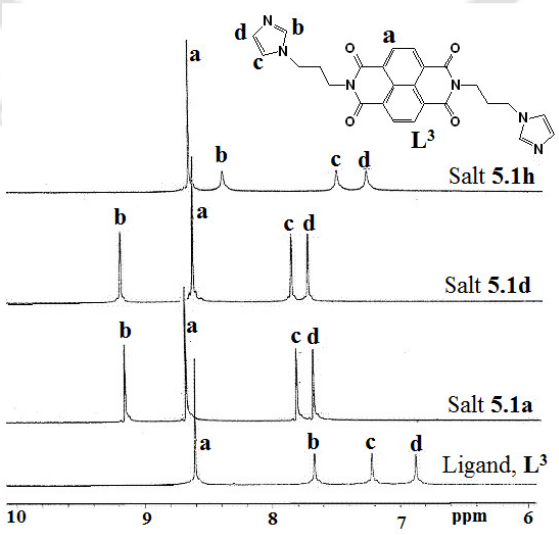

Figure 5.3: *Overlay of the aromatic region of the* ^{1}*H-NMR spectra of the* ***L*** ^{3} *and its chloride salt (**5.1a**), bisulfate salt (**5.1d**) and hexafluorosilicate salt (**5.1h**).*

This change of chemical shift with respect to ligand occurs due to the protonation of imidazole nitrogen causing the deshielding effect on the imidazole protons. Chemical shifts in ^{1}H-NMR of the salts are similar, but the chemical shifts of the salt having SiF_6^{2-} are different from that of the others. Moreover, differences in chemical shift values in the aromatic region of chloride (**5.1a**), bisulfate (**5.1d**) and hexafluorosilicate (**5.1h**) salts are attributed to the increase in electrostatic interactions upon change of charge.

The crystallographic study have revealed that chloride and bromide salts **5.1a** and **5.1b** are isostructural and isomorphous. This means that crystals of the salts belong to same space group having similar structure, but differ in bond parameters. They crystallized in triclinic *P-1* space group. Structures of **5.1a** and **5.1b** are highly symmetric and in each case two halves of the $[H_2(\mathbf{L^3})^{2+}]$ ions appear in the respective asymmetric unit. In the structure of both the salts it is observed that the cationic part, namely the $[H_2(\mathbf{L^3})^{2+}]$, lies about the inversion centres. The π···π and C-H···π interactions between the symmetry independent $[H_2(\mathbf{L^3})^{2+}]$ ions lead to the formation of a 2-D lamellar structure. Environments of the two chloride ions are different. Cl1 interacts with imidazole rings of three $[H_2(\mathbf{L^3})^{2+}]$ ions and interacts with one molecule of water of crystallization. On the other hand, the Cl2-ion is linked to three different $[H_2(\mathbf{L^3})^{2+}]$ and two lattice water molecules. The weak interactions generate a hydrogen bonded chain having two water molecules and two chloride ions as repeat units. Hydrogen bond parameters are listed in Table **5.1**. There is a great challenge to search for systems that have anion-π interactions.[1,2] Chloride ions form hydrogen bonds with water molecules. Chain like aquated structures has relevance in ion transport [42-43, 57-62] and in biological systems. Such chain-like structures are observed in metallo-organic compounds. Chains having alternate water bridges[63] as well as chains with dimeric chloride bridged by water molecules are well known in the literature.[59] The water channels formed by imidazole quartets in biological systems find application in ion transport across a membrane.[57] Our observation that the halogen bridged aqua chain held by imidazole is similar to the water chain in the imidazole-quartet in biology is significant. In the present study two intervening water molecules are bridged by two symmetry non-equivalent chloride ions. The chloride ions are placed on top of the naphthalenediimide ring through a C17-H···Cl^- interaction and further the chloride (Cl1) has anion-π interaction with the naphthalenediimide ring. Such interaction is revealed in the distance between the chloride (Cl1) and the centroid of an imide ring of **5.1a** being 3.49 Å (Figure **5.4a**).

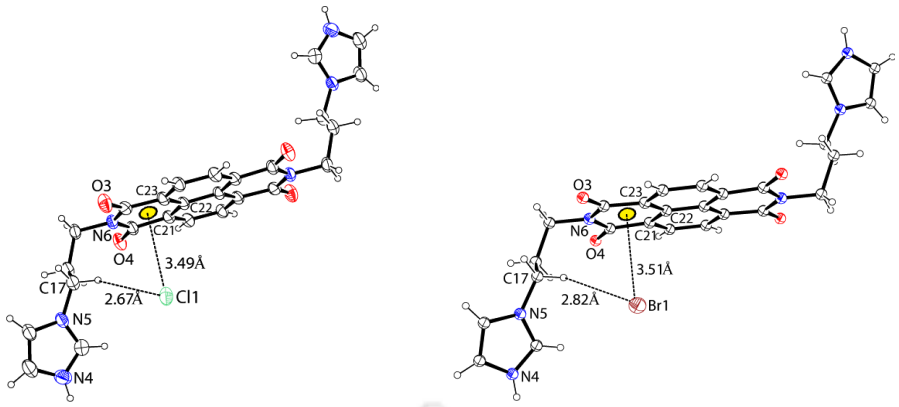

(a) (b)

***Figure 5.4**: Anion···π interactions and the position of (a) chloride ion in salt **5.1a**, (b) bromide ion in salt **5.1b** with respect to naphthalenediimide ring.*

On the other hand, in the salt **5.1b** the bromide ion is observed at a distance 3.51 Å from the centroid of an imide ring (Figure **5.4b**). The $d_{H\cdots A}$ distance of the chloride and bromide ion involved in C17-H interactions in the salts **5.1a** and **5.1b** are 2.67 Å and 2.82 Å, respectively. Theoretical calculation[1] has revealed that such a C-H···Cl^- interaction with an optimal $d_{H\cdots A}$ distance of 2.84 Å is favorable to have a perfect anion-π interaction.

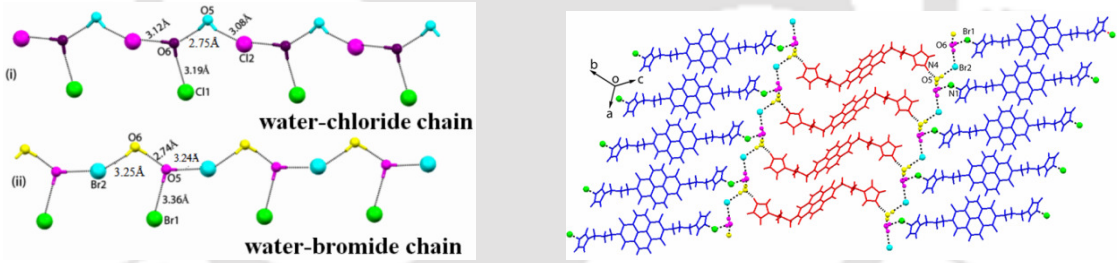

(a) (b)

***Figure 5.5**: (a) Water assisted chain of (i) chloride ions in **5.1a** and (ii) bromide ions in **5.1b**, (b) The chain of water-bromide ions in the lattice of **5.1b**.*

Thus, the results are in very good agreement with the analogous systems predicted by theory. The bromide ion has a bigger size than the chloride ion (1.14 times higher in terms of ionic radius), leading to a different separation than the chloride ion with the π-aromatic ring in the two structures. In the case of **5.1b** both the Br^- anions are hydrogen bonded to three $[H_2(\mathbf{L}^3)^{2+}]$ ions, via N^+-H···Br^- and C-H···Br^- interactions. Due to the size difference, the coordination of bromide ion differs from chloride ion. The Br1 ion interacts with one C-H proton on the imidazole ring, two aliphatic C-H protons from methylene groups, one imidazolium N^+-H proton and one O-H proton from one of the lattice water molecules. The Br2 anion also has interaction with two C-H bonds of imidazole ring and

one Br2···π interaction. Further, there are two strong O-H···$Br2^-$ interactions with two lattice water molecules. The coordination numbers of the two bromide ions are five in each case. The bromide ions form an infinite bromide-water chain where Br2 bridges the two intervening water molecules in the chain. On the other hand, the Br1 ion forms hydrogen bonds with the N^+-H proton of the $[H_2(\mathbf{L^3})^{2+}]$. Such interaction is not present in the case of the chloride salt. The hydrated bromide ions constitute an unusual polymeric chain, which propagates between two layers of $[H_2(\mathbf{L^3})^{2+}]$ ions. The literature suggests that the bromide ions binding to water molecules form a water cluster [64-66] in which water molecules have analogous hydrogen bonds to those present in liquid water.

Table 5.1**: Selected hydrogen bond parameters of the salts **5.1a-5.1b.

Compd. no.	D-H···A [symmetry]	$d_{D\cdots H}$(Å)	$d_{H\cdots A}$(Å)	$d_{D\cdots A}$(Å)	∠D-H···A(°)
5.1a	N1-H1···Cl1 [1-x,1-y,1-z]	0.86	2.26	3.112(3)	175
	N4-H4···O5 [1-x,-y,1-z]	0.86	1.87	2.706(6)	165
	O5-H5···O6 [1-x,1-y,-z]	0.84(6)	1.95(6)	2.757(7)	160(6)
	O5-H5···Cl2 [1-x,1-y,-z]	0.84(4)	2.29(4)	3.087(4)	159(4)
	O6-H6···Cl2 [1+x,y,z]	0.84(4)	2.29(5)	3.123(5)	171(5)
	O6-H6···Cl1 [1-x,1-y,1-z]	0.84(3)	2.36(4)	3.195(6)	178(11)
	C1-H1···O3 [-x,1-y,1-z]	0.93	2.27	3.122(5)	151
	C6-H6···O1	0.97	2.34	2.709(5)	102
	C14-H14···O2 [1-x,-y,1-z]	0.93	2.49	3.147(5)	127
5.1b	N1-H1A···Br1 [1-x,-y,1-z]	0.86	2.41	3.268(4)	176
	N4-H4···O5	0.86	1.87	2.709(7)	163
	O5-H5M···Br2 [1-x,1-y,-z]	0.84	2.43	3.243(5)	163(4)
	O5-H5N···O6 [-x,1-y,-z]	0.85(5)	1.93(7)	2.749(8)	162(8)
	O6-H6M···Br2	0.83	2.44(5)	3.252(7)	165(6)
	O6-H6N···Br1 [-1+x,y,z]	0.83(3)	2.54(3)	3.364(6)	175(7)
	C1-H1···O3 [1-x,-y,1-z]	0.93	2.30	3.158(7)	154
	C1-H1···Br2 [-x,-y,1-z]	0.93	2.84	3.719(6)	157
	C6-H6B···O1	0.97	2.35	2.718(6)	101
	C14-H14···O2 [-x,1-y,1-z]	0.93	2.51	3.159(7)	127
	C19-H19A···O3	0.97	2.35	2.735(6)	103

In the present case we observe a zigzag chain, in which each bromide ion is separated by two hydrogen bonded water molecules. The bromide ions being held in metallo-organic frame holding two layers of water molecules has been demonstrated earlier.[58] The difference observed in the present pattern is that it has water molecules as intervening molecules between the anions along a chain. A selected list of hydrogen bond parameters of the salt **5.1a** and **5.1b** are given in the Table **5.1**. Thermogravimetry of the hydrated salt **5.1a** (Figure **5.16a** in the experimental section) shows loss of water molecules in the temperature range 74-94 °C (wt. loss experimental 5.24 %, calcd. 6.09 %); whereas the water molecules in case of **5.1b** are lost in the temperatures range 70-102 °C (wt. loss experimental 5.16 %, calcd. 5.29 %). Comparing the simulated powder X-ray diffraction patterns with experimental patterns of **5.1b** (Figure **5.16b** in the experimental section) it

were found that there were similarities between the two which confirmed the bulk purity of the salts.

Among the salts having tetrahedral anions, the perchlorate salt **5.1c** crystallized in *P2₁/n* space group. In this structure the cationic part lies about an inversion centre. Asymmetric unit of the perchlorate salt contains two halves of $[H_2(\mathbf{L}^3)^{2+}]$ and two perchlorate anions.

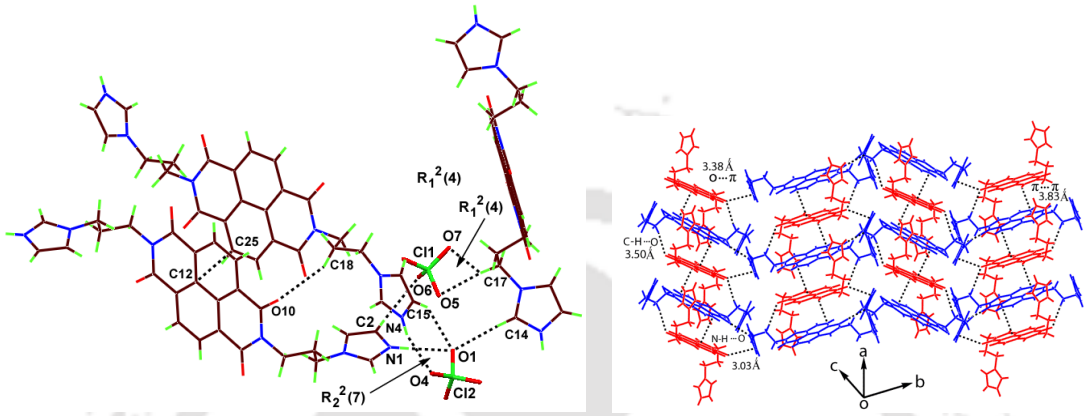

(a) (b)

***Figure 5.6**: (a) Weak interaction among perchlorate anions and the protonated ligand forming cyclic hydrogen bond, (b) 2D lamellar structure in salt **5.1c**.*

Each perchlorate ion shows eight-fold coordination, which is provided by weak N-H···O and C-H···O interactions with six $[H_2(\mathbf{L}^3)^{2+}]$ cations. However, the binding environments of the two perchlorate anions are different with respect to each other. One of the perchlorate ions (bearing Cl1) is engaged with $[H_2(\mathbf{L}^3)^{2+}]$ ions through two N-H···O and six C-H···O interactions; whereas the other perchlorate bearing Cl2 interacts with $[H_2(\mathbf{L}^3)^{2+}]$ ions only through eight C-H···O interactions without an N-H···O interaction (Figure **5.6a**). Oxygen atoms on both perchlorate ions involved in two types of cyclic $R_2^2(7)$ and $R_1^2(4)$ hydrogen bond as shown in Figure **5.6a**. The weak interactions in the lattice contribute to the formation of the 2-D layers (Figure **5.6b**).

The bisulphate salts (**5.1d**) and methyl sulfate salt (**5.1e**) both having tetrahedral anions, crystallized in the *P2₁/c* (with Z' = 0.5) space group. Z' is a quantity associated with the number of molecules in the asymmetric unit and it guides the overall packing pattern. The crystallographic asymmetric unit of the bisulfate salt consists of one half of the $[H_2(\mathbf{L}^3)^{2+}]$ ion, a bisulfate anion and a water molecule of crystallization. In both the cases the cationic part lies about an inversion centre as in the case of **5.1c**. Each bisulfate anion is associated with four neighbouring $[H_2(\mathbf{L}^3)^{2+}]$ and two lattice waters.

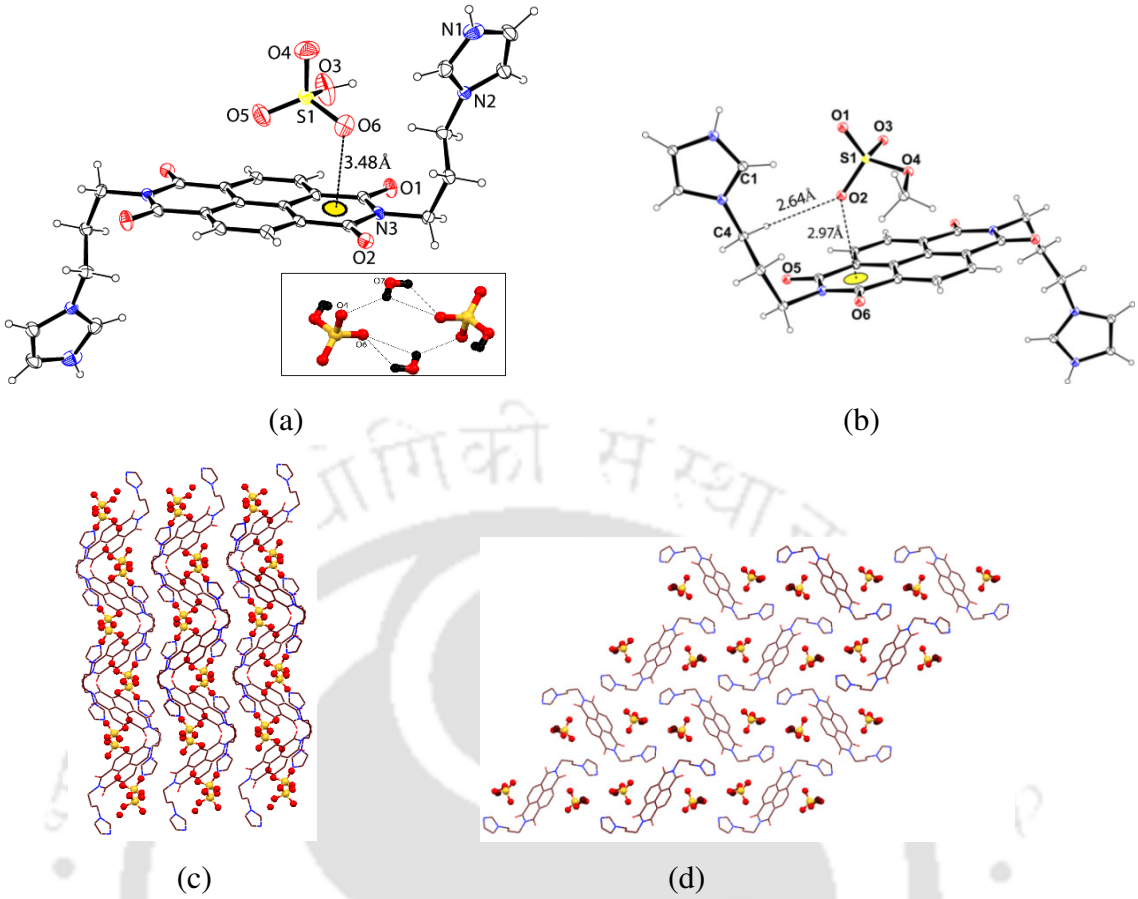

Figure 5.7: *The position of a (a) bisulfate anion (inset is water bridged dimeric assembly of bisulfate anion) in salt* ***5.1d****, (b) methyl sulfate anion with respect to naphthalenediimide ring in* ***5.1e,*** *(c) helical assembly holding the bisulfate anions in salt* ***5.1d*** *viewed along c-crystallographic axis and (d) packing diagram showing the position of methyl sulfate in salt* ***5.1e*** *viewed along a-crystallographic axis.*

The water molecules connect bisulfate anions through bridges in pairs to form bowl-like structures (inset of Figure **5.7a**). The cations interact with two hydrogen sulfates of such assemblies. These intermolecular interactions lead to the formation of helical supramolecular arrangements of cations. The bisulphate anions come close to the proximity of the naphthalenediimide ring to have anion···π interactions. The distance between atom O6 and the centroid of a ring is 3.48 Å (Figure **5.7a**). Bisulfate salts find applications in various devices, such as sensors and fuel cells.[67-71] Bisulfate anion also has structural analogy to the biologically relevant biphosphate anion.[72-73] Such anions are generally stabilized by crown ethers[74] and 3,5-diphenylpyrazole[75] ligands and their formation from conventional acids are often less selective. So the stabilization of bisulfate anions derived from sulfuric acid under ambient conditions is important. The bisulfate salt adapts a helical arrangement of cations formed by weak interactions; the anions are held in the groves of such helices (Figure **5.7c**).

From the thermogram of the salt **5.1d** (Figure **4.17a** in the experimental section) shows a 4.86 % weight loss from 90 to 130 °C. It corresponds to loss of one water molecule of crystallization (calcd. wt. loss 5.03 %).

***Table 5.2**: Selected hydrogen bond parameters of the salts **5.1c**-**5.1e**.*

Compd no.	D-H···A [symmetry]	$d_{D-H(Å)}$	$d_{H\cdots A(Å)}$	$d_{D\cdots A(Å)}$	∠D-H···A(°)
5.1c	N1-H1A···O1	0.86	2.33	3.134(8)	155
	N4-H4···O4 [-1/2+x,1/2-y,-1/2+z]	0.86	2.30	3.005(10)	139
	N4-H4···O12 [1/2+x,1/2-y,-1/2+z]	0.86	2.47	3.031(9)	123
	C1-H1···O7 [1+x,y,z]	0.93	2.42	3.166(10)	137
	C4-H4B···O6 [1-x,-y,1-z]	0.97	2.48	3.400(7)	158
	C6-H6A···O9	0.97	2.31	2.731(6)	105
	C9-H9···O2 [x,y,1+z]	0.93	2.52	3.148(10)	126
	C14-H14···O1	0.93	2.35	3.280(10)	175
	C15-H15···O1 [-1/2+x,1/2-y,-1/2+z]	0.93	2.47	3.271(9)	144
	C17-H17A···O4 [-1+x,y,z]	0.97	2.49	3.429(9)	162
5.1d	N1-H1A···O3 [1-x,1/2+y,1/2-z]	0.86	2.05	2.824(9)	149
	O7-H7A···O6 [x,1/2-y,1/2+z]	0.85(7)	2.32(7)	2.753(8)	112(6)
	O7-H7B···O6 [x,1/2-y,1/2+z]	0.84(16)	2.25(15)	2.753(8)	118(10)
	C1-H1···O6	0.93	2.49	3.296(8)	146
	C1-H1···O7 [1-x,1/2+y,1/2-z]	0.93	2.51	3.132(9)	124
	C2-H2···O5 [1-x,1/2+y,1/2-z]	0.93	2.48	3.145(8)	129
	C3-H3···O4 [-1+x,y,z]	0.93	2.32	3.100(9)	141
	C6-H6A···O1	0.97	2.35	2.737(7)	103
	C6-H6A···O5 [-1+x,y,z]	0.97	2.51	3.291(7)	137
	C12-H12···O4 [1-x,-1/2+y,1/2-z]	0.93	2.53	3.377(7)	151
	N1-H1A···O3 [1-x,1/2+y,1/2-z]	0.86	2.05	2.824(9)	149
	C13-H13···O3 [x,1/2-y,-1/2+z]	0.93	2.49	3.246(9)	138
5.1e	N1-H1C···O1 [1-x,-1/2+y,1/2-z]	0.86	1.85	2.707(4)	174
	C1-H1···O1 [x,1/2-y,-1/2+z]	0.93	2.40	3.265(5)	154
	C1-H1···O2 [x,1/2-y,-1/2+z]	0.93	2.59	3.336(5)	138
	C2-H2···O5 [1-x,-1/2+y,1/2-z]	0.93	2.31	3.142(5)	149
	C3-H3···O3	0.93	2.33	3.203(5)	156
	C4-H4B···O6 [-1+x,y,z]	0.97	2.59	2.991(5)	105
	C6-H6A···O5	0.97	2.38	2.741(5)	101

Structure of the methyl sulfate salt (**5.1e)** is also highly symmetric and it contains half of $[H_2(\mathbf{L^3})^{2+}]$ and a methyl sulfate anion in its asymmetric unit. Methyl sulfate anions also lie in the proximity of the naphthalenediimide ring as in the case of bisulfate anion to have anion-π interactions. Methyl sulfate anion binds to four units of $[H_2(\mathbf{L^3})^{2+}]$. There are one N^+-H, four C-H···O and one O···π interactions (3.29 Å). In the packing diagram of methyl sulfate salts (Figure **5.7d**) the anions are found on opposite faces of the naphthalenediimide ring to have weak anion-interactions, as illustrated in Figure **5.7b**. Although methyl sulfate anion is unstable, it can be easily stabilized in a supramolecular environment,[76-78] so $\mathbf{L^3}$ is an example of a substrate to stabilize methyl sulfate anions.

Hydrogen phosphate or biphosphate salt (**3.1f**) crystallized in a primitive triclinic space group. Asymmetric unit contains a hydrogen phosphate anion, one water molecule and two halves of the protonated $\mathbf{L^3}$. The N^+-H groups of the cationic part act as H-bond donors and interact very strongly with hydrogen phosphate anions. The interactions between the O-H of water molecules and C-H of the $[H_2(\mathbf{L^3})^{2+}]$ with hydrogen phosphate anion leads to the formation of a 2D lamellar structure, the layers are separated by

hydrogen phosphate-water chains, as shown in Figure **5.8b**. The HPO_4^{2-} anions form a water bridged polymeric inter anionic chain structure along c-crystallographic axis with R_2^2 (8) type cyclic hydrogen bonding, as shown in Figure **5.8a**.

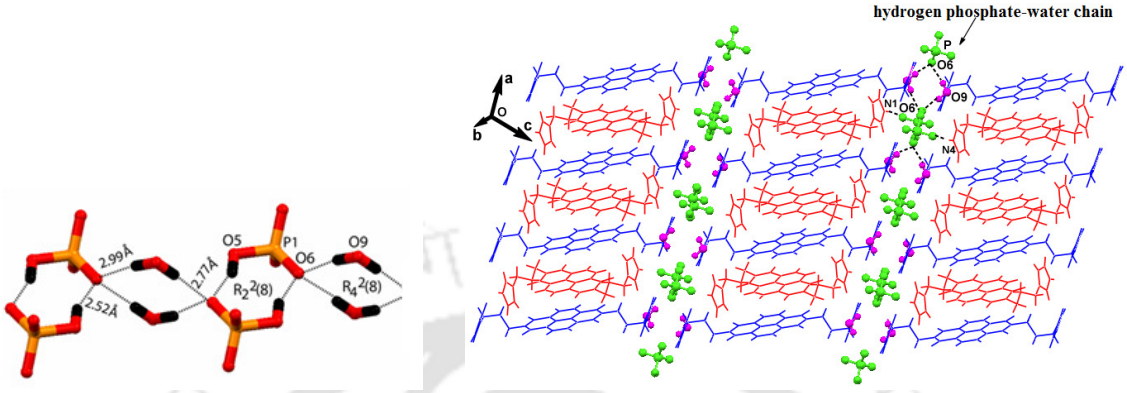

(a) (b)

***Figure 5.8**: (a) One dimensional water bridged hydrogen phosphate chain along c-axis, (b) Hydrogen-bonded 2D lamellar structure separated by hydrogen phosphate-water chain in lattice of **5.1f**.*

Each of the HPO_4^{2-} anions interacts with two O-H···O interactions. O6 and O8 act as a trifurcated H-bond acceptor with D···A distance ranging from 2.52 Å to 3.32 Å. Here the O···O (2.52 Å) and N···O (2.58 Å and another HPO_4^{2-} anion through 2.69 Å) bonds are much shorter and stronger than the normal hydrogen bond distance (OH···O ≥ 2.8 Å).[79] H-bond between O5 and O6 (with $d_{O\cdots O}$ = 2.52 Å) is attributed to low energy barrier H-bonds and these type of H-bonds are very important in biology; they exist in protein interiors and have roles in protein functions, such as enzyme catalysis and in the stabilization of specific intermediates. [80-81]

Different kinds of dimeric hydrogen phosphate, phosphate-water chains and cyclic octamers of dihydrogen phosphate anion have been reported [82-83] and in the present case here is yet another important chain formed within a lamellar structure.

From thermogravimetric analysis of **5.1f** (Figure **5.17b** in the experimental section) it was observed that a weight loss of 3.87 % which can be corroborated to the loss of the lattice water molecule (calcd. loss 3.0 wt. %).

Similarity between the simulated PXRD patterns with experimental patterns of salt **5.1f** confirmed the phase purity of the compound. The PXRD patterns of the salt **5.1f** are shown in Figure **5.18a** in the experimental section.

Asymmetric unit of the nitrate salt **5.1g** has half of the $[H_2(\mathbf{L}^3)^{2+}]$ ions with an anion. Planar nitrate ions are held by four $[H_2(\mathbf{L}^3)^{2+}]$ ions in one plane. The $[H_2(\mathbf{L}^3)^{2+}]$ ions lie

about inversion centres in the structure of the nitrate salt. Nitrate anions occur in pairs in which the two oxygen atoms come face to face (O4···O4 = 3.03 Å). Thus one of the interesting features of the salt is the $NO_3^-\cdots NO_3^-$ interactions present in the assembly (Figure **5.9a**); such O···O interactions were observed in urea nitrate and shown that they

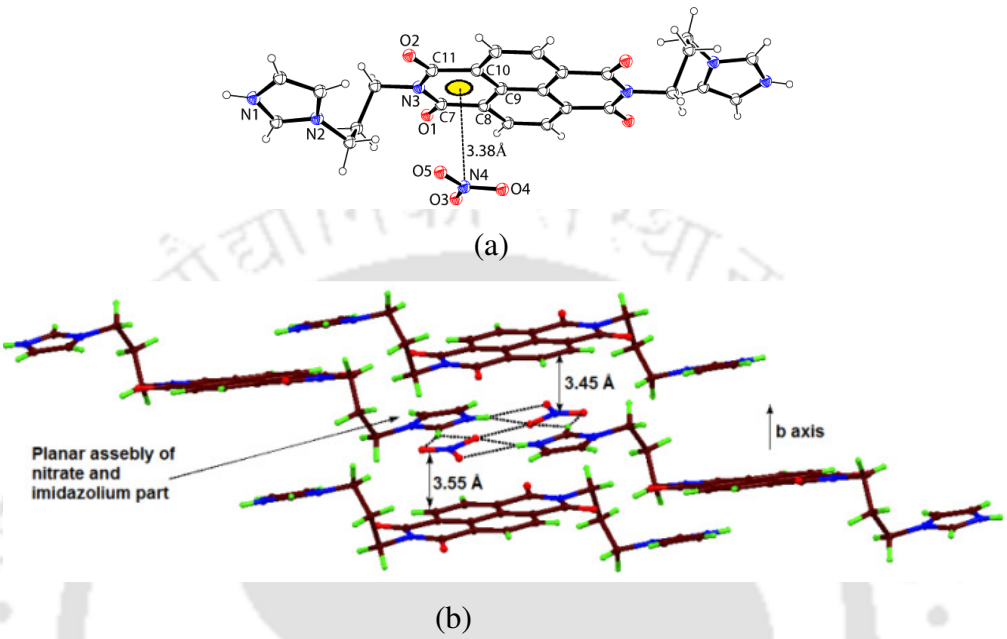

Figure 5.9*: (a) The position of a nitro-group with respect to a naphthalenediimide ring in the salt* ***5.1g****, (b) sandwiched nitrate anions stack between ring components of the salt* ***5.1g****.*

influence the structure of the nitrate salts.[84] The position of a nitro group with respect to a naphthalenediimide ring is shown in Figure **5.9a**, the distance of separation of the centroid of plane of nitrate anion to the two centroid of the naphthalenediimide plane is 3.38 Å. Planar nitrate anions and imidazole rings are sandwiched between the layers of naphthalenediimide rings and the distance of separation lies between 3.4-3.6 Å, as shown in Figure **5.9b**. The weak interactions in this salt lead to the formation of 2D layered structure. Similarity between the simulated PXRD patterns with experimental patterns of salt **5.1g** confirmed the compound was in pure form (Figure **5.18b** in the experimental section).

When $\mathbf{L^3}$ is reacted with hydrofluoric acid in a glass vessel, it resulted the formation of salt $[H_2(\mathbf{L^3})(SiF_6)]\cdot 1.5H_2O$ (**5.1h**) which has a SiF_6^{2-} dianion formed by etching of the glass. Etching of glass by hydrofluoric acid leading to SiF_6^{2-} ions was also reported earlier.[64] Salt **5.1h**, having an octahedral hexafluorosilicate anion, crystallized in the monoclinic $P2_1/c$ space group and the asymmetric unit of the salt contains two $[H_2(\mathbf{L^3})^{2+}]$

ions, two SiF_6^{2-} anions along with one and a half water molecules of crystallization (Z' = 2).

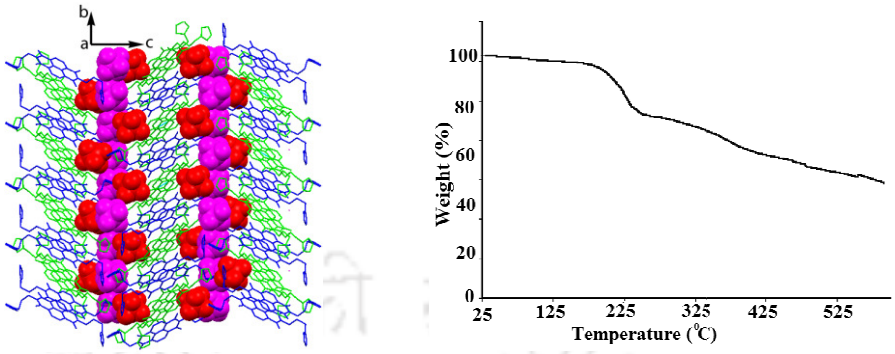

(a) (b)

***Figure 5.10**: (a) Spiral arrangement of SiF_6^{2-} ions in **5.1h,** (b) thermogram of **5.1h** (5 °C/ min).*

These two SiF_6^{2-} ions are hydrogen bonded to seven $[H_2(\mathbf{L^3})^{2+}]$ ions via N-H···F and C-H···F interactions. The anions in the lattice form spiral chain like arrangements in between the stacked layer of $[H_2(\mathbf{L^3})^{2+}]$ cations (Figure **5.10a**). From the thermogravimetric analysis (Figure **5.10b**) of **5.1h** it is clear that no water molecules are lost at low temperature; the weight loss occurs around 192 °C probably due to loss of hydrofluoric acid.

***Table 5.3**: Selected hydrogen bond parameters of the salt **5.1f-5.1g**.*

Compd. no.	D-H···A [symmetry]	$d_{D\text{-}H(Å)}$	$d_{H\cdots A(Å)}$	$d_{D\cdots A(Å)}$	∠D-H···A(°)
5.1f	N1-H1A···O8 [2-x,-y,1-z]	0.86	1.89	2.696(4)	155
	N4-H4C···O(7)	0.89(3)	1.70(3)	2.582(4)	175(4)
	O5-H5···O6 [2-x,-y,1-z]	0.82	1.74	2.526(4)	159
	O9-H9A···O6 [1-x,1-y,1-z]	0.87	2.12	2.992(4)	173
	O9-H9B···O6 [x,1+y,z]	0.97	1.82	2.774(4)	164
	N1-H1A···O8 [2-x,-y,1-z]	0.86	1.89	2.696(4)	155
	C14-H14···O8 [2-x,1-y,1-z]	0.93	2.32	3.237(5)	167
	C15-H15···O9 [x,-1+y,z]	0.93	2.52	3.375(5)	153
	C16-H16···O7 [-1+x,y,z]	0.93	2.52	3.346(5)	149
	C19-H19A···N5	0.97	2.60	2.939(4)	101
	C19-H19B···O3	0.97	2.37	2.707(4)	100
5.1g	N1-H1A···O4 [-1/2+x,1/2-y,-1/2+z]	0.86	1.86	2.712(16)	168
	C1-H1···O4 [1/2-x,-1/2+y,1/2-z]	0.93	2.31	3.049(19)	136
	C1-H1···O5 [1/2-x,-1/2+y,1/2-z]	0.93	2.26	3.17(2)	167
	C2-H2···O3 [1/2-x,1/2+y,1/2-z]	0.93	2.46	3.02(2)	118
	C4-H4B···O5 [-1+x,y,z]	0.97	2.38	3.16(2)	137
	C5-H5B···O1	0.97	2.59	3.113(19)	114
	C6-H6B···O2	0.97	2.38	2.758(19)	103

To explain the orientations of the imidazole rings, we define the two types of torsion angles across the naphthalenediimide ring as shown in Figure **5.11**. We also make a distinction while numbering between two symmetry equivalent halves by adding a prime on the atom number (Two arms of a particular unit were denoted by arm **I** and arm **II**). Besides these, there are symmetry independent molecules in these structures; so the same

sequence of atoms for torsion angles are analysed but they are demarcated by different numbers to show that they are from two different symmetry independent molecules. In case of salt **5.1g** there are four non-equivalent arms in the symmetry independent cations; these are numbered independently.

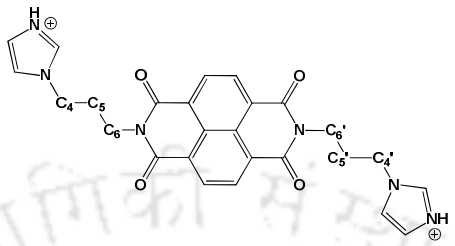

***Figure 5.11**: Torsion angles of the two arms of $[H_2(L^3)^{2+}]$.*

Torsion angles are listed in Table **5.4**. In all the cases the transoid type of arrangement across the naphthalenediimide ring is observed. Generally, two principal types of orientation of the flexible part are observed, they are reflected in the dihedral angle between two planes, one plane containing $N_{imidazole}$-$C_{methylene}$

***Table 5.4**: Torsion angles of $[H_2(L^3)^{2+}]$ showing the orientation of the imidazole rings.*

Compd. no.	Torsion angle	Angle (°)	Z′; asymmetric unit ; Symmetry to generate equivalent part
5.1a	Arm **I** (N2-C4-C5-C6)	170.8(3)	1; two halves of cation H_2L^{2+}; (x,y,z) and (-x, -y, -z)
	Arm **II** (N2'-C4'-C5'-C6')	-170.8(3)	
	Arm **I** (N5-C17-C18-C19)	174.2(3)	
	Arm **II** (N5'-C17'-C18'-C19')	-174.2(3)	
5.1b	Arm **I** (N2-C4-C5-C6)	170.0(4)	1 ; two halves of cation H_2L^{2+}; (x, y, z) and (-x, -y, -z)
	Arm **II** (N2'-C4'-C5'-C6')	-170.0(4)	
	Arm **I** (N5-C17-C18-C19)	174.5(4)	
	Arm **II** (N5'-C17'-C18'-C19')	-174.5(4)	
5.1c	Arm **I** (N2-C4-C5-C6)	173.7(4)	1; two halves of cation H_2L^{2+}; (x, y, z), (1/2-x, 1/2-y, 1/2-z) (-x,-y,-z) and (1/2+x, 1/2-y, 1/2+z)
	Arm **II** (N2'-C4'-C5'-C6')	-173.7(4)	
	Arm **I** (N5-C17-C18-C19)	66.7(6)	
	Arm **II** (N5'-C17'-C18'-C19')	-66.7(6)	
5.1d	Arm **I** (N2-C4-C5-C6)	179.4(4)	0.5; one half of cation H_2L^{2+}; (x, y, z), (-x,-y,-z), (-x, 1/2+y, 1/2-z) and (x, 1/2-y,1/2+z)
	Arm **II** (N2'-C4'-C5'-C6')	-179.4(4)	
5.1e	Arm **I** (N2-C4-C5-C6)	177.7(3)	0.5; One half of cation H_2L^{2+}; (x, y, z), (-x,-y,-z), (-x, 1/2+y, 1/2-z) and (x, 1/2-y,1/2+z)
	Arm **II** (N2'-C4'-C5'-C6')	-177.7(3)	
5.1f	Arm **I** (N2-C4-C5-C6)	173.7(3)	1; two halves of cation H_2L^{2+}; (x,y,z) and (-x, -y, -z)
	Arm **II** (N2'-C4'-C5'-C6')	-173.7(3)	
	Arm **I** (N5-C17-C18-C19)	57.2(4)	
	Arm **II** (N5'-C17'-C18'-C19')	-57.2(4)	
5.1g	Arm **I** (N2-C4-C5-C6)	68(2)	0.5, one half of cation H_2L^{2+}; (x, y, z), (-x,-y,-z), (1/2-x, 1/2+y, 1/2-z) and (1/2 + x, 1/2-y, 1/2+z)
	Arm **II** (N2'-C4'-C5'-C6')	-68(2)	
5.1h	Arm **I** (N2-C4-C5-C6)	-62(1)	2; two independent molecules in the asymmetric unit, thus there are four arms in different orientations. (x, y, z), (-x,-y,-z), (-x, 1/2+y, 1/2-z) and (x, 1/2-y, 1/2+z)
	Arm **II** (N5-C23-C22-C21)	-55(1)	
	Arm **I** (N8-C30-C31-C32)	-64(1)	
	Arm **II** (N11-C49-C48-C47)	67(1)	

and another plane containing $C_{methylene}$–$C_{methylene}$ bond. More quantitatively, these torsion angles are found to be close to 170° or between 55-70°. Recently, cadmium complexes of pyridine tethered imide based scaffolds, which are guided by anions,[85] have been shown to have variations in conformations. A close analysis suggests that the position of the flexible

part in $[H_2(\mathbf{L^3})^{2+}]$ is decided by weak interactions with the respective counter ion and these guide the position of the cations in different ways, leading to different Z' values. We clearly see that the orientations of the imidazole are guided by the anions. For example, the chloride, bromide and perchlorate are mono-anionic and have a spherical charge distribution; they show similar torsion angles in each case. In the case of the bromide and chloride two halves of symmetry independent molecules appear in their asymmetric unit, showing that the cations occurs in pairs of repeat units; and each component in the pair has two different orientations. Bisulfate and methyl sulfate shows a similar pattern of orientations, they occur as overall one cation per repeat unit, whereas the pairs of symmetry non-equivalent molecules in **5.1g** has altogether different orientations of the imidazole ring with respect to the chloride or bromides. All the anions compared in **5.1a-5.1f** are mono-anionic and the orientation across the naphthalenediimide is transoid in each case. Thus, the formation of water-assisted ion chains influences the orientation of the imidazole rings, bringing the anions close to the naphthalenediimide ring to have π-anion interactions. Whereas in the case of perchlorate there are no such interactions, and in the case of bisulphate and methyl sulfate as well as nitrate, the geometrical arrangement and the distances favor weak anion-π interactions. The electron clouds in these oxy-acid cases are π-delocalised, which makes a distinction from the halides.

5.3 Fluorescence emission studies of L^3 with different acids:

Ligand, $\mathbf{L^3}$ shows an emission maximum at 397 nm upon excitation at 340 nm. This emission was changed on addition of different acids and such changes are characteristics of individual anions. The solution state studies of the ligand were carried out by monitoring the changes in the fluorescence emission on gradual addition of various acid solutions.

The fluorescence intensity of $\mathbf{L^3}$ decreases on gradual addition of hydrochloric acid and hydrobromic acid (Figure **5.12a-b**). On the other hand fluorescence intensity of $\mathbf{L^3}$ increases on addition of oxy-acids such as perchloric acid, sulphuric acid, phosphoric acid and nitric acid which are shown in Figure **5.12c-f**. We also observed enhancement of fluorescence intensity of $\mathbf{L^3}$ upon addition of hydrofluoric acid. Solid state photoluminescence spectra of all salts were also recorded to check whether it is similar or different from that of the solution state. We found analogy between the solid and solution state. A representative solid state spectrum is shown in Figure **5.13** where overlay of $\mathbf{L^3}$,

salt **5.1b** and salt **5.1g** are drawn. Anions are known to quench fluorescence emission of aromatic fluorophore.[86] There are also examples in which fluorescence emission of receptors gets enhanced by interaction with anions.[57] Thus, it is of interest to understand changes caused by protonation in the geometrical features of the tethers attached to naphthalimides as they could play an important role in fluorescence emission.[28-29] In the present case the changes in fluorescence help us to distinguish hydrofluoric acid from hydrochloric and hydrobromic acid, as the hydrofluoric acid causes fluorescence ON; whereas, hydrochloric acid and hydrobromic acid cause OFF.

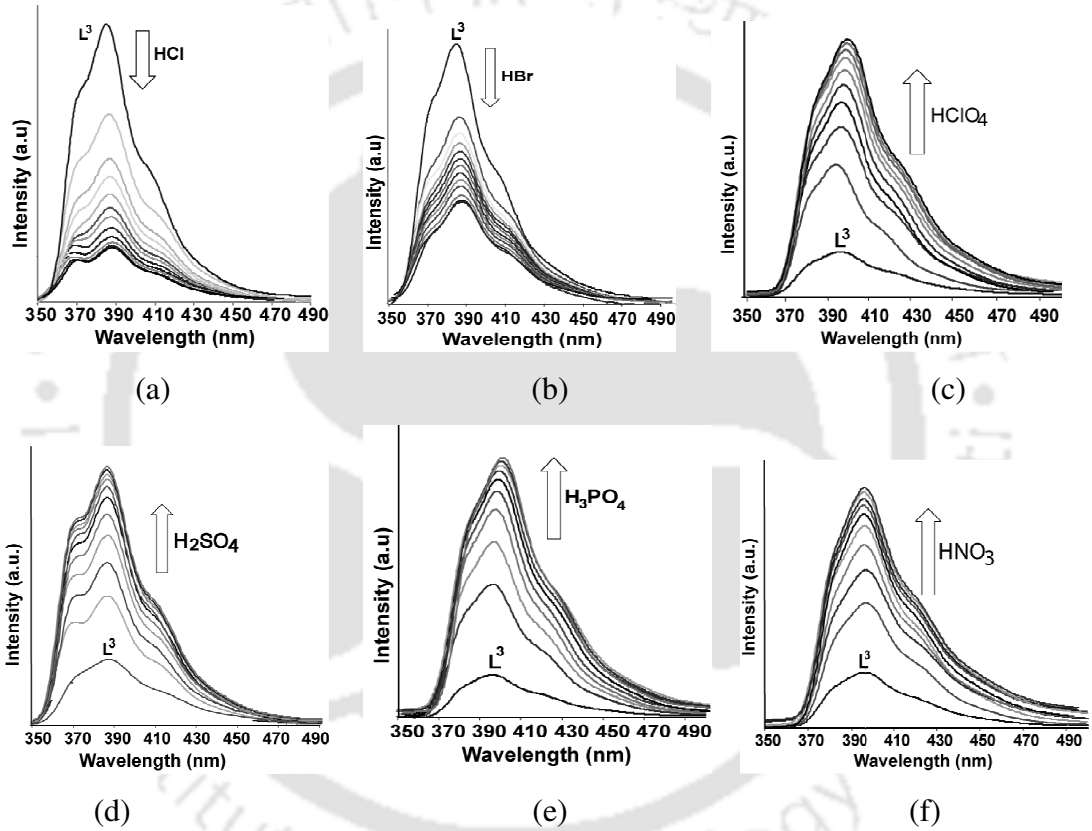

***Figure 5.12**: Changes in fluorescence emission intensity (λex = 340 nm) of **L³** (2ml of 10^{-5} M solution in methanol) with (a) HCl, (b) HBr, (c) $HClO_4$, (d) H_2SO_4, (e) H_3PO_4, and (f) HNO_3 (10 µl in each aliquot from each of the acid solution of concentration 10^{-2} M each).*

The π···π stacking interactions generally quench fluorescence.[87] From the existing literature it is clear that the anions form exciplexes with anions,[86] thereby fluorescence quenching takes place.

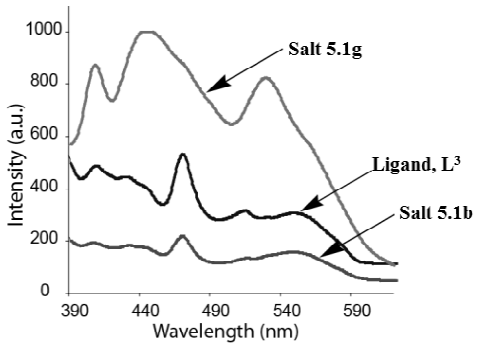

***Figure 5.13**: Solid state fluorescence emission of **L**^{3} and its bromide and nitrate salts (λ_{ex} = 380 nm).*

The parent **L**^{3} is in a native state, in which the lone pair of electrons on the nitrogen atoms of the imidazole are in the proximity of the naphthalenediimide ring, as illustrated in Figure **5.14a**. The participation of the lone pairs to form an N-H bond by protonation is expected to enhance the (Figure **5.14c**) fluorescence emission.

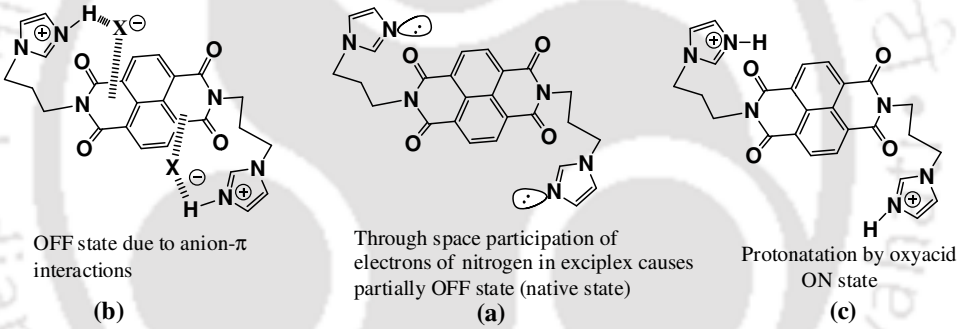

***Figure 5.14**: Three different stages of **L**^{3} (a) free ligand in partially OFF state, (b) OFF state due to anion-π interactions and (c) ON state due to the protonations by oxyacids.*

Thus, in the case of the acids having π-delocalised oxy-anions or the one having no anion-π interactions, enhancement of fluorescence was observed. In the protonated state generated by hydrochloric acid and hydrobromic acid, the chloride and bromide ions are positioned in such a way that they cause quenching of fluorescence (Figure **5.14b**) by interacting with the naphthalenediimide unit through anion-π interactions (Figure **5.3**) by forming an exciplex state.[85]

5.3 Conclusion:

Anion assisted assemblies of imidazole tethered naphthalenediimide is shown. This is the first structural evidence showing anion-π interactions in naphthalenediimide derivatives to depict the geometries and also making a correlation on affects of anion-pi interactions.

Chloride and bromide ions have significant anion-π interactions and are also anions that are hydrogen bonded to water molecules in the form of a chain held between the layers of cations. The size and shape of the anions dictates the orientations of the imidazole rings. Two types of orientations of imidazole rings in the respective salts of **L^3** with $C_{methylene}$-$C_{methylene}$ bonds, namely parallel (dihedral angle close to 170°) and perpendicular (dihedral angle close to 70°) orientations are observed in these salts. Nitrate ions occur in pairs and are sandwiched between the aromatic rings of naphthalenediimides. Quenching of the fluorescence of **L^3** by chloride and bromide anion occurs due to anion-π interactions whereas the protonation of **L^3** by oxyacid causes fluorescence enhancement in a conventional manner that is observed in naphthalimide padent groups containing nitrogen atoms. Salt of **L^3** are in the forms of different interesting anion assisted assemblies. Another interesting observation is different aquated anionic chains within the channel like structures of the protonated **L^3.**

5.4 Experimental Section:

The detailed synthetic methodologies for synthesis of salts are described. Analytical data listed along with each compound. The instrumental details and the crystallographic parameters are provided in Appendix.

Synthesis of N,N'-bis(3-imidazol-1-ylpropyl)naphthalenediimide: 1,4,5,8-naphthalenetetracarboxylic acid dianhydride (540 mg, 2 mmol) was dissolved in warm DMF. To this solution 3-(1H-imidazol-1-yl)propan-1-amine (480 mg, 4 mmol) was added and the reaction mixture was refluxed 24 h. To the reaction mixture ice cold water added. A brown precipitate of the compound **L^3** was formed which was filtered and washed with methanol and dried in air. Yield 55%. ^{1}H-NMR (400 MHz, DMSO-d_6): 8.60 (*s*, 1H), 7.66 (*s*, 1H), 7.22 (*s*, 1H), 6.87 (*s*, 1H), 4.12 (*t*, 2H, 6.8Hz), 4.08 (*t*, 2H, 7.2Hz), 2.28 (*m*, 2H, 6.8Hz). IR (KBr, cm^{-1}): 3555 (s), 3385 (m), 1699 (s), 1650 (s), 1581(m), 1505 (w), 1454 (m), 1376 (s), 1340 (s), 1305 (m), 1246 (s), 1171 (m), 1057 (m), 972 (w), 769 (s), 592 (w). ^{13}C-NMR (150 MHz, DMSO-d_6) (Figure **5.15a**): 162.7 (carbonyl carbon), 137.3 (naphalene carbon), 130.4, 126, 119.3 (imidazole carbon), 128.3 (imide ring carbon), 44, 37.8, 29 (methylene carbon). HR-ESI MS (M+1) 483.1772 (calcd. 483.1703) (Figure **5.15b**).

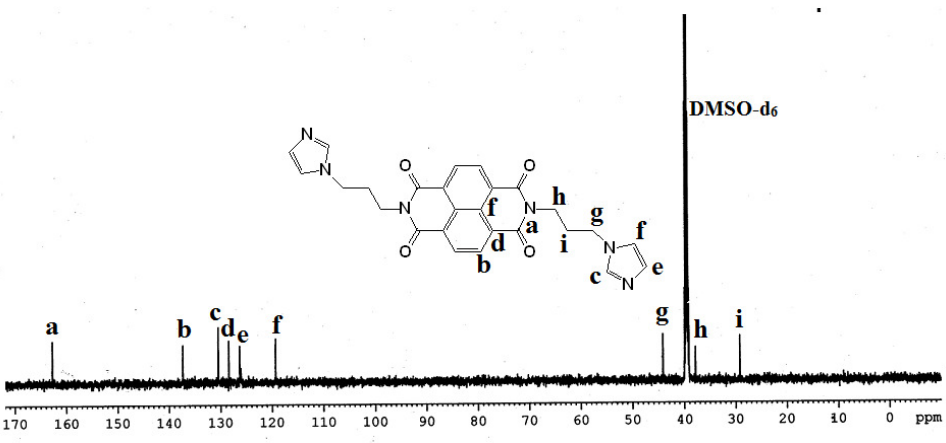

(a)

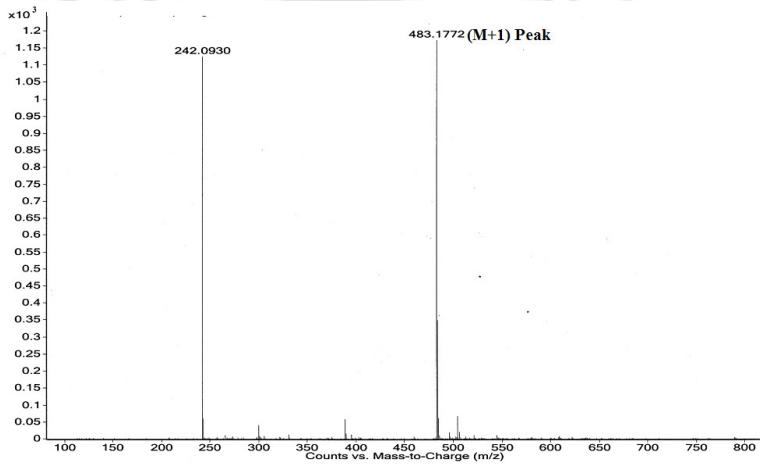

(b)

Figure 5.15: *(a)* ^{13}*C-NMR (150 MHz, DMSO-d$_6$) and (b) HR-ESI MS of ligand* ***L^3*****.**

Salt 5.1a: To a methanolic solution of **L^3** (482 mg, 1 mmol), 0.3 mL of 70 % HCl was added and stirred for 30 min. A clear solution was obtained and it was filtered and kept undisturbed at room temperature. On standing, light pink rod shaped crystals appeared after 7-8 d. Yield 45 %. ^{1}H-NMR (400 MHz, DMSO-d$_6$): 9.15 (*s*, 1H), 8.67 (*s*, 1H), 7.81 (*s*, 1H), 7.68 (*s*, 1H), 4.33 (*t*, 2H, 7.2Hz), 4.08 (*t*, 2H, 6.4Hz), 2.25 (*m*, 2H, 6.8Hz). IR (cm^{-1}): 3391 (b), 3137 (w), 1695 (s), 1660 (s), 1580 (s), 1548 (w), 1454 (s), 1383 (s), 1334 (s), 1246 (s), 1166 (m), 1055 (m), 972 (w), 833 (m), 766 (s), 623 (w).

Salt 5.1b: Reddish brown crystals after 6 d were obtained reacting **L^3** (1 mmol) with HBr (48 %, 0.3 mL). Yield 58 %. ^{1}H-NMR (400 MHz, DMSO-d$_6$): 9.18 (*s*, 1H), 8.67 (*s*, 1H), 7.84 (*s*, 1H), 7.71 (*s*, 1H), 4.34 (*t*, 2H, 7.6Hz), 4.10 (*t*, 2H, 6.4Hz), 2.26 (*m*, 2H, 7.2Hz). IR (KBr, cm^{-1}): 3410 (b), 2964 (m), 1696 (s), 1659 (s), 1581 (s), 1547 (m), 1453 (s), 1377 (s), 1334 (s), 1260 (w), 1246 (s), 1170 (m), 1083 (w), 1054 (m), 970 (w), 855 (m), 803 (s), 766 (m).

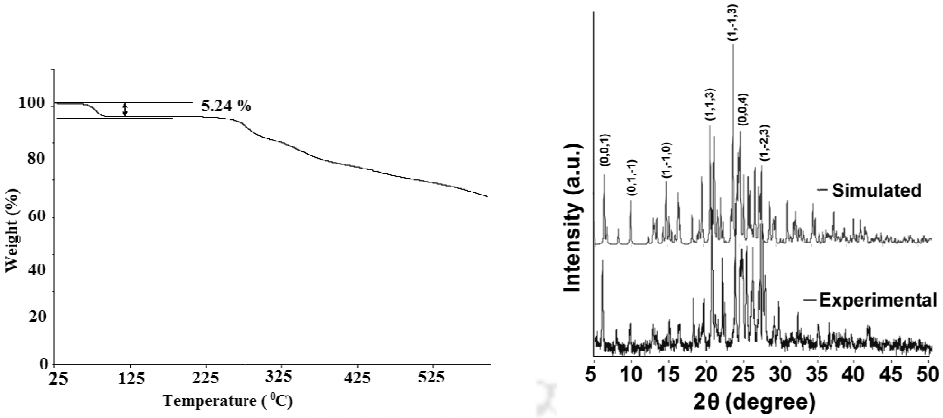

(a) (b)

Figure 5.16*: (a) Thermogram of salt* ***5.1a*** *(heating rate 5 °C/min) and (b) Comparison of simulated (top) and experimental (bottom) PXRD patterns of the salt* ***5.1b****.*

Salt 5.1c: Reaction of 0.3 mL of 70 % of perchloric acid with 1 mmol $\mathbf{L^3}$ gave light pink crystals of salt **5.1c** after 4-5 d. Yield 48 %. ^{1}H-NMR(400 MHz, DMSO-d$_6$): 9.10 (*s*, 1H), 8.68 (*s*, 1H), 7.81 (*s*, 1H), 7.69 (*s*, 1 H), 4.32 (*t*, 2H, 7.2Hz), 4.10 (*t*, 2H, 6.4Hz), 2.26 (*m*, 2H, 7.2Hz). IR (KBr, cm^{-1}): 3410 (b), 3133 (w), 1695 (s), 1660 (s), 1581 (s), 1547 (m), 1454 (s), 1379 (s), 1346 (m), 1334 (s), 1309 (w), 1296 (w), 1246 (s), 1143 (w), 1117 (m), 1083 (s), 965 (w), 855 (m), 823 (m), 784 (w), 765 (s), 728 (w), 624 (s).

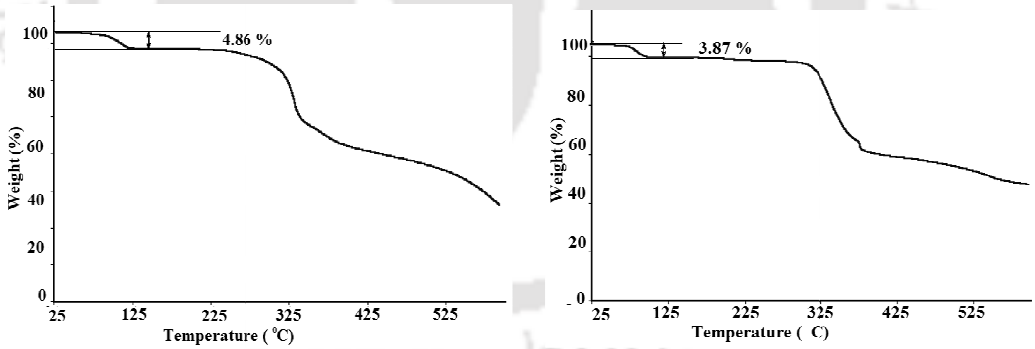

(a) (b)

Figure 5.17*: Thermogram of (a) salt* ***5.1d*** *and (b) salt* ***5.1f*** *(heating rate 5 °C/min).*

Salt 5.1d: It was obtained by treating 0.1 ml of concentrated sulphuric acid with a solution of $\mathbf{L^3}$ (482 mg, 1 mmol) in 25 mL methanol. Red crystals were obtained after 10-12 d. Yield 58 %. ^{1}H-NMR (400 MHz, DMSO-d$_6$) : 9.14 (*s*, 1H), 8.59 (*s*, 1H), 7.83 (*s*, 1H), 7.70 (*s*, 1H), 4.34 (*t*, 1H, 7.2 Hz), 4.07 (*t*, 2H, 6.4Hz), 2.26 (*m*, 2H, 6.4Hz). IR (cm^{-1}): 3420 (b), 1695 (s), 1660 (s), 1582 (s), 1548 (m), 1455 (s), 1379 (s), 1334 (s), 1246 (s), 1090 (w), 1055 (s), 1002 (m), 970 (w), 856 (m), 824 (w), 766 (s), 590 (m).

Salt 5.1e: Few drops of concentrated sulfuric acid to a solution of $\mathbf{L^3}$ (482 mg, 1 mmol) in a binary mixture of DMF-methanol led to **5.1e**. After 9-10 d brown crystals of **5.1e** were obtained. Yield: 56 %. ^{1}H-NMR (400 MHz, DMSO-d_6): 9.13 (*s*, 1H), 8.68 (*s*, 1H), 7.82 (*s*, 1H), 7.70 (*s*, 1H), 4.33 (*t*, 2H, 7.2Hz), 4.10 (*t*, 2H, 6.8 Hz), 2.2 (*m*, 2H, 7.2 Hz). IR (KBr, cm^{-1}): 3120 (w), 1705 (s), 1660 (s), 1580 (s), 1548 (s), 1456(s), 1431 (w), 1378 (s), 1338 (s), 1313 (w), 1300 (w), 1277 (m), 1247 (m), 1053 (s), 1001 (s), 971 (m), 908 (m), 888 (m), 861 (m), 781 (s), 767 (s), 755 (s), 738 (s), 638 (s), 576 (s), 536 (w).

***Table 5.5**: Selected hydrogen bond parameters of the salt **5.1h**.*

Compd. no.	D-H···A [symmetry]	$d_{D\text{-}H(Å)}$	$d_{H\cdots A(Å)}$	$d_{D\cdots A(Å)}$	∠D-H···A(°)
5.1h	N1-H1···O2 [1-x, 1-y, -z]	0.86	2.59	3.337(17)	146
	N6-H6···F10 [x, 2+y, z]	0.86	2.48	3.098(16)	130
	N7-H7···F7 [x, -1/2-y, -1/2+z]	0.86	1.96	2.811(10)	171
	N12-H12···F9 [1-x,1/2+y,1/2-z]	0.86	2.50	2.958(12)	114
	C2 -H2···F4 [1-x,1-y, -z]	0.93	1.99	2.780(15)	141
	C2 -H2···F6 [1-x, 1-y, -z]	0.93	2.13	2.913(16)	142
	C3 -H3···F11 [x, 1/2-y, -1/2+z]	0.93	2.26	3.173(14)	168
	C6 -H6A···O1	0.97	2.38	2.702(13)	102
	C15-H15···F6 [x, 1+y, z]	0.93	2.30	3.102(12)	144
	C21-H21B···O(4)	0.97	2.36	2.720(12)	101
	C21-H21B···N5	0.97	2.60	2.957(14)	102
	C23-H23B···F8 [x, 1+y, z]	0.97	2.32	3.138(11)	142
	C24-H24···F12 [x, 2+y, z]	0.93	2.46	3.029(18)	120
	C25-H25···F(1) [1-x, 1/2+y, 1/2-z]	0.93	1.82	2.741(12)	168
	C26-H26···F9 [x, 1+y, z]	0.93	2.21	3.112(11)	164
	C26-H26···F(11) [x, 1+y, z]	0.93	2.50	3.189(12)	131
	C27-H27···F8 [-x, -y, -z]	0.93	2.09	3.023(14)	177
	C29-H29···F11 [x, 1/2-y, -1/2+z]	0.93	2.44	3.170(12)	136
	C32-H32B···O6	0.97	2.36	2.702(13)	100
	C35-H35···O3 [-x, 2-y, -z]	0.93	2.44	3.163(12)	135
	C47-H47B···O8	0.97	2.36	2.732(12)	102
	C51-H51···F9 [1-x,1/2+y,1/2-z]	0.93	2.35	2.883(12)	116
	C51-H51···F10 [1-x,1/2+y,1/2-z]	0.93	1.77	2.702(13)	175
	C52-H52···F5	0.93	2.41	3.011(12)	122

Salt 5.1f: $\mathbf{L^3}$ was dissolved in a mixture of DMSO-MeOH (1:1 v/v) and a few drops of orthophosphoric acid were added. A clear solution was obtained. The solution was filtered to make free from any residue and kept at room temperature for two weeks. Block-shaped crystals suitable for X-ray analysis were obtained. Yield: 60 %. ^{1}H-NMR (400 MHz, DMSO-d_6): 8.61 (*s*, 1H), 7.78 (*s*, 1H), 7.26 (*s*, 1H), 6.93 (*s*, 1H), 4.11 (*t*, 2H, 6.8Hz), 4.05 (*m*, 2H, 6.8Hz), 2.12 (*t*, 2H, 6.8Hz). IR (cm^{-1}): 3383 (br), 3124 (m), 1703 (s), 1663 (s), 1579(m), 1454 (s), 1375 (m), 1342 (s), 1246 (s), 1068 (br), 952 (m), 768 (m), 662 (w), 517 (m).

Salt 5.1g: Addition of nitric acid (0.3 mL of 69 %) to a methanolic solution of $\mathbf{L^3}$ (482 mg, 1 mmol) gave **5.1g**. Brown rod shaped crystals of **5.1g** appeared after 5 d. Yield 62 %. ^{1}H-NMR (400 MHz, DMSO-d_6): 9.13 (*s*, 1H), 8.68 (*s*, 1H), 7.82 (*s*, 1H), 7.70 (*s*, 1 H), 4.33 (*t*, 2H, 7.2Hz), 4.10 (*t*, 2H, 6.4Hz), 2.28 (*m*, 2H, 6.4Hz). IR (cm^{-1}): 3432 (b), 3106 (w), 1701 (s), 1658 (s), 1575 (s), 1456 (m), 1383 (s), 1334 (m), 1260 (w), 1245 (m), 1174

(m), 1100 (w), 1084 (w), 1038 (w), 926 (w), 889 (m), 851 (w), 823 (w), 773 (m), 749 (m), 718 (w), 669 (w), 634 (w).

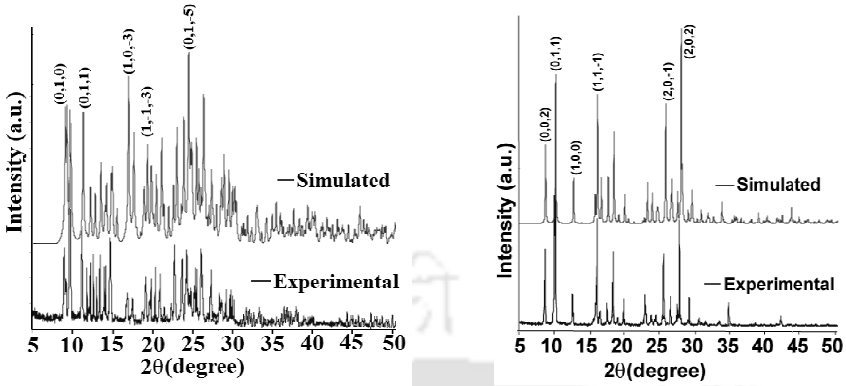

***Figure 5.18**: (a) Comparison of simulated (top) and experimental (bottom) PXRD patterns of (a) salt **5.1f** and (b) salt **5.1g**.*

Salt 5.1h: It was obtained by adding hydrofluoric acid (0.2 mL of 48 %) to a methanol solution of **L**^{3} (482 mg, 1 mmol) in a glass test tube. A clear solution obtained was kept for crystallization at room temperature. Brown needle shaped crystals were obtained after 12-14 h on the wall of the test tube. ^{1}H-NMR (400 MHz, DMSO-d$_6$): 8.67 (*s*, 1H), 8.4 (*s*, 1H), 7.52 (*s*, 1H), 4.21 (*t*, 2H, 7.2Hz), 4.08 (*t*, 2H, 6.8Hz), 2.32 (*m*, 2H, 7.2Hz). IR (cm^{-1}): 3416 (br), 3149 (w), 1696 (s), 1660 (s), 1581 (s), 1547 (m), 1454 (s), 1380 (m), 1346 (s), 1334 (s), 1295 (w), 1246 (s), 1167 (m), 1085 (w), 1055 (m), 890 (s), 856 (w), 824 (m), 765 (s), 483 (s).

5.6 References:

1. Dawson, R. E.; Hennig, A.; Wemann, D. P.; Emery, D.; Ravikumar, V.; Montenegero, J.; Takeuchi, T.; Gabutti, S.; Mayor, M.; Mareda, J.; Shalley, C.; Matile, S. *Nat. Chem.* **2010**, *2*, 533-537.
2. Gale, P. A. *Chem. Soc. Rev*. **2010**, *39*, 3746-3771.
3. Beer, P.D.; Gale, P.A. *Angew. Chem., Int. Ed*. **2001**, *40*, 486-516.
4. Sessler, J. L.; Gale, P. A.; Cho, W. -S.; Anion Receptor Chemistry: *Monographs in Supramolecular Chemistry*, RSC, Cambridge, U.K. **2006.**
5. He, J. J.; Quiocho, F. A. *Science* **1991**, *251*, 1479-1481.
6. Bianchi, A.; James, K. B.; Espana, E. G. *Supramolecular Chemistry of Anions*, Wiley-VCH, New-York, **1997.**
7. Martinez-Manez, R.; Sancenon, F. *Chem. Rev.* **2003**, *103*, 4419-4476.

8. An, H.; Bradshaw, J. S.; Izatt, R. M. *Chem. Rev*. **1992**, *92*, 543-572.
9. An, H.; Bradshaw, J. S.; Izatt, R. M.; Yan, Z. *Chem. Rev*. **1994**, *94*, 939-991.
10. Conn, M. M.; Jr. Rebek, *J. Chem. Rev*. **1997**, *97*, 1647-1668.
11. Nath, B.; Baruah, J. B. *Cryst. Growth Des*. **2012**, *12*, 1671-1682.
12. Burkhard, P.; Tai, C. H.; Jansonius, J. N.; Cook, P. F. *J. Mol. Biol*. **2000**, *303*, 279-286.
13. Burlington, B. T.; Widlanski, T. S. *J. Org. Chem*. **2001**, 66, 7561-7567.
14. Tai, C. H.; Burkhard, P.; Gani, D.; Jenn, T.; Johnson, C.; Cook, P. F. *Biochemistry* **2001**, *40*, 7446-7452.
15. Courtemanche, R. J. M.; Pinter, T.; Hof, F. *Chem. Commun*. **2011**, *47*, 12688-12690.
16. Schottel, B. L.; Chifotides, H. T.; and K. D. Dunbar, *Chem. Soc. Rev*. **2008**, *37*, 68-83.
17. Bao, X.-P.; Wang, L.; Wu, L.; Li, Z. -Y. *Supramol. Chem*. **2008**, *20*, 467-472.
18. Lakshminarayanan, P. S.; Ravikumar, I.; Suresh, E.; Ghosh, P. *Inorg. Chem*. **2007**, *46*, 4769-4771.
19. Kondo, S. -I.; Hiraoka, Y.; Kurumatani, N.; Yano, Y. *Chem. Commun*. **2005**, 1720-1722.
20. Steed, J. W.; *Chem. Soc. Rev*. **2010**, *39*, 3686-3699.
21. Gale, P. A. *In Encyclopedia of Supramolecular Chemistry*, ed. Atwood, J. L.; Steed, J. W.; Dekker, M. New York, **2004**, 31-41.
22. Gale, P. A. *Chem. Commun*. **2008**, 4525-4540.
23. Sessler, J. L.; Cho, D. -G.; Lynch, V. *J. Am. Chem. Soc*. **2006**, *128*, 16518-16519.
24. Schug, K. A.; Lindner, W. *Chem. Rev*. **2005**, *105*, 67-113.
25. Guha, S.; Saha, S. *J. Am. Chem. Soc*. **2010**, *132*, 17674-17677.
26. Guha, S.; Goodson, F. S.; Corson, L. J.; Saha, S. *J. Am. Chem. Soc*. **2012**, *134*, 13679-13691.
27. Thomine, S.; Barbier-Brygod, H. *Nature* **2010**, *467*, 1058-1059.
28. Duke, R. M.; Veale, E. B.; Pfeffer, F. M.; Kruger, P. E.; Gunnaluagsson, T. *Chem. Soc. Rev*. **2010**, *39*, 3936-3953.
29. Silva, A. P. De.; Gunaratne, H. Q. N.; Gunnlaugsson, T.; Huxley, A. J. M.; McCoy, C. P.; Rademacher, J. T.; Rice, T. E. *Chem. Rev*. **1997**, *97*, 1515-1566.
30. McDonald, K. P.; Ramabhardan, R. O.; Lee, S.; Raghavchari, K.; Flood, A. H. *Org. Lett*. **2011**, *13*, 6260-6263.
31. Ali, H. D. P. P.; Kruger, E.; Gunnlauglsson, T. *New J. Chem*. **2008**, *32*, 1153-1161.
32. Veale, E. B.; Gunnauglgsson, T. *J. Org. Chem*. **2010**, *75*, 5513-5525.
33. Gan, J.; Chen, K.; Chang, C. -P.; Tian, H. *Dyes Pigm*. **2003**, *57*, 21-28.
34. Gan, J.; Tian, H.; Wang, Z.; Chen, K.; Hill, J.; Lane, P. A.; Rahn, M. D.; Fox, A. M.; Bradley, D. D. C. J. *Organomet. Chem*. **2002**, *645*, 168-175.
35. Bao, X. -P.; Wang, L.; Wu, L.; Li, Z. -Y. *Supramol. Chem*. **2008**, *20*, 467-477.

36. Gunnlaugsson, T.; Kruger, P. E.; Jensen, P.; Tiemey, J.; Ali, H. D. P.; Hussey, G. M. *J. Org. Chem.* **2005**, *70*, 10875-10878.
37. Gunnlaugsson, T.; Glynn, M.; Tocci, G. M.; Kruger, P. E.; Pfeffer, F. M. *Coord. Chem. Rev.* **2006**, *250*, 3094-3117.
38. Barooah, N.; Sarma, R. J.; Baruah, J. B. *CrystEngComm.* **2006**, *8*, 608-615.
39. Barooah, N.; Baruah, J. B. *J. Mol. Struct*. **2008**, *872*, 205-211.
40. Jentzsch, A. V.; Emery, D.; Mareda, J.; Metrangolo, P.; Resnati, G.; Matile, S. *Angew. Chem., Int. Ed*. **2011**, *50*, 11675-11678.
41. Gamez, P.; Mooibroek, T. J.; Teat, S. J.; Reedijk, J. *Acc. Chem. Res*. **2007**, *40*, 435-444.
42. Gorteau, V.; Bollot, G.; Mareda, J.; Perz-velasco, A.; Matile, S. *J. Am. Chem. Soc*. **2006**, *128*, 14788-14789.
43. Davis, J. T. *Nat. Chem*. **2010**, *2*, 516-517.
44. Zhao, Y.; Beuchat, C.; Domoto, Y.; Gajewy, J.; Wilson, A.; Mareda, J.; Sakai, N.; Matile, S. *J. Am. Chem. Soc*. **2014**, *136*, 2101-2111.
45. Zhao, Y.; Sakai, N.; Matile, S. *Nature Commun*. **2014**, *5*, 1-5.
46. Gabriel, G. J.; Iverson, B. L. *J. Am. Chem. Soc*. **2002**, *124*, 15174-15175.
47. Degenhardt III, C. F.; Lavin, J. M.; Smith, M. D.; Shimizu, K. D. *Org. Lett*. **2005**, *7*, 4079-4081.
48. Baruah, J. B.; Karmakar, A.; Barooah, N. *CrystEngComm* **2008**, *10*, 151-154.
49. Barooah, N.; Sarma, R. J.; Baruah, J. B. *CrystEngComm* **2006**, *8*, 608-615.
50. Kishikawa, K.; Tsubokura, S.; Kohmoto, S.; Yamamoto, M.; Yamguchi, K. *J. Org. Chem.* **1999**, *64*, 7568-7578.
51. Kishikawa, K.; Furusawa, S.; Yamaki, T.; Kohmoto, S.; Yamamoto, M.; Yamaguchi, K. *J. Am. Chem. Soc*. **2002**, *124*, 1597-1605.
52. Chong, Y. S.; Dial, B. E.; Burns, W. G.; Shimizu, K. D. *Chem. Commun*. **2012**, *48*, 1296-1298.
53. Chong,Y. S.; Carroll, W. R.; Burns, W. G.; Smith, M. D.; Shimizu, K. D. *Chem. Eur. J*. **2009**, *15*, 9117-9126.
54. Rasberry, R. D.; Smith, M. D.; Shimizu, K. D. *Org. Lett*. **2008**, *10*, 2889-2892.
55. Lavin, J. M.; Shimizu, K. D. *Chem. Commun*. **2007**, 228-230.
56. Molina, P.; Tarraga, A.; Oton, F. *Org. Biomol. Chem*. **2012**, *10*, 1711-1724.
57. Kubo, Y.; Kobayashi, A.; Ishida, T.; Misawa, Y.; James, T. D. *Chem. Commun*. **2005**, 2846-2848.
58. Duc, Y. L.; Michau, M.; Gilles, A.; Gence, V.; Legrand, Y. -M.; Lee, A. V.; Tingry, S.; Barboiu, M. *Angew. Chem., Int. Ed*. **2011**, *50*, 11366-11372.
59. Bai, S. Q.; Quek, G. Y. H.; Koh, L. L.; Hor, T. S. A. *CrystEngComm*. **2010**, *12*, 226-233.

60. Dutzler, R.; Campbell, E. B.; Cadene, M.; Chait, B. T.; MacKinnon, R. *Nature* **2002**, *415*, 287-294.
61. Saha, M. K.; Bernal, I. *Inorg. Chem. Commun*. **2005**, *8*, 871-873.
62. Srinivasan, B. R.; Mhalsikar, R. G.; Rane, K. S.; Nather, C.; Bensch, W. *J. Chem. Sci.* **2007**, *119*, 21-27.
63. Chow, H. S.; Constable, E. C.; Housecroft, C. E.; Neuburgerm, M.; Schaffner, S. *Dalton Trans.* **2006**, 2881-2890.
64. Das, M. C.; Ghosh, S. K.; Bharadwaj, P. K. *Dalton Trans.* **2009**, 6496-6506.
65. Wan, C. -Q.; Li, G. -S.; Chen, X. -D.; Mak, T. C. W. *Cryst. Growth Des*. **2008**, *8*, 3897-3901.
66. Hoog, P. De.; Gamez, P.; Mutikainen, I.; Turpeinen, U.; Reedjik, J. *Angew. Chem., Int. Ed.* **2004**, *43*, 5814-5817.
67. Haile, S. M.; Boyens, D. A.; Chisholm, C. R. I.; Merie, R. B. *Nature* **2001**, *410*, 910-913.
68. Chisholm, C. R. I.; Haile, S. M. *Solid State Ionics* **2000**, *229*, 136-137.
69. Haile, S. M. *Mater. Res. Soc. Symp. Proc*. **1999**, *547*, 315-326.
70. Lipkowski, J.; Baranowski, B.; Lunden, A. *Pol. J. Chem*. **1993**, *67*, 1867-1876.
71. Bruce, P. G. *Dalton Trans*. **2006**, 1365-1369.
72. Braga, D.; Maini, L.; Polito, M.; Grepioni, F. *Struct. Bonding* **2004**, *111*, 1-32.
73. Braga, D.; D'Oria, E.; Grepioni, F.; Mota, F.; Novoa, J. J.; Rovira, C. *Chem. Eur. J*. **2002**, *8*, 1173-1180.
74. Braga, D.; Gandolfi, M.; Lusi, M.; Polito, M.; Rubini, K.; Grepioni, F. *Cryst. Growth Des.* **2007**, *7*, 919-924.
75. Singh, U. P.; Kashyap, S.; Singh, H. J.; Butcher, R. J. *CrystEngComm*. **2011**, *13*, 4110-4120.
76. Sarma, R. J.; Baruah, J. B. *Solid State Sci*. **2008**, *10*, 580-586.
77. Bott, S. G.; Coleman, A. W.; Atwood, J. L. *J. Am. Chem. Soc*. **1988**, *110*, 610-611.
78. Blake, A. J.; Hubberstey, P.; Suksangpanya, U.; Wilson, C. L. *J. Chem. Soc., Dalton Trans.* **2000**, 3873-3880.
79. Day, V. W.; Hossain, M. A.; Kang, S. O.; Powell, D.; Lushington, G.; Bowman-James, K. *J. Am. Chem. Soc*. **2007**, *129*, 8692-8693.
80. Cleland, W. W.; Kreevoy, M. M. *Science* **1994**, *264*, 1887-1890.
81. Frey, P. A.; Whitt, S. A.; Tobin, J. B. *Science* **1994**, *264*, 1927-1930.
82. Ilioudis, C. A.; Georganopoulou, D. G.; Steed, J. W. *J. Mater. Chem*. **2002**, *4*, 26-36.
83. Hossain, M. A.; Isklan, M.; Pramanik, A.; Saeed, M. A.; Fronczek, F. R. *Cryst. Growth Des.* **2012**, *12*, 567-571.
84. Nelyubina, Y. V.; Lyssenko, K. A.; Golovanov, D. G.; Antipin, M. Y. *CrystEngComm* **2007**, *9*, 991-996.

85. Yu, Z. -Q.; Pan, M.; Jiang, J. -J.; Liu, Z. -M.; Su, C. -Y. *Cryst.Growth Des*. **2012**, *12*, 2389-2396.

86. Shizuka, H.; Nakamura, M.; Morlta, T. *J. Phys. Chem*. **1980**, *84*, 989-994.

87. Xu, Z.; Singh, N. J.; Lim, J.; Pan, J.; Kim, H. N.; Park, S.; Kim, K. S.; Yoon, J. *J. Am. Chem. Soc*. **2009**, *131*, 15528-15533.

CHAPTER 6

Self-assemblies of solvates and salts of a chiral zwitterionic host N-(2-imidazol-5-yl-1-carboxyethyl)-1, 8-naphthalimide

Self-assembled supramolecular systems usually show distinct properties compared to discrete molecules of the parent counterparts.[1-2] This opens diverse scope to explore various types of applications of such assemblies. [3-14] In particular, different supramolecular systems based on chiral organic molecules have found application in enantioselective catalysis[15-17] and molecular recognition[18-19] in biologically relevant systems. Among such molecules having self assembling properties, naphthalimides are of special interest due to their extensive use to construct scaffolds for host-guest chemistry.[20-26] As mentioned in the earlier chapter, the advantage of such systems lies on the dipolar nature of cyclic aromatic imides controlling their packing patterns in the solid state.[27-43] In addition, attaching a chiral unit to these systems provides avenues for new supramolecular synthons.[44-46] Achiral 1,8-naphthalimide derivatives show helical fiber-like morphologies on gelation in a wide range of polar solvents, which are tunable by adding a chiral substrate such as tartaric acid through the formation of intermolecular H-bonds.[47] Besides, naphthalimides containing chiral amino side chains are highly efficient artificial nucleases and antitumor agents,[48] serving as intercalators to DNA molecules.[49] On the other hand, solvent and various weak interactions (e.g., C-H$\cdots\pi$ and C-H$\cdots$O) are important in self-assembly processes which influence chirality[50] or molecular recognition.[51-52] However, there is no systematic study on the assemblies of chiral amino acid functionalized naphthalimides to understand the packing patterns in the solid state, although such materials may have a potential application as chiral supramolecular systems with new opto-electronic properties.

Based on such observations and keeping in mind that imidazole functionalities are present in two naturally occurring aromatic amino acids (tryptophan and histidine, respectively) with a recognized biological function, we have taken up studying of a chiral carboxylic acid bearing both 1,8-naphthalimide and imidazole groups, namely (–)-N-(2-imidazol-5-yl-1-carboxyethyl)-1,8-naphthalimide (H$\mathbf{L^4}$), and the structural aspects of its solvates and salts. Different solvents molecules used for interaction study are shown in Figure **6.1a**. Compound H$\mathbf{L^4}$ can exhibit both acidic and basic properties due to the presence of

carboxylic acid and imidazole group. There are different possibilities of hydrated and anhydrous HL^4 moieties to form supramolecular assemblies by interactions with different hydrogen bonding species such as solvent or anions (a few possible ways are shown in Figure **6.1b**).

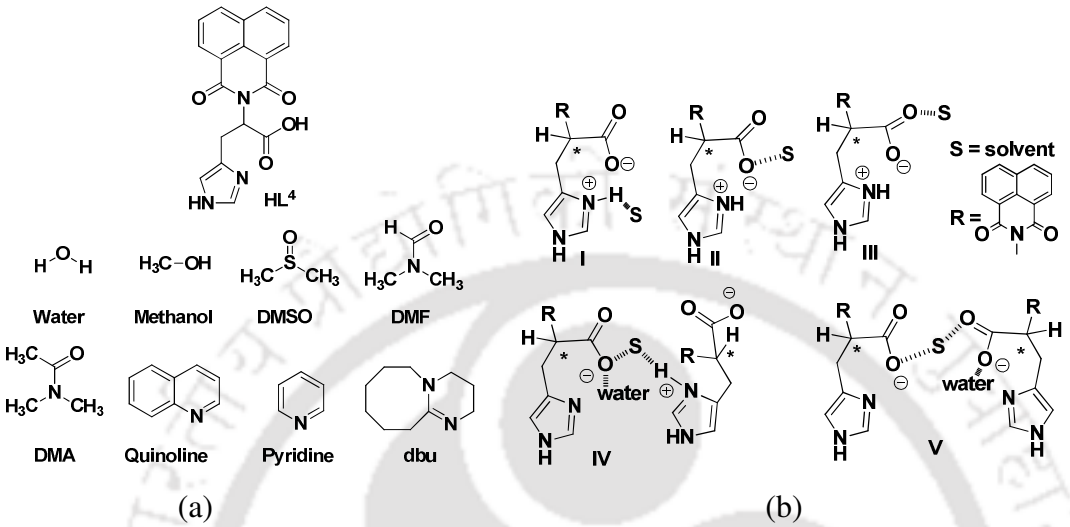

***Figure 6.1**: (a) N-(2-imidazol-5-yl-1-carboxyethyl)-1,8-naphthalimide (HL^4) and different substrates (solvents) used for interaction study and (b) A few of the possible ways for self-assembling of solvates or salts with HL^4.*

Furthermore, multiple functional groups in HL^4 can participate in diversified hydrogen bonds either within the neighboring host molecules or additionally involving guest solvent moieties and/or counter ions. It is of particular interest to study the resulting supramolecular networks from a topological viewpoint. In fact, the topological analysis has become a very important tool in crystal engineering research, enabling he classification, identification, and prediction of different topological motifs in various coordination and supramolecular compounds.[53-60] Despite the fact that a vast number of topologies have been either theoretically predicted or experimentally determined, the identification of new topological types is a sweeping research direction, as corroborated by a constantly growing number of research publications on this topic that also include the state-of-the-art reviews and perspective articles.[53-60] In particular, topological analysis and classification of hydrogen-bonded networks[59-60] are interesting owing to their high complexity, and thus represent a rather good potential not only to reveal the new topological types but also to identify some theoretically predicted topological motifs. Therefore the topological analysis of hydrogen-bonded networks can contribute to the

rationalisation and prediction of supramolecular motifs facilitating a possible design of the desired structures.[54]

In the preceding discussion, the anion recognition properties of a naphthalenediimide derivative (**L**^{3}) and the fluorescence intensity changes caused by anions are discussed.

6.1 Synthesis of N-(2-imidazol-5-yl-1-carboxyethyl)-1,8-naphthalimide (HL^{4}):

N-(2-imidazol-5-yl-1-carboxyethyl)-1,8-naphthalimide was synthesized by condensation of L-histidine and 1,8-naphthalic anhydride, following the procedure as discussed the experimental section. The compound was characterized with various spectroscopic techniques such as FT-IR, ^{1}H-NMR, ^{13}C-NMR and mass spectrometry. IR stretching frequencies for the carbonyl group appears at 1697 cm^{-1} and 1660 cm^{-1}; and for the hydroxyl group appears at 3482 cm^{-1} (Figure **6.2a**). In ^{1}H-NMR (DMSO-d$_6$) of H**L**^{4}**,** multiplet at 3.40-3.50 ppm appears for the -CH$_2$- protons adjacent to the chiral centre whereas the signals for the chiral proton appeared at 5.91 ppm as doublet of doublet. Signals for imidazole protons appear at 6.67 ppm and 7.30 ppm as singlet; whereas naphthalene protons show chemical shift at 8.50 ppm, 8.48 ppm and 7.88 ppm (Figure **6.2b**).

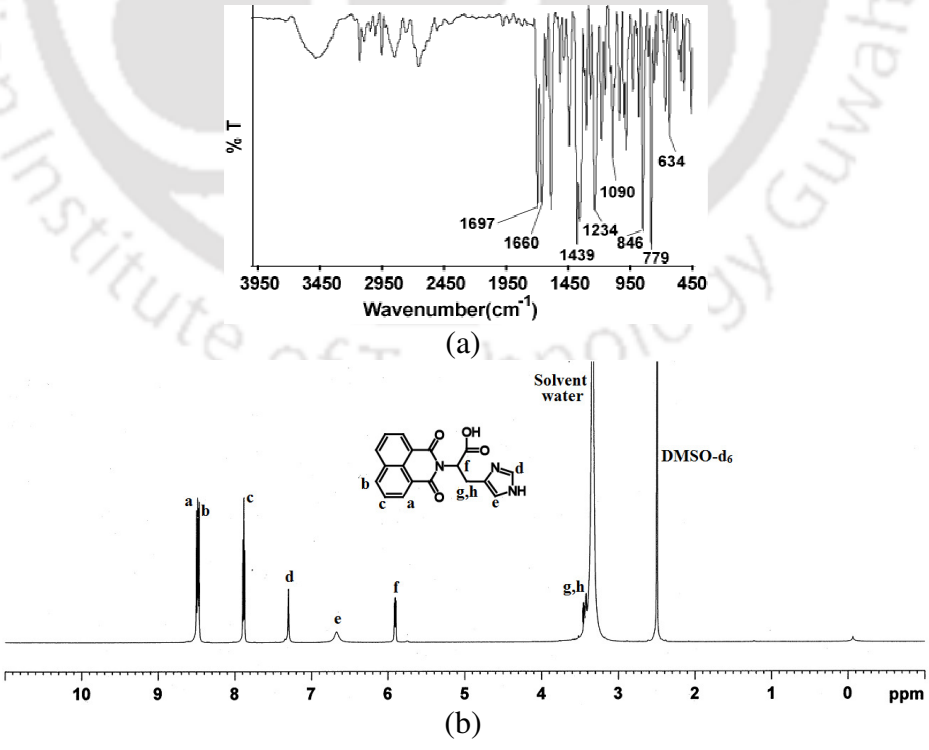

Figure 6.2: *(a) IR spectrum and (b) ^{1}H-NMR spectrum of* ***HL^{4}.***

In ^{13}C-NMR (DMSO-d_6) signals at 169.7 ppm and 162.9 ppm are due to the carboxylic carbon and carbonyl carbon respectively. Naphthalene carbons 'c', 'd' and 'h' appear at 134.8 ppm, 134.2 ppm and 127.5 ppm respectively; whereas tertiary carbons on naphthalene ring show signals at 128.3 ppm, 124.5 ppm and 123.2 ppm. Signals at 131.5, 130.8 and 121.1 ppm are due to imidazolyl carbons; whereas chiral carbon and aliphatic carbons show signal at 52.9 and 21.3 ppm respectively (Figure **6.19a** in the experimental section). The Mass spectrum H**L**^{4} shows a peak at 336.7502 (calcd. 336.3135) which corresponds to (M+1) peak (Figure **6.19b** in the experimental section).

6.2 Solvates and salts of N-(2-imidazol-5-yl-1-carboxyethyl)-1,8-naphthalimide:

Eight different solvates **6.1a**-**6.1h**, namely H**L**^{4}·H_2O (**6.1a**), H**L**^{4}·MeOH·3H_2O (**6.1b**) (MeOH = methanol), H**L**^{4}·DMSO (**6.1c**), H**L**^{4}·DMF (**6.1d**), H**L**^{4}·DMA (**6.1e**), H**L**^{4}·2quinoline (**6.1f**), H**L**^{4}·pyridine (**6.1g**) and **L**^{4}·Hdbu·2H_2O (**6.1h**) (dbu =1,8-Diazabicyclo[5.4.0]undec-7-ene), as well as four salts **6.1i**-**6.1l** formulated as [H**L**^{4}]Br·0.5MeOH (**6.1i**), [H**L**^{4}]I·0.5MeOH (**6.1j**), [H**L**^{4}]$_2SO_4$·DMF·H_2O (**6.1k**) and [H**L**^{4}]NO_3 (**6.1l**) were prepared by crystallization from respective solvent and acid as described in the experimental section. They are structurally characterized by single crystal X-ray diffraction and other conventional techniques. All the solvates and salts crystallized in chiral space group $P2_1$ (**6.1a**, **6.1b**, **6.1f**-**6.1j** and **6.1l**), $P4_32_12$ (**6.1c**-**6.1e**), $P1$ (**6.1h**) and $P2_12_12_1$ (**6.1g** and **6.1k**). In solvates 6.**1a**-**6.1g**, H**L**^{4} molecules exist as zwitterions, in **6.1g** **L**^{4} is anionic, whereas in four salts **6.1j**-**6.1l** it adopts a cationic [H_2**L**^{4}]$^{+}$ form. Solvates **6.1c**-**6.1e**, **6.1g** and **6.1b** crystallized in a 1:1 host-guest ratio, compound **6.1h** is a 1:1:2 dbu solvate dihydrate, whereas quinoline solvate **6.1f** shows a 1:2 host-guest ratio. Bromide and iodide salts **6.1i** and **6.1j** are isostructural and contain 0.5 molecule of methanol, the sulfate derivative **6.1k** has one DMF and one water molecule, whereas **6.1l** is an anhydrous nitrate salt. Powder X-ray diffraction (PXRD) patterns of **6.1a**-**6.1l** were recorded to ascertain their phase homogeneity. We found a good agreement of the experimental and simulated PXRD data which suggested uniformity of the bulk materials. Slight deviations in matching were observed in few cases possibly due to the loss of solvent molecules. As a representative case the powder XRD of the DMA solvate (**6.1e**) and nitrate salt (**6.1l**) are shown in Figure **6.21** in the experimental section**.** The agreement of all the peaks suggests the phase purity in bulk samples. The indexing is done as per the simulated diffraction pattern by using MERCURY program. The host molecule as well as

solvates and salts are chiral; their chirality was confirmed by measuring specific rotation and by recording circular dichroism spectra of selected compounds (experimental section Figure **6.20**). Desiraju and coworkers[61] have used IR spectroscopy as a tool to identify various synthons of cocrystals and polymorphs. Solvates and salts of H**L**^{4} reveal the characteristic stretching vibrations for each derivative. Significant stretching frequencies with the corresponding assignment are listed in Table **6.1**. It is clear that each solvate has the characteristic bands of their solvent components, whereas salts also show additional vibrations due to the presence of anions such as nitrate and sulfate.

***Table 6.1**: Characteristic stretching vibrations observed in the IR spectra of **6.1a-6.1l**.*

Compd. no.	Maximum of IR band in cm^{-1} with assignment in parenthesis
6.1a	3502 (ν_{OH}/ν_{NH}), 3022 (ν_{ArH}), 1701 ($\nu^{s}_{C=O}$), 1659 ($\nu^{as}_{C=O}$)
6.1b	3445 (ν_{OH}/ν_{NH}), 3021 (ν_{ArH}), 1700 ($\nu^{s}_{C=O}$), 1658 ($\nu^{as}_{C=O}$)
6.1c	3477 (ν_{OH}/ν_{NH}), 3006 (ν_{ArH}), 2937 (ν_{CH}), 1695 ($\nu^{s}_{C=O}$), 1656 ($\nu^{as}_{C=O}$), 1055 ($\nu_{S=O}$)
6.1d	3445 (ν_{OH}/ν_{NH}), 3019(ν_{ArH}), 2938(ν_{CH}), 2916 ($\nu_{CH(DMF)}$), 1698 ($\nu^{s}_{C=O}$), 1658 ($\nu^{as}_{C=O}$)
6.1e	3466 (ν_{OH}/ν_{NH}), 3012 (ν_{ArH}), 2937 (ν_{CH}), 1698 ($\nu^{s}_{C=O}$), 1658 ($\nu^{as}_{C=O}$)
6.1f	3489 (ν_{OH}/ν_{NH}), 3028 (ν_{ArH}), 2965 (ν_{CH}), 1695 ($\nu^{s}_{C=O}$), 1656 ($\nu^{as}_{C=O}$), 1498 ($\nu_{C=N}$)
6.1g	3446 (ν_{OH}/ν_{NH}), 3019 (ν_{ArH}), 1702 ($\nu^{s}_{C=O}$), 1659 ($\nu^{as}_{C=O}$), 1516 ($\nu_{C=N}$)
6.1h	3501 (ν_{OH}/ν_{NH}), 2940 (ν_{CH}), 1700 ($\nu^{s}_{C=O}$), 1656 ($\nu^{as}_{C=O}$), 1515 ($\nu_{C=N}$)
6.1i	3475 (ν_{OH}/ν_{NH}), 3000 (ν_{ArH}), 1706 ($\nu^{s}_{C=O}$), 1662 ($\nu^{as}_{C=O}$)
6.1j	3475 (ν_{OH}/ν_{NH}), 3013 (ν_{ArH}), 1704 ($\nu^{s}_{C=O}$), 1661 ($\nu^{as}_{C=O}$)
6.1k	3445(ν_{OH}/ν_{NH}), 3031 (ν_{ArH}), 1700 ($\nu^{s}_{C=O}$), 1657 ($\nu^{as}_{C=O}$), 1380 ($\nu_{S=O}$)
6.1l	3502(ν_{OH}/ν_{NH}), 3040 (ν_{ArH}), 1738 ($\nu^{s}_{C=O}$), 1697 ($\nu^{ss}_{C=O}$), 1385 (ν_{NO3})

There are four symmetry nonequivalent H**L**^{4} units in the unit cell of **6.1a** which interact intermolecularly through multiple N-H···O hydrogen bonds between the imidazole moieties and carboxylate groups (Figure **6.3a**). Moreover, there are four symmetry nonequivalent crystallization water molecules that further bridge two symmetry independent host moieties, resulting in the complex hydrogen-bonded 2D double layers.

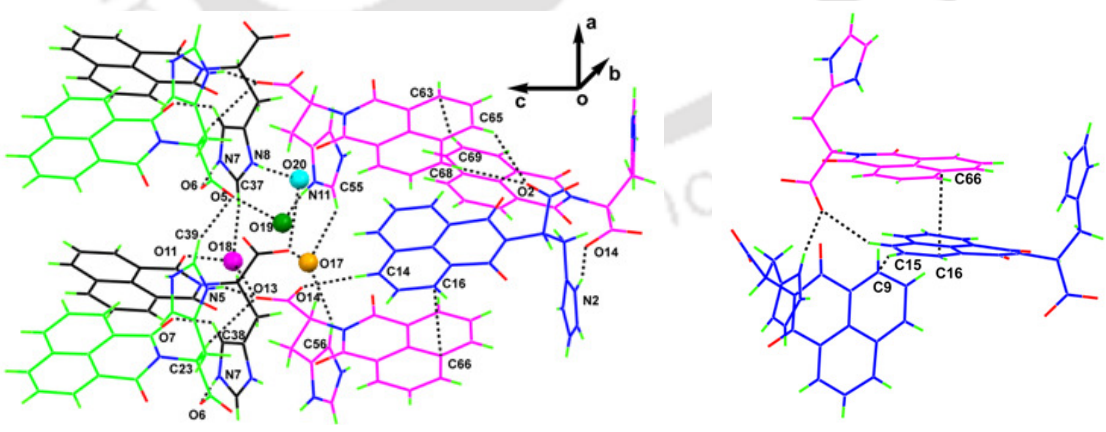

(a) (b)

***Figure 6.3:** Structural fragments of **6.1a**: (a) H-bonding interactions showing environments of four symmetry non-equivalent host molecules and (b) C-H···π contacts and π-stacking interactions in the lattice, helping the naphthalimide rings to adopt different orientations.*

Apart from this, there are other weak C-H···O,[62-65] C-H···π and π···π interactions[66-67] (Figure **6.2b**) that help to hold the guest H_2O molecules. A few selected hydrogen bond parameters are listed in Table **6.2**.

Table 6.2: *Selected hydrogen bond parameters of the hydrate* ***6.1a.***

Compd. no.	D-H···A [symmetry]	$d_{D\cdots H}$(Å)	$d_{H\cdots A}$(Å)	$d_{D\cdots A}$(Å)	∠D-H···A(°)
6.1a	N1-H1A···O1 [1+x,y,z]	0.8(3)	1.9(4)	2.67(4)	153.00
	N2-H2A···O14 [x,1+y,z]	0.9(3)	1.8(4)	2.64(4)	164.00
	N4-H4···O10 [x,-1+y,z]	0.8(6)	2.0(2)	2.74(5)	155.00
	N5-H5A···O13	0.9(2)	1.8(3)	2.66(4)	162.00
	N7-H7···O6	0.86(15)	1.79(19)	2.65(4)	177.00
	N8-H8···O20	0.85(18)	1.8(3)	2.66(6)	163.00
	N10-H10A···O2	0.9(2)	1.8(2)	2.65(5)	164.00
	N11-H11A···O19	0.8(3)	1.8(3)	2.64(7)	164.00
	C1-H1···O5 [1+x,1+y,z]	0.93	2.56	3.02(5)	111.00
	C4-H4A···O4	0.97	2.31	2.93(4)	120.00
	C4-H4B···O1	0.97	2.39	2.77(4)	103.00
	C5-H5···O3	0.98	2.26	2.76(4)	110.00
	C20-H20···O12 [x,-1+y,z]	0.90(3)	2.5(3)	3.24(5)	151(18)
	C22-H22A···O8	0.97	2.37	2.93(4)	116.00
	C23-H23···O7	0.98	2.23	2.73(4)	110.00
	C29-H29···O10 [2-x,-1/2+y,1-z]	0.93	2.55	3.26(5)	133.00
	C40-H40A···O9	0.97	2.50	2.86(5)	102.00
	C40-H40B···O12	0.97	2.25	2.88(5)	122.00
	C41-H41···O11	0.98	2.19	2.69(5)	110.00
	C50-H50···O6 [1-x,1/2+y,1-z]	0.93	2.47	3.20(5)	135.00
	C55-H55···O17 [-1+x,y,z]	0.94	2.37	3.12(6)	138.00
	C58-H58A···O16	0.97	2.41	2.99(5)	118.00
	C59-H59···O15	0.98	2.20	2.72(4)	111.00

Asymmetric unit of the solvate **6.1b** contains four symmetry independent H**L**^{4}, one MeOH and three H_2O molecules. Thus, its packing pattern differs due to the presence of a MeOH molecule in lieu of a water molecule in hydrate **6.1a**. Packing patterns in both the cases are guided by host molecules via donor and acceptor type interactions involving carboxylate and imidazole groups (Figure **6.3a**). Difference is caused by one C-H functionality of methanol that interacts with the -COO group of another symmetry nonequivalent molecule via C73-H···O5 bond. There is an intermolecular H-bond between the carboxyl group and imidazole moiety of similar set and also among different sets of host molecules. Strong N4-H···O5 hydrogen bonds within the similar set of host molecules and N5-H···O10, N7-H···O6, N11-H···O9, and N5-H···O6 hydrogen-bonds among different host molecules are observed. In addition, independent host molecules are interconnected via various weak C-H···O and C-H···π interactions which lead to the formation of cyclic $R_2^1(6)$ and $R_3^3(11)$ hydrogen bond motifs.[68] Both carboxyl groups of two H**L**^{4} and one imidazole moiety of another H**L**^{4} molecule are involved in hydrogen-bond formation with the methanol molecule either directly or through bridging water. One of the water molecules O7 of the solvate is involved in the formation of other cyclic hydrogen-bonded motifs in the structure of **6.1b**. Such cyclic units contain three H**L**^{4} moieties (three each have independent symmetry), one methanol and one water molecule (Figure **6.4b**).

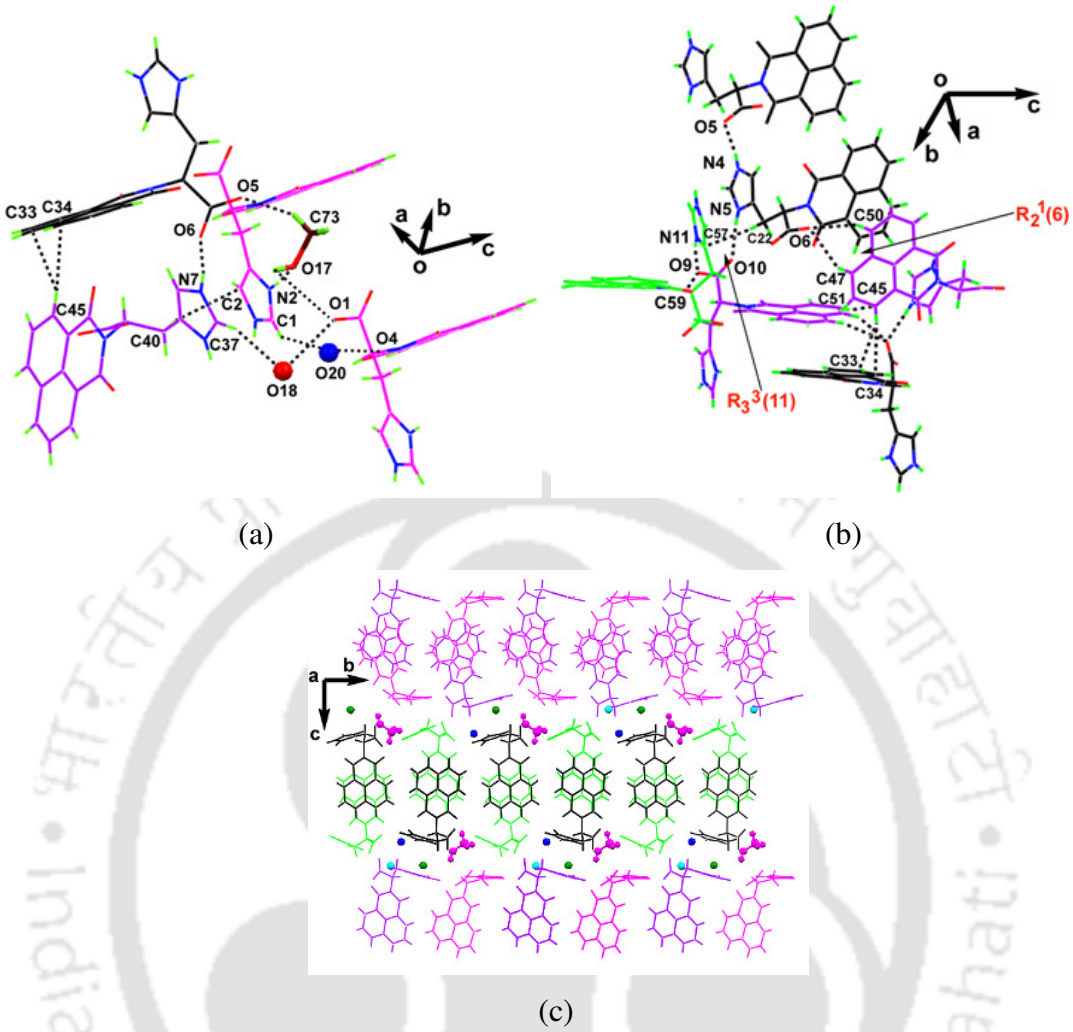

***Figure 6.4**: (a) Structural fragments of **6.1b** showing: (a) Weak interactions of MeOH and H_2O with the host molecules to make a tightly packed structure, (b) Intermolecular interactions among the host molecules to form different cyclic hydrogen-bonded motifs and (c) 3D supramolecular assembly in which the hydrophobic layers separated by hydrophilic channel containing solvent methanol and water molecules.*

A few selected hydrogen bond parameters are listed in Table **6.3**. The host molecules are further π-stacked forming a 3D supramolecular assembly in which the hydrophobic layers remain separated by hydrophilic channel containing solvent methanol and water molecules (Figure **6.4c**). Similar to **6.1a**, water molecules in **6.1b** also help in the formation of assemblies of four HL^4 units, and the replacement of one H_2O by MeOH molecule simplifies an overall H-bonded network, that is reflected in topological relationship[53-55] between the underlying H-bonded nets in **6.1a** and **6.1b**. Thus, it is clear that in the course of the formation of solvate **6.1b** there is a competition between the water and methanol molecules, which results in the formation of hydrated methanol solvate.

***Table 6.3**: Selected hydrogen bond parameters of the solvate **6.1b**.*

Compd. no.	D-H···A [symmetry]	$d_{D\cdots H}$(Å)	$d_{H\cdots A}$(Å)	$d_{D\cdots A}$(Å)	∠D-H···A(°)
6.1b	N1-H1A···O14 [x,-1+y,z]	0.86	1.82	2.640(9)	158.00
	N2-H2A···O17	0.86	1.87	2.727(11)	173.00
	N4-H4···O5 [-1+x,y,z]	0.86	1.76	2.609(8)	170.00
	N5-H5A···O10	0.86	1.81	2.662(9)	169.00
	N10-H6A···O2	0.86	2.01	2.764(9)	145.00
	N7-H7···O6 [x,1+y,z]	0.88(4)	1.71(5)	2.581(10)	169(7)
	N8-H8···O19	0.86	1.85	2.694(11)	168.00
	N11-H11A···O9	0.86	1.77	2.593(9)	160.00
	C4-H4A···O1	0.97	2.56	2.894(9)	100.00
	C4-H4B···O3	0.97	2.29	2.903(10)	120.00
	C5-H5···O4	0.98	2.18	2.680(11)	110.00
	C11-H11···O14 [1-x,-1/2+y,-z]	0.93	2.46	3.197(12)	136.00
	C19-H19···O13 [-1+x,y,z]	0.93	2.54	2.955(10)	108.00
	C22-H22A···O7	0.97	2.31	2.913(9)	120.00
	C22-H22B···O5	0.97	2.35	2.739(9)	103.00
	C23-H23···O8	0.98	2.25	2.745(9)	110.00
	C37-H37···O18	0.94(6)	2.46(6)	3.199(13)	135(7)
	C40-H40A···O9	0.97	2.48	2.807(10)	100.00
	C40-H40B···O12	0.97	2.43	3.006(10)	117.00
	C41-H41···O11	0.98	2.19	2.708(9)	111.00
	C58-H58B···O15	0.97	2.36	2.926(10)	117.00
	C59-H59···O16	0.98	2.22	2.722(10)	110.00
	C63-H63···O15	0.94(5)	2.34(4)	2.851(12)	114(4)
	C68-H68···O2 [-x,1/2+y,-z]	0.93	2.55	3.217(10)	128.00
	C70-H70···O16	0.92(4)	2.44(5)	2.815(10)	104(3)

In DMSO solvate **6.1c**, host molecules form dimeric units via two bridging DMSO moieties with the help of C-H···O (C-O distances ranging from 2.95 to 3.46 Å) and N-H···O (N-O distance of 2.72 Å) interactions (Figure **6.5a**). Oxygen atom of S=O group serves as a pivot for a bifurcated H-bond and interacts with the N2H and C1H atoms of H**L**[4]; which results in a $R_2^1(5)$ cyclic hydrogen bond motif. One carboxylate O atom acts as a tetrafurcated hydrogen bond acceptor and is connected to two C-H groups of a DMSO molecule via the C-H···O and N-H···O1 interactions (Figure **6.5b**). Hydrogen bonds driven by solvents such as DMF (Figure **6.6a**) and DMSO (Figure **6.6b**) with organic molecules were analyzed earlier and the association of these solvents with host molecules is favored by strong and weak hydrogen-bonds,based on which a high probability of solvent inclusion in the crystals was suggested.[69] As guest molecule, DMSO has a tendency to exist as a dimmer within itself or with acids and amides. In our case, we have observed the latter type of dimers. Thus, DMF or DMA molecules prefer to act as stabilizers of linear chains formed by ionic type of interactions between the hosts, but DMSO favors such interactions between two nearby molecules to yield dimeric assemblies. In these three isostructural solvates, no interactions between the guest molecules are observed. A few selected hydrogen bond parameters of solvate **6.1c** and **6.1d** are listed in Table **6.4**.

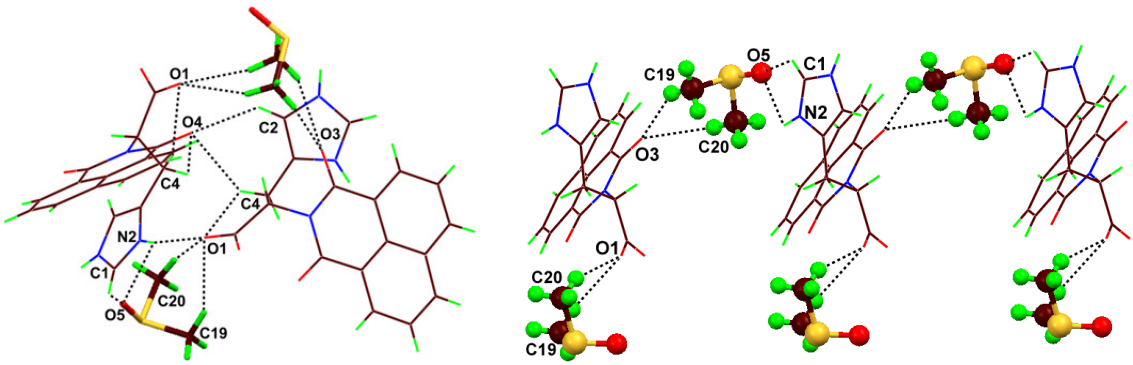

(a) (b)

***Figure 6.5**: (a) Dimeric assembly of solvate **6.1c** and interactions with DMSO molecules, and (b) bridging of HL^4 molecules by DMSO in **6.1c** involving carbonyl oxygen atoms in bifurcated hydrogen bond on one side and oxygen atom of S=O on another side.*

Single point contact of the solvent molecules forming $R_4^2(11)$ types of cyclic hydrogen-bond through C-H···O interactions are observed in the case of DMF solvate (Figure **6.6a**). Whereas in case of DMA solvate two point contact of the solvent molecules forming $R_2^1(7)$ types of cyclic H-bond through C-H···O interactions (Figure **6.6b**) are observed. In all the three solvates **6.1c**, **6.1d** and **6.1e** linear chain like hydrogen bonded assemblies are formed. A few selected hydrogen bond parameters of solvate **6.1e** are listed in Table **6.4**.

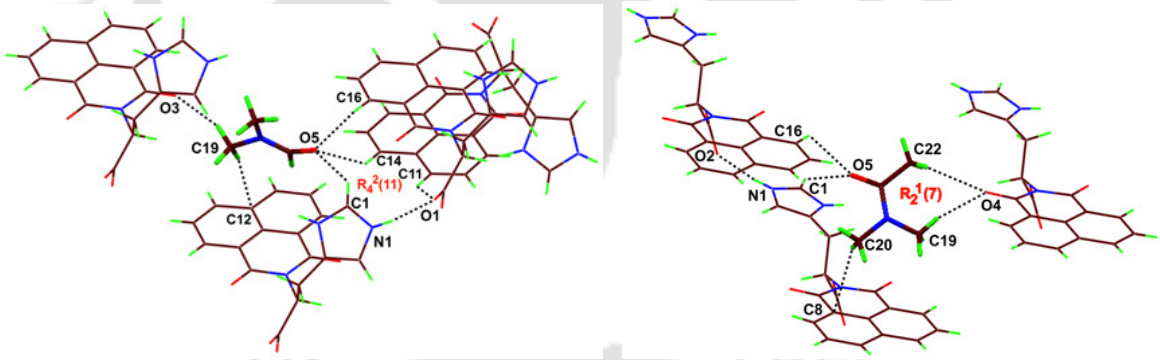

(a) (b)

***Figure 6.6**: (a) Assembling of host molecules by DMF in **6.1d** via trifurcated H-bonds and C-H···π interactions, (b) host molecules bridged by DMA through C-H···π and C-H···O interactions and bifurcated cyclic hydrogen-bonded $R_2^1(7)$ motifs in **6.1e**.*

An asymmetric unit of quinoline solvate **6.1f** contains one molecule of HL^4 host and two symmetry nonequivalent guest quinoline molecules. One of the quinoline molecules interacts weakly with the $-COO^-$ group of host via the C34-H···O2 bonds (Figure **6.7a**). Hydrogen atom of this quinoline ring also forms a bifurcated donor hydrogen-bond with the carbonyl oxygen of one HL^4 and an aromatic ring of another quinoline molecule via the C29-H···O3 and C-H···π ($d_{C29\cdots\pi}$ = 3.854 Å) interactions. Another symmetry

nonequivalent quinoline molecule associates with the HL^4 host via the C15-H···N4 interactions, while one of the C-H hydrogen atoms of this quinoline also interact with the

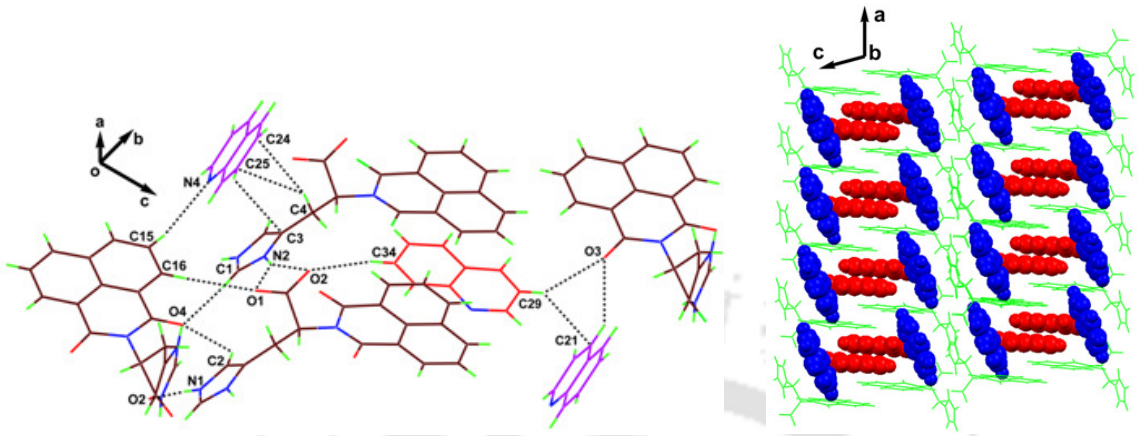

(a) (b)

***Figure 6.7**: (a) Self-assembling of the quinoline solvate **6.1f** showing the π-stacking of quinoline sandwiched between two naphthalimide moieties above and below quinoline ring and (b) 3D supramolecular channel-like structure along the b axis in solvate **6.1f**.*

***Table 6.4**: Selected hydrogen bond parameters of the solvate **6.1c**-**6.1e**.*

Compd. no.	D-H···A [symmetry]	$d_{D\cdots H}$(Å)	$d_{H\cdots A}$(Å)	$d_{D\cdots A}$(Å)	∠D-H···A(°)
6.1c	N1-H1A···O2 [x,1+y,z]	0.86	1.81	2.663(4)	170.00
	N2-H2A···O1 [-1/2+x,1/2-y,1/4-z]	0.86	1.93	2.721(4)	152.00
	C1-H1··· O5 [-1+x,y,z]	0.93	2.38	2.953(6)	119.00
	C2-H2··· O4 [1/2+x,1/2-y,1/4-z]	0.93	2.50	3.241(5)	137.00
	C4-H4A···O1	0.97	2.45	2.782(5)	100.00
	C5-H5···O3	0.98	2.26	2.732(5)	108.00
	C19-H19A···O1 [1/2+x,1/2-y,1/4-z]	0.96	2.59	3.462(8)	150.00
	C19-H19B···O3	0.96	2.52	3.363(8)	146.00
	C20-H20B···O3	0.96	2.59	3.437(7)	148.00
	C20-H20C···O1 [1/2+x,1/2-y,1/4-z]	0.96	2.48	3.367(7)	153.00
6.1d	N1-H1···O1 [x,1+y,z]	0.84(2)	1.87(2)	2.703(4)	170(4)
	N2-H2···O2 [-1/2+x,1/2-y,1/4-z]	0.84(3)	1.85(4)	2.677(4)	165(5)
	C1-H1A···O5 [-1+x,y,z]	0.95(4)	2.26(4)	2.943(7)	129(3)
	C2-H2A···O4 [1/2+x,1/2-y,1/4-z]	0.94(3)	2.40(4)	3.147(5)	136(3)
	C4-H4B···O2	0.97	2.45	2.807(5)	101.00
	C5-H5···O3	0.98	2.28	2.736(5)	108.00
	C19-H19B···O3	0.96	2.48	3.169(8)	129.00
	C20-H20A···O5	0.96	2.30	2.713(10)	105.00
6.1e	N1-H1A···O2	0.85(2)	1.928(18)	2.770(3)	171(3)
	N2-H2A···O1	0.84(2)	1.86(2)	2.665(3)	161(3)
	C1-H1···O5	0.93(2)	2.37(2)	3.091(4)	134(2)
	C2-H2···O3	0.94(2)	2.46(2)	3.252(3)	143(2)
	C4-H4B···O1	1.05(3)	2.41(3)	2.825(3)	102.1(19)
	C5-H5···O4	0.98(3)	2.33(3)	2.726(3)	103.2(19)
	C9-H9···O4	0.94(3)	2.38(3)	2.808(4)	107(2)
	C16-H16···O5	0.95(2)	2.51(3)	3.053(4)	116.5(18)
	C19-H19A···O4	0.96	2.30	3.237(5)	165.00

aromatic imidazole ring via C-H···π ($d_{C29\cdots\pi}$ = 3.789 Å) contact. In the crystal lattice of **6.1e**, the host molecules associate with each other through a set of two N2-H^+···$O1^-$ and N2-H^+···O2 strong hydrogen-bonds between the carboxylate and imidazole functional groups to produce the $R_1^2(4)$ H-bond motifs. Oxygen atom of C=O group is involved in a bifurcated H-bond with imidazole moiety of two different host molecules through C-H···O

***Table 6.5**: Selected hydrogen bonding parameters of the solvate **6.1f-6.1h**.*

Compd. no.	D-H···A [symmetry]	$d_{D\cdots H}$(Å)	$d_{H\cdots A}$(Å)	$d_{D\cdots A}$(Å)	∠D-H···A(°)
6.1f	N1-H1A···O2 [2-x,-1/2+y,1-z]	0.86(3)	1.89(3)	2.749(4)	176(4)
	N2-H2A···O1 [-1+x,y,z]	0.85(3)	2.18(3)	2.920(4)	145(3)
	N2-H2A···O2 [-1+x,y,z]	0.85(3)	2.32(4)	3.112(3)	156(3)
	C1-H1···O4 [1-x,-1/2+y,1-z]	0.93	2.27	3.195(4)	175.00
	C2-H2···O1	0.93	2.57	3.044(4)	112.00
	C2-H2···O4 [2-x,-1/2+y,1-z]	0.93	2.57	3.138(4)	120.00
	C4-H4B···O4	0.97	2.45	2.845(4)	104.00
	C5-H5···O3	0.98	2.23	2.725(3)	110.00
	C34-H34···O2 [2-x,-1/2+y,1-z]	0.93	2.49	3.315(7)	148.00
6.1g	N1-H1A··· O2 [1+x,y,z]	0.852(18)	1.809(19)	2.657(2)	173(3)
	N2-H2A···O1 [-x,1/2+y,1/2-z]	0.85(2)	1.81(2)	2.622(2)	162(2)
	C4-H4A···O1	1.06(3)	2.37(3)	2.781(3)	101.7(17)
	C4-H4A··· O3 [-x,-1/2+y,1/2-z]	1.06(3)	2.55(3)	3.547(3)	157(2)
	C4-H4B···O3	1.02(3)	2.46(3)	3.024(3)	114.3(15)
	C5-H5···O4	0.956(19)	2.235(19)	2.722(3)	110.5(14)
	C15-H15···O2 [1/2+x,3/2-y,-z]	0.95(2)	2.48(3)	3.290(3)	144(3)
	C22-H22···N2	0.93	2.58	3.485(11)	163
6.1h	N1-H1A···O1 [x,1+y,z]	0.86	2.51	3.111(4)	127.00
	N1-H1A···O2 [x,1+y,z]	0.86	2.11	2.947(4)	163.00
	N6-H6···O5 [1+x,-1+y,z]	0.86	2.31	3.137(4)	162.00
	N6-H6···O6 [1+x,-1+y,z]	0.86	2.30	3.009(4)	140.00
	N9-H7···O1	0.80(4)	2.02(4)	2.790(4)	163(5)
	C2-H2···O4	0.93	2.56	3.366(5)	145.00
	C4-H4A···O3	0.97	2.45	3.030(4)	118.00
	C5-H5···O4	0.98	2.22	2.725(4)	111.00
	C19-H19B···O2	0.97	2.31	3.248(4)	163.00
	C27-H27A···O3 [-1+x,y,z]	0.97	2.56	3.365(6)	141.00
	C31-H31A···O7	0.97	2.29	2.837(5)	115.00
	C32-H32···O8	0.98	2.24	2.657(4)	104.00
	C42-H42···O4	0.93	2.58	3.327(4)	138.00
	C46-H46A···O5 [1+x,-1+y,z]	0.97	2.32	3.283(5)	175.00

interactions. The N1-H···O2 bond holds carboxylate oxygen atom O2 with imidazole hydrogen. A few selected hydrogen bond parameters are listed in Table **6.5**. Besides these interactions, there are π-stacks ($d_{\pi\cdots\pi}$ = 3.575 Å) between the quinolines and host molecules to construct a 3D supramolecular channel-like structure along the *b* axis (Figure **6.7b**). Quinolines are well known for their assembling through π-stacking in host-guest complexes,[70-74] and in the solvate **6.1f** we observe the sandwiching of quinoline molecules between the naphthalimide rings of two independent hosts.

Asymmetric unit of the solvate **6.1g** contains one host H**L**^{4} and one pyridine molecule. Interactions between them are similar to those in solvate **6.1f**. Hence, pyridine associates with H**L**^{4} via weak C-H···O bonding interactions with both carboxylate and C=O groups of the host. Some selected hydrogen bond parameters are listed in Table **6.5**. However, some differences in the packing patterns of **6.1f** and **6.1g** arise because the pyridyl nitrogen does not form a hydrogen bond with host molecules. Strong π-stacking ($d_{\pi\cdots\pi}$ = 3.612 Å) between the pyridine and H**L**^{4} molecules enhances the stability of supramolecular assembly (Figure **6.8a**). In host-guest chemistry, pyridine molecules commonly show π- stacking, and several examples of pyridine dimers in host-guest compounds are known.[75-76]

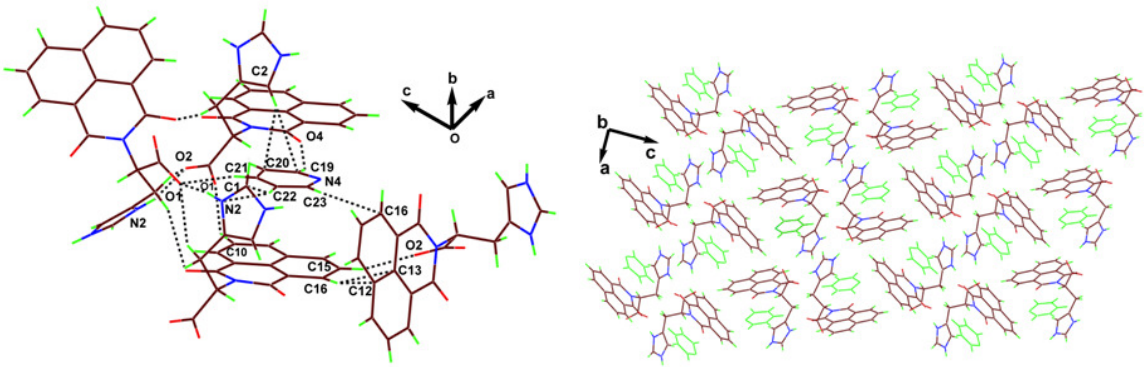

(a) (b)

***Figure 6.8**: Structural fragments showing: (a) weak interactions in pyridine solvate **6.1g** and self-assembling of host molecules to hold pyridine molecule through C-H···π interaction and (b) 3D supramolecular channel-like structure in **6.1g**.*

Host molecules in **6.1g** are packed through various hydrogen-bonds forming a triangular 3D supramolecular channel-like structure in which the pyridine guests are present in the lattice (Figure **6.8b**).

From the structures of **6.1c**-**6.1g**, it is clear that the aprotic solvents such as DMF, DMA, DMSO, quinoline, and pyridine do not require water, and the host molecules can be assembled via interactions of imidazolium and carboxylate moieties, resulting in packing patterns that can hold the solvent molecules. The similarity of DMF and DMA solvate is that they tend to favor a hydrogen-bonded chain-like arrangement between the host molecules. In contrast, DMSO has a high polarity index and is able to disrupt a chainlike structure formed through N-H···O interactions, leading to a DMSO bridged assembly between the parent molecules. Owing to the aromatic character of pyridine and quinoline, they can easily form stacking arrangements leading to inclusion derivatives.

Asymmetric unit of solvate $\mathbf{L^4}\cdot$Hdbu$\cdot 2H_2O$ (**6.1h**) contains two host, two protonated Hdbu, and four crystallization water molecules. In contrast to other solvates, dbu generates anionic $(\mathbf{L^4})^-$ host rather than a zwitterionic form. In solid state, one set of host molecules is assembled through strong hydrogen-bonds and weak C1-H···O4 interactions (Figure **6.9a**). Such a set of host molecules is connected to the other set by the C42-H···O4 interactions which exist between the carbonyl oxygen atoms and naphthalimide rings. A few selected hydrogen bond parameters are listed in Table **6.5**. Lattice water molecules

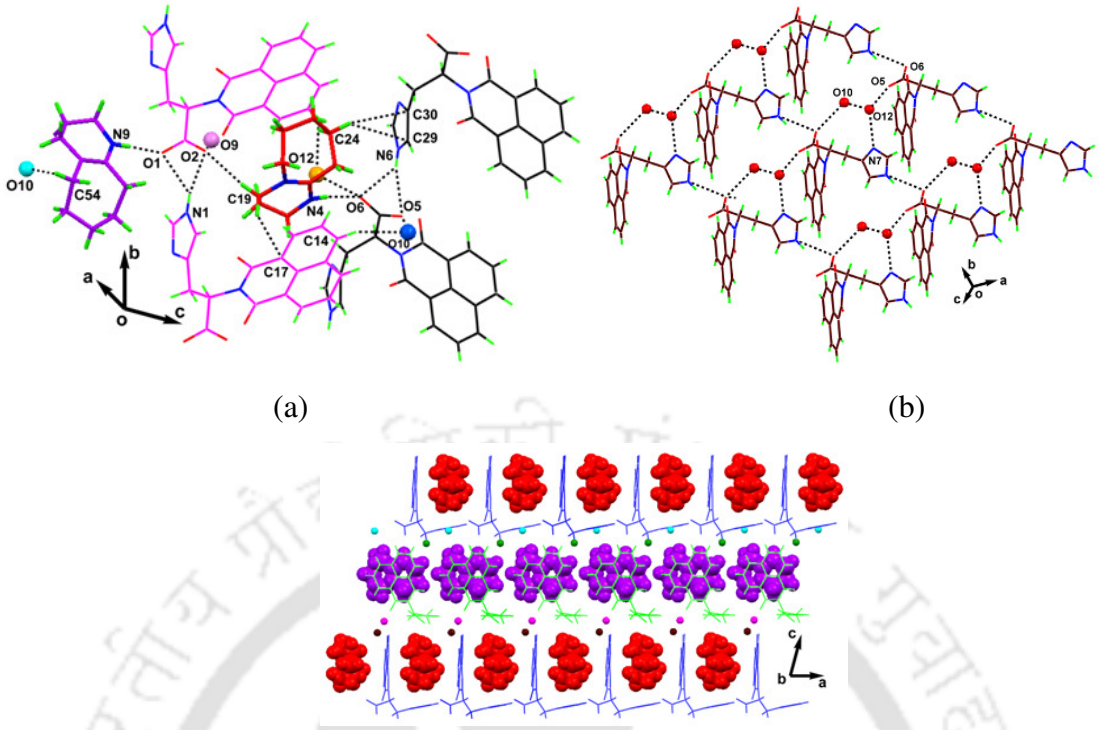

(a) (b)

(c)

***Figure 6.9**: Structural fragments of **6.1h** showing: (a) hydrogen-bonds between different host molecules of **6.1h** and weak interactions of dbu and water molecules, (b) 2D hydrogen-bonded assembly of the host and water molecules and (c) 3D supramolecular channel-like structure in which the Hdbu guests are incorporated.*

also act as connectors among the host molecules which form 2D hydrogen bonded assembly (Figure **6.9b**). In this case, a 3D supramolecular channel-like structure[77] is generated in which the Hdbu guests are incorporated (Figure **6.9c**).

Bromide and iodide salts **6.1i** and **6.1j** are isostructural. There are two types of anionic environments observed around halide ions. Br1 atom in **6.1i** is held by one N-H^{+}···Br^{-}, one O-H···Br^{-} and two C-H···Br^{-} interactions in a distorted tetrahedral geometry (Figure **6.10a**). The Br2 atom shows one N-H^{+}···Br^{-} interaction, one N-H···Br^{-} and two C-H···Br^{-} interactions (Figure **6.10b**). A few selected hydrogen bond parameters are listed in Table **6.6**. Bromide assisted assemblies adopt different hydrogen bond environments,[78-79] among which T-shape geometry is common. Interestingly, in our case we get dissimilar environments for bromide ions in the same salt.

On the other hand, in **6.1j** one iodide participates in two N-H and one C-H interactions, while the other iodide contacts to one O-H, one $^{+}$N-H and two C-H groups (Figure **6.11a** and **6.11b**).

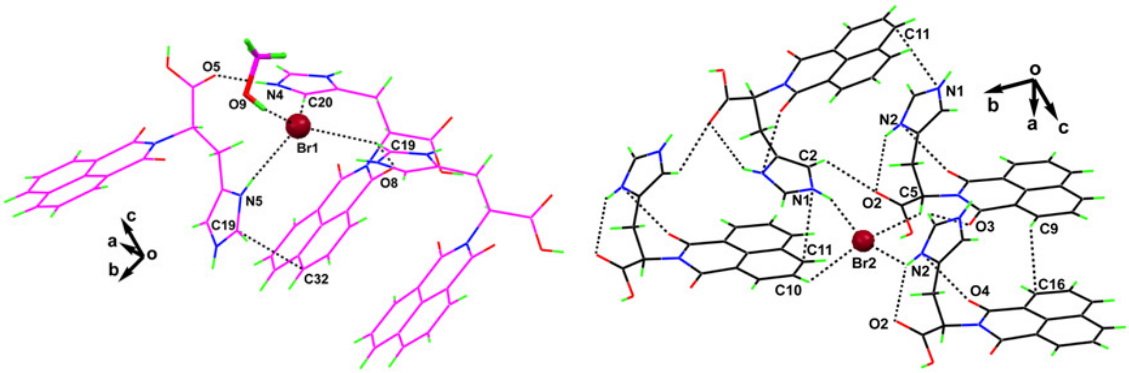

(a) (b)

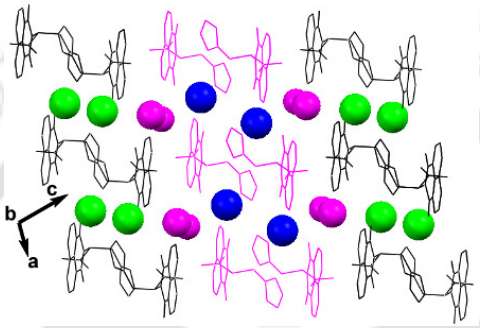

(c)

***Figure 6.10**: Structural fragments of **6.1i** showing hydrogen bond environments around (a) Br1 and (b) Br2 anions and their participation in self-assembling of supramolecular architecture. (c) 2D bromide-methanol supramolecular motifs which separate two hydrophobic 1D chains of $[H_2L^4]^+$.Green and blue color balls indicate bromide ions; purple color bals indicate methanol.*

In both the salts **6.1i** and **6.1j**, host cations form close packed structure by interacting with each other through strong O-H···O and N-H···O and weak C-H···O hydrogen bonds. A few selected hydrogen bond parameters are listed in Table **6.6**.

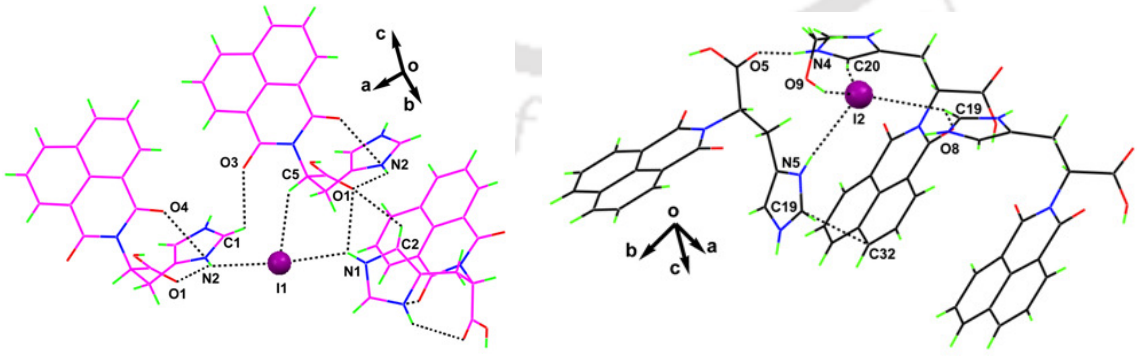

(a) (b)

Figure 6.11**: Coordination environments around (a) I1 and (b) I2 in the salt **6.1j.

There are π-stacking interactions present among the naphthalimide rings and also between the naphthalimide and imidazole.

Table 6.6: *Selected hydrogen bond parameters of the salts* ***6.1i-6.1j.***

Compd. no.	D-H···A [symmetry]	$d_{D\cdots H}$(Å)	$d_{H\cdots A}$(Å)	$d_{D\cdots A}$(Å)	∠D-H···A(°)
6.1i	N1-H1···Br2 [-x,1/2+y,-z]	0.86	2.70	3.455(10)	148
	O1-H1M··· O6 [x,1+y,z]	0.82	1.78	2.561(10)	159
	N2-H2A···O2	0.85(11)	2.24(12)	2.992(11)	149(9)
	N4-H4··· O5 [1-x,1/2+y,1-z]	0.84(6)	1.90(6)	2.717(11)	164(8)
	N5-H5A···Br1	0.86	2.53	3.320(9)	154
	O6-H6···O1 [x,-1+y,z]	0.82	2.12	2.561(10)	114
	O6-H6···O9 [-1+x,y,z]	0.82	2.55	3.10(3)	125
	C1-H1A···O3 [-1+x,y,z]	0.93	2.56	2.950(14)	106
	C2-H2···O2 [-x,-1/2+y,-z]	0.93	2.49	3.049(13)	119
	C5-H5···O3	0.98	2.21	2.689(13)	109
	C14-H14···O6	0.93	2.51	3.345(14)	150
	C19-H19···Br1 [2-x,1/2+y,1-z]	0.93	2.91	3.576(11)	130
	C20-H20···Br1 [1-x,1/2+y,1-z]	0.93	2.78	3.710(12)	177
	C22-H22A···O8	0.97	2.55	3.072(12)	114
	C23-H23···O7	0.98	2.25	2.741(12)	109
6.1j	N1-H1A···I2 [-1+x,y,z]	0.86	2.84	3.562(17)	143
	O2-H2M···N3	0.82	2.39	2.81(3)	112
	N4-H4···O5 [1-x,1/2+y,-z]	0.85	1.99	2.73(3)	144
	N5-H5A···I1	0.87	2.68	3.50(2)	157
	O6-H6···O9 [1+x,y,z]	0.82	2.29	3.08(9)	163
	C1-H1···O3 [-1+x,y,z]	0.93	2.59	3.07(3)	113
	C2-H2···O1 [-x,-1/2+y,1-z]	0.93	2.53	3.05(3)	116
	C5-H5···O3	0.98	2.25	2.73(3)	109
	C5-H5···I2 [1-x,1/2+y,1-z]	0.98	3.06	3.83(2)	137
	C19-H19···I1 [-x,1/2+y,-z]	0.93	3.01	3.66(4)	128
	C20-H20··· I1 [1-x,1/2+y,-z]	0.93	2.89	3.81(4)	169.
	C22-H22A···O8	0.97	2.58	3.07(4)	112
	C23-H23···O7	0.98	2.23	2.73(4)	111
	C37-H37B···I1	0.96	3.00	3.75(6)	135
	C37-H37C···O4	0.96	2.55	3.32(7)	137

Halides and solvent molecules form 2D halide-methanol supramolecular motifs which separate two hydrophobic 1D chains of $[H_2\mathbf{L^4}]^+$. One of the representative 2D supramolecular motifs in the case of salt **6.1i** is shown in Figure **6.10c**. In our earlier work,[80] we have found that anion-π interactions of halides in imidazole tethered naphthalenediimide derivative, however, no anion-π interactions are found in halide salts **6.1i** and **6.1j**.

In order to compensate the charge on divalent sulfate ion in **6.1k**, there are two protonated $[H_2\mathbf{L^4}]^+$ moieties present per anion, in addition to one H_2O and DMF molecule of crystallization. Sulfate ions form dimers of host molecules with cyclic $R_1^2(5)$ H-bond motifs (Figure **6.12a**). Sulfate O9 atom forms a trifurcated H-bond acceptor with one carboxylic group, one imidazole moiety of the same set of two $[H_2\mathbf{L^4}]^+$ cations and with one water molecule. Oxygen atom O10 also form trifurcated hydrogen bonds with $[H_2\mathbf{L^4}]^+$ cations, although the H-bonds formed are slightly weaker compared to those of other sulfate oxygen atoms. Similarly, O11 acts as a trifurcated H-bond acceptor to form hydrogen-bonds with two symmetry non-equivalent host molecules, whereas O12 acts as a birfurcated hydrogen-bond acceptor with strong O2-H···O12 and N1-H···O12 interactions (Figure **6.12b**). A few selected hydrogen bond parameters are listed in Table **6.7**. All these

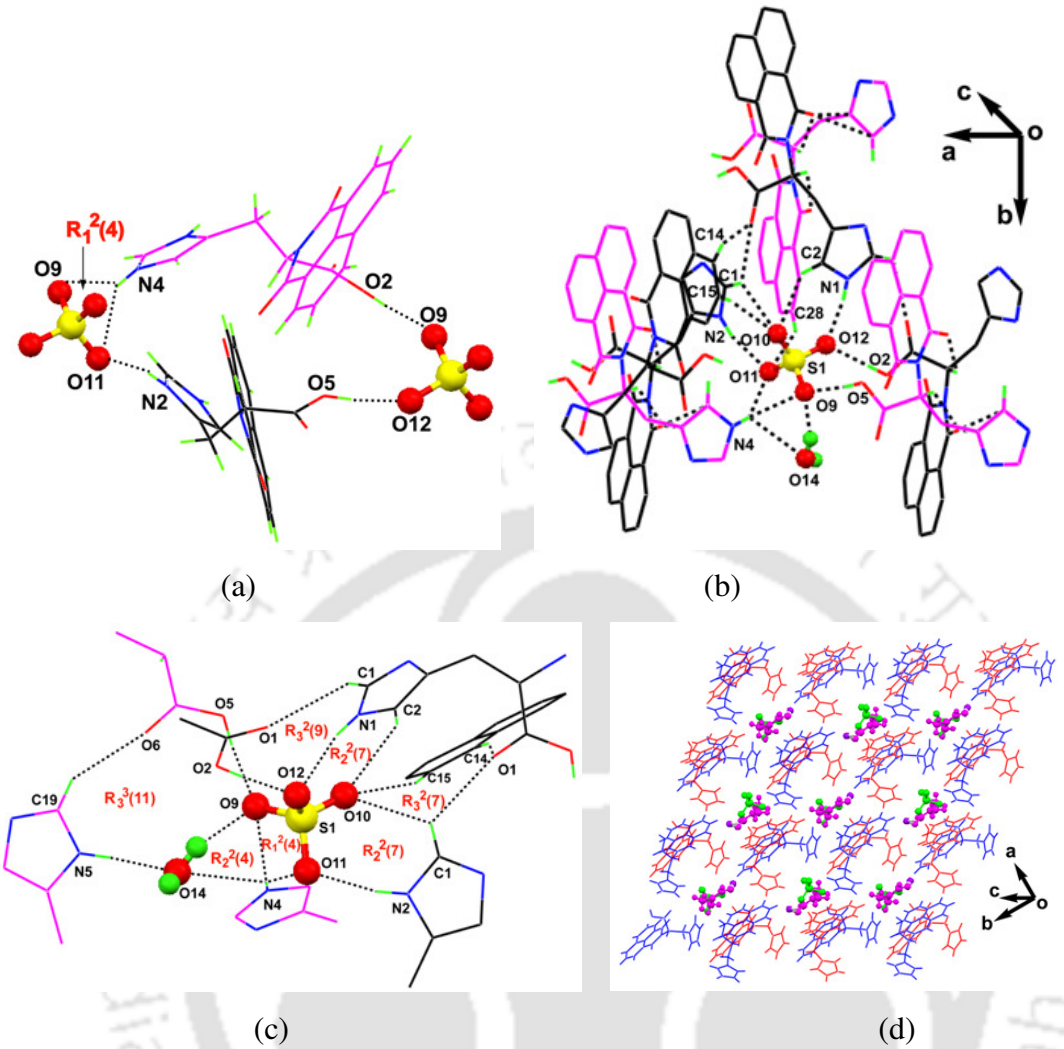

***Figure 6.12**: Structural fragments of **6.1k**: (a) dimers of $[H_2L^4]^+$ hosts driven by sulfate anions which show two different bridging modes, (b) hydrogen-bonding environment around sulfate anion held to water molecule, leading to self-assembling of host molecules (some C-H bonds are omitted for clarity of presentation), (c) different types of cyclic hydrogen bond motif in salt **6.1k** (only interacting parts of host molecules are shown) and (d) supramolecular channel-like architecture in the salt **6.1k**.*

interactions among the host cations, sulfate anions and water molecules generate various types of cyclic H-bonded motifs such as $R_1^2(4)$, $R_2^2(4)$, $R_2^2(7)$, $R_3^2(7)$, $R_3^2(9)$ and $R_3^3(11)$ (Figure **6.12c**). These motifs and π-stacking ($d_{\pi\cdots\pi}$ = 3.592 Å) between the naphthalimide rings of $[H_2\mathbf{L}^4]^+$ cations provide channel-like supramolecular structures to encapsulate the DMF molecules as shown in Figure **6.12d**.

Asymmetric unit of salt **6.1l** contains two non-equivalent $[H_2\mathbf{L}^4]^+$ moieties and two nitrate anions. There are two types of H-bond environment for NO_3^- ions. In one type, nitrate ions are hydrogen-bonded to $[H_2\mathbf{L}^4]^+$ through N-H···O bonds and -CH protons of imidazole, while the naphthalimide ring also interacts with the anion. Another set of nitrate anions

***Table 6.7**: Selected hydrogen bond parameters of the salt **6.1k**.*

Compd. no.	D-H···A [symmetry]	$d_{D\cdots H}$(Å)	$d_{H\cdots A}$(Å)	$d_{D\cdots A}$(Å)	∠D-H···A(°)
6.1k	N1-H1A ···O12 [1-x,-1/2+y,1/2-z]	0.84(3)	1.98(3)	2.804(4)	166(4)
	N2-H2A···O11 [3/2-x,-y,-1/2+z]	0.84(3)	1.96	2.803(3)	165
	O2-H2M···O12 [1/2-x,-y,-1/2+z]	0.86	1.77	2.591(3)	174
	N4-H4M···O9 [1-x,1/2+y,1/2-z]	0.84(4)	2.34(3)	2.988(4)	134 (3)
	N4-H4M···O11 [1-x,1/2+y,1/2-z]	0.84(5)	2.27(3)	3.024(4)	149(3)
	N5-H5A···O14	0.86(4)	1.88	2.735(4)	172
	O5-H5M···O9 [-x,1/2+y,1/2-z]	0.93	1.78(4)	2.618(3)	175(3)
	O14-H14A ···O9 [1/2-x,-y,-1/2+z]	0.93	1.96(5)	2.775(4)	160(6)
	O14-H14B···O13	0.93	1.86(3)	2.687(5)	160(7)
	C1-H1···O10 [3/2-x,-y,-1/2+z]	0.97	2.55	3.147(4)	122
	C1-H1···O1 [1/2+x,-1/2-y,-z]	0.98	2.50	3.087(4)	122
	C2-H2···O10 [1-x,-1/2+y,1/2-z]	0.93	2.53	3.180(4)	127
	C4-H4A···O4	0.93	2.47	2.926(4)	109
	C5-H5···O3	0.93	2.21	2.710(4)	110
	C14-H14···O1 [1-x,1/2+y,1/2-z]	0.97	2.45	3.295(5)	152
	C15-H15···O10	0.97	2.57	3.427(5)	154
	C19-H19···O6 [1/2+x,1/2-y,-z]	0.98	2.36	3.177(4)	147
	C22-H22A···O6	0.93	2.44	2.890(5)	108
	C22-H22B···O8	0.96	2.57	2.931(4)	102
	C23-H23···O7	0.98	2.24	2.744(4)	111
	C29-H29···O8 [-x,1/2+y,1/2-z]	0.93	2.47	3.312(5)	151
	C37-H37A ···O13	0.96	2.37	2.752(6)	103

has two interacting imidazole moieties and an aliphatic C-H group (Figure **6.13a**). Two symmetry non-equivalent $[H_2\mathbf{L}^4]^+$ moieties are above and below the nitrate plane, thus facilitating anion-π interactions of unequal strength with the NO_3^-···centroid (anion-π) contact distances of 3.205 and 3.687 Å. The O-H···nitrate hydrogen bonds have donor-

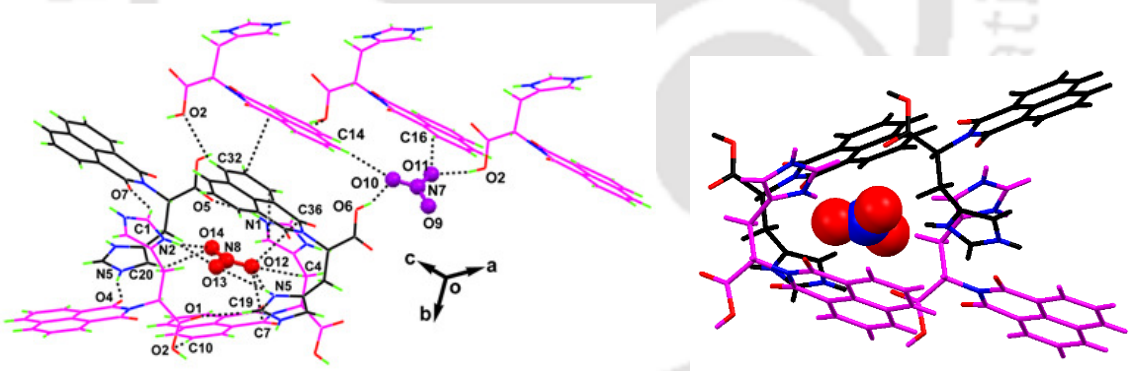

(a) (b)

***Figure 613**: Structural fragments of **6.1l**: (a) weak interactions in nitrate salt **6.1l** and (b) a channel-like structure formed by cationic host molecules encapsulating a nitrate ion.*

acceptor distances in the 2.584-2.619 Å range. The $N_{imidazole}$-H···nitrate separations are in the 2.833-3.314 Å interval and the C-H···nitrate H-bonds vary from 3.340 to 3.572 Å. A few selected hydrogen bond parameters are listed in Table **6.8**.

Anion-π interactions are considered based on the separation distance for such contacts.[81-85] Host cations are assembled to form a channel-like structure. One set of nitrate ions is located inside the channel formed by host molecules, while a different set of anions forms

***Table 6.8**: Selected hydrogen bonding parameters of the salt **6.1l**.*

Compd. no.	D-H···A [symmetry]	$d_{D\cdots H}$(Å)	$d_{H\cdots A}$(Å)	$d_{D\cdots A}$(Å)	∠D-H···A(°)
6.1l	N1-H1A···O5 [1-x,-1/2+y,1-z]	0.86(6)	1.92(6)	2.757(5)	162(6)
	O2-H2A···O11 [-1+x,y,1+z]	0.82	1.81	2.619(4)	170
	N2-H2M···O13 [-1+x,y,1+z]	0.84(3)	2.03(3)	2.834(4)	161(3)
	N2-H2M···O14 [-1+x,y,1+z]	0.84(3)	2.59(3)	3.315(5)	145(3)
	N4-H4M···O4 [-x,1/2+y,1-z]	0.85(3)	2.01(3)	2.808(5)	157(3)
	N5-H5A···O12 [1-x,1/2+y,1-z]	0.85(2)	2.04(3)	2.859(4)	161(6)
	N5-H5A···O13 [1-x,1/2+y,1-z]	0.85(2)	2.58(4)	3.215(4)	133(4)
	O6-H6···O10	0.82	1.82	2.584(5)	155
	C1-H1···O7 [-x,-1/2+y,1-z]	0.93	2.20	2.977(5)	141
	C4-H4A···O3	0.97	2.59	3.097(4)	113
	C4-H4B···O1	0.97	2.46	2.803(4)	100
	C5-H5···O4	0.98	2.22	2.706(4)	109
	C14-H14···O10	0.93	2.49	3.412(6)	174
	C16-H16···O11 [-1+x,y,z]	0.93	2.49	3.191(5)	132
	C19-H19···O1 [-x,1/2+y,2-z]	0.93	2.19	3.066(5)	156
	C20-H20···O14 [1-x,1/2+y,-z]	0.93	2.54	3.340(5)	145
	C23-H23···O7	0.98	2.27	2.714(5)	107
	C28-H28···O8 [-1+x,y,z]	0.93	2.57	3.363(5)	143

a chain-like structure between two adjacent channels (Figure **6.13b**). Nitrate anions in organic nitrate salts can generate dimeric assemblies,[86-87] which are not observed in the present study. On the other hand, parallel stacked nitrate ions with an aromatic ring show anion-π interactions;[88-89] or there may be anion-π interactions between the oxygen atoms of nitrate ions to have O···π type interactions with a π-cloud of a host.[90] Such interactions are generally put forward on the basis of distance of separation between the anion and a π-cloud and from similar point of view, we have observed stacking type interactions in **6.1l**. Nitrate anions are slightly oblique with respect to the plane of an interacting naphthalimide ring to facilitate effective encapsulation of nitrate within a channel like structure.

6.3 Topological analysis of H-bonded networks in 6.1a-6.1l:

As discussed above, the structures **6.1a-6.1l** exhibit multiple weak interactions and conventional (strong) hydrogen bonds between the neighbouring HL^4 (**6.1a-6.1h**) or $[H_2L^4]^+$ (**6.1i-6.1l**) units and also involve lattice solvent molecules and/or counter anions, thus giving rise to the generation of various supramolecular networks. To get further insight into the structure of these networks, we have carried out their topological analysis following the concept of the simplified underlying net.[53-60] Therefore, the host molecules were reduced to their centroids which, along with the centroids of lattice solvent molecules and/or counteranions, resulted in the underlying H-bonded nets. These nets were assembled by taking into consideration only the conventional (strong)[53] hydrogen bonds D–H···A [H···A <2.50 Å, D···A <3.50 Å, ∠(D–H···A) >120°; D and A stand for donor and acceptor atoms respectively]; in some cases hydrogen bonds (short contacts) were considered without H atoms on crystallization solvent molecules. The underlying

networks in **6.1a**-**6.1l** were topologically classified[53-55] and the obtained results are summarized in Table **6.9** and Figure **6.14**. It may be noted that some interactions in **6.1i** and **6.1j** around halide atoms do not fall within the above parameters for strong H-bonds and thus were not considered in the topological analysis. An underlying H-bonded network of **6.1a** can be topologically classified as a very complex hexanodal 3,3,4,4,5,5-connected 2D double layer (Figure **6.14a**) with unique topology[11] defined by the point symbol of $(3.5.6)(3.5^2.6^2.8)(3.5^6.6.7.8)(5^2.7)(5^3.6^3)(5^8.6.8)$.

***Table 6.9**. Topological classification of underlying H-bonded nets in **6.1a**-**6.1l**.*

Compd. no.	Underlying H-bonded net	Topology, point symbol, nodes/linkers
6.1a	hexanodal 3,3,4,4,5,5-connected 2D double layer[a]	**new** topology, $(3.5.6)(3.5^2.6^2.8)(3.5^6.6.7.8)(5^2.7)$-$(5^3.6^3)(5^8.6.8)$, 3-c H_2O, 4- and 5-c HL^4 nodes
6.1b	binodal 3,4-connected 2D double layer[a]	**3,4L127** topology, $(6^3)(6^5.8)$, 3-c and 4-c HL^4 nodes, 2-c H_2O and MeOH linkers
6.1c-6.1h	uninodal 4-connected 2D zigzag layer	**skl** topology, $(4^4.6^2)$, 4-c HL^4 nodes[b]
6.1i-6.1j	uninodal 2-connected 1D zigzag chain	**2C1** topology, no circuits, 2-c $[H_2L^4]^+$ nodes
6.1k	binodal 3,6-connected 2D double layer	**kgd** topology, $(4^3)_2(4^6.6^6.8^3)$, 3-c $[H_2L^4]^+$ and 6-c SO_4^{2-} nodes, 2-c H_2O linkers
6.1l	uninodal 4-connected 3D framework	**lon** topology, (6^6), 4-c $[H_2L^4]^+$ nodes, 2-c NO_3^- linkers

[a]Hydrogen bonds (short contacts) were considered without H on crystallization H_2O molecules; 2-c, 3-c, 4-c, 5-c, or 6-c stand for 2-, 3-, 4-, 5-, and 6-connected nodes or linkers. [b] In **6.1h**, there are also 2-c H_2O linkers.

In a related solvate **6.1b** containing one MeOH and three H_2O molecules, an underlying network features a much simpler binodal 3,4-connected double layer with the **3,4L127** topology and the point symbol of $(6^3)(6^5.8)$, as shown in Figure **6.14b**. Interestingly, further simplification of the underlying nets in **6.1a** and **6.1b** by omitting all the crystallization solvent molecules leads, in both cases, to an unreported 3,3,4-connected trinodal 2D network with the point symbol of $(5.6^4.8)(5^2.6)(5^2.8)$.[53-55]

From the topological point of view, solvates **6.1c**-**6.1g** with DMSO, DMF, DMA, quinoline and pyridine guest molecules are similar. Their underlying H-bonded nets are driven by conventional H-bonds between the adjacent HL^4 moieties. These nets can be described as uninodal 4-connected 2D zigzag layers (for **6.1c**, Figure **6.14c**) with the **skl** topology and the point symbol of $(4^4.6^2)$. The same topological type is also observed in the H-bonded network of **6.1h** which, however, reveals the presence of additional H_2O linkers.

The underlying nets of the bromide (**6.1i**) and iodide (**6.1j**) salts of $[H_2L^4]^+$ are uninodal 2-connected 1D zigzag chains with a simple **2C1** topology (for **6.1i**, Figure **6.14d**).

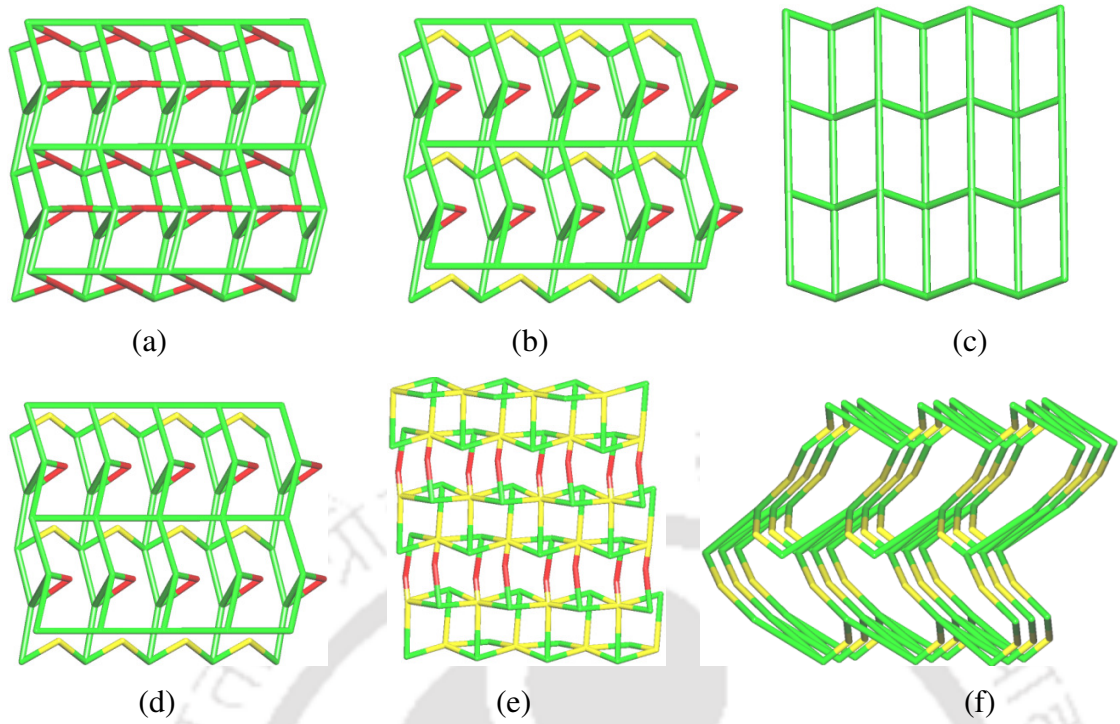

***Figure 6.14**: Topological representations of the simplified underlying H-bonded nets in (a) **6.1a**, (b) **6.1b**, (c) **6.1c**, (d) **6.1i**, (e) **6.1k** and (f) **6.1l**. Further details: (a) topologically unique hexanodal 3,3,4,4,5,5-connected 2D double layer, (b) binodal 3,4-connected 2D double layer with the **3,4L127** topology, (c) uninodal 4-connected 2D zigzag layer with the **skl** topology, (d) uninodal 2-connected 1D zigzag chains with the **2C1** topology, (e) binodal 3,6-connected 2D layer with the **kgd** topology and (f) uninodal 4-connected 3D net with the **lon** topology; (a, b, c, e) view along the c axis; (d, f) view along the a axis; Color codes: green-centroids of HL^4 (a-c) or $[H_2L^4]^+$ (e-f) nodes, red-centroids of H_2O (a, b, e) nodes/linkers, yellow-centroids of MeOH linkers (b) or SO_4^{2-} nodes (e) or NO_3^- linkers (f).*

However, the dimensionality of an H-bonded network increases to 2D in the sulfate salt **6.1k**, which features a binodal 3,6-connected layer (Figure **6.14e**) with the **kgd** topology defined by the point symbol of $(4^3)_2(4^6.6^6.8^3)$. Interestingly, the H-bonded network of the nitrate salt **6.1l** can be classified as a uninodal 4-connected 3D net (Figure **6.14f**) with the **lon** topology and the point symbol (6^6).[53-55]

Hence, three distinct topological types of H-bonded networks were identified in different solvates of HL^4 (**6.1a**-**6.1h**), although all of them show 2D underlying nets. In contrast, various $[H_2L^4]^+$ salts (**6.1i**-**6.1l**) reveal different H-bonded nets that are quite distinct not only in the topology but also in the dimensionality that increases from 1D in halide salts **6.1i** and **6.1j** to 2D in sulfate derivative **6.1k** and 3D in nitrate compound **6.1l**.

6.4 Thermogravimetric analyses of solvates and salts:

In this study we have observed a self-assembly of zwitterionic host molecules with trapping of solvent molecules. Further, we have also obtained solvated salts of the host. To compare the solvent loss temperature in these solvates with a different imidazole containing host[91] where self-assemblies are not occurring through zwitterionic interactions, we have carried out thermogravimetric analyses (TGA) on all solvates and salts, also aiming to probe their thermal stabilities. Thermogram of some of the solvates and salts are shown in Figure **6.15** and some of them are shown in experimental section Figure **6.19** and Figure **6.22**. Temperature intervals during which the solvent molecules are released from compounds **6.1a**-**6.1l** are listed in Table **6.10**. In this table, we have also given the comparative temperature ranges of the solvent removal from different solvates of bis(4-hydroxy-3,5-dimethylphenyl)-(4-N,N-dimethylaminophenyl)-methane (**L**) host.[91] It appears that the temperatures at which the solvents are lost from solvates **6.1c** (Figure **6.15a**) and **6.1e** are higher than those of the corresponding solvates of **L**. In the case of **L**, host-guest assemblies are through hydrogen bonds[91] without any electrostatic interactions,

***Table 6.10**: Results of thermogravimetric analyses summarizing the removal of solvent molecules from the solvates and salts (**6.1a**-**6.1l**) and related solvates of **L**.*

Compd. no.	Temperature-range (°C)	Weight loss, % Exp. (calcd.)	Lost solvent molecule(s)	Temperature range (°C) for solvent loss in solvates of **L**[a]
$HL^4 \cdot H_2O$ (**6.1a**)	65-116	5.7 (5.1)	$-H_2O$	
$4HL^4 \cdot MeOH \cdot 3H_2O$ (**6.1b**)	50-132	6.9 (6.0)	–MeOH, $-3H_2O$	
$HL^4 \cdot DMSO$ (**6.1c**)	185-235	20.1 (19.1)	–DMSO	110-195
$HL^4 \cdot DMF$ (**6.1d**)	152-230	17.9 (17.9)	–DMF	
$HL^4 \cdot DMA$ (**6.1e**)	150-235	21.4 (20.6)	–DMA	100-180
$HL^4 \cdot 2$quinoline (**6.1f**)	121-161	20.1 (21.7)	–quinoline (1st)	
	162-258	26.2 (27.8)	–quinoline (2nd)	
$HL^4 \cdot$pyridine (**6.1g**)	90-152	20.1 (19.0)	–pyridine	
$L^4 \cdot Hdbu \cdot 2H_2O$ (**6.1h**)	65-125	35.2 (36.1)	–dbu, $-2H_2O$	75-120
$[H_2L^4]Br \cdot 0.5MeOH$ (**6.1i**)	75-105	4.1 (3.7)	–0.5MeOH	
$[H_2L^4]I \cdot 0.5MeOH$ (**6.1j**)	75-105	3.7 (3.3)	–0.5MeOH	
$[H_2L^4]_2SO_4 \cdot DMF \cdot H_2O$ (**6.1k**)	80-195	9.1 (10.5)	–DMF, $-H_2O$	

[a]Given for comparison from ref. 91.

whereas HL^4 adapts a packing pattern through strong ionic interactions, thus providing a higher thermal stability to the tightly packed structure. In the case of dbu solvate, the temperatures loss for dbu are comparable, since the structures in the both cases are guided by bulk of dbu that leads to relatively weak packing patterns.

Solvate **6.1f** liberates two equivalents of quinoline molecules in two steps between 121°C and 258 °C. In the first step (121-161 °C), 20.4 % weight loss occurs corresponding to the loss of one quinoline molecule (calcd. 21.8 %). Further, a 26.2% weight loss (162-258 °C) is associated with the release of the second quinoline molecule (Figure **6.15c**). These results point out that there are two independent environments for quinoline in the crystal

lattice. Solvate **6.1g** releases pyridine in the 90-152 °C range (20.1 % weight loss, calcd. 19.1 %). In solvate **6.1h**, dbu along with two water molecules are lost at 65-125 °C (35.2 % weight loss, calcd. 36.1 %). In spite of being in protonated form, dbu is released at relatively low temperature, probably due the easy removal of a bulky amine to adapt a zwitterionic structure by parent host molecules.

In the case of isostructural salts **6.1i** and **6.1j**, methanol molecule is lost in the 75-105 interval °C (weight loss 4.1% and 3.7%; calcd. 3.7% and 3.3% for **6.1i** and **6.1j**, respectively).

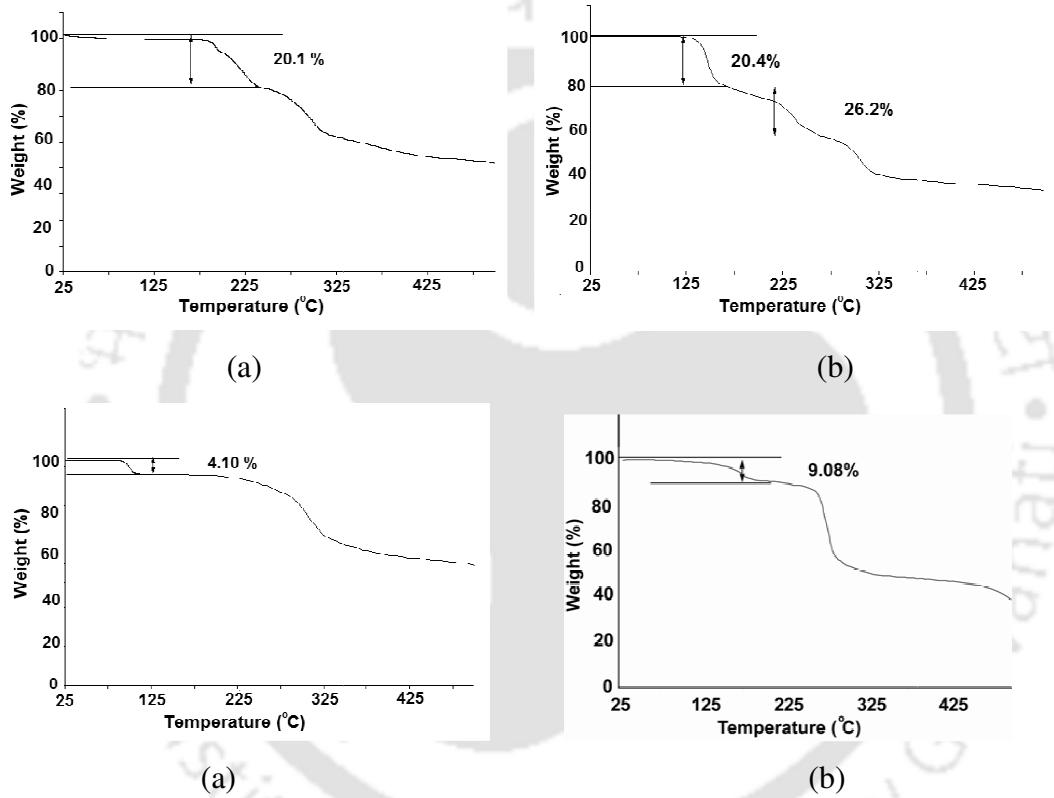

Figure 6.15**: Thermogram (heating rate 7 °C/min.) of (a) solvate **6.1c, (c)** solvate **6.1f**, (c) salt **6.1i** and (d) salt **6.1k.

There is a gradual decrease in weight loss (theoretical 10.5% and observed 9.1%) occurring at 75-195 °C in **6.1k**, which is due to the simultaneous removal of water and DMF molecules. The salt **6.1l** shows no weight loss below 200 °C indicating the absence of any solvent molecule in its lattice. In most of the solvates and salts, organic moieties start to decompose above 225 °C except solvate **6.1d** that decomposes at 258 °C. It is interesting to compare the DMF loss from the solvate **6.1d** and salt **6.1k**. It occurs at the 152-230 °C intervals in **6.1d**, shifting to 75-195 °C in **6.1k**. Thermogram of the salts **6.1i**

and salt **6.1k** are shown in Figure **6.15c** and Figure **6.15d** respectively. Packing patterns of both compounds are guided by electrostatic interactions.

6.5 UV-visible and fluorescence emission studies of solvate and salts:

UV-visible spectra of H**L**^{4}, solvates **6.1a**-**6.1h** and salts **6.1i**-**6.1l** were recorded in the solid state (Figures **6.17a** and **6.17b**). The spectrum of free host has two absorption bands at 320 and 364 nm, which are attributed to the π → π* and n → π* transitions. All other solvates except **6.1h** show similar absorption bands that are slightly red shifted in

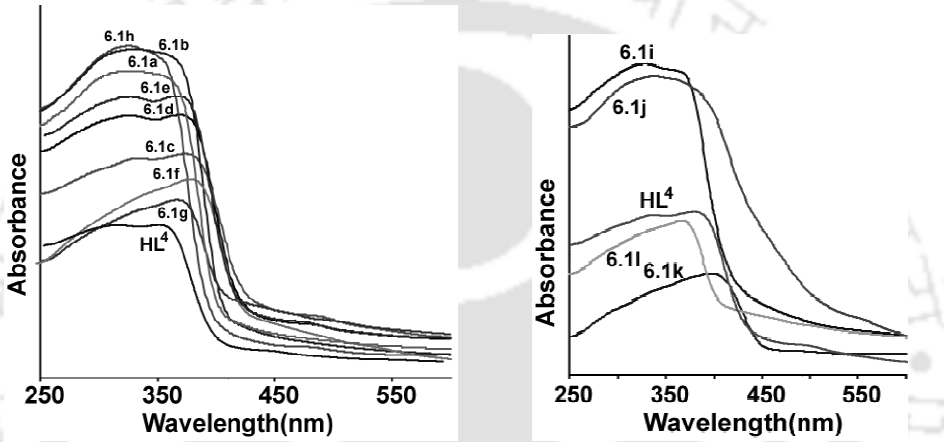

(a) (b)

***Figure 6.16**: Solid state UV-visible spectra of (a) solvate **6.1a**-**6.1h** and (b) salt **6.1i**-**6.1l**.*

comparison to those of free H**L**^{4}. This clearly indicates the distinction of the dbu derivative **6.1h** in which the host molecule exist as anionic form as illustrated in the structural discussion.

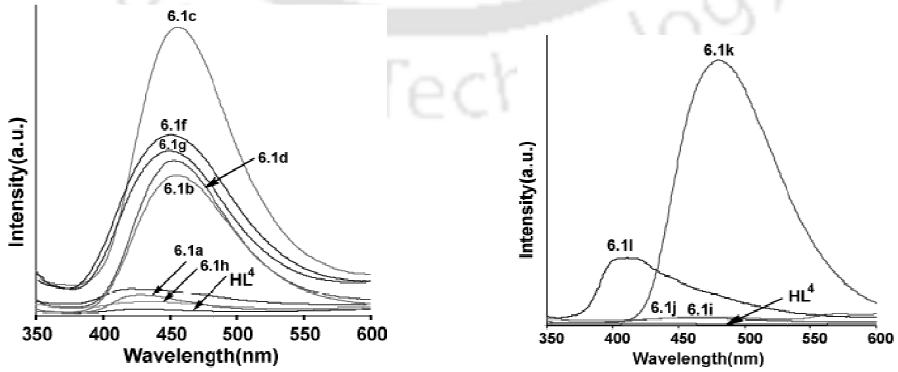

(a) (b)

***Figure 6.17**: Solid state fluorescence emission spectra of (a) solvate **6.1a**-**6.1h** and (b) salt **6.1i**-**6.1l**.*

Fluorescence emission of analogous naphthalimide compounds have been reported due to their excellent photoemissive properties and usage as fluorescent brighteners,[92-93] as well as emission in the blue spectral region.[94-96] Fluorescence emission is commonly guided by photo-electron transfer (PET) mechanism in N-functionalized naphthalimides.[97-99] Solid state fluorescence emission spectra were recorded at λ_{ex} 330 nm which are shown in Figures **6.18a** and **6.18b**. The host H**L**^{4} exhibits emission at 427 nm, while all other solvates and salts show strong emission bands in the 428-487 nm regions with an enhancement of fluorescence intensity than that of the host molecule. This is due to the interaction of lone pair of electrons on nitrogen atom contributing to PET mechanism in the starting compound, which gets involved in hydrogen bonding in solvates and protonated salts.

6.6 Conclusions:

Different packing in supramolecular assemblies of chiral zwitterionic host N-(2-imidazol-5-yl-1-carboxyethyl)-1,8-naphthalimide is established. These results contributed to understand the zwitterionic organic molecule holding a number of solvent guest molecules with distinct supramolecular arrangements. Majority of solvates comprise of tetrameric assemblies of host molecules which are readjusted in geometries to accommodate the solvent molecules. The arrangements of organic hosts in hydrate as well as water/methanol solvates have similar characteristics. The former can be constructed by assembling of four neighboring hosts knitted by water molecules, whereas methanol solvate has three organic host molecules knitted by water connected to another host molecule by methanol and water molecules. On the other hand, the cyclic assemblies present in solvates are broken in the structures of salts. Halide ions help in the generation of 1D zig-zag chains of host cations. Sulfate anions break the assemblies of host cations to give discrete units, whereas nitrate anions stabilize dimeric units of hosts acting as connectors between them.

Topological analysis shows six distinct topological networks in these solvates and salts. These include 1D zigzag chains with the **2C1** topology in **6.1i** and **6.1j**, 2D layers with the **3,4L127** (in **6.1b**), **skl** (in **6.1c**-**6.1h**) and **kgd** (in **6.1k**) topologies, the 3D network with the **lon** topology in **6.1l**, as well as a topologically unique 3,3,4,4,5,5-connected 2D double layer in **6.1a**.

Fluorescence emission studies of these solvates show strong emission bands with distinct maxima in the range of 428-487 nm. In particular, a high fluorescence emission ability of

sulfate salt and DMSO solvate are explained by the structural setting of the host molecules and by reducing the PET effect of lone pair of electrons.

6.7 Experimental section:

The detailed synthetic methodologies for synthesis of solvates and salts are described. Analytical data are listed along with each compound. The instrumental details and the crystallographic parameters are provided in Appendix.

Synthesis of N-(2-imidazol-5-yl-1-carboxyethyl)-1,8-naphthalimide (HL^4): L-histidine monohydrochloride (0.84 g, 4 mmol) was stirred with lithium hydroxide monohydrate (0.17 g, 6 mmol) in 20 mL methanol for 15 min. The reaction mixture was then poured in a round bottom flask containing DMF solution (15 mL) of 1,8-naphthalic anhydride (0.80 g, 4 mmol). After refluxing the solution at 100 ºC for 12 h, it was cooled and poured into a beaker containing ice cold water. A white precipitate was obtained which was then filtered and dried in air. Yield: 80 %. IR (KBr, cm^{-1}): 3482 (br), 3126 (w), 1697 (s), 1660 (s), 1625 (m), 1586 (s), 1514 (m), 1439 (s), 1379 (m), 1302 (s), 1234 (s), 1181 (s), 1090 (s), 1034 (s), 981 (s), 880 (s), 846 (s), 779 (s), 665 (s), 634 (s), 515 (m), 465 (m). ^{1}H-NMR (600 MHz, DMSO-d_6): 8.50 (*d*, 1H, 6 Hz), 8.48 (*d*, 1H, 7.2 Hz), 7.88 (*t*, 1H, 7.8 Hz), 7.30 (*s*, 1H), 6.67 (*s*, 1H), 5.91 (*dd*, 1H), 3.45 (*dd*, 2H, 4.8 Hz), 3.42 (*dd*, 2H, 4.2 Hz). ^{13}C-NMR (DMSO-d_6): 169.7, 162.9, 134.8, 134.2, 131.5, 130.8, 128.3, 127.5, 124.5, 123.2, 121.1, 52.9, 21.3. HR-ESI MS (M+1) 336.7502 (calcd. 336.0906). Specific rotation, $[\alpha]_D^{25}$ (°) = -101.

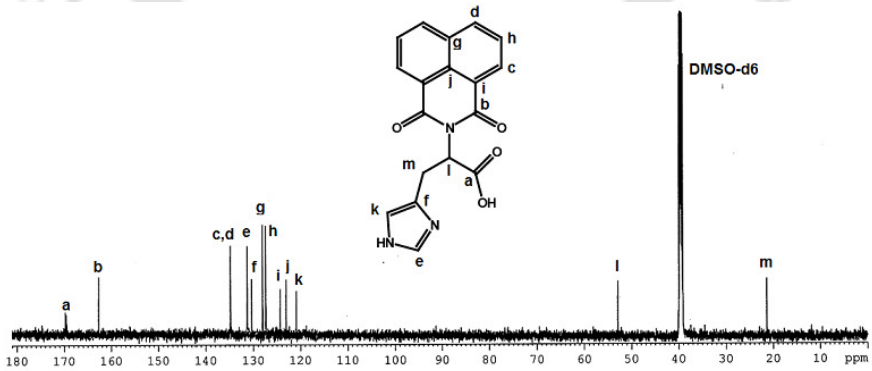

(a)

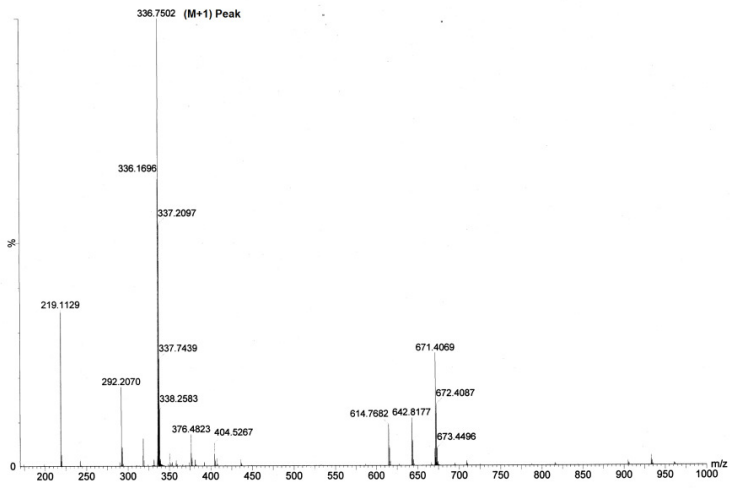

(b)

***Figure 6.18**: (a) [13]C-NMR (150 MHz, DMSO-d_6) and (b) HR-ESI MS of HL[4].*

Hydrate 6.1a: H**L**[4] (340 mg) was dissolved in 15 mL water by slight warming. Resulting solution was filtered and kept for crystallization. After one week of evaporation in air, colorless crystals appeared. Yield: 78 %. IR (KBr, cm^{-1}): 3502 (br), 3140 (w), 3022 (w), 1701 (s), 1659 (s), 1585 (s), 1437 (w), 1379 (s), 1236 (s), 1174 (w), 1087 (w), 949 (w), 849 (m), 778 (s), 665 (s), 631 (s), 517 (w). ^{1}H-NMR (600 MHz, DMSO-d_6): 8.48 (*d*, 1H, 8.4 Hz), 8.46 (*d*, 1H, 8.4 Hz), 7.88 (*t*, 1H, 7.8Hz), 7.36 (*s*, 1H), 6.65 (*s*, 1H), 5.79 (*dd*, 1H), 3.43 (*dd*, 1H), 3.35 (*dd*, 1H). Specific rotation, $[\alpha]_D^{25}(^\circ)$ = -109.

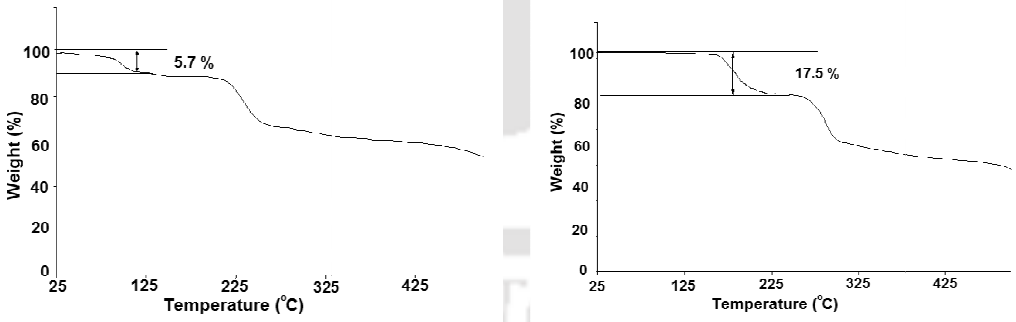

(a) (b)

***Figure 6.19:** Thermogram (heating rate 7 °C/min) of (a) hydrate of HL[4] (**6.1a**) and (b) DMF solvate (**6.1d**).*

Methanol solvate 6.1b: A solution of H**L**[4] (340 mg) in 10 mL methanol was left to slowly evaporate in air for one week to give the white crystals of **6.1b**. Yield: 72 %. IR (KBr, cm^{-1}): 3445 (br), 3140 (m), 3021 (w), 1700 (s), 1658 (s), 1585 (s), 1437 (w), 1379 (m), 1236 (s), 1174 (w), 1024 (m), 948 (m), 849 (m), 778 (s), 708 (w), 665 (s), 631 (s), 517 (m). ^{1}H-NMR (600 MHz, DMSO-d_6): 8.49 (*d*, 1H, 8.4 Hz), 8.46 (*d*, 1H, 8.4 Hz), 7.88 (*t*, 1H, 7.8

Hz), 7.36 (*s*, 1H), 6.65 (*s,* 1H), 5.79 (*dd*, 1H), (-CH_2- peak merged with water peak), 1.95 (*s*, 3H). Specific rotation, $[\alpha]_D^{25}$ (°) = -114.

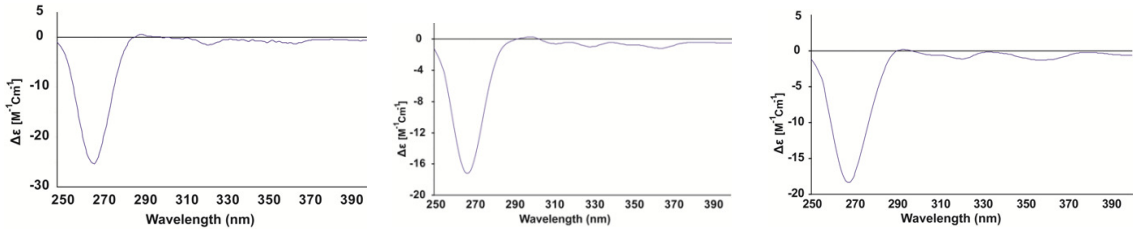

(a) (b) (c)

Figure 6.20*: Circular dichroism spectra of (a) HL*[4]*, (b) solvate* ***6.1c*** *and (c) salt* ***6.1l****.*

DMSO solvate 6.1c: HL[4] (340 mg) was dissolved in 10 mL DMSO and the resulting solution was filtered and kept undisturbed at room temperature for crystallization. Brown colored crystals of **6.1c** were obtained after 4 d by slow evaporation in air. Yield: 44 %. IR (KBr, cm^{-1}): 3477 (br), 3006 (w), 3152 (w), 1695 (s), 1656 (s), 1583 (s), 1435 (s), 1378 (s), 1336 (m), 1235 (s), 1187 (m), 1055 (s), 1024 (m), 956 (s), 871 (w), 775 (s), 661 (s), 608 (m), 566 (m), 512 (s). ^{1}H-NMR (600 MHz, DMSO-d_6): 8.49 (*d*, 1H, 9 Hz), 8.46 (*d*, 1H, 9.2 Hz), 7.88 (*t*, 1H, 7.8Hz), 6.65 (*s*, 1H), 5.80 (*dd*, 1H, 4.8 Hz), 3.43 (*dd*, 1H), 3.35 (*dd*, 1H), 2.53 (*s*, 1H). Specific rotation, $[\alpha]_D^{25}$ (°) = -104.

DMF solvate (6.1d): HL[4] (340 mg) was dissolved in a minimum volume of DMF. Obtained solution was kept undisturbed for crystallization. Colorless block crystals of **6.1d** appeared after one week by slow evaporation in air. Yield 82 %. IR (KBr, cm^{-1}): 3445 (br), 3154 (w), 3019 (w), 1696 (w), 1657 (s), 1585 (s), 1437 (s), 1378 (s), 1336 (m), 1236 (s), 1191 (s), 1056 (s), 956 (s), 872 (w), 776 (s), 662 (s), 511 (s). ^{1}H-NMR (600 MHz, DMSO-d_6): 8.49 (*d*, 1H, 8.4Hz), 8.46 (*d*, 1H, 8.6 Hz), 7.95(*s*, DMF proton), 7.89 (*t*, 1H, 7.8 Hz), 7.35 (*s*, 1H), 6.65 (*s*, 1H), 5.80 (*dd*, 1H, 4.8 Hz), (-CH_2- peak has been merged with solvent water peak), 2.53 (s, 3H). Specific rotation, $[\alpha]_D^{25}$ (°) = -102.

DMA solvate (6.1e): Colorless crystals were obtained from a solution of HL[4] (340 mg) in 10 mL DMA after one week of slow evaporation in air. Yield: 34 %. IR (KBr, cm^{-1}): 3466 (br), 3157 (w), 3012 (w), 1698 (m), 1658 (s), 1587 (m), 1438 (m), 1379 (s), 1237 (s), 1192 (m), 1057 (m), 958 (m), 874 (w), 781 (s), 663 (s), 512 (m). ^{1}H-NMR (600 MHz, DMSO-d_6): 8.49 (*d*, 1H, 8.4 Hz), 8.66 (*d*, 1H, 8.2), 7.88 (*t*, 1H, 7.2), 7.36 (*s*, 1H), 6.65 (*s*, 1H), 5.79 (*dd*, 1H, 5.4 Hz), (-CH_2- peak has been merged with solvent water peak), 2.94 (*s*, 3H), 1.95 (*s*, 3H). Specific rotation, $[\alpha]_D^{25}$ (°) = -99.

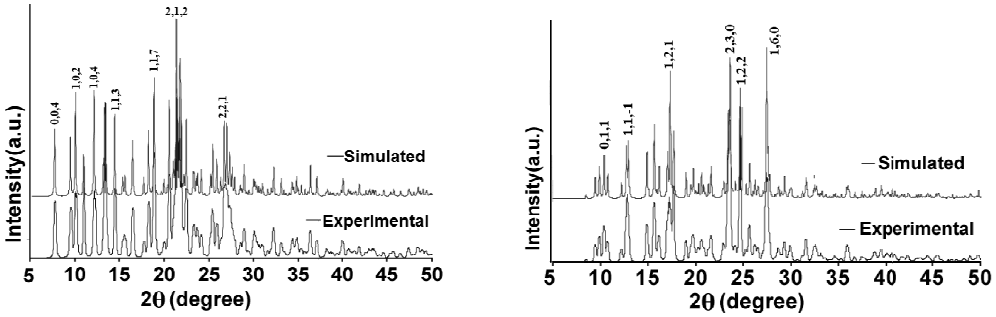

(a) (b)

Figure 6.21**: Comparison of simulated (top) and bottom (experimental) PXRD patterns of (a) DMA solvate **6.1e** and (d) salt **6.1l.

Quinoline solvate (6.1f): Brown colored crystals were obtained from a solution of H**L**^{4} (340 mg) in a minimum volume of quinoline after one week of slow evaporation in air. Yield: 69 %. IR (KBr, cm^{-1}): 3489 (br), 3114 (w), 3028 (w) 1695 (s), 1656 (s), 1626 (m), 1586 (s), 1498 (m), 1380 (m), 1260 (m), 1181 (w), 1025 (s), 854 (s), 802 (s), 665 (s), 630 (s), 536 (m), 474 (m). ^{1}H-NMR (600 MHz, DMSO-d$_6$): 8.91 (*dd*, 1H), 8.48 (*t*, 1H, 9 Hz), 8.38 (*d*, 1H, 7.8 Hz), 8.03 (*d*, 1H, 8.4 Hz), 7.99 (*d*, 1H, 8.4 Hz), 7.88 (*t*, 1H, 7.2 Hz), 7.78 (*m*, 1H), 7.63 (*t*, 1H, 1.2 Hz), 7.54 (*m*, 1H), 7.36 (*s*, 1H), 6.65 (s), 5.79 (*dd*, 1H), (-CH_2- peak has been merged with solvent water peak). Specific rotation, $[\alpha]_D^{25}$ (°) = -113.

Pyridine solvate (6.1g): H**L**^{4} (340 mg) was dissolved in a minimum volume of pyridine and filtered off. The filtrate was kept undisturbed for crystallization. Colorless block crystals of **6.1g** were obtained after one week by slow evaporation in air. Yield: 84 %. IR (KBr, cm^{-1}): 3446 (br), 3019 (w), 1700 (s), 1659 (s), 1585 (s), 1436 (m), 1379 (s), 1236 (s), 1175 (m), 1024 (s), 952 (s), 851 (m), 778 (s), 664 (s), 633 (m), 541 (w), 515 (w). ^{1}H-NMR (600 MHz, DMSO-d$_6$): 8.64 (*t*, 1H, 7.2Hz), 8.49 (*d*, 1H, 8.4 Hz), 8..48 (*d*, 1H, 7.2 Hz), 7.88 (*t*, 1H, 7.8 Hz), 7.62 (*t*, 1H, 8 Hz), 7.41 (*s*, 1H), 7.15 (*t*, 1H, 7.8Hz), 6.68 (*s*, 1H), 5.80 (*dd*, 1H), 3.44 (*dd*, 1H), 3.35 (*dd*, 1H). Specific rotation, $[\alpha]_D^{25}$ (°) = -111.

Dbu solvate (6.1h): Slow evaporation of the solution of H**L**^{4} (340 mg) in 5 mL dbu led to the formation of **6.1h** as colorless crystals after six days. Yield: 38 %. IR (KBr, cm^{-1}): 3501 (br), 2940 (w), 1700 (s), 1656 (s), 1585 (s), 1440 (s), 1384 (s), 1343 (m), 1239 (s), 1204 (m), 1105 (w), 1084 (m), 981 (s), 953 (s), 857 (s), 783 (s), 631 (w), 513 (w), 467 (w). ^{1}H-NMR (600 MHz, DMSO-d$_6$): 8.42 (*d*, 1H, 7.8 Hz), 8.40 (*d*, 1H, 8.2Hz), 7.84 (*t*, 1H, 7.8 Hz), 7.32 (*s*, 1H), 6.44 (*br*, 1H), 5.30 (*br*, 1H), 3.51 (*t*,1H, 7.8 Hz), 3.43 (*t*, 1H, 6 Hz), 3.21 (*t*, 2H, 5.4 Hz), 2.65 (*t*, 2H, 6 Hz), 1.86 (*m*, 2H), 1.63 (*t*, 2H, 5.4 Hz), 1.57 (*d*, 2H, 4.8 Hz). Specific rotation $[\alpha]_D^{25}$ (°) = -90.

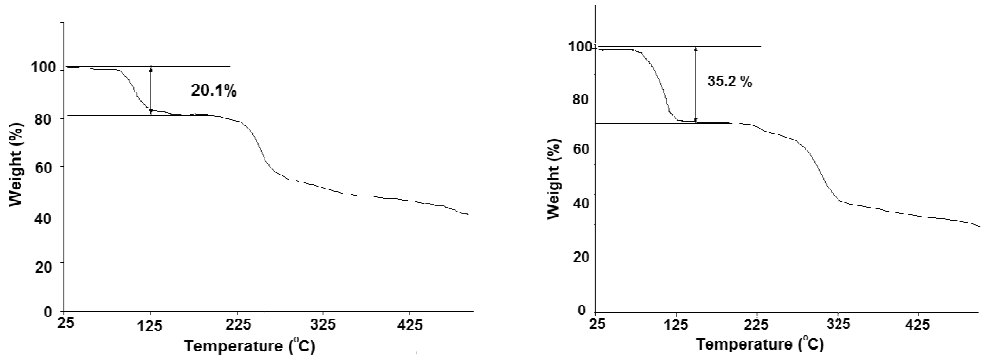

(a) (b)

***Figure 6.22**: Thermogram (heating rate 7 °C/min.) of (a) solvate **6.1g** and (b) solvate **6.1h**.*

Bromide salt (6.1i): Brown crystals of **6.1i** were obtained after 8-10 d by slow evaporation in air from a mixture prepared by adding 48 % aqueous hydrobromic acid (0.5 ml) to a solution of H**L**^{4} (340 mg) in 10 mL methanol. Yield: 68 %. IR (KBr, cm^{-1}): 3475 (br), 3000 (w), 1706 (s), 1662 (s), 1586 (s), 1465(m), 1436 (w), 1376 (m), 1238 (s), 1147 (w), 1021 (w), 921 (w), 842 (w), 777 (s), 659 (m), 625 (m), 459 (m). ^{1}H-NMR (600 MHz, DMSO-d$_6$): 8.51 (*d*, 1H, 12.6 Hz), 8.49 (*d*, 1H, 8.4 Hz), 8.18 (*s*, 1H), 7.89 (*t*, 1H, 2.4 Hz), 7.06 (*s*, 1H), 5.80 (*dd*, 1H), 3.55 (*dd*, 1H), 3.44 (*dd*, 1H), 2.61 (*s*, 3H). Specific rotation $[\alpha]_D^{25}$ (°) = -98.

Iodide salt (**6.1j**): 57 % aqueous hydroiodic acid (0.5 mL) was mixed with H**L**^{4} (340 mg) in 10 mL methanol. After a week brown crystals of **6.1j** were observed by slow evaporation in air. Yield: 64 %. IR (KBr, cm^{-1}): 3475 (br), 3013 (w), 1704 (s), 1661 (s), 1586 (s), 1462 (m), 1375 (m), 1298 (w), 1237 (s), 1145 (w), 1020 (w), 922 (w), 841 (w), 775 (s), 734 (w), 659 (m), 620 (m), 534 (w), 460 (w). ^{1}H-NMR (600 MHz, DMSO-d$_6$): 8.51 (*d*, 1H, 8.4 Hz), 8.49 (*d*, 1H, 7.2 Hz), 8.18 (*s*, 1H), 7.89 (*t*, 1H, 7.8 Hz), 7.07 (*s*, 1H), 5.80 (*m*, 1H), 3.56 (*dd*, 3.40), 2.61 (*s*, 3H). Specific rotation $[\alpha]_D^{25}$ (°) = -96.

Sulfate salt (6.1k): This compound was obtained by treating 0.1 mL of concentrated sulfuric acid with a solution of H**L**^{4} (340 mg, 1 mmol) in 25 mL methanol. Yellowish white crystals were obtained after one week by slow evaporation in air. Yield 75 %. IR (KBr, cm^{-1}): 3445 (br), 3031 (w), 1700 (s), 1657 (s), 1587 (s), 1438 (s), 1380 (s), 1354 (w), 1240 (s), 1112 (s), 1027 (w), 847 (w), 779 (s), 621 (s), 453 (w). ^{1}H-NMR (600 MHz, DMSO-d$_6$): 8.51 (*d*, 1H, 8.4 Hz), 8.49 (*d*, 1H, 7.2 Hz), 8.14 (*s*, 1H), 7.95 (aldehydic proton of DMF), 7.89 (*t*, 1H, 7.8 Hz), 7.05 (*s*, 1H), 5.80 (*m*, 1H), 3.56 (*dd*, 3.40), 3.00 (*s*, 3H). Specific rotation $[\alpha]_D^{25}$ (°) = -115.

Nitrate salt (6.1l): Addition of 69 % nitric acid (0.3 ml) to a methanolic solution (10 ml) of HL^4 (340 mg, 1 mmol) gave colorless crystals of **6.1l** after one week of slow evaporation in air. Yield 62 %. IR (KBr, cm^{-1}): 3502 (br), 3143 (w), 3040 (w), 1738 (s), 1697 (s), 1665 (w), 1624 (m), 1587 (s), 1459 (m), 1383 (s), 1282 (m), 1243 (s), 1145 (m), 1108 (m), 1081 (w), 961 (w), 849 (m), 781 (s), 650 (m), 626 (s), 513 (s), 456 (w). ^{1}H-NMR (600 MHz, DMSO-d_6): 8.89 (*s*, 1H), 8.55 (*d*, 1H, 9.6 Hz), 8.50 (*d*, 1H, 7.8 Hz), 7.90 (*t*, 1H, 7.8 Hz), 7.42 (*s*, 1H), 5.80 (*dd*, 1H), 3.66 (*dd*, 1H), 3.41 (*dd*, 1H). Specific rotation $[\alpha]_D^{25}$ (°) = -110.

References:

1. Joyce, G. F. *Nature* **2002**, *418*, 214-221.
2. Valev, V. K.; Baumberg, J. J.; Sibilia, C.; Verbiest, T. *Adv. Mater.* **2013**, *25*, 2517-2534.
3. Wong, K. M. -C.; Yam, V. W. -W. *Acc. Chem. Res.,* **2011**, *44*, 424-434.
4. Maggini, L.; Bonifazi, D. *Chem. Soc. Rev.* **2012**, *41*, 211-241.
5. Kim, Y.; Li, W.; Shin, S.; Lee, M.; *Acc. Chem. Res*. **2013**, *46*, 2888-2897.
6. Korevaar, P. A.; George, S. J.; Markvoort, A. J.; Smulders, M. M. J.; Hilbers, P. A. J.; Schenning, A. P. H. J.; De Greef, T. F. A.; Meijer, E. W. *Nature* **2012,** *481*, 492-496.
7. Mateos-Timoneda, M. A.; Crego-Calama, M.; Reinhoudt, D. N. *Chem. Soc. Rev*. **2004**, *33*, 363-372.
8. Aida, T.; Meijer, E. W.; Stupp, S. I. *Science* **2012,** *335*, 813-817.
9. Shin, S.; Lim, S.; Kim, Y.; Kim, T.; Choi, T.-L.; Lee, M. *J. Am. Chem. Soc.* **2013,** *135*, 2156-2159.
10. Zhu, L.; Li, X.; Wu, S.; Nguyen, K. T.; Yan, H.; Agren, H.; Zhao, Y. *J. Am. Chem. Soc.* **2013**, *135*, 9174-9180.
11. Gopal, A.; Hifsudheen, M.; Furumi, S.; Takeuchi, M.; Ajayaghosh, A. *Angew. Chem. Int. Ed.* **2012**, *51*, 10505-10509.
12. Zhu, L.; Li, X.; Zhang, Q.; Ma, X.; Li, M.; Zhang, H.; Luo, Z.; Agren, H.; Zhao, Y. *J. Am. Chem. Soc.* **2013**, *135,* 5175-5182.
13. Oh, H. S. ; Liu, S.; Jee, H.; Baev, A.; Swihart, M. T.; Prasad, P. N. J. *Am. Chem. Soc.* **2010**, *132*, 17346-17348.
14. Huang, Z.; Kang, S. -K.; Banno, M.; Yamaguchi, T.; Lee, D.; Seok, C.; Yashima, E.; Lee, M. *Science* **2012**, *337*, 1521-1526.
15. Roelfes, G.; Feringa, B. L. *Angew. Chem. Int. Ed.* **2005**, *44*, 3230-3232.
16. Boersma, A. J.; Coquiere, D.; Geerdink, D.; Rosati, F.; Feringa, B. N.; Roelfes, G. *Nat. Chem.* **2010**, *2*, 991-995.

17. Wang, J.; Feringa , B. L. *Science* **2011**, *331,* 1429-1432.
18. Kuhnle, A.; Linderoth, T. R.; Hammer, B.; Besenbacher, F. *Nature* **2002**, *415*, 891-893.
19. Gawronski, J.; Gawronska, K.; Skowronek, P.; Holmen, A. *J. Org. Chem.* **1999,** *64,* 234-241.
20. Cheney, M. L.; McManus, G. J.; Perman, J. A.; Wang, Z.; Zaworotko, M. J. *Cryst. Growth Des.* **2007**, *7*, 616-617.
21. Degenhardt III, C.; Shortell, D. B.; Adams, R. D.; Shimizu, K. D. *Chem. Commun*. **2000**, 929-930.
22. Iwanaga, T.; Nakamoto, R.; Yasutake, M.; Shinmyozu, T. *Angew. Chem., Int. Ed.* **2006**, *45*, 3643-3647.
23. Rasberry, R. D.; Smith, M. D.; Shimizu, K. D. *Org. Lett.* **2008**, *13*, 2889-2892.
24. Colquhoun, H. M.; Williams, D. J.; Zhu, Z. *J. Am. Chem. Soc.* **2002**, *124*, 13346-13347.
25. Cagulada, A. M.; Hamilton, D. G. *J. Am. Chem. Soc.* **2009**, *131*, 902-903.
26. Hosokawa, T.; Datta, S.; Sheth, A. R.; Brooks, N. R.; Young, V. G.; Jr. and Grant D. J. W. *Cryst. Growth Des.* **2004**, *4*, 971-977.
27. Barooah, N.; Sarma, R.J.; Baruah, J. B. *CrystEngComm* **2006**, *8*, 608-615.
28. Baruah, J. B.; Karmakar, A.; Barooah, N. *CrystEngComm* **2008**, *10*, 151-154.
29. Barooah, N.; Sarma, R. J.; Baruah, J. B. *Cryst. Growth Des.* **2003**, *3,* 639-642.
30. Flamigni, L.; Johnston, M. R.; Giribabu, L. *Chem. Eur. J.* **2002**, *8*, 3938-3847.
31. Du, M.; Zhang, Z. H.; Zhao, X. J. *Cryst. Growth Des.* **2005**, *5*, 1199-1202.
32. Takahashi, S.; Katagiri, T.; Uneyama, K. *Chem. Commun.* **2005**, 3658-3660.
33. Weatherhead-Kloster, R. A.; Selby, H. D.; Miller, W. B.; Mash, E. A. *J. Org. Chem.* **2005**, *70*, 8693-8702.
34. Zhang, J. P.; Lin, Y.-Y.; Huang, X. C.; Chen, X. M. *Chem. Commun.* **2005**, 1258-1260.
35. Vangala, V. R.; Bhogala, B. R.; Dey, A.; Desiraju, G. R.; Broder, C. K.; Smith, P. S.; Mondal, R.; Howard, J. A. K.; Wilson, C. C. *J. Am. Chem. Soc*. **2003,** *125*, 14495-14509.
36. Kishikawa, K.; Iwashima, C.; Yamguchi, K.; Yamamoto, M. *J. Chem. Soc. Perkin. Trans.* **2000**, *1*, 2217-2221.
37. Kishikawa, K.; Tsubokura, S.; Kohomoto, S.; Yamamoto, M. *J. Org. Chem.***1999**, *64*, 7568-7578.
38. Singh, D.; Baruah, J. B. *Tetrahedron Lett.* **2008**, *49*, 4374-4377.
39. Zhou, Q.-Z.; Jiang, X.-K.; Shao, X.-B.; Chen, G.-J.; Jia, M.-X.; Li, Z.-T. *Org. Lett.* **2003**, *5*, 1955-1958.
40. Mukhopadhyay, P.; Iwashita, Y.; Shirakawa, M.; Kawano, S.; Fujita, N.; Shinkai, S. *Angew. Chem., Int. Ed.* **2006**, *45*, 1592-1595.
41. Pantos, G. D.; Pengo, P.; Sanders, J. K. M. *Angew. Chem., Int. Ed.* **2007**, *46*, 194-197.

42. Cairns, A. J.; Perman, J. A.; Wojtas, L.; Kravtsov, V. C.; Alkordi, M. H.; Eddaoudi, M.; Zaworotko, M. J. *J. Am. Chem. Soc*. **2008**, *130*, 1560-1561.
43. Nath, J. K.; Mondal, A.; Powell, A. K. and Baruah, J. B. *Cryst. Growth Des.* **2014**, *14*, 4735-4748.
44. Gawronski, J.; Gawronska, K.; Skowronek, P.; Holmen, A. *J. Org. Chem.* **1999**, *64*, 234-241.
45. Saito, I.; Takayama, M.; Kawanishi, S. *J. Am. Chem. Soc.* **1995**, *117*, 5590-5591.
46. Banerjee, S.; Veale, E. B.; Phelan, C. M.; Murphy, S. A.; Tocci, G. M.; Gillespie, L. J.; Frimannsson, D. O.; Kelly, J. M.; Gunnlaugsson, T. *Chem. Soc. Rev*. **2013**, *42,* 1601-1618.
47. Cao, X.; Zhang, M.; Liu, K.; Mao, Y.; Lan, H.; Liu, B.; Yi, T.; *Chinese Sci. Bull.* **2012**, *57*, 4272-4277.
48. Zhu, H.; Huang, M.; Yang, F.; Chen, Y.; Miao, Z.; Qian, X.; Xu, Y.; Qin, Y.; Luo, H.; Shen, X.; Geng, M.; Cai, Y.; Ding, *J. Molecular Cancer Therapeut.* **2007**, *6*, 484-495.
49. Yang, Q.; Yang, P.; Qian, X.; Tong, L.; *Bioorg. Med. Chem. Lett.* **2008**, *18*, 6210-6213.
50. Pietropaolo, A.; Nakano, T. *J. Am. Chem. Soc.* **2013**, *135,* 5509-5512.
51. Barooah, N.; Sarma, R. J.; Baruah, J. B. *CrystEngComm* **2006**, *8*, 608-615.
52. Barooah, N.; Baruah, J. B. *J. Mol. Struct.* **2008**, *872*, 205-211
53. Blatov, V. A. *IUCr CompComm Newsletter* **2006**, *7*, 4-38.
54. Blatov, V. A.; Shevchenko, A. P.; Proserpio, D. M. *Cryst. Growth Des.* **2014**, *14*, 3576-3586.
55. Peresypkina, E. V.; Blatov, V. A. *Acta Cryst.* **2000**, *B56*, 1035-1045.
56. O'Keeffe, M.; Yaghi, O. M. *Chem. Rev.* **2012**, *112*, 675-702.
57. O'Keeffe, M.; Peskov, M. A.; Ramsden, S. J.; Yaghi, O. M. *Acc. Chem. Res.* **2008**, *30*, 1782-1789.
58. Li, M.; Li, D.; O'Keeffe, M.; Yaghi, O. M. *Chem. Rev*. **2014**, *114*, 1343-1370.
59. Zolotarev, P. N.; Arshad, M. N.; Asiri, A. M.; Al-amshany, Z. M.; Blatov, V. A. *Cryst. Growth Des.* **2014**, *14*, 1938-1949.
60. Baburin, I. A.; Blatov, V. A.; Carlucci, L.; Ciani, G.; Proserpio, D. M. *CrystEngComm* **2008**, *10*, 1822-1838.
61. Mukherjee, A.; Tothadi, S.; Chakraborty, S.; Ganguly, S.; Desiraju, G. R. *CrystEngComm* **2013**, *15*, 4640-4654.
62. Desiraju, G. R.; Steiner, T. In *The Weak Hydrogen Bond: In Structural Chemistry and Biology*; Desiraju, G. R., Steiner, T., Eds.; Oxford University Press Inc.: New York, **1999**.
63. Dunitz, J. D.; Gavezzotti, A. *Angew. Chem., Int. Ed*. **2005**, *44*, 1766-1787.
64. Vishweshwar, P.; Thaimattam, R.; Jaskólski, M.; Desiraju, G. R. *Chem.Commun*. **2002**, 1830-1831.
65. Takahashi, O.; Kohno, Y.; Nishio, M. *Chem. Rev*. **2010**, *110*, 6049-6076.

66. Nishio, M. *CrystEngComm.* **2004**, *6*, 130-158.
67. Nishio, M.; Umezawa, Y.; Suezawa, H.; Tsuboyama, S. In *The Importance of π-Interactions in Crystal Engineering: Frontiers in Crystal Engineering*; Tiekink, E. R. T.; Zukerman-Schpector, J.; Eds.; John Wiley & Sons Ltd: New York, **2012**.
68. Etter, M. C. *Acc. Chem. Res.***1990**, *23*, 120-126.
69. Nangia, A.; Desiraju, G. R. *Chem. Commun*. **1999**, 605-606.
70. Singh, D.; Baruah, J. B. *CrystEngComm.* **2009**, *11*, 2688-2694.
71. Singh, D.; Baruah, J. B. *Cryst. Growth Des*. **2011**, *11*, 768-777.
72. Singh, D.; Baruah, J. B. *Cryst. Growth Des*. **2012**, *12*, 2109-2121.
73. Singh, D.; Baruah, J. B. *Cryst. Growth Des.* **2012**, *12*, 3169-3180.
74. Das, B.; Crans, D. C.; Baruah, J. B. *Inorg. Chim. Acta* **2013**, *408*, 204-208.
75. Singh, D.; Bhattacharyya, P.; Baruah, J. B. *Cryst.Growth Des*. **2010**, *10*, 348-356.
76. Biradha, K.; Zaworotko, M. J. *J. Am. Chem. Soc.* **1998**, *120*, 6431-6432.
77. Duc, Y. L.; Michau, M.; Gilles, A.; Gence, V.; Legrand, Y.-M.; Lee, A. V. D.; Tingry, S.; Barboiu, M. *Angew. Chem., Int. Ed*. **2011**, *50*, 11366-11372.
78. Chen, W.-J.; Long, L.-S.; Huang, R.-B.; Zheng, L.-S. *Cryst. Growth Des.* **2013**, *13*, 2507-2513.
79. Bakhoda, A.; Khavasi, H. R.; Safari, N. *Cryst. Growth Des.* **2011**, *11*, 933-935.
80. Nath, J. K.; Baruah, J. B. *New J. Chem*. **2013**, 37, 1509-1519.
81. Dawson, R. E.; Hennig, A.; Wemann, D. P.; Emery, D.; Ravikumar, V.; Montenegero, J.; Takeuchi, T.; Gabutti, S.; Mayor, M.; Mareda, J.; Shalley, C.; Matile, S. *Nat. Chem.* **2010**, *2*, 533-537.
82. F Fujisawa, K.; Beuchat, C.; Humbert-Droz, M.; Wilson, A.; Wesolowski,T. A.; Mareda, J.; Sakai, N.; Matile, S. *Angew. Chem., Int. Ed.* **2014**, *53*, 11266-11269.
83. Frontera, A.; Gamez, P.; Mascal, M.; Mooibroek, T. J.; Reedijk, J. *Angew. Chem. Int. Ed.* **2011**, *50,* 9564-9583.
84. Zhao, Y.; Domoto, Y.; Orentas, E.; Beuchat, C.; Emery, D.; Mareda, J.; Sakai, N.; Matile, S. *Angew. Chem., Int. Ed.* **2013**, *52*, 9940-9943.
85. Misek, J.; Jentzsch, A. V.; Sakurai, S.-I.; Emery, D.; Mareda, J.; Matile, S. *Angew. Chem., Int. Ed.* **2010**, *49*, 7680-7683.
86. Marivel, S.; Arunachalam, M.; Ghosh, P. *Cryst. Growth Des*. **2011**, *11,* 1642-1650.
87. Nelyubina, Y. V.; Lyssenko, K. A.; Golovanov, D. G.; Antipin, M. Y. *CrystEngComm.* **2007**, *9*, 991-996.
88. Casellas, H.; Massera, C.; Buda, F.; Gamez, P.; Reedjik, J. *New. J. Chem.* **2006,** *30*, 1561-1566.
89. Vlaencia, L.; Bastda, R.; Gracia-Espana, E.; de Julian-Ortiz, J. V.; Llinares, J. M.; Macias, A.; Lourido, P. P. *Cryst. Growth Des.* **2010,** *10,* 3418-3423.

90. Wang, D. -X.; Wang, M. -X. *J. Am. Chem. Soc.* **2013**, *135,* 892-897.

91. Nath, B.; Baruah, J. B. *Cryst. Growth Des.* **2012**, *12*, 6173-6180.

92. Reger, D. L.; Debreczeni, A.; Horger, J. J.; Smith, M. D. *Cryst. Growth Des.* **2011**, *11*, 4068-4079.

93. Alexiou, M. S.; Tychopoulos, V.; Ghorbanian, S.; Tyman, J. H. P.; Brown, R. G.; Brittain, P. I. *J. Chem. Soc. Perkin Trans*. **1990**, *2*, 837-842.

94. DeSilva, A.P.; Gunaratne, H. Q. N.; Gunnlaugsson, T.; Huxley, A. J. M.; McCoy, C. P.; Rademacher, J.; Rice, T. E. *Chem. Rev*. **1997**, *97*, 1515-1566.

95. Guha, S.; Goodson, F.S.; Corson, L. J.; Saha, S. *J. Am. Chem. Soc.* **2012**, *134*, 13679-13691.

96. Nath, J. K.; Baruah, J.B. *J. Fluoresc.* **2014**, *24*, 649-655.

97. DeSilva, A. P.; Gunaratne, H. Q. N.; Gunlaugsson, T. *Tetrahedron Lett.* **1998**, *39*, 5077-5080.

98. DiCesare, N.; Adhikari, D. P.; Heynekamp, J. J.; Heagy, M. D.; Lakowicz, J. R. *J. Fluoresc.* **2002**, *12*, 147-154.

99. Trupp, S.; Schweitzer, A.; Mohr, G. *J. Org. Biomol. Chem.* **2006**, *4*, 2965-2968.

Conclusion

Taking advantages of hydrolytic ring opening reaction of cyclic anhydride and synergic π-stacking interactions of ligands metallacycles of some first row transition metal ions with different nuclearities were prepared. Depending on the ancillary ligand and central metal ions dinuclear, tetranuclear, hexanuclear metallacycles were selectively formed under ambient conditions. Tetranuclear metallacycles of cobalt (II) and zinc (II) were formed in the reaction of naphthalic anhydride, 2,2'-bipyridine and respective metal acetate. Whereas use of 1,10-phenenthroline as ancillary ligand resulted in the formation of hexanuclear metallacycle of cobalt (II) or nickel (II) ions. Nuclearities of such complexes depend on π···π interactions between the naphthalene ring and ancillary ligands. Cobalt (II) tetranuclear and hexanuclear metallacycle shows dominant antiferromagnetic interactions, whereas nickel (II) metallacycles showed as intramolecular ferromagnetic interactions.

Similar reactions carried out with copper (II) salts have resulted in trapping of intermediate ester complex formed during solvolytic ring opening in methanol medium. This enabled us to show an unprecedented example of solid state transformation of ester in solid state to form dicarboxylate complexes. From such solid state transformation mediated by moisture or moistening with solvent coordination polymer or dinuclear metallacycle through fast hydrolysis of ester group in such copper (II) precursors were shown. This novel solid state transformation provides new avenues to explore solvent mediated solid state transformations. Possible topological correlations between the starting ester complex and final coordination polymer or dicarboxylate complex are analysed. Diphenic anhydride did not yield intermediate species which is attributed to steric factor. Extension of these hydrolytic or solvolytic ring opening reactions to imides were carried out with copper (II) acetate as well as cadmium (II) acetate to prepare coordination polymers.

To understand modulation of emission properties of 1,8-naphthalimide at a remote site from a metal ion, 1,8-naphthalimide was tethered to imidazole through a propylene unit and a series of mononuclear metal complexes were prepared. Possibility of ambidenticity of thiocyanate ligand in such complexes was explored with an anticipation to prepare coordination polymers, but in each case we observed mononuclear complexes. Difference in geometrical arrangement caused to the flexible propylene unit of the tether provided different orientation of imidazole ring with respect to naphthalimide group, consequence of which were reflected in their fluorescence properties. Fluorescence behaviour of such

complexes was correlated with solid state structures. Complexes having bent geometries caused emission at shorter wavelength, whereas complex having stretched geometry show emission at longer wavelength.

In another approach dicarboxylic acids were taken as the primary unit for formation of coordination polymers in which pyridine tethered naphthalimide were used as ancillary ligands to understand magnetic properties as well as fluorescence properties. A series of different transition metal coordination polymers are prepared in which supramolecular interactions associated with naphthalimide rings and the flexibility of dicarboxylic acids guided coordination modes of different carboxylates. Changes in coordination and assembling properties caused by supramolecular interactions of naphthalimide group on these coordination polymers decide their photoluminescence and magnetic properties. At low temperature cobalt and nickel coordination polymers thus prepared showed weak anti-ferromagnetic behaviour, similar behaviour with copper coordination polymers other than copper malonate coordination polymer was observed. In the later case ferromagnetic interactions was observed. On the other hand a manganese adipate coordination polymer was identified among these complexes which showed single chain magnetic behaviour due to weak interactions between polymer chains. Based on their packing patterns in these coordination polymers fluorescence have been modulated.

Both the nitrogen atoms of naphthalenediimide were functionalized to anchor imidazole through intervening propylene units. This system has the ability to hold anions and serves as a model to understand different anion assisted assemblies of protonated naphthalenediimide derivatives. From such supramolecular assemblies we could depict clearly the first structural evidence showing anion-π interactions in naphthalenediimde derivatives and been able to establish geometries. We also have made a correlation on effects of anion-π interactions. Quenching of fluorescence of the ligand by chloride or bromide anions was observed due to anion-π interactions, whereas the protonation of the ligand by oxyacid caused conventional fluorescence enhancement observed in naphthalimide having nitrogen atoms containing pendant groups.

Finally we have depicted the packing patterns generated by different solvents when they are solvated to an optically pure histidine based naphthalimide zwitterionic derivative. Majority of solvates comprise of tetrameric assemblies of host molecules which are readjusted in geometries to accommodate the solvent molecules. Thermal studies were carried out to establish the stability of the solvates. Topological analyses reveal that there

are six distinct topological networks observed in the solvates and salts of the host. This zwitterionic derivative is capable of forming various anions with distinct supramolecular arrangements.

Appendix

Details of the analytical instruments:

X-ray crystallography:

X-ray diffraction data were collected on Bruker 3-circle diffractometer with CCD area detectors ProteumM APEX or SMART 6000 or Bruker Nonius Apex 2, using graphite-monochromated Mo-Kα radiation (λ= 0.71073Å) from a 60W micro-focus Bede Microsourse® with glass polycapillary optics or sealed tube.

X-ray diffraction data for all crystals were collected using Bruker SMART software. This software is also used for indexing and determination of the unit cell parameters. Some data were also collected in Oxford SuperNova diffractometer and data refinement refinement and cell reductions were carried out by CrysAlisPro.

Cell structures were solved by direct method and refined by full-matrix least squares against F^2 of all data, using SHELXTL software. The CIF of all the compounds synthesized and characterised are included in the soft copy.

All the non H-atoms were refined by full-matrix least squares in anisotropic, all H-atoms in isotropic approximation, against F^2 of all reflections. All non H-atoms were refined by full matrix least squares in anisotropic approximation and the hydrogen atoms attached to these atoms were treated as 'riding' in calculated positions and in some of the cases the hydrogen atoms have been located on the difference Fourier maps. In all the cases the H-atoms attached to the polar atoms such as O and N were located on the difference Fourier maps and refined in the final structure in isotropic approximation. The crystallographic tables for all the compounds are given at the end of this section, which includes the crystal parameters and the refinement factor.

Powder X-ray Diffraction data were collected on Bruker D2 phaser diffractometer in Bragg- Brentano θ-θ geometry with CuKα source (λ = 154 Å) on a glass surface of air dried sample using a secondary curved graphite monochromator. Diffraction patterns were collected over a 2θ range of 5-45°C at a scan rate of 2° per minute.

UV-visible spectroscopy, Fluorescence spectroscopy and IR Spectroscopy:

UV-visible absorption spectra were recorded using Perkin-Elmer Lambda 750 spectrophotometer equipped with double cell compartments. All the chemicals and solvents used were as obtained from the standard suppliers such as Merck Germany, Sigma Aldrich USA, Ranbaxy India. The solvents for optical spectroscopy were of HPLC grade (Aldrich or Merck) and used as obtained. The fluorescence spectra were recorded using a Perkin-Elmer LS 55 spectrofluorometer and Fluoromax 4 fluorimeter. FT-IR spectra were recorded on Perkin-Elmer spectrum one spectrometer in the range 4000-450 cm^{-1}.

NMR Spectroscopy:

The NMR spectra were recorded on Bruker 400 MHz and 600 MHz spectrometers. The chemical shifts in the NMR spectra are all given in ppm and tetramethylsilane was used as the internal standard.

EPR spectroscopy:

Solid state X band electron paramagnetic resonance spectra were recorded on a JES-FA200 ESR spectrometer and DPPH was used as internal standard.

Magnetic susceptibility measurements:

Magnetic susceptibility measurements were performed on Quantum Design SQUID MPMS XL instruments under the applied magnetic field of 1000 Oe and in the temperature range of 300 K to 2 K. Field-dependent magnetization was measured in the field range of 0 to 7 T under different temperatures (1.8 K to 5 K) and at 2 K and 3 K. The AC-susceptibility measurements recorded at H_{dc} = 1500 Oe with H_{ac} = 3.5 Oe in the temperature range of 15 K-2 K at various frequencies.

Thermogravimetric Studies and Elemental Analysis:

The thermogravimetric studies were performed using a Mettlar Toledo TGA/ STDA 851 thermal analyser and also with TA instrument with model no. SDTQ600. Typically about 4-10 mg of the samples were mounted on platinum crucibles and the TG profiles recorded

at the heating rate of 5˚C/min or in some cases 7˚C/min and under nitrogen atmosphere. Elemental analyses were done on a Parkin-Elmer PE 2400 II CHN analyser 2400.

Crystallographic data and refinement parameters for the compounds:

Compound No.	**2.1a**	**2.1b**	**2.1c**	**2.1d**
Formulae	$C_{88}H_{88}Co_4N_8O_{32}$	$C_{144}H_{148}Co_6N_{12}O_{56}$	$C_{22}H_{15}N_2NiO_8$	$C_{144}H_{148}N_{12}Ni_6O_{56}$
CCDC No.	869362	869363	1049808	891414
Mol. wt.	1989.26	3269.44	494.05	3295.00
Space group	*P-1*	*R-3*	*P2$_1$/c*	*R-3*
a (Å)	14.8783(3)	19.6128(3)	10.7477(13)	19.5194(7)
b (Å)	15.8120(4)	19.6128(3)	15.4242(18)	19.5194(7)
c (Å)	20.9566(5)	30.6440(5)	16.3400(15)	30.6641(12)
α (°)	110.6520(10)	90.00	90.00	90.00
β (°)	91.7890(10)	90.00	128.668(5)	90.00
γ (°)	91.7960(10)	120.00	90.00	120.00
V (Å^3)	4606.37(19)	10208.3(3)	2114.9(4)	10118.0(6)
Density (Mgm^{-3})	1.423	1.583	1.548	1.597
Abs. Coeff. (mm^{-1})	0.794	0.818	0.971	0.926
F(000)	2008	4962	1008	4980
Total no. of reflections	16498	4116	3746	3795
Reflections, *I > 2σ(I)*	9915	3654	2897	2086
Max.2 θ (°)	50.50	50.50	50.44	49.58
Ranges (h, k, l)	-17 ≤ h ≤ 17 -18 ≤ k ≤ 18 -25 ≤ l ≤ 24	-23 ≤ h ≤ 23 -22 ≤ k ≤ 23 -36 ≤ l ≤ 36	-12 ≤ h ≤ 12 -18 ≤ k ≤ 14 -17 ≤ l ≤ 15	-20 ≤ h ≤ 14 -20 ≤ k ≤ 21 -35 ≤ l ≤ 30
Complete to 2θ (%)	98.9	100.0	98.1	98.2
Data/ Restraints/Parameters	16498 / 0/ 1189	4116/0/330	3746 / 0 / 298	3795/0/
Goof (F^2)	1.164	1.069	1.117	1.066
R indices [*I > 2σ(I)*]	0.0647	0.0450	0.0814	0.0655
R indices (all data)	0.0963	0.0508	0.2287	0.1147

Compound No.	**2.1d**	**2.1e**	**2.2a**	**2.2b**
Formulae	$C_{88}H_{68}N_8O_22Zn_4$	$C_{48}H_{34}N_4O_{11}Zn_2$	$C_{24}H_{22}CuN_4O_8$	$C_{28}H_{28}Cu_2N_8O_{10}$
CCDC No.	892000	898078	972841	972840
Mol. wt.	1850.98	973.52	558.00	763.66
Space group	*I4$_1$/a*	*P-1*	*C2/c*	*P2$_1$/n*
a (Å)	15.2011(5)	10.5241(7)	12.5530(6)	8.8941(3)
b (Å)	15.2011(5)	11.4978(7)	8.4912(6)	22.4052(8)
c (Å)	33.989(2)	18.8532(14)	24.4976(13)	16.1449(6)
α (°)	90.00	90.077(4)	90.00	90.00
β (°)	90.00	100.663(3)	100.436(3)	105.428(2)
γ (°)	90.00	109.580(2)	90.00	90.00
V (Å^3)	7854.0(6)	2107.3(2)	2568.0(3)	3101.33(19)
Density (Mgm^{-3})	1.565	1.533	1.443	1.631
Abs. Coeff. (mm^{-1})	1.292	1.208	0.905	1.442
F(000)	3760	994	1148	1560
Total no. of reflections	3551	7498	2297	5534
Reflections, *I > 2σ(I)*	2071	5594	2071	3654
Max. 2θ (°)	50.48	50.50	50.50	50.50

Ranges (h, k, l)	-17 ≤ h ≤ 17 -18 ≤ k ≤ 17 -40 ≤ l ≤ 40	-11 ≤ h ≤ 10 -12 ≤ k ≤ 12 -22 ≤ l ≤ 19	-14 ≤ h ≤ 14 -10 ≤ k ≤ 4 -24 ≤ l ≤ 29	-10 ≤ h ≤ 10 -26 ≤ k ≤ 24 -19 ≤ l ≤ 19
Complete to 2θ (%)	99.9	99.2	99.4	98.3
Data/ Restraints/Parameters	3551/0/277	7498/5/606	2297/4/201	5534/4/449
Goof (F^2)	1.055	0.978	1.097	1.077
R indices [$I > 2\sigma(I)$]	0.0467	0.0528	0.0304	0.0516
R indices (all data)	0.0948	0.0928	0.0337	0.0981

Compound No.	**2.2c**	**2.2d**	**2.2e**	**2.3**
Formulae	$C_{38}H_{34}CuN_8O_8$	$C_{36}H_{38}Cu_2N_6O_{12}$	$C_{36}H_{30}CuN_4O_8$	$C_{14}H_{13}N_3O_2$
CCDC No.	972843	972839	972842	908078
Mol. wt.	794.28	873.80	710.18	255.27
Space group	$P2_1/c$	$P2_1/n$	$P2_1/c$	C2/c
a (Å)	8.5178(13)	11.9671(8)	8.077(2)	20.0864(9)
b (Å)	26.117(4)	13.7220(6)	12.926(3)	8.5847(3)
c (Å)	9.9434(16)	12.2072(8)	17.252(4)	14.8489(6)
α (°)	90.00	90.00	90.00	90.00
β (°)	125.233(10)	112.352(8)	114.682(10)	102.617(3)
γ (°)	90.00	90.00	90.00	90.00
V ($Å^3$)	1806.8(5)	1853.97(19)	1636.6(7)	2498.65(17)
Density (Mgm^{-3})	1.453	1.565	1.441	1. 357
Abs. Coeff. (mm^{-1})	0.670	1.220	0.727	0.094
F(000)	822	900	734	1072
Total no. of reflections	3210	3349	2939	2234
Reflections, $I > 2\sigma(I)$	2035	2768	2423	1682
Max. 2θ (°)	50.50	50.50	50.48	50.50
Ranges (h, k, l)	-10 ≤ h ≤ 9 -31 ≤ k ≤ 31 -11 ≤ l ≤ 11	-14 ≤ h ≤ 14 -14 ≤ k ≤ 16 -14 ≤ l ≤ 14	-9 ≤ h ≤ 9 -15 ≤ k ≤ 15 -20 ≤ l ≤ 20	-23 ≤ h ≤ 23 -10 ≤ k ≤ 10 -12 ≤ l ≤ 17
Complete to 2θ (%)	98.2	99.9	99.1	98.8
Data/ Restraints/Parameters	3210/2/251	3349/2/264	2939/0/224	2234 / 0 / 172
Goof (F^2)	1.196	1.013	1.059	1.095
R indices [$I > 2\sigma(I)$]	0.1598	0.0510	0.0311	0.0440
R indices (all data)	0.1885	0.0624	0.0401	0.0507

Compound No.	**2.3a**	**2.3b**	**2.3c**	**2.3d**
Formulae	$C_{56}H_{52}Cl_2CuN_{12}O_{20}$	$C_{56}H_{53}CuN_{14}O_{19}$	$C_{56}H_{52}Cu_2N_{12}O_{23}$	$C_{46}H_{45}Cd\ N_9O_{12}$
CCDC No.	908075	908076	908074	908077
Mol. wt.	1347.54	1289.66	1388.18	1028.31
Space group	P-1	C2/c	$I4_1/a$	$P2_1/c$
a (Å)	7.4414(8)	27.1427(13)	20.2203(9)	7.8545(4)
b (Å)	12.8615(13)	16.3589(13)	20.2203(9)	32.9348(16)
c (Å)	18.5332(18)	14.2208(8)	17.4841(13)	17.4647(8)
α (°)	103.824(6)	90.00	90.00	90.00
β (°)	99.430(6)	92.483(4)	90.00	101.076(3)
γ (°)	101.889(4)	90.00	90.00	90.00
V ($Å^3$)	1642.5(3)	6308.5(7)	7148.6(7)	4433.7(4)
Density (Mgm^{-3})	1.362	1.358	1.290	1.541
Abs. Coeff. (mm^{-1})	0.493	0.428	0.673	0.569

F(000)	695	2672	2856	2112
Total no. of reflections	5825	5616	3324	7816
Reflections, $I > 2\sigma(I)$	2786	3232	2124	4695
Max. 2θ (°)	50.50	50.50	50.98	50.00
Ranges (h, k, l)	-8 ≤ h ≤ 7 -13 ≤ k ≤ 15 -21 ≤ l ≤ 21	-30 ≤ h ≤ 32 -17 ≤ k ≤ 19 -17 ≤ l ≤ 17	-24 ≤ h ≤ 24 -23 ≤ k ≤ 24 -20 ≤ l ≤ 21	-9 ≤ h ≤ 7 -38 ≤ k ≤ 39 -20 ≤ l ≤ 20
Complete to 2θ (%)	98.2	98.5	99.8	99.9
Data/ Restraints/Parameters	5825/ 0 / 412	5616 / 0 / 410	3324 / 0 / 212	7816 / 2 / 615
Goof (F^2)	1.205	1.298	0.867	1.045
R indices [$I > 2\sigma(I)$]	0.0992	0.0765	0.0585	0.0778
R indices (all data)	0.1687	0.1254	0.1010	0.1322

Compound No.	**3.1a**	**3.1b**	**3.1c**	**3.1d**
Formulae	$C_{36}H_{30}Cl_2N_6O_4Zn$	$C_{36}H_{30}Cl_2N_6O_4Cd$	$C_{36}H_{30}Cl_2N_6O_4Hg$	$C_{78}H_{66}N_{16}O_8S_2Mn$
CCDC No.	928185	928178	928182	928183
Mol. wt.	746.93	973.96	882.15	1474.53
Space group	C2/c	C2/c	C2/c	P-1
a (Å)	14.6120(18)	14.6314(6)	14.7824(3)	10.6242(7)
b (Å)	11.9825(18)	11.9993(4)	12.0395(3)	11.2787(6)
c (Å)	19.488(3)	19.7572(8)	19.7994(5)	15.7505(9)
α (°)	90.00	90.00	90.00	95.575(4)
β (°)	104.612(11)	105.630(2)	104.923(2)	103.794(4)
γ (°)	90.00	90.00	90.00	99.258(4)
V ($Å^3$)	3276.9(8)	3340.4(2)	3404.91(14)	1790.86(18)
Density (Mgm^{-3})	1.514	1.579	1.721	1.367
Abs. Coeff. (mm^{-1})	0.964	0.864	4.727	0.312
F(000)	1536	1608	1736	767
Total no. of reflections	2919	3032	3066	6370
Reflections, $I > 2\sigma(I)$	2156	2638	2402	4095
Max. 2θ (°)	50.50	50.50	50.48	50.50
Ranges (h, k, l)	-16 ≤ h ≤ 17 -14 ≤ k ≤ 12 -22 ≤ l ≤ 22	-17 ≤ h ≤ 17 -14 ≤ k ≤ 10 -23 ≤ l ≤ 23	-17 ≤ h ≤ 17 -13 ≤ k ≤ 14 -23 ≤ l ≤ 23	-12 ≤ h ≤ 12 -13 ≤ k ≤ 13 -18 ≤ l ≤ 18
Complete to 2θ (%)	98.1	99.8	99.0	98.3
Data/ Restraints/Parameters	2919 / 0 / 222	3032 / 0 / 255	3066 / 0 /222	6370 / 0 / 476
Goof (F^2)	0.984	1.043	1.104	1.005
R indices [$I > 2\sigma(I)$]	0.0488	0.0351	0.0720	0.0433
R indices (all data)	0.0627	0.0427	0.1093	0.0790

Compound No.	**31.e**	**3.1f**	**3.1g**	**4.1a**
Formulae	$C_{78}H_{66}N_{16}O_8S_2Co$	$C_{38}H_{30}N_8O_4S_2Zn$	$C_{62}H_{59}N_{13}O_8S_2Cd$	$C_{42}H_{40}MnN_4O_{12}$
CCDC No.	928180	928184	928179	976310
Mol. wt.	1478.52	792.19	1290.74	847.72
Space group	P-1	$P2_1/c$	*P-1*	*P-1*
a (Å)	10.6146(8)	14.5214(4)	10.3324(3)	5.5839(12)
b (Å)	11.2239(12)	14.1478(5)	16.9948(4)	12.097(3)
c (Å)	15.7625(14)	22.8454(8)	17.5964(4)	14.595(3)
α (°)	95.493(8)	90.00	91.4080(10)	107.883(11)

β (°)	104.366(7)	128.618(2)	95.6650(10)	100.455(11)
γ (°)	99.105(8)	90.00	106.9570(10)	97.851(12)
V (Å^3)	1778.3(3)	3667.1(2)	2936.48(13)	903.0(3)
Density (Mgm^{-3})	1.381	1.435	1.460	1.552
Abs. Coeff. (mm^{-1})	0.370	0.836	0.511	0.442
F(000)	769	1632	1332	437
Total no. of reflections	6422	6629	10470	3218
Reflections, $I > 2\sigma(I)$	4116	4765	7921	1695
Max. 2θ (°)	50.50	50.50	50.50	50.50
Ranges (h, k, l)	-12 ≤ h ≤ 12 -11 ≤ k ≤ 13 -18 ≤ l ≤ 18	-16 ≤ h ≤ 17 -16 ≤ k ≤ 16 -26 ≤ l ≤ 27	-12 ≤ h ≤ 12 -19 ≤ k ≤ 18 -21 ≤ l ≤ 20	-6 ≤ h ≤ 6 -14 ≤ k ≤ 14 -17 ≤ l ≤ 17
Complete to 2θ (%)	99.8	99.8	98.3	98.5
Data/ Restraints/Parameters	6422 / 0 / 476	6629 / 0 / 478	10470 / 0 / 779	3218 / 1 / 273
Goof (F^2)	1.019	1.114	1.044	0.987
R indices [$I > 2\sigma(I)$]	0.0699	0.0473	0.0320	0.0778
R indices (all data)	0.1076	0.0732	0.0450	0.1531

Compound No.	**4.1b**	**4.1c**	**4.1d**	**4.1e**
Formulae	$C_{40}H_{34}CoN_4O_{12}$	$C_{42}H_{40}CoN_4O_{12}$	$C_{22}H_{22}N_2NiO_{10}$	$C_{40}H_{28}CuN_4O_9$
CCDC No.	976311	976312	976313	976314
Mol. wt.	821.65	851.72	533.13	772.21
Space group	*P2$_1$/a*	*P-1*	*P2$_1$/a*	*P-1*
a (Å)	9.0212(5)	5.5869(4)	9.1127(3)	8.8003(5)
b (Å)	13.2138(9)	12.0319(13)	13.0832(5)	14.7244(10)
c (Å)	30.273(2)	14.5280(15)	18.4154(7)	16.5169(14)
α (°)	90.00	107.552(9)	90.00	98.647(6)
β (°)	91.213(6)	100.654(7)	97.724(3)	93.170(6)
γ (°)	90.00	97.990(7)	90.00	98.561(5)
V (Å^3)	3607.8(4)	895.09(15)	2175.63(13)	2085.7(3)
Density (Mgm^{-3})	1.505	1.573	1.628	1.226
Abs. Coeff. (mm^{-1})	0.550	0.557	0.956	0.578
F(000)	1684	439	1104	790
Total no. of reflections	6532	3231	3924	7553
Reflections, $I > 2\sigma(I)$	5221	2751	3313	4276
Max. 2θ (°)	50.50	50.48	50.48	50.50
Ranges (h, k, l)	-10 ≤ h ≤ 10 -10 ≤ k ≤ 15 -32 ≤ l ≤ 36	-6 ≤ h ≤ 6 -13 ≤ k ≤ 14 -17 ≤ l ≤ 17	-10 ≤ h ≤ 10 -9 ≤ k ≤ 15 -19 ≤ l ≤ 22	-10 ≤ h ≤ 10 -17 ≤ k ≤ 17 -19 ≤ l ≤ 18
Complete to 2θ (%)	99.8	99.9	99.8	99.8
Data/ Restraints/Parameters	6532 / 4 / 528	3231 / 2 / 276	3924 / 8 / 327	7553 / 0 / 487
Goof (F^2)	1.087	1.068	1.032	1.168
R indices [$I > 2\sigma(I)$]	0.0936	0.0561	0.0514	0.0877
R indices (all data)	0.1105	0.0670	0.1688	0.1458

Compound No.	**4.1f**	**4.1g**	**5.1a**	**5.1b**
Formulae	$C_{21}H_{16}CuN_2O_7$	$C_{126}H_{101}Cu_3N_{12}O_{27}$	$C_{26}H_{28}Cl_2N_6O_6$	$C_{26}H_{28}Br_2NO_6$
CCDC No.	976315	976316	911758	911757
Mol. wt.	471.90	2405.85	591.44	680.36

Space group	*Pbca*	*P-1*	*P-1*	*P-1*
a (Å)	15.1823(11)	17.0180(5)	7.0527(12)	7.2916(3)
b (Å)	7.8010(6)	17.8705(7)	13.808(2)	13.7926(5)
c (Å)	31.418(2)	20.8120(7)	14.472(2)	14.4930(6)
α (°)	90.00	65.116(3)	78.038(5)	78.306(2)
β (°)	90.00	83.339(3)	83.616(5)	82.839(2)
γ (°)	90.00	69.993(3)	81.133(5)	80.576(2)
V ($Å^3$)	3721.1(5)	5392.3(3)	1357.7(4)	1401.72(10)
Density (Mgm^{-3})	1.685	1.479	1.447	1.612
Abs. Coeff. (mm^{-1})	1.225	0.674	0.292	2.943
F(000)	1928	2476	616	688
Total no. of reflections	3321	28001	4886	4982
Reflections, $I > 2\sigma(I)$	2036	25971	2535	3062
Max. 2θ (°)	50.50	57.54	50.46	50.48
Ranges (h, k, l)	$-17 \le h \le 17$ $-8 \le k \le 8$ $-36 \le l \le 37$	$-17 \le h \le 22$ $-23 \le k \le 23$ $-23 \le l \le 27$	$-7 \le h \le 8$ $-16 \le k \le 16$ $-14 \le l \le 17$	$-8 \le h \le 8$ $-16 \le k \le 14$ $-17 \le l \le 16$
Complete to 2θ (%)	98.5	99.8	99.1	98.3
Data/ Restraints/Parameters	3321 / 0 / 285	28001 / 0 / 1514	4886 / 4 / 377	4982 / 4 / 377
Goof (F^2)	1.001	1.072	0.962	0.962
R indices [$I > 2\sigma(I)$]	0.0406	0.0640	0.0647	0.0444
R indices (all data)	0.0890	0.1032	0.1116	0.0770

Compound No.	**5.1c**	**5.1d**	**5.1e**	**5.1f**
Formulae	$C_{26}H_{24}Cl_2N_6O_{12}$	$C_{26}H_{30}N_6O_{14}S_2$	$C_{28}H_{30}N_6O_{12}S_2$	$C_{26}H_{27}N_6O_9P$
CCDC No.	911763	911759	911760	916142
Mol. wt.	683.41	714.68	706.70	598.51
Space group	$P2_1/n$	$P2_1/c$	$P2_1/c$	*P-1*
a (Å)	9.5472(5)	8.5912(4)	6.691(3)	7.5861(4)
b (Å)	24.1664(10)	12.5950(6)	13.879(6)	10.2212(6)
c (Å)	12.7016(5)	14.3918(7)	17.851(7)	18.4816(14)
α (°)	90.00	90.00	90.00	100.062(6)
β (°)	101.922(2)	106.760(2)	109.63(2)	98.722(5)
γ (°)	90.00	90.00	90.00	106.368(5)
V ($Å^3$)	2867.3(2)	1491.13(12)	1561.3(11)	1322.86(14)
Density (Mgm^{-3})	1.583	1.592	1.503	1.503
Abs. Coeff. (mm^{-1})	0.304	0.262	0.245	0.172
F(000)	1408	744	736	624
Total no. of reflections	4989	2668	2791	4778
Reflections, $I > 2\sigma(I)$	2652	2098	1964	3450
Max. 2θ (°)	50.00	50.50	50.48	50.50
Ranges (h, k, l)	$-11 \le h \le 11$ $-28 \le k \le 27$ $-15 \le l \le 14$	$-9 \le h \le 10$ $-14 \le k \le 12$ $-16 \le l \le 14$	$-7 \le h \le 8$ $-16 \le k \le 16$ $-21 \le l \le 21$	$-9 \le h \le 9$ $-12 \le k \le 8$ $-22 \le l \le 22$
Complete to 2θ (%)	98.7	98.7	98.6	99.8
Data/ Restraints/Parameters	4989 / 0 / 415	2668 / 6 / 226	2791 / 0 / 218	4778 / 10 / 387
Goof (F^2)	1.031	0.908	0.998	1.000
R indices [$I > 2\sigma(I)$]	0.0733	0.0875	0.0554	0.0572
R indices (all data)	0.1470	0.0962	0.0831	0.0807

Compound No.	**5.1g**	**5.1h**	**6.1a**	**6.1b**
Formulae	$C_{26}H_{24}N_8O_{10}$	$C_{104}H_{102}F_{24}N_{24}O_{19}Si_4$	$C_{18}H_{13}N_3O_5$	$C_{73}H_{56}N_{12}O_{20}$
CCDC No.	911761	911762	1021687	1021686
Mol. wt.	608.53	2560.60	351.31	1421.30
Space group	$P2_1/n$	$P\ 2_1/c$	$P2_1$	$P2_1$
a (Å)	6.9112(9)	19.277(6)	8.3033(6)	8.4504(5)
b (Å)	9.5788(11)	9.226(3)	14.3166(9)	14.1551(9)
c (Å)	20.126(2)	34.761(10)	27.1828(15)	27.2253(16)
α (°)	90.00	90.00	90	90
β (°)	94.476(8)	116.698(19)	90.998(6)	92.716(5)
γ (°)	90.00	90.00	90	90
V (Å^3)	1328.3(3)	5523(3)	3230.9(3)	3253.0(3)
Density (Mgm^{-3})	1.521	1.536	1.444	1.451
Abs. Coeff. (mm^{-1})	0.120	0.175	0.108	0.108
F(000)	632	2624	1456	1476
Total no. of reflections	2384	9817	5999	5998
Reflections, $I > 2\sigma(I)$	1127	3639	5195	4982
Max. 2θ (°)	50.48	50.50	50.50	50.50
Ranges (h, k, l)	-7 ≤ h ≤ 8 -10 ≤ k ≤ 10 -23 ≤ l ≤ 22	-23 ≤ h ≤ 23 -11 ≤ k ≤ 10 -41 ≤ l ≤ 41	-9 ≤ h ≤ 9 -17 ≤ k ≤ 16 -30 ≤ l ≤ 32	-10 ≤ h ≤ 9 -16 ≤ k ≤ 15 -20 ≤ l ≤ 32
Complete to 2θ (%)	99.0	98.6	99.0	98.0
Data/ Restraints/Parameters	2384 / 0 / 200	9817 / 0 / 793	5999/17/970	5998/35/1002
Goof (F^2)	1.166	1.116	0.999	1.006
R indices [$I > 2\sigma(I)$]	0.0528	0.0817	0.0656	0.0894
R indices (all data)	0.0754	0.1156	0.0996	0.1736

Compound No.	**6.1c**	**6.1d**	**6.1e**	**6.1f**
Formulae	$C_{20}H_{19}N_3O_5S$	$C_{21}H_{20}N_4O_5$	$C_{22}H_{22}N_4O_5$	$C_{36}H_{27}N_5O_4$
CCDC No.	1021689	1021688	1021691	1021695
Mol. wt.	413.45	408.41	422.44	593.63
Space group	$P4_32_12$	$P4_32_12$	$P4_32_12$	$P2_1$
a (Å)	9.1474(3)	9.2737(3)	9.4259(3)	7.0609(3)
b (Å)	9.1474(3)	9.2737(3)	9.4259(3)	13.0523(6)
c (Å)	45.447(2)	45.268(2)	45.174(3)	15.6203(8)
α (°)	90	90	90	90
β (°)	90	90	90	98.512(4)
γ (°)	90	90	90	90
V (Å^3)	3802.8(3)	3893.1(2)	4013.6(3)	1423.73(11)
Density (Mgm^{-3})	1.444	1.394	1.398	1.385
Abs. Coeff. (mm^{-1})	0.209	0.102	0.101	0.093
F(000)	1728	1712	1776	620
Total no. of reflections	2099	2139	2202	2689
Reflections, $I > 2\sigma(I)$	1857	1866	1943	2418
Max. θ (°)	50.48	50.46	50.50	50.48
Ranges (h, k, l)	-10 ≤ h ≤ 4 -10 ≤ k ≤ 5 -54 ≤ l ≤ 27	-6 ≤ h ≤ 11 -10 ≤ k ≤ 5 -54 ≤ l ≤ 52	-11 ≤ h ≤ 8 -11 ≤ k ≤ 10 -28 ≤ l ≤ 54	-8≤ h ≤ 8 -12 ≤ k ≤ 15 -10 ≤ l ≤ 18

Complete to 2θ (%)	99.0	99.0	99.0	99.0
Data/ Restraints/Parameters	3436/0/264	2139/7/289	2202/22/335	2689/3/414
Goof (F^2)	1.026	0.997	1.034	1.018
R indices [$I > 2\sigma(I)$]	0.0631	0.0645	0.0471	0.0439
R indices (all data)	0.0766	0.0715	0.0539	0.0493

Compound No.	**6.1g**	**6.1h**	**6.1i**	**6.1j**
Formulae	$C_{23}H_{18}N_4O_4$	$C_{27}H_{31}N_5O_6$	$C_{37}H_{32}Br_2N_6O_9$	$C_{37}H_{31}I_2N_6O_9$
CCDC No.	1021694	1021685	1021690	1021692
Mol. wt.	414.41	521.57	864.49	958.49
Space group	$P2_12_12_1$	$P1$	$P2_1$	$P2_1$
a (Å)	8.8106(3)	8.6816(3)	7.8903(7)	8.1686(5)
b (Å)	9.3624(3)	9.2680(3)	11.6558(8)	11.7670(4)
c (Å)	24.5159(7)	18.9183(5)	20.221(2)	20.2208(9)
α (°)	90	85.672(2)	90	90
β (°)	90	79.851(2)	97.454(8)	98.256(5)
γ (°)	90	62.346(2)	90	90
V (Å^3)	2022.28(11)	1327.17(7)	1844.0(3)	1923.48(16)
Density (Mgm^{-3})	1.361	1.300	1.557	1.655
Abs. Coeff. (mm^{-1})	0.096	0.094	2.262	1.696
F(000)	864	548	876	948
Total no. of reflections	2869	4701	3471	3592
Reflections, $I > 2\sigma(I)$	2582	3571	3030	2764
Max. θ (°)	57.06	50.50	50.50	50.50
Ranges (h, k, l)	-11≤ h ≤ 11 -10 ≤ k ≤ 12 -32 ≤ l ≤ 31	-10≤ h ≤ 10 -11 ≤ k ≤ 11 -22 ≤ l ≤ 20	-9 ≤ h ≤ 9 -12 ≤ k ≤ 13 -24 ≤ l ≤ 14	-7 ≤ h ≤ 9 -14 ≤ k ≤ 13 -24 ≤ l ≤ 16
Complete to 2θ (%)	98.4	98.0	99.0	98.0
Data/ Restraints/Parameters	2869/62/320	4701/16/690	3471/38/497	3592/58/481
Goof (F^2)	1.071	1.068	1.039	1.048
R indices [$I > 2\sigma(I)$]	0.0578	0.0476	0.0775	0.0550
R indices (all data)	0.0761	0.0583	0.1070	0.0646

Compound No.	**6.1k**	**6.1l**
Formulae	$C_{39}H_{37}N_7O_{14}S$	$C_{18}H_{14}N_4O_7$
CCDC No.	1021696	1021693
Mol. wt.	859.82	398.33
Space group	$P2_12_12_1$	$P2_1$
a (Å)	11.2039(4)	9.1427(4)
b (Å)	16.6610(7)	20.8064(10)
c (Å)	20.7290(9)	9.5488(4)
α (°)	90	90
β (°)	90	101.925(4)
γ (°)	90	90
V (Å^3)	3869.5(3)	1777.24(14)
Density (Mgm^{-3})	1.476	1.489
Abs. Coeff. (mm^{-1})	0.165	0.117
F(000)	1792	824
Total no. of reflections	3896	3269

Reflections, $I > 2\sigma(I)$	3035	3052
Max. θ (°)	50.50	50.50
Ranges (h, k, l)	$-13 \leq h \leq 9$ $-19 \leq k \leq 18$ $-24 \leq l \leq 15$	$-10 \leq h \leq 10$ $-24 \leq k \leq 24$ $-11 \leq l \leq 10$
Complete to 2θ (%)	99.0	99.0
Data/ Restraints/Parameters	3896/8/573	3269/5/541
Goof (F^2)	1.015	0.998
R indices [$I > 2\sigma(I)$]	0.0433	0.0427
R indices (all data)	0.0556	0.0548

List of Publication

1. **J. K. Nath,** A. M. Kirillov, J. B. Baruah. Synthesis, structure and topological studies of solvates and salts of a chiral zwitterionic host N-(2-imidazol-5-yl-1-carboxyethyl)-1,8-naphthalimide.
   Crystal Growth and Design, 2015, **15**, 737-751.

2. **J. K. Nath,** A. Mondal, A. K. Powell, J. B. Baruah. Structures, magnetic properties and photoluminescence of dicarboxylate coordination polymers of Mn, Co, Ni, Cu having N-(4-pyridylmethyl)-1,8-naphthalimide.
   Crystal Growth and Design, 2014**, 14**, 4735-4748.

3. **J. K. Nath,** A. M. Kirillov, J. B. Baruah. Unusual solvent-mediated hydrolysis of dicarboxylate monoester ligands in copper (II) complexes toward simultaneous crystallization of new dicarboxylate derivatives.
   RSC Advances, 2014**, 4**, 47876-47886.

4. **J. K. Nath,** J. B. Baruah. Twisted conformations in complexes of N-(3-imidazol-1-yl-propyl)-1,8-naphthalimide and fluorescence properties.
   Inorganic Chemistry Frontiers, 2014**, 1**, 342-351.

5. **J. K. Nath,** J. B. Baruah. Water assisted anion chains and anion dependent fluorescence emission in salts of *N,N'*-bis(3-imidazol-1-ylpropyl)naphthalenediimide.
   New Journal of Chemistry, 2013**, 37**, 1509-1519.

6. **J. K. Nath,** Y. Lan, A. K. Powell, J. B. Baruah. Effect of ancillary ligands in hydrolysis of 1,8-naphthalic anhydride for synthesis of metallacycles of Co^{2+}, Ni^{2+} and Zn^{2+}.
   Zeitschrift für anorganische und allgemeine Chemie, 2013**, 639,** 2250-2257.

7. **J. K. Nath,** J. B. Baruah. Copper (II) and cadmium (II) complexes with an imide tethered imidazole and a copper (II) coordination polymer through ring opening reaction.
   Inorganic Chemistry Communication, 2013, **30**, 128-132.